



**Universidade do Minho**

I3Bs - Instituto de Investigação em Biomateriais, Biodegradáveis e Biomiméticos

Marta Alexandra Rodrigues Casanova

**Surface biofunctionalization of polycaprolactone fibrous meshes for skeletal and neural tissue advanced therapies**

Surface biofunctionalization of polycaprolactone fibrous meshes for skeletal and neural tissue advanced therapies

Marta Casanova

UMinho | 2019

**FCT** Fundação para a Ciência e a Tecnologia  
MINISTÉRIO DA CIÊNCIA, TECNOLOGIA E ENSINO SUPERIOR

**PD + F**  
FCT PhD PROGRAMMES

**PO PH**  
PROGRAMA OPERACIONAL POTENCIAL HUMANO

**QR**  
QUADRO DE REFERÊNCIA ESTRATÉGICO NACIONAL  
PORTUGA. 2007.2013

**GOVERNO DA REPÚBLICA PORTUGUESA**

**UNIÃO EUROPEIA**  
Fundo Social Europeu





**Universidade do Minho**

I3Bs - Instituto de Investigação em Biomateriais, Biodegradáveis e Biomiméticos

Marta Alexandra Rodrigues Casanova

**Surface biofunctionalization of  
polycaprolactone fibrous meshes for  
skeletal and neural tissue advanced  
therapies**

Tese de Doutoramento

Doutoramento em Engenharia de Tecidos, Medicina  
Regenerativa e Células Estaminais

Trabalho efetuado sob a orientação do

**Professor Nuno João Meleiro das Neves**

**Doutor Albino Manuel Pereira Martins**

Outubro de 2019

## **DIREITOS DE AUTOR E CONDIÇÕES DE UTILIZAÇÃO DO TRABALHO POR TERCEIROS**

Este é um trabalho académico que pode ser utilizado por terceiros desde que respeitadas as regras e boas práticas internacionalmente aceites, no que concerne aos direitos de autor e direitos conexos.

Assim, o presente trabalho pode ser utilizado nos termos previstos na licença abaixo indicada.

Caso o utilizador necessite de permissão para poder fazer um uso do trabalho em condições não previstas no licenciamento indicado, deverá contactar o autor, através do RepositóriUM da Universidade do Minho.

*Licença concedida aos utilizadores deste trabalho*



**Atribuição**

**CC BY**

**<https://creativecommons.org/licenses/by/4.0/>**

## ACKNOWLEDGMENTS

The help and support provided by others during this PhD was crucial to the success of the work. Therefore, I would like to express my sincere thanks to the people that made this thesis possible. I would like to start by expressing my gratitude to my supervisor Prof. Nuno M. Neves, I am deeply grateful for accepting me as a PhD student, and believing in me. I express a really special recognition for his constructive criticism, the scientific brainstorming and clarifying the importance of the scientific policy. For the orientation and support throughout this PhD, getting me to this stage. I would like to express my gratitude to my co-supervisor Dr. Albino Martins, for the support, help and suggestions during these 4 years. Hence, I thank him for his trust and especially for all the patience and serenity he transmitted along these years. Lastly, but not least, to the director of the 3B's Research Group, Prof. Dr. Rui L. Reis, for giving me the opportunity to join this prestigious research group. I am truly grateful to him for providing me the opportunity to have such experience during these past years, which prepared me to the competitive scientific world.

To the financial support of the Portuguese Foundation for Science and Technology to make possible this PhD by awarded me with a PhD scholarship (PD/BD/113797/2015) under the Doctoral Program on Advanced Therapies for Health (FSE/POCH/PD/169/2013). The experimental work was funded by the projects SPARTAN (PTDC/CTM-BIO/4388/2014) and FRONthera (NORTE-01-0145-FEDER-0000232).

I would like to acknowledge the co-authors of my research papers, presented in this thesis. Your contribution was critical in order to achieve this personal milestone. I thank all 3B's Research Group members for their availability and expertise, which somehow contributed to the success of this PhD work. To all my fellow colleagues from the 3B's Research Group, I would like to thank for all their support and friendship, in specially Alexandra Brito, Bárbara Mendes, Carla Abreu and Marta Guedes.

I would like to thank my family for all the unconditional love and support, playing a very important role throughout my civic and academic formation. To my godmother, I am really thankful for the person that I am today. I would like also to thank my friends for all the emotional support. To my godson and his sister, I want to thank the unconditional love.

Finally, I would like to express thankfulness to my partner, my world, the love of my life Jorge Ferreira. Thank you for always staying by my side in the best and hardest moments. Thus, this thesis is dedicated to you, to us.

## **STATEMENT OF INTEGRITY**

I hereby declare having conducted this academic work with integrity. I confirm that I have not used plagiarism or any form of undue use of information or falsification of results along the process leading to its elaboration.

I further declare that I have fully acknowledged the Code of Ethical Conduct of the University of Minho.

## **Surface biofunctionalization of polycaprolactone fibrous meshes for skeletal and neural tissue advanced therapies**

### **ABSTRACT**

Damage of the skeletal and neural tissues has a significant impact over the quality-of-life of patients and high socio-economical costs. Current treatment options are not effective in long term, due to the suboptimal integration with the host tissue and limited bioactivity of implantable biomaterials. The immobilization of biomolecules at the surface of biomedical devices has attracted increasing interest, allowing for their local bioavailability avoiding systemic side effects and longer half-life.

Envisioning the development of advanced therapies, the electrospun nanofibrous meshes (NFMs) were used as a substrate due to their fibrous structure mimic the extracellular matrix (ECM) of many tissues, allowing cell-cell and cell-biomaterial interactions. For that, the surface of polycaprolactone NFMs was activated and functionalized with amine groups allow for covalent immobilization of defined antibodies, with the capacity to selectively bind autologous biomolecules. Different biofunctional substrates with chondrogenic inductive properties were developed through the surface biofunctionalization of NFM with endogenous human fibronectin, extracellular vesicles or the combination of endogenous Transforming Growth Factor- $\beta$ 3 and Insulin-like Growth Factor-I. All these biofunctional substrates successfully induced the chondrogenic differentiation of human bone marrow-derived mesenchymal stem cells (hBM-MSCs) under basal culture conditions. Blood-derived Nerve Growth Factor bound to the surface of NFMs remains bioactive, being an effective inducer of the neurogenic differentiation of a relevant cell line. Additionally, we developed a biofunctional system able to mimic the vasculature of bone tissue, comprising Bone Morphogenetic Protein 2 and Vascular Endothelial Growth Factor in a parallel pattern design. This biofunctional system enabled a spatially defined osteogenic and angiogenic differentiation of hBM-MSCs.

The surface biofunctionalization of biomaterial substrates enables developing biofunctional systems envisioning patient-specific devices promoting skeletal and neural tissue regeneration that can maximize and extend the local efficacy and minimize the side effects of the use of biologic based therapies in patients.

**Keywords:** Antibodies Immobilization; Bone; Cartilage; Electrospun Nanofibrous Meshes; Nerve;

**Biofuncionalização da superfície de membranas fibrosas de policaprolactona para terapias avançadas de tecido esquelético e neural**

## RESUMO

A deterioração dos tecidos esquelético e neural têm um impacto significativo na qualidade de vida dos pacientes e um elevado custo socioeconómico. Os tratamentos atualmente disponíveis não são eficazes a longo termo, devido à inadequada integração com o tecido hospedeiro e à baixa bioatividade dos biomateriais implantados. A imobilização de biomoléculas constitui uma estratégia alternativa, permitindo a biodisponibilidade local das biomoléculas evitando efeitos colaterais sistêmicos.

Ambicionando desenvolver terapias avançadas, malhas fibrosas produzidas por “electrospinning” (NFMs) foram usadas como substratos poliméricos devido à sua estrutura fibrosa similar a matriz extracelular (ECM) de muitos tecidos, promovendo as interações célula-célula e célula-biomaterial. Para isso, NFMs de policaprolactona foram ativadas e funcionalizadas com grupos amina, permitindo a imobilização covalente de anticorpos pré-definidos, com capacidade de ligar seletivamente biomoléculas autólogas. Foram desenvolvidos diferentes substratos biofuncionais, com propriedades indutoras de diferenciação condrogénica, mediante ligação de fibronectina humana, vesículas extracelulares ou a combinação do fator de transformação do crescimento beta 3 com o fator de crescimento semelhante à insulina tipo I. Todos estes substratos biofuncionalizados foram capazes de induzir a diferenciação condrogénica de células estaminais mesenquimais derivadas de medula óssea humana (hBM-MSCs) sendo cultivadas em condições basais. O fator de crescimento nervoso ligado à superfície das NFMs permanece bioativo, sendo um indutor eficaz da diferenciação neurogénica de uma linha celular relevante. Numa outra abordagem, foi desenvolvido um sistema biofuncional capaz de mimetizar a vasculatura de um tecido ósseo, ligando paralelamente a proteína morfogenética óssea 2 e o fator de crescimento do endotélio vascular sobre uma mesma NFM. Este sistema biofuncional permitiu a diferenciação osteogénica e angiogénica de hBM-MSCs espacialmente definida.

Concluindo, a biofuncionalização de substratos produzidos por “electrospinning” permite o desenvolvimento de dispositivos biomédicos personalizados, capazes de promover a regeneração do tecido esquelético e neural, maximizando a eficácia local e minimizando os efeitos colaterais do uso de terapias biológicas em pacientes.

**Palavras-chave:** Cartilagem; Imobilização de Anticorpos; Malhas fibrosas produzidas por “electrospinning”; Nervo; Osso;



## TABLE OF CONTENTS

ACKNOWLEDGMENTS .....	III
STATEMENT OF INTEGRITY.....	IV
ABSTRACT.....	V
RESUMO.....	VI
TABLE OF CONTENTS .....	VII
LIST OF ABBREVIATIONS.....	XIII
LIST OF FIGURES.....	XIX
LIST OF SUPPLEMENTARY FIGURES.....	XXVIII
LIST OF TABLES .....	XXIX
SHORT <i>CURRICULUM VITAE</i> .....	XXX
LIST OF PUBLICATIONS.....	XXXI
INTRODUCTION TO THE THESIS FORMAT .....	XXXVI
SECTION 1.....	1
GENERAL INTRODUCTION.....	1
CHAPTER I- SURFACE BIOFUNCTIONALIZATION TO IMPROVE THE EFFICACY OF A BIOMATERIAL SUBSTRATE FOR USE IN REGENERATIVE MEDICINE .....	3
Abstract.....	3
I-1. Introduction.....	4
I-2. Advanced strategies in Tissue Engineering and Regenerative Medicine.....	5
I-2.1. Cell Sources .....	6
I-2.2. Requirements of a Biomaterial Scaffold .....	8
I-2.3. Bioactive Molecules .....	9
I-2.4. Sources of Bioactive Molecules.....	18
I-3. Biofunctionalization strategies .....	20
I-3.1. Non-covalent Immobilization .....	27
I-3.2. Covalent Immobilization .....	27
I-3.3. Combined Techniques .....	29

I-4.	Applications of Biofunctional Strategies .....	30
I-4.1.	Cartilage Repair .....	30
I-4.2.	Nerve Regeneration.....	31
I-4.3.	Bone Regeneration .....	32
I-5.	Final Remarks.....	33
I-6.	References .....	34
SECTION 2.....		60
EXPERIMENTAL DESIGN .....		60
CHAPTER II - MATERIALS AND METHODS.....		62
Overview.....		62
II-1.	Materials .....	63
II-1.1.	Polycaprolactone (PCL) .....	63
II-1.2.	Antibodies.....	63
II-1.3.	Bioactive Proteins .....	65
II-2.	Reagents .....	66
II-3.	Biomaterial Substrate Fabrication and (Bio)Functionalization .....	66
II-3.1.	The Electrospinning processing technique .....	67
II-3.2.	Surface Functionalization of Electrospun Nanofibers .....	69
II-3.3.	Antibodies Immobilization Strategy – Biofunctionalization.....	71
II-3.4.	Bound bioactive molecules.....	76
II-3.5.	Biological Assays.....	81
II-3.6.	<i>In vivo</i> angiogenesis evaluation .....	94
II-4.	Statistical analysis .....	96
II-5.	References .....	97
SECTION 3.....		105
STRATEGIES FOR CARTILAGE REPAIR.....		105
CHAPTER III - FIBRONECTIN BOUND TO A FIBROUS SUBSTRATE HAS CHONDROGENIC-INDUCTIVE PROPERTIES.....		107
Abstract.....		107
III-1.	Introduction.....	108
III-2.	Materials and Methods .....	109

III-2.1.	Production of activated and functionalized PCL NFMs .....	109
III-2.2.	Biofunctionalization of NFMs.....	110
III-2.3.	Biological activity.....	111
III-2.4.	Statistical analysis.....	113
III-3.	Results .....	114
III-3.1.	Biofunctionalization of nanofibrous substrates with human plasma fibronectin .....	114
III-3.2.	Biological activity of fibronectin over hBM-MSCs .....	115
III-4.	Discussion.....	121
III-5.	Conclusions.....	123
III-6.	Acknowledgements .....	124
III-7.	References .....	124
CHAPTER IV - EXTRACELLULAR VESICLES DELIVERY SYSTEMS CAPABLE OF INDUCING THE CHONDROGENIC DIFFERENTIATION.....		130
Abstract.....		130
IV-1.	Introduction.....	131
IV-2.	Materials and Methods .....	132
IV-2.1.	Isolation and expansion of hACs.....	132
IV-2.2.	Isolation and expansion of hBM-MSCs.....	132
IV-2.3.	Extracellular Vesicles .....	133
IV-2.4.	Preparation of activated and functionalized PCL NFMs .....	134
IV-2.5.	Engineered EVs delivery systems .....	134
IV-2.6.	Biological activity of EVs delivery systems into uncommitted Homotypic cells .....	135
IV-2.7.	Statistical analysis.....	138
IV-3.	Results .....	138
IV-3.1.	Development and characterization of the EVs delivery systems .....	138
IV-3.2.	EVs delivery systems elicit hBM-MSCs chondrogenic commitment .....	140
IV-4.	Discussion.....	144
IV-5.	Conclusions.....	146
IV-6.	Acknowledgments.....	147
IV-7.	References .....	147
IV-8.	Supplementary material.....	151

CHAPTER V -	CHONDROGENESIS-INDUCTIVE	NANOFIBROUS
SUBSTRATE USING BOTH BIOLOGICAL FLUIDS AND MESENCHYMAL STEM		
CELLS FROM AN ENDOGENOUS SOURCE ..... 153		
Abstract.....		153
V-1. Introduction.....		154
V-2. Materials and Methods .....		155
V-2.1. Production and Characterization.....		155
V-2.2. Biological Assay .....		158
V-2.3. Statistical analysis .....		162
V-3. Results .....		162
V-3.1. Single Immobilization.....		162
V-3.2. Mixed Immobilization.....		164
V-3.3. Biological Activity.....		167
V-4. Discussion.....		171
V-5. Conclusions.....		173
V-6. Acknowledgments.....		174
V-7. References .....		174
SECTION 4.....		179
STRATEGIES FOR NERVE REGENERATION.....		179
CHAPTER VI -	GUIDED NERVE REGENERATION	MEDIATED BY
ENDOGENOUS NGF BOUND AT THE SURFACE OF AN ELECTROSPUN FIBROUS		
MESH ..... 181		
Abstract.....		181
VI-1. Introduction.....		182
VI-2. Materials and Methods .....		183
VI-2.1. Rat blood plasma .....		183
VI-2.2. Production of amine functionalized electrospun fibrous meshes (NFM) .....		184
VI-2.3. Nerve growth factor functionalized electrospun fibrous meshes .....		184
VI-2.4. Biological <i>in vitro</i> assays .....		185
VI-2.5. Statistical analysis.....		188
VI-3. Results .....		188
VI-3.1. Physicochemical properties of the NFM functionalized with NGF .....		188



CHAPTER VIII - GENERAL CONCLUSIONS AND FUTURE PERSPECTIVES..	234
VIII-1. General conclusions .....	234
VIII-2. Future Perspectives .....	238

## LIST OF ABBREVIATIONS

### A

Abs – Absorbance

ABTS – 2,2'-azino-bis(3-ethylbenzthiazoline-6-sulphonic acid

ACI – Autologous chondrocyte implantation

ADSCs – Adipose-derived mesenchymal stem cells

Akt – Protein kinase

ALP – Alkaline phosphatase

$\alpha$ -MEM – Alpha-Minimum Essential Medium

ANOVA – Analysis of variance

ASCs – Adult stem cells

ATB – Antibiotic/Antimycotic

ATP – Adenosine triphosphate

Au – Gold

### B

Basal – Basal medium

BCA – Bicinchoninic acid assay

b-FGF – Basic fibroblast growth factor

BM – Basal medium

BMP – Bone morphogenetic protein

BMP-2 – Bone morphogenetic protein 2

BSA – Bovine serum albumin

### C

CAM – Chorioallantoic membrane

cDNA – Complementary DNA

cFN – Commercial fibronectin

cFN bound – Biofunctionalized nanofibrous substrates comprising bound fibronectin from commercial-origin

cFN soluble – Commercial fibronectin soluble

Chondro – Standard chondrogenic differentiation medium

CO<sub>2</sub> – Carbon dioxide

COL I $\alpha$ 1 – Collagen type I alpha 1

COL II – Collagen type II

COL X – Collagen type X

COMP – Cartilage oligomeric matrix protein

CM – Standard chondrogenic differentiation medium

## **D**

DAB – 3, 3 -diaminobenzidine

DAPI – 4,6-diamidino-2-phenylindole

DM – Differentiation medium of hACs

DMB – Dimethylmethylene blue

DMEM – Dulbecco's modified Eagle's medium.

DNA – Deoxyribonucleic acid

dsDNA – Double stranded DNA

## **E**

ECM – Extracellular matrix

EDC – 1-Ethyl-3-(3-dimethylaminopropyl)carbodiimide

EDS – Energy dispersive X-ray spectroscopy

eFN – Endogenous fibronectin

eFN bound – Biofunctionalized nanofibrous substrates comprising bound fibronectin from commercial-origin

ELISA – Enzyme-linked immunosorbent assay

EM – Expansion medium of hACs

EGF – Epidermal growth factor

EVs – Extracellular vesicles

EV<sup>BM</sup> – Biofunctional NFM with EVs derived from hBM-MSCs under basal medium



$EV^{CM}$  – Biofunctional NFM with EVs derived from hBM-MSCs under standard chondrogenic differentiation medium

$EV^{DM}$  – Biofunctional NFM with EVs derived from hACs under differentiation medium

$EV^{EM}$  – Biofunctional NFM with EVs derived from hACs under expansion medium

*BMP-2* – Engineered biofunctional system comprising BMP-2 in parallel pattern

*VEGF* – Engineered biofunctional system comprising VEGF in parallel pattern

*BMP-2|VEGF* – Engineered biofunctional system comprising BMP-2 and VEGF in combined parallel pattern

## **F**

FBS – Fetal bovine serum

FDA – U.S. Food and Drug Administration

FLISA – Fluorescence-linked immunosorbent assay

FN – Fibronectin

## **G**

GAPDH – Glyceraldehydes-3-phosphate-dehydrogenase

GFs – Growth factors

GPC – Gel permeation chromatography

GAG – Glycosaminoglycan

GAP-43 – Growth-associated protein 43

## **H**

hACs – Human articular chondrocytes

hASCs – Human adipose stem cells

hBM-MSCs – Human bone marrow-derived mesenchymal stem cells

HMD – Hexamethylenediamine

HS – Horse serum

## **I**

Ig – Immunoglobulin

IGF – Insulin-like growth factor

ITS – Insulin-transferrin-selenium

## **M**

MACI – Matrix-induced autologous chondrocyte implantation

MAP-2 – Microtubule-associated protein 2

MAPK – Mitogen-activated protein kinase

MES – 2-(N-morpholino)-ethanesulfonic acid

mRNA – Messenger RNA

MSC – Mesenchymal stem cells

MTS–3-(4,5-dimethylthiazol-2-yl)-5-(3-carboxymethoxyphenyl)-2-(4-sulfophenyl)-2H-tetrazolium

## **N**

NaCl – Sodium chloride

NADPH – Nicotinamide adenine dinucleotide phosphate

NADH – Nicotinamide adenine dinucleotide

NaOH – Sodium hydroxide

NF-160 – Neurofilament 160

NF-200 – Neurofilament 200

NFM – Nanofibrous mesh

NFM- – NFM in basal medium without recombinant NGF

NFM+ – NFM in basal medium with 100 ng/mL recombinant NGF

NFM-NGF – NFM functionalized with endogenous NGF

NFM-pNGF – NFM functionalized with plasma-derived NGF in basal medium

NFM-rNGF – NFM functionalized with recombinant NGF in basal medium

NGF – Nerve growth factor

NH<sub>2</sub> – Amine group

NHS – N-hydroxysuccinimide

## **O**

Osteo – Standard osteogenic differentiation medium

## **P**

PATH – Doctoral Program on Advanced Therapies for Health

PBS – Phosphate-buffered saline

PC12 – Rat pheochromocytoma cells

PCL – Polycaprolactone

PCR – Polymerase chain reaction

pDNA – Plasmid Deoxyribonucleic acid

PDGF – Platelet derived growth factor

PECAM – Platelet and endothelial cell adhesion molecule

PEM – Polyelectrolyte multilayer

PKC – Protein kinase C

PL – Platelet lysate

PLGA-GCH – Poly-(lactic-co-glycolic acid)-gelatin/chondroitinsulfate/hyaluronic acid

PLGA – Poly [(lactic acid) -co- (glycolic acid)]

pNGF – plasma-derived nerve growth factor

PPP – Platelet-poor plasma

PRP – Platelet-rich plasma

## **R**

RGD – Arginine-glycine-aspartic acid

RNA – Ribonucleic acid

rNGF – Recombinant nerve growth factor

RPM – Rotations per minute

RT – Room temperature

RT-PCR – Real-time polymerase chain reaction

Runx 2 – Runt-related transcription factor 2

## **S**

SD – Standard deviation

SEM – Scanning Electron Microscopy

SOX 9 – Sry-type high mobility group box 9

SPSS – Statistical Package for the Social Sciences

sulfo-NHS – Sulfo-N-hydroxysuccinimide

Syn1 – Synapsin-1

## **T**

2D – Two-dimensional

3D – Three-dimensional

TERM – Tissue Engineering and Regenerative Medicine

TGF- $\beta$  – Transforming growth factor Beta

TMB – Tetramethylbenzidine

TrkA – Tropomyosin receptor kinase A

## **U**

UV – Ultraviolet light

UV-O – Ultraviolet-ozone

## **V**

VEGF – Vascular endothelial growth factor

VEGF A – Vascular endothelial growth factor A

VEGFR2 – Vascular endothelial growth factor receptor 2

vWF – Von willebrand factor

## LIST OF FIGURES

Figure I-1 The extracellular microenvironment (a) and cell signaling by soluble factors (b) [122, 125].....	10
Figure I-2 Fibronectin primary structure and its binding domains. ....	11
Figure I-3 Schematic overview of the wound healing process and the biomolecules involved [174].....	13
Figure I-4 Schematic diagram showing different biofunctionalization techniques. (A) Strategies for non-covalent immobilization of the bioactive molecules, leveraging the natural affinity of biomolecules to these biomaterials. (B) Strategies to covalently attach bioactive molecules to biomaterials using chemical or enzymatic tools. (C) Combined strategies to employ endogenous ECM as the delivery biomatrix by engineering fusions of bioactive molecules with ECM binding domains.....	21
Figure II-1 Chemical structure of polycaprolactone. ....	63
Figure II-2 Structure of an Antibody.....	64
Figure II-3 The common setup and working principle of electrospinning [26]. ....	68
Figure II-4 Scanning electron microscopy analysis of an electrospun polycaprolactone nanofibrous mesh.....	69
Figure II-5 Surface activation and functionalization of the electrospun PCL nanofibers.....	70
Figure II-6 EDC reacts preferentially with the carboxyl groups forming O-acylisourea, an unstable reactive ester. In combination with NHS forms a semi-stable amine-reactive ester. This NHS ester can readily react with the available amine groups at the surface of electrospun nanofibers. ....	71
Figure II-7 Antibody and antigen immobilization strategy implemented to activated and functionalized NFMs. ....	72
Figure II-8 Schematic representation of the mixed antibodies immobilized at the surface of activated and functionalized NFMs.....	74
Figure II-9 Schematic representation of the compartments in the patterning device that allows the immobilization of antibodies in a parallel design of a single NFM. ....	75
Figure II-10 Separation of blood components by a whole blood centrifugation [49].....	77

Figure III-1 Top: Maximum immobilization capacity of fibronectin antibody at the surface of activated and functionalized NFM (a). Data were analyzed by the one-way ANOVA test, followed by the Tukey's HSD test ( $p < 0.001$ ): a denotes significant differences compared to concentration 0  $\mu\text{g/mL}$ ; b denotes significant differences compared to concentration 2  $\mu\text{g/mL}$ ; c denotes significant differences compared to concentration 4  $\mu\text{g/mL}$  and d denotes significant differences compared to concentration 6  $\mu\text{g/mL}$ ; Spatial distribution of anti-fibronectin (b) immobilized at the surface of activated and functionalized nanofibrous substrates at 8  $\mu\text{g/mL}$ . The negative control sample (c) was not incubated with the primary antibody. Bottom: Quantification of fibronectin (d) present in 3 independent human blood plasma samples and in a pool of six independent donors. The endogenous fibronectin binding capacity of the biofunctionalized nanofibrous substrate (e)..... 114

Figure III-2 Biochemical performance (i.e. cell viability (a) and proliferation (b), total protein synthesis(c)) and cell morphology (d) of the hBM-MSCs cultured over biofunctionalized nanofibrous substrates comprising bound fibronectin from different sources (i.e. commercial [*cFN bound*] and endogenous [*eFN bound*]), under basal culture conditions. Non-biofunctionalized nanofibrous substrates in basal medium (*Basal*), basal medium supplemented with commercial fibronectin (*cFN soluble*) and standard chondrogenic differentiation medium (*Chondro*) were used as controls. Data were analyzed by the Kruskal-Wallis test, followed by the Tukey's HSD test ( $p < 0.001$ ): a denotes significant differences compared to *Basal*; b denotes significant differences compared to *Chondro*; ..... 116

Figure III-3 Analysis of the sulfated glycosaminoglycans content (a) and staining by Alcian blue (b) of the hBM-MSCs cultured over biofunctionalized nanofibrous substrates comprising bound fibronectin from different sources (i.e. commercial [*cFN bound*] and endogenous [*eFN bound*]), under basal culture conditions. Non-biofunctionalized nanofibrous substrates in basal medium (*Basal*), basal medium supplemented with commercial fibronectin (*cFN soluble*) and standard chondrogenic differentiation medium (*Chondro*) were used as controls. Data were analyzed by the Kruskal-Wallis test, followed by the Tukey's HSD test ( $p < 0.001$ ): a denotes significant differences compared to *Basal*; b denotes significant differences compared to *Chondro*; c denotes significant differences compared to *cFN soluble*; ..... 117

Figure III-4 Top: Relative expression of chondrogenic markers (i.e. *Sox 9* (a), *Collagen type II* (b), *COMP* (c) and *Aggrecan* (d)) by hBM-MSCs cultured on biofunctionalized

nanofibrous substrates comprising bound fibronectin from different sources (i.e. commercial [*cFN bound*] and endogenous [*eFN bound*]), under basal culture conditions. Non-biofunctionalized nanofibrous substrates in basal medium (*Basal*), basal medium supplemented with commercial fibronectin (*cFN soluble*) and standard chondrogenic differentiation medium (*Chondro*) and standard osteogenic differentiation medium (*Osteo*) were used as controls. The expression was normalized against the GAPDH gene and the quantification was performed according to the Livak method. Data were analyzed by the Kruskal-Wallis test, followed by the Tukey's HSD test ( $p < 0.001$ ): *a* denotes significant differences compared to *Osteo*; *b* denotes significant differences compared to *Chondro*; *c* denotes significant differences compared to *cFN soluble*; Bottom: Immunolocalization of collagen type II (e) of the hBM-MSCs cultured over biofunctionalized or non-biofunctionalized nanofibrous substrates..... 119

Figure III-5 Top: Relative expression of hypertrophic markers (i.e. *Collagen type X* (a), *Collagen type I $\alpha$*  (b), *Runx 2* (c) and *Alkaline Phosphatase* (d)) by hBM-MSCs cultured on biofunctionalized nanofibrous substrates comprising bound fibronectin from different sources (i.e. commercial [*cFN bound*] and endogenous [*eFN bound*]), under basal culture conditions. Non-biofunctionalized nanofibrous substrates in basal medium (*Basal*), basal medium supplemented with commercial fibronectin (*cFN soluble*), standard chondrogenic differentiation medium (*Chondro*) and standard osteogenic differentiation medium (*Osteo*) were used as controls. The expression was normalized against the GAPDH gene and the quantification was performed according to the Livak method. Data were analyzed by the Kruskal-Wallis test, followed by the Tukey's HSD test ( $p < 0.001$ ): *a* denotes significant differences compared to *Osteo*; *b* denotes significant differences compared to *Chondro*; *c* denotes significant differences compared to *cFN soluble*; Bottom: Immunolocalization of collagen type *I $\alpha$*  (e) of the hBM-MSCs cultured over biofunctionalized or non-biofunctionalized nanofibrous substrates..... 120

Figure IV-1 Maximum immobilization capacity of CD63 antibody at the surface of activated and functionalized NFM (a). Data were analyzed by the one-way ANOVA test, followed by the Tukey's HSD test ( $*p < 0.01$ ;  $**p < 0.001$ ;  $***p < 0.0001$ ): *a* denotes significant differences compared to concentration 0  $\mu\text{g mL}^{-1}$ ; *b* denotes significant differences compared to concentration 1  $\mu\text{g mL}^{-1}$  and *c* denotes significant differences compared to concentration 2  $\mu\text{g mL}^{-1}$ . Spatial distribution of anti-CD63 immobilized at the surface of activated and functionalized nanofibrous substrates at 4  $\mu\text{g mL}^{-1}$  (b). The negative control

sample was not incubated with the primary antibody (c). Quantification of extracellular vesicles derived from hACs and hBM-MSCs, and bound to the biofunctional nanofibrous system (d)..... 139

Figure IV-2 Distribution of EVs bound at the surface of the biofunctional nanofibrous system (a); EDS spectrum of the EVs-delivery system surface (b); Fluorescence micrographs of the EVs markers CD63 (c), CD81 (d) and CD9 (e). ..... 140

Figure IV-3 Biochemical performance (i.e. cell viability (a), proliferation (DNA content) (b), total protein synthesis(c)) and sulfated glycosaminoglycans (GAGs) content (d) of hBM-MSCs cultured on biofunctional nanofibrous systems comprising EVs derived from different sources (i.e. hACs under expansion medium [ $EV^{EM}$ ], hACs under differentiation medium [ $EV^{DM}$ ], hBM-MSCs under basal medium [ $EV^{DM}$ ] and hBM-MSCs under chondrogenic medium [ $EV^{CM}$ ]), under basal culture conditions. hACs cultured on non-biofunctionalized nanofibrous substrates under expansion medium ( $EM$ ) or differentiation medium ( $DM$ ), and hBM-MSCs cultured on non-biofunctionalized nanofibrous substrates under basal medium ( $BM$ ) or chondrogenic medium ( $CM$ ) were used as controls. Data were analyzed by the Kruskal-Wallis test, followed by the Tukey's HSD test ( $*p < 0.01$ ;  $**p < 0.001$ ;  $***p < 0.0001$ ):  $a$  denotes significant differences compared to  $EM$ ;  $b$  denotes significant differences compared to  $DM$ ;  $c$  denotes significant differences compared to  $BM$ ;  $d$  denotes significant differences compared to  $CM$ ;  $e$  denotes significant differences compared to  $EV^{EM}$ ;  $f$  denotes significant differences compared to  $EV^{DM}$ ;  $g$  denotes significant differences compared to  $EV^{BM}$ . ..... 141

Figure IV-4 Relative expression of chondrogenic (i.e. *Sox 9* (a), *COMP* (b), *Aggrecan* (c) and *Collagen type II* (d)) and hypertrophic transcripts (i.e. *Collagen type I $\alpha$*  (e), *Collagen type X* (f)) by hBM-MSCs cultured on biofunctional nanofibrous systems comprising EVs derived from different sources (i.e. hACs under expansion medium [ $EV^{EM}$ ], hACs under differentiation medium [ $EV^{DM}$ ], hBM-MSCs under basal medium [ $EV^{DM}$ ] and hBM-MSCs under chondrogenic medium [ $EV^{CM}$ ]), under basal culture conditions. hACs cultured on non-biofunctionalized nanofibrous substrates under expansion medium ( $EM$ ) or differentiation medium ( $DM$ ), and hBM-MSCs cultured on non-biofunctionalized nanofibrous substrates under basal medium ( $BM$ ) or chondrogenic medium ( $CM$ ) were used as controls. Data were analyzed by the Kruskal-Wallis test, followed by the Tukey's HSD test ( $*p < 0.01$ ;  $**p < 0.001$ ;  $***p < 0.0001$ ):  $a$  denotes significant differences compared to  $EM$ ;  $b$  denotes significant differences compared to  $DM$ ;  $c$  denotes significant differences



compared to *BM*; *d* denotes significant differences compared to *CM*; *e* denotes significant differences compared to *EV<sup>EM</sup>*; *f* denotes significant differences compared to *EV<sup>DM</sup>*; *g* denotes significant differences compared to *EV<sup>BM</sup>*..... 143

Figure IV-5 Morphology of hBM-MSCs cultured during 28 days on biofunctional nanofibrous systems comprising EVs derived from different sources (i.e. hACs under expansion medium [*EV<sup>EM</sup>*], hACs under differentiation medium [*EV<sup>DM</sup>*], hBM-MSCs under basal medium [*EV<sup>DM</sup>*] and hBM-MSCs under chondrogenic medium [*EV<sup>CM</sup>*]), under basal conditions, analyzed by scanning electron microscopy (SEM) (a); stained with alcian blue for sulfated glycosaminoglycans (b); and immunolocalized collagen type II (c) and type I $\alpha$  (d)..... 144

Figure V-1 Top: Maximum immobilization capacity of a single antibody at the surface of activated and functionalized NFM: immobilization of anti-TGF- $\beta$ 3 (a) and immobilization of anti-IGF-I (b). Data were analyzed by the one-way ANOVA test, followed by the Tukey's HSD test ( $p < 0.006$ ): a denotes significant differences compared to concentration  $0 \mu\text{g mL}^{-1}$ ; b denotes significant differences compared to concentration  $2 \mu\text{g mL}^{-1}$ . Bottom: Spatial distribution of anti-TGF- $\beta$ 3 (d) or anti-IGF-I (e) immobilized at the surface of activated and functionalized nanofibrous substrates at  $4 \mu\text{g mL}^{-1}$ . The negative control sample (c) was not incubated with the primary antibody. .... 163

Figure V-2 Capability of the biofunctionalized nanofibrous substrate to bind different concentrations of recombinant proteins from TGF- $\beta$ 3 (a) and IGF-I (b). Data were analyzed by the Kruskal-Wallis test, followed by the Tukey's HSD test ( $p < 0.01$ ): in the FLISA, a denotes significant differences compared to concentration  $0 \mu\text{g mL}^{-1}$ ; b denotes significant differences compared to concentration  $1 \mu\text{g mL}^{-1}$ ; c denotes significant differences compared to concentration  $2 \mu\text{g mL}^{-1}$ ; in the ELISA, A denotes significant differences compared to concentration  $0 \mu\text{g mL}^{-1}$ ; B denotes significant differences compared to concentration  $1 \mu\text{g mL}^{-1}$ ..... 164

Figure V-3 Top: Single or mixed immobilization capacity of anti-TGF- $\beta$ 3 (a) and anti-IGF-I (b) at the surface of activated and functionalized electrospun nanofibers. Data were analyzed by the Kruskal-Wallis test, followed by the Tukey's HSD test ( $p < 0.01$ ): a denotes significant differences compared to negative control. Bottom: Spatial distribution of the simultaneously immobilization of TGF- $\beta$ 3 and IGF-I antibodies over the same substrate, in a mixed fashion, at the 1:10 proportion: anti-TGF- $\beta$ 3 (d); anti-IGF-I (e); and

merged view (f). Activated and functionalized nanofibrous substrates without primary antibodies immobilization (c). .....	165
Figure V-4 Single or mixed immobilization capacity of recombinant TGF- $\beta$ 3 (a) and IGF-I (b) at the surface of activated and functionalized electrospun nanofibers, assessed by the FLISA or the ELISA (c). Data were analyzed by the Kruskal-Wallis test, followed by the Tukey's HSD test ( $p < 0.01$ ): a denotes significant differences compared to negative control. ....	166
Figure V-5 Biochemical performance (i.e. metabolic activity (a) and proliferation (b), total protein (c) and GAG/DNA ratio (d) synthesis) of the hBM-MSCs cultured on biofunctionalized biomaterial system. Data were analyzed by the Kruskal-Wallis test, followed by the Tukey's HSD test ( $p < 0.01$ ). No significant differences were observed between culturing conditions. ....	168
Figure V-6 Relative expression of chondrogenic and hypertrophic markers by hBM-MSCs cultured on biofunctionalized biomaterial system. The expression was normalized against the <i>GAPDH</i> gene and the quantification was performed according to the Livak method. Data were analyzed by the Kruskal-Wallis test, followed by the Tukey's HSD test ( $p < 0.01$ ): a denotes significant differences compared to the positive condition (Chondro medium). ....	169
Figure V-7 Morphological analysis of the hBM-MSCs cultured for 28 days by scanning electron microscopy (SEM); staining of sulfated glycosaminoglycans by Alcian blue; immunolocalization of collagen type II (brown staining). ....	170
Figure VI-1 Maximum immobilization capacity of anti-NGF- $\beta$ antibody at the surface of activated and functionalized NFM (a). Data were analyzed by the one-way ANOVA test, followed by the Tukey's HSD test ( $p < 0.01$ ): a denotes significant differences compared to concentration 0 $\mu\text{g/mL}$ ; b denotes significant differences compared to concentration 1 $\mu\text{g/mL}$ ; c denotes significant differences compared to concentration 2 $\mu\text{g/mL}$ ; d denotes significant differences compared to concentration 4 $\mu\text{g/mL}$ ; e denotes significant differences compared to concentration 6 $\mu\text{g/mL}$ and f denotes significant differences compared to concentration 8 $\mu\text{g/mL}$ . Spatial distribution of anti-NGF immobilized at the NFM at 10 $\mu\text{g/mL}$ (b). The negative control sample was not incubated with the primary antibody (c). ....	189

Figure VI-2 Top: Biochemical performance (i.e. metabolic activity (a), proliferation (b) and protein synthesis (c)) of the PC12 cells cultured on NFM functionalized with NGF $\beta$  from different sources, under basal medium. NFMs cultured with PC12 cells under basal (NFM-) or neuronal differentiation media (NFM+) were used as controls. Data were analysed by the Kruskal-Wallis test, followed by the Tukey's HSD test ( $p < 0.01$ ): a denotes significant differences compared to NFM- and b denotes significant differences compared to NFM+; \* $p < 0.01$ ; \*\* $p < 0.001$ ; \*\*\* $p < 0.0001$ ; Bottom: Morphological analysis of the PC12 cells on different culture condition, along culturing time, by scanning electron microscopy (SEM) (d)..... 191

Figure VI-3 Top: Percentage of neurite-bearing PC12 cells on different culture condition along culturing time (a). Data were analysed by the Kruskal-Wallis test, followed by the Tukey's HSD test ( $p < 0.01$ ): a denotes significant differences compared to NFM-; b denotes significant differences compared to NFM+ and c denotes significant differences compared to NFM-rNGF; \* $p < 0.01$ ; \*\* $p < 0.001$ ; \*\*\* $p < 0.0001$ ; Bottom: Immunocytochemistry with beta-III Tubulin (brown) of PC12 cells on different culture condition along culturing time (b)..... 192

Figure VI-4 Relative expression of GAP-43 (a), MAP2 (b), NF160 (c), NF200 (d) and Syn1 (e) genes by PC12 cells cultured on different culture condition, along culturing time. The expression was normalized against the GAPDH gene and the quantification was performed according to the Livak method, considering the negative control (NFM-) as calibrator. Data were analysed by the Kruskal-Wallis test, followed by the Tukey's HSD test ( $p < 0.01$ ): a denotes significant differences compared to NFM-; b denotes significant differences compared to NFM+; and c denotes significant differences compared to NFM-rNGF; \* $p < 0.01$ ; \*\* $p < 0.001$ ; \*\*\* $p < 0.0001$ ;..... 193

Figure VI-5 Immunoexpression of GAP-43, NF-200 and Syn1 proteins by the PC12 cells cultured on the different condition, at the 7<sup>th</sup> day. .... 194

Figure VII-1 Schematic representation of the compartments in the patterning device that allows the immobilization of antibodies in a parallel pattern design of a single NFM. .... 208

Figure VII-2 Maximum immobilization capacity of a single antibody at the surface of activated and functionalized NFM: immobilization of anti-BMP-2 (a) and immobilization of anti-VEGF (b). Data were analyzed by the one-way ANOVA test, followed by the Tukey's HSD test ( $p < 0.01$ ): a denotes significant differences compared to concentration 0  $\mu\text{g mL}^{-1}$

<p><sup>1</sup>; <i>b</i> denotes significant differences compared to concentration 2 <math>\mu\text{g mL}^{-1}</math> and <i>c</i> denotes significant differences compared to concentration 4 <math>\mu\text{g mL}^{-1}</math>. .....</p>	214
<p>Figure VII-3 Spatial distribution of immobilized primary antibodies at the surface of activated and functionalized nanofibrous substrates, in a parallel pattern design: 4 <math>\mu\text{g mL}^{-1}</math> anti-BMP-2 (a); 4 <math>\mu\text{g mL}^{-1}</math> VEGF (b); merged view (c) and activated and functionalized nanofibrous substrates without primary antibodies immobilization (d). .....</p>	215
<p>Figure VII-4 Biochemical performance (i.e. metabolic activity (a) and proliferation (b), total protein synthesis (c) and ALP activity (d) of the hBM-MSCs cultured on nanofibrous substrates with endogenous BMP-2 and/or VEGF parallel bound, under basal medium. Activated NFMs cultured with hBM-MSCs under standard Osteogenic or Angiogenic differentiation media were used as positive controls, while NFM/hBM-MSCs constructs cultured under Basal medium was used as negative control. Data were analysed by the Kruskal-Wallis test, followed by the Tukey's HSD test (<math>p &lt; 0.01</math>): <i>a</i> denotes significant differences compared to <i>Basal medium</i>; <i>b</i> denotes significant differences compared to <i>Osteogenic medium</i>; <i>c</i> denotes significant differences compared to <i>Angiogenic medium</i>; <i>d</i> denotes significant differences compared to <i>BMP-2</i>; <i>e</i> denotes significant differences compared to <i>VEGF</i>; .....</p>	217
<p>Figure VII-5 Relative expression of osteogenic markers by hBM-MSCs cultured on engineered biofunctional systems. The expression was normalized against the GAPDH gene and the quantification was performed according to the Livak method. Data were analysed by the Kruskal-Wallis test, followed by the Tukey's HSD test (<math>p &lt; 0.01</math>): <i>a</i> denotes significant differences compared to Basal medium; <i>b</i> denotes significant differences compared to <i>Osteogenic medium</i>; <i>c</i> denotes significant differences compared to <i>Angiogenic medium</i>; <i>d</i> denotes significant differences compared to <i>BMP-2</i>; <i>e</i> denotes significant differences compared to <i>VEGF</i>; .....</p>	218
<p>Figure VII-6 Relative expression of angiogenic markers by hBM-MSCs cultured on engineered biofunctional systems. The expression was normalized against the GAPDH gene and the quantification was performed according to the Livak method. Data were analysed by the Kruskal-Wallis test, followed by the Tukey's HSD test (<math>p &lt; 0.01</math>): <i>a</i> denotes significant differences compared to <i>Basal medium</i>; <i>b</i> denotes significant differences compared to <i>Osteogenic medium</i>; <i>c</i> denotes significant differences compared to <i>Angiogenic medium</i>; <i>d</i></p>	

denotes significant differences compared to <i>BMP-2</i> ; e denotes significant differences compared to <i>VEGF</i> ;	219
Figure VII-7 Immunoexpression of osteogenic (Collagen I $\alpha$ ; Osteocalcin; Osteopontin) and angiogenic (CD31; vWF) markers in engineered biofunctional systems, after 21 days of culture (10X magnifications).	220
Figure VII-8 Stereomicroscope photographs of <i>ex ovo</i> NFM substrates after incubation on the chorioallantoic membrane of the chick embryo (a). Macroscopic quantification of blood vessels converging towards implanted structures (b). Vascular Length Density (i.e. ratio of skeletonized vasculature area to total area) (c), and Vascular Density (i.e. ratio of vasculature area to total selection area) (d). Data were analysed by the Kruskal-Wallis test, followed by the Tukey's HSD test (* $p < 0.01$ ; ** $p < 0.001$ ; *** $p < 0.0001$ ): a denotes significant differences compared to <i>CTR<sub>CAM</sub></i> ; b denotes significant differences compared to <i>NFM</i> ; c denotes significant differences compared to <i>BMP-2</i> ; d denotes significant differences compared to <i>VEGF</i> ;	221

## LIST OF SUPPLEMENTARY FIGURES

Supplementary Figure IV-1 Biochemical performance (i.e. proliferation (DNA content) (a), total protein synthesis(b)), sulfated glycosaminoglycans (GAGs) content (c) and relative expression of chondrogenic (i.e. *Sox 9* (d), *COMP* (e), *Aggrecan* (f) and *Collagen type II* (g)) and hypertrophic transcripts (i.e. *Collagen type I $\alpha$*  (h), *Collagen type X* (i)) by hACs cultured on non-biofunctionalized nanofibrous substrates under expansion medium (*EM*) or differentiation medium (*DM*), and hBM-MSCs cultured on non-biofunctionalized nanofibrous substrates under basal medium (*BM*) or chondrogenic medium (*CM*). Data were analyzed by the Kruskal-Wallis test, followed by the Tukey's HSD test ( $*p<0.01$ ;  $**p<0.001$ ): *a* denotes significant differences compared to *EM*; *b* denotes significant differences compared to *DM*; *c* denotes significant differences compared to *BM*..... 151

## LIST OF TABLES

Table I-1 Most relevant growth factors in the TERM field.....	14
Table I-2 Biofunctionalization strategies applied in TERM approaches. ....	22
Table II-1 Primer sequences used for RT-PCR procedures <sup>a)</sup> . ....	92
Table III-1 Primer sequences used for RT-PCR procedures <sup>a)</sup> .....	113
Table IV-1 Experimental conditions used in the Cell Biology assays.....	136
Table IV-2 Primer sequences used for RT-PCR procedures <sup>a)</sup> . ....	137
Table V-1 Primer sequences used for RT-PCR procedures <sup>a)</sup> . ....	161
Table V-2 Quantification of TGF- $\beta$ 3 and IGF-I present in 3 independent human PL samples and in a PL pool. The GFs binding capacity of the biofunctionalized nanofibrous substrate. .....	166
Table VI-1 Experimental conditions used in the Cell Biology assays.....	185
Table VI-2 Primer sequences used for RT-PCR procedures <sup>a)</sup> . ....	187
Table VI-3 Quantification of NGF recombinant or derived from rat blood plasma) and the binding capacity of the NFM-NGF system.....	189
Table VII-1 The engineered biofunctional systems. ....	210
Table VII-2 Primer sequences used for RT-PCR procedures <sup>a)</sup> .....	211
Table VII-3 Quantification of the growth factors of interest (i.e. BMP-2, VEGF) derived from human PL samples and the binding capacity of the engineered biofunctional system. .	216

## ***SHORT CURRICULUM VITAE***

Marta Alexandra Rodrigues Casanova was born on the 2<sup>th</sup> of July 1990, in Vila Nova de Famalicão, Portugal. She received her Bachelor degree in (2011) in Biomedical Sciences, at the Department of Biomedical Sciences and Medicine, University of Algarve, Faro, Portugal with a final grade of 14 /20. She proceeds with a Master degree (2015) in Molecular Genetics at School of Sciences, University of Minho, Braga, Portugal that she finished with a final grade of 18/20. In May 2015, she started her PhD with an awarded Foundation for Science and Technology (FCT) PhD scholarship (PD/BD/113797/2015) at the 3B's Research Group (Biomaterials, Biodegradables and Biomimetics), of the University of Minho, Headquarters of the European Institute of Excellence on Tissue Engineering and Regenerative Medicine at Avepark, Caldas das Taipas, Guimarães, Portugal, under the supervision of Prof. Dr. Nuno M. Neves and Dr. Albino Martins.

As a result of her research work, she is the author or co-author of 7 papers in international journals (1 published, 6 submitted), 1 book chapter, 1 abstract published in international conference proceedings and 4 published online, 3 oral presentations, and 13 poster presentations.



## LIST OF PUBLICATIONS

The work performed during the PhD period resulted in the publications listed below.

### *Papers in international scientific journals with referees*

1. **Casanova M. R.**, Reis R. L., Martins A. and Neves N. M., “Surface Biofunctionalization to Improve the Efficacy of Biomaterial Substrates to be used in Regenerative Medicine”, (Submitted), 2019.
2. **Casanova M. R.**, Reis R. L., Martins A. and Neves N. M., “Fibronectin Bound to a Fibrous Substrate has Chondrogenic-inductive Properties”, (Submitted), 2019.
3. **Casanova M. R.**, Reis R. L., Martins A. and Neves N. M., “Extracellular Vesicles Delivery Systems Capable of Inducing the Chondrogenic Differentiation”, (Submitted), 2019.
4. **Casanova M. R.**, Reis R. L., Martins A. and Neves N. M., “Guided Nerve Regeneration Mediated by Endogenous NGF bound at the surface of an Electrospun Fibrous Mesh”, (Submitted), 2019.
5. **Casanova M. R.**, Oliveira C., Fernandes E. M., Reis R. L., Silva T. H., Martins A. and Neves N. M., “Spatial Immobilization of Endogenous Growth Factors to Control Vascularization in Bone Tissue Engineering”, (Submitted), 2019.
6. **Casanova M. R.**, Alves da Silva M., Costa-Pinto A. R., Reis R. L., Martins A., Neves N. M., “Chondrogenesis-inductive nanofibrous substrate using both biological fluids and mesenchymal stem cells from an autologous source”, *Materials Science and Engineering: C*, vol. 98, issue 2019, pp. 1169-1178, doi: 10.1016/j.msec.2019.01.069., 2019.
7. Alves da Silva M.\*, **Casanova M. R.\***, Costa-Pinto A. R., Reis R. L., Neves N. M., Nogueira-Silva C., “Human Amniotic Membrane Stem Cells Isolation and Characterization”, (Submitted), 2019. \*The authors contributed equally.

### *Conference abstracts published in international scientific journals*

1. **Casanova M. R.**, Fernandes E. M., Reis R. L., Martins A., and Neves N. M., "Parallel binding of autologous BMP-2 and VEGF envisioning a vascularized bone tissue engineering approach", Abstracts from the 45<sup>th</sup> ESAO Congress, 12–15

September 2018, Madrid, Spain. *The International Journal of Artificial Organs*, vol. 41(9), O169, pg. 561-562, doi: doi.org/10.1177/0391398818785526, 2018.

#### ***Conference abstracts published online***

1. **Casanova M. R.**, Reis R. L., Martins A., and Neves N. M., "Chondrogenic Inductive Nanofibrous Mesh Biofunctionalized with Human Fibronectin", Transactions of the 42<sup>nd</sup> Annual Meeting, Society For Biomaterials 2019 Annual Meeting, Volume XL, pg. 797, (<https://abstracts.biomaterials.org/data/papers/2019/abstracts/961.pdf>), 2019.
2. **Casanova M. R.**, Fernandes E. M., Reis R. L., Martins A., and Neves N. M., "Vascularized bone tissue engineered system comprising autologous growth differentiation factors and mesenchymal stem cells", 5<sup>th</sup> TERMIS World Congress, a92434, 03-P185, ([https://www2.convention.co.jp/termis-wc2018/pdf/s\\_poster3.pdf](https://www2.convention.co.jp/termis-wc2018/pdf/s_poster3.pdf)), 2018.
3. **Casanova M. R.**, Alves da Silva M. L., Costa-Pinto A. R., Reis R. L., Martins A., and Neves N. M., "Chondrogenesis-inductive nanofibrous substrate biofunctionalized with autologous growth factors from platelet lysates for stem cell based therapies ", eCM Meeting Abstracts 2017, Collection 2; TERMIS EU P830, ([https://ecmconferences.org/abstracts/2017/Collection2/pdf/collection2\\_poster.pdf](https://ecmconferences.org/abstracts/2017/Collection2/pdf/collection2_poster.pdf)), 2017.
4. **Casanova M. R.**, Alves da Silva M. L., Costa-Pinto A. R., Reis R. L., Martins A., and Neves N. M., "Chondrogenic-Inductive Nanofibrous Substrates Biofunctionalized with Immobilized Autologous TGF- $\beta$ 3 and IGF-I", Transactions of the Society For Biomaterials 2017 Annual Meeting, Volume XXXVIII, pg. 510, (<https://abstracts.biomaterials.org/data/papers/2017/abstracts/0700.pdf>), 2017.

#### ***Book Chapter***

1. **Casanova M. R.**, Reis R. L., Martins A. and Neves N. M., "The Use of Electrospinning Technique on Osteochondral Tissue Engineering", Osteochondral Tissue Engineering - Nanotechnology, Scaffolding-Related Developments and Translation, Eds. Oliveira J. M., Pina S., Roman J. S., and Reis R. L., Springer International Publishing AG, vol. 1058, pp. 247 - 263, doi: doi.org/10.1007/978-3-319-76711-6\_11, 2018.

### ***Oral communications***

1. **Casanova M. R.**, Fernandes E. M., Reis R. L., Martins A., and Neves N. M., "Parallel binding of autologous BMP-2 and VEGF envisioning a vascularized bone tissue engineering approach", XLV ESAO Congress, September 2018, Madrid, Spain.
2. **Casanova M. R.**, Reis R. L., Martins A., and Neves N. M., "Nanofibrous substrate functionalized with fibronectin is able to conduct the chondrogenesis of mesenchymal stem cells", CHEM2NATURE and GENE2SKIN Summer School, June, 2018, Porto, Portugal.
3. **Casanova M. R.**, Alves da Silva M. L., Costa-Pinto A. R., Reis R. L., Martins A., and Neves N. M., "Chondrogenesis-inductive nanofibrous substrate comprising autologous TGF- $\beta$ 3 and IGF-I from platelet lysates", CHEM2NATURE First School, November, 2016, Guimarães, Portugal.

### ***Posters presentations***

1. **Casanova M. R.**, Reis R. L., Martins A., and Neves N. M., "Autologous NGF Immobilized at the Surface of a Nanofibrous Mesh for Guided Nerve Regeneration", 1<sup>st</sup> Discoveries Forum on Regenerative and Precision Medicine, September, 2019, Porto, Portugal.
2. **Casanova M. R.**, Reis R. L., Martins A., and Neves N. M., "Autologous NGF Immobilized on a Nanofibrous Substrate as an Approach to Guided Nerve Regeneration", Achilles Conference and FoReCaST Workshop, July, 2019, Porto, Portugal.
3. **Casanova M. R.**, Reis R. L., Martins A., and Neves N. M., "Chondrogenic Inductive Nanofibrous Mesh Biofunctionalized with Human Fibronectin", Society for Biomaterials Annual Meeting and Exposition 2019, April, 2019, Seattle, United States.
4. **Casanova M. R.**, Reis R. L., Martins A., and Neves N. M., "Adjacent immobilization of autologous BMP-2 and VEGF envisioning a vascularized bone tissue engineering approach", European Society for Biomaterials, September, 2018, Maastricht, Netherlands.
5. **Casanova M. R.**, Reis R. L., Martins A., and Neves N. M., "Endogenous fibronectin bound to nanofibrous substrate is able to conduct the chondrogenesis of

mesenchymal stem cells", GENE2SKIN and CHEM2NATURE FINAL CONFERENCE, October, 2018, Guimarães, Portugal.

6. **Casanova M. R.**, Fernandes E. M., Reis R. L., Martins A., and Neves N. M., "Vascularized bone tissue engineered system comprising autologous growth differentiation factors and mesenchymal stem cells", 5<sup>th</sup> TERMIS World Congress, September, 2018, Kyoto, Japan.
7. **Casanova M. R.**, Reis R. L., Martins A., and Neves N. M., "Personalized advanced therapies for skeletal tissue regeneration", Ciência 2018 - Encontro com a Ciência e Tecnologia em Portugal, July, 2018, Lisbon, Portugal.
8. **Casanova M. R.**, Fernandes E. M., Reis R. L., Martins A., and Neves N. M., "Vascularized bone tissue engineered platform comprising autologous BMP-2 and VEGF parallel immobilized", Winter School Gene2Skin and 1<sup>o</sup> Workshop do FoReCaST -The Tumour Microenvironment, November, 2017, Porto, Portugal.
9. Alves da Silva M., Costa-Pinto A. R., **Casanova M. R.**, Reis R. L., Nogueira-Silva C., Neves N. M., "Human Amniotic Membrane Stem Cells Isolation and Characterization", Winter School Gene2Skin and 1<sup>o</sup> Workshop do FoReCaST -The Tumour Microenvironment, November, 2017, Porto, Portugal.
10. **Casanova M. R.**, Alves da Silva M. L., Costa-Pinto A. R., Reis R. L., Martins A., and Neves N. M., "Chondrogenesis-inductive nanofibrous substrate biofunctionalized with autologous growth factors from platelet lysates for stem cell-based therapies ", TERMIS-EU 2017 Conference, June, 2017, Davos, Switzerland.
11. **Casanova M. R.**, Fernandes E. M., Reis R. L., Martins A., and Neves N. M., "Adjacent immobilization of autologous BMP-2 and VEGF envisioning a vascularized bone tissue engineering approach", CHEM2NATURE Second School, June, 2017, Porto, Portugal.
12. **Casanova M. R.**, Alves da Silva M. L., Costa-Pinto A. R., Reis R. L., Martins A., and Neves N. M., "Chondrogenic-Inductive Nanofibrous Substrates Biofunctionalized with Immobilized Autologous TGF- $\beta$ 3 and IGF-I", Society for Biomaterials 2017 Annual Meeting and Exposition, April, 2017, Minneapolis, United States.
13. **Casanova M. R.**, Alves da Silva, ML, Costa-Pinto A. R., Reis R. L., Martins A., and Neves N. M., "Chondrogenesis-inductive nanofibrous substrate comprising

autologous TGF- $\beta$ 3 and IGF-I from platelet lysates", GENE2SKIN Conference & TERM STEM, October, 2016, Guimarães, Portugal.

***Awards***

1. Quiz Time organized as part of the First Achilles Conference – “Molecular and Biological Mechanisms of Tendon Homeostasis and Repair” held from July 8 | 10, 2019 in Porto, Portugal.
2. Contest CHEM2BRAIN organized as part of the CHEM2NATURE Summer School, held from June 03 | 06, 2018 in Porto, Portugal.

***Awarded grant***

1. Foundation for Science and Technology (FCT) PhD scholarship (PD/BD/113797/2015).

## INTRODUCTION TO THE THESIS FORMAT

The present thesis is divided into six main **Sections (1 to 6)** comprising eight **Chapters (I to VIII)**. This structure allows organizing the data presented in the various chapters, according with the specific aims of each work, the nature of the experiments performed and the results achieved. The **Section 1** includes a general introduction to the biofunctionalization of biomaterial substrates, as well as the characterization of the state-of-art on strategies implemented for cartilage, nerve and bone regeneration (**Chapters I**). A detailed overview of the materials and methods used in this thesis is presented in **Section 2 (Chapter II)**. The experimental results are presented and discussed in **Sections 3 to 5**, focusing on the production of highly biofunctional nanofibrous substrates envisioning patient-specific strategies, based on the target tissue, namely Cartilage (**Section 3**), Nerve (**Section 4**) and Bone (**Section 5**). The main body of the thesis is based on a series of papers published in international journals or submitted for publication, which are identified in the front page of each chapter. Therefore, each thesis chapter is presented in an adapted version of the published or submitted manuscript style, keeping its contents, but intended to have a consistent structure between the various thesis chapters. A list of relevant references is also provided as a subsection within each chapter. Finally, **Section 6 (Chapter VIII)** completes this thesis with the concluding remarks of the experimental work, as well as the future perspectives of the developed technologies.

### *Section I – General introduction*

Chapter I – Surface biofunctionalization to improve the efficacy of a biomaterial substrate for use in regenerative medicine: This chapter provides a general overview of the latest advances in surface functionalization strategies, by covering the different methods and techniques that can be used in the Tissue Engineering and Regenerative Medicine (TERM).

### *Section II – Detailed description of experimental materials and methodologies*

Chapter II – Materials and Methods: This chapter provides a detailed analysis of the materials used, the processing techniques, the surface biofunctionalization strategies and the techniques used for the physicochemical characterization of the scaffolds. The biological tests with both model cell lines and primary cultures of human bone marrow mesenchymal stem cells or human articular chondrocytes are also described. The biological assays include the analysis of the cell viability and proliferation, the total protein synthesis and the quantification of a

neurogenic, chondrogenic and osteoblastic markers by immunohistochemistry and quantitative PCR. The *in vivo* angiogenesis evaluation is also described.

### ***Section III – Strategies for Cartilage repair***

Chapter III – Fibronectin bound to a fibrous substrate has chondrogenic-inductive properties: This chapter described the development of a biofunctional electrospun nanofibrous substrate able to specifically bind endogenous fibronectin from a pool of human blood plasma samples. The role of the bound fibronectin was evaluated in the chondrogenic differentiation of human bone marrow-derived mesenchymal stem cells (hBM-MSCs).

Chapter IV – Extracellular Vesicles Delivery Systems Capable of Inducing the Chondrogenic Differentiation: This chapter aims to report on a biofunctional system based on extracellular vesicles (EVs) derived from human articular chondrocytes (hACs) or chondrogenically induced hBM-MSCs. The regenerative potential of these EVs delivery systems were confirmed by assessing their contribution to induce the chondrogenic differentiation of hBM-MSCs *in vitro*.

Chapter V – Chondrogenesis-inductive nanofibrous substrate using both biological fluids and mesenchymal stem cells from an endogenous source: In this chapter, we report on the production and testing of a biofunctional system with chondrogenic induction capacity, through the immobilization of endogenous TGF- $\beta$ 3 and IGF-I retrieved from platelet lysates. The chondrogenesis potential of this biofunctional nanofibrous substrate was assessed by culturing hBM-MSCs, confirming those successfully induced chondrogenesis.

### ***Section IV – Strategies for Nerve regeneration***

Chapter VI – Guided Nerve Regeneration Mediated by Endogenous NGF bound at the surface of an Electrospun Fibrous Mesh: This chapter describes the selective immobilization of endogenous nerve growth factor (NGF), derived from rat blood plasma, at the surface of an electrospun nanofibrous substrate. The neurogenic potential of this biofunctional nanofibrous substrate was confirmed by culturing rat pheochromocytoma (PC12) cells during 7 days, without any further induction.

### ***Section V – Strategies for Bone regeneration***

Chapter VII – Spatial immobilization of endogenous growth factors to control vascularization in bone tissue engineering: This chapter describes a proof-of-principle study,

aiming to demonstrate that two growth factors can be bound in a spatial controlled way over the same nanofibrous substrate. The developed biofunctional system is able to bind endogenous BMP-2 and VEGF from human platelet lysates, envisioning an autologous vascularized bone tissue engineering strategy. The bioactivity of the bound growth factors was tested with hBM-MSCs, confirming the simultaneous induction of osteogenesis and angiogenesis of the cells by the nanofibrous substrate. The *in vivo* angiogenic potential of the biofunctional system was confirmed by testing the efficacy of this device in a chick chorioallantoic membrane (CAM) assay.

### ***Section VI – Concluding remarks***

Chapter VIII – General Conclusions and Future Perspectives: The final section of the thesis presents the overall conclusions achieved from the collection of research works previously reported. It is also discussed the future perspectives and research lines to be followed.



*“Believe in yourself and all that you are.  
Know that there is something inside you that is greater than any obstacle”*

***Christian D. Larson***

*“One, remember to look up at the stars and not down at your feet.*

*Two, never give up work.*

*Work gives you meaning and purpose and life is empty without it.*

*Three, if you are lucky enough to find love, remember it is there and don't throw it away.”*

***Stephen Hawking***

# **SECTION 1**

## **GENERAL INTRODUCTION**

# **Chapter I**

## **Surface**

### **Biofunctionalization to Improve the Efficacy of a Biomaterial Substrate for use in Regenerative Medicine**

## Chapter I

### **Surface Biofunctionalization to Improve the Efficacy of a Biomaterial Substrate for use in Regenerative Medicine\***

#### **ABSTRACT**

Surface biofunctionalization has emerged in the past decade as a promising tool in Tissue Engineering and Regenerative Medicine (TERM) approaches. The development of a biomaterial with regenerative properties is challenging, primarily owing to the requirement of achieving a surface that enhance cell attachment, proliferation and maturation/differentiation. There are numerous possible approaches for biofunctionalizing a biomaterial, which can be classified as non-covalent and covalent immobilization. However, an important aspect to have into consideration is the maintenance of stable/available bioactive molecule. Bioactive molecules, such as growth factors, play a pivotal role in the wound healing cascade mediating a wide range of cellular activities. Therefore, the immobilization of such bioactive molecules at the surface of biomaterial substrates has attracted tremendous interest in TERM approaches. In this review, we will discuss a wide range of bioactive molecules, different biofunctionalization strategies, and the most relevant results addressed by novel promising strategies.

---

\* This chapter is based on the following publication:

Casanova M. R., Reis R. L., Martins A. and Neves N. M., "Surface Biofunctionalization to Improve the Efficacy of Biomaterial Substrates to be used in Regenerative Medicine", Submitted for publication.

## I-1. INTRODUCTION

Loss of tissue and organ function caused by injuries or diseases can lead to a dysfunctional physiological response of the body. Furthermore, the auto-regenerative process may not lead to restore the normal structure and function of those tissues/organs [1, 2]. Currently, the transplantation of organs (e.g. kidney, liver, heart, lung, pancreas), tissue transplants (e.g. autografts, allograft, xenografts and other substitutes), the administration of bioactive factors and the implantation of artificial devices (e.g. metal-alloys, ceramics and inert prosthesis), are the optional clinical therapies available for those conditions [1, 3, 4]. However, the efficacy of these methods in restoring tissue structure and function is low, insufficient biocompatibility, owing to immune rejection, chronic inflammation and lack of clinical predictability [5, 6]. Therefore, tissue and organ regeneration remain an enormous clinical challenge, becoming an increasingly common worldwide health problem. Alternative methods for tissue and organs regeneration are being investigated in the Tissue Engineering and Regenerative Medicine (TERM) field, opening new solutions and strategies. The main aim of TERM is thus to repair or replace damaged or injured tissues [1, 2]. The development of effective strategies relies on the increasing our knowledge on wound healing and tissue formation physiology, as well as on the advances made in material science and cell biology [2, 7].

The biomaterial substrates significantly influence the attachment, proliferation and function of regenerative cells [8]. Therefore, the development of suitable biodegradable biomaterials as candidates for TERM is an active field of research [9-12]. It is important to keep in mind that the cell-biomaterial interface has to be compatible and able to integrate with the host tissue in order to allow for a precise control of cell fate.

Over the years, studies on biofunctionalization of biomaterial substrates (i.e., modification with biologically relevant and effective molecules) have been of great importance for TERM [13-16]. In a biofunctionalization strategy, the introduction of functional groups at the surface of the biomaterial substrate will act as cell recognition site or as focal points for further modification with bioactive molecules. Therefore, the biomolecular modifications could lead to promising bioactive biomaterial substrates with ability to control interactions with cell receptors (e.g. integrins), enhancing cell proliferation, differentiation, production and organization of extracellular matrix (ECM). There are different immobilization strategies that can be performed into biomaterial substrates for their biofunctionalization [17, 18]. Nevertheless, it is important to ensure the preservation of the bioactive molecule functionality.

Covalent immobilization meets some of these requirements, leading to the development of bioactive biomaterial substrates with functionality and to the possibility to achieve a localized and prolonged bioactivity of the immobilized bioactive molecules [16, 19, 20]. Biological samples like platelet rich plasma (PRP) have gained special interest as an autologous source of a variety of bioactive molecules envisioning a personalized therapy.

This section discusses different biofunctionalization strategies covering the different methods and techniques that can be used in the TERM field. In particular, the modification with biologically relevant and effective molecules are reviewed in great detail, emphasizing their potential applications in nerve, cartilage and bone regeneration.

## **I-2. ADVANCED STRATEGIES IN TISSUE ENGINEERING AND REGENERATIVE MEDICINE**

TERM is an emerging field focused on the development of alternative therapies for tissue/organ repair or regeneration. Those strategies require biomaterials interaction and its integration with the most tissue and cells, incorporating appropriated physical and cellular signals.

In general terms, a TERM approach consists on the combination of three different fundamental factors, namely cells (exogenous or autologous), biomaterials/scaffolds (supporting the formation of tissues *in vitro* or delivery of cells *in vivo*), and bioactive molecules (provided by the culture medium, the scaffold or the host). The most common implemented approaches may include the following: (i) the delivery of healthy cells directly into the defect site, in order to overcome the loss of cells resulting from the diseased tissue or trauma; (ii) the delivery of morphogens or tissue healing molecules that stimulate the host cells; and (iii) the implantation of a 3D matrix or scaffold biomaterial in which the cells grow to create a living 3D tissue substitute [21-24]. All these strategies involve either the design of a pre-formed scaffold or/and injectable biomaterial substrate, able to properly delivery and maintain the seeded cells or mobilize endogenously recruited cells in the site of action. Therefore, the surface biofunctionalization can be exploited both with seeded or with unseeded biomaterial substrates in order to enhance the efficacy of the tissue repair.

## I-2.1. Cell Sources

The cell is the basic structural, functional and biological unit of a living organism. Multicellular organisms are composed of many different cell types with specialized functions. Therefore, depending on the final application and the tissue to be repaired by the TERM approaches, different cell sources can be selected such as the blood, skin, bone, muscle or epithelium cells [25]. A reliable cells source should be easily isolated and expandable, non-immunogenic and have the ability to differentiate into a phenotype similar to the tissue that will be regenerated. An autologous strategy consists of obtaining a donor biopsy, followed by cells isolation and expansion *in vitro*, and, finally their implantation back into the donor [24]. The cells can be also xenogenic (such as bovine or porcine) or allogenic (from the same species but from a different individual). Due to the limitation of growing terminally differentiated cell types to obtain therapeutically relevant quantities, stem cells have emerged as strong alternatives. Stem cells have the remarkable capacity to renew themselves through cell division (the self-renewal capacity) and to differentiate into various cell types (the differentiation capacity) under certain physiologic or experimental conditions [26, 27].

Based on differentiation capability to form multiple cells types, stem cells can be classified as ‘totipotent’, ‘pluripotent’, ‘multipotent’ fetal stem cells and ‘multipotent’ adult stem cells (ASCs). ‘Totipotent’ cells have the capability to form all embryonic and extra-embryonic tissues, namely the embryo and the trophoblast of the placenta [28]. ‘Pluripotent’ cells are capable to origin almost all cells that arise from the three germ lines, but not the embryo because they are not able to origin the placenta and supporting tissues. The inner cell mass (ICM) also known as embryonic stem cells, are considered to be ‘pluripotent’ cells. However, the application of the embryonic stem cells in tissue engineering applications have some drawbacks, namely tumorigenic and immunological incompatibility [29, 30]. The multipotent fetal stem cells derived from the three embryonic germ layers (i.e. ectoderm, mesoderm and endoderm) are capable to origin particular cells, such as organs and tissues [28].

Induced pluripotent stem cells (iPS cells) are a type of pluripotent stem cell recently described as another promising stem cell source. IPS cells are artificially derived by transfection of certain stem cell-associated genes into non-pluripotent cells, such as adult fibroblasts [31, 32]. After transfection cells become morphologically and biochemical similar to pluripotent cells. This similarity includes the expression of certain stem cell genes and proteins, doubling time, embryoid body, teratoma and viable chimera formation, as the ability to form multiple



cells types [32, 33]. However, the full extent of their exact relation to “natural” pluripotent stem cells is still under study [34].

ASCs are a type of multipotent stem cells, which are presented in fully differentiated adult tissues. These stem cells are highly exploited for TERM applications [16, 35-39], since in the body they are responsible for the growth, maintenance, regeneration and repair of diseased or damaged tissue. Among the ASCs, the Mesenchymal Stem Cells (MSCs) were originally identified in the bone marrow and have been demonstrated prominent therapeutic proprieties [40]. It has been reported that MSCs secrete a variety of autocrine/paracrine factors that support regenerative processes, induce angiogenesis, protect cells from apoptosis and modulate the immune system. Indeed, MSCs from different sources have been reported to act as potent regulators of immune response. They were shown to inhibit the activation of T-, B- and dendritic cells while inducing the generation of Treg and regulatory macrophages [41]. Currently, there are ongoing clinical trials using MSCs for the treatment of some immune disorders [41, 42].

MSCs can be isolated from many types of adult tissues such as bone marrow [43], umbilical cord [44], fat [45], synovial fluid [46], dental pulp [47] and muscle [48], and are characterized by their ability to undergo extensive self-renewal *in vitro* and to go through multilineage. The immunophenotypic analysis of MSCs are characterized in a minimalist fashion as a plastic-adherent cell population with the following surface markers: CD13, CD44, CD73, CD90, CD105 positive, CD14, CD11b, CD 34, CD45, CD79 and HLA-DR negative [49]. The use of MSCs has several advantages, as they have unique biological properties, including their capability to extensive *in vitro* replication in an undifferentiated state, and to differentiate along multiple pathways [50].

MSCs have become one the main cell source for tissue repair, being an interesting candidate for cell-based therapeutics and regenerative medicine when compared to differentiated cells [51, 52]. Specifically, Bone Marrow-derived MSCs (BM-MSCs) and Adipose-derived MSCs (ADSCs) are the most common sources used in the TERM field [53]. Both have an identical potential to differentiate into cells and tissues of mesodermal origins, namely adipocytes, cartilage, bone and skeletal muscle [54-56]. The BM-MSCs has a greater ability to differentiate into chondrogenic and osteogenic lineage than do ADSCs [54, 56, 57]. Therefore, the BM-MSCs have been extensively studied in cartilage [58-63] and bone [64-66] tissue engineering.

## I-2.2. Requirements of a Biomaterial Scaffold

In TERM strategies, the scaffold plays a unique role, as it is designed to serve as a temporary support for cell proliferation, migration and differentiation, in order to form a hybrid tissue construct *in vitro* [67]. Therefore, the development of suitable biodegradable biomaterials as candidates for TERM is an active field of research [9-12]. It is important ensure that the cell-biomaterial interface is compatible and integrate with the host tissue in order to allow for precisely control of cell fate. Biomaterial substrates must behave as bioactive instructive scaffolds with the capacity to direct the cell behavior. These interactions are governed by surface energy, chemical composition, stiffness, as well as roughness and topography of the biomaterial surface in contact with the host micro-environment [68].

A suitable biomaterial substrate should possess adequate pore size, level of porosity, mechanical stability, degradation kinetics, and good biocompatibility. For a successful applicability in clinical TERM strategies, the scaffolds should have the following properties: (a) promote cell-biomaterial and cell-cell interactions, cell adhesion and ECM deposition [69-71]; (b) the porosity and the pore size should allow for the cell ingrowth and facilitate diffusion of nutrients and metabolites [1, 72, 73]; (c) permit sufficient transport of gases, nutrients and other soluble factors to allow cell survival [74-77]; (d) biodegradability in a rate compatible with that of the neo-tissue growth [78-80]; (e) act as delivery vehicles for cells, biomolecules and bioactive factors [39, 81-83]; (f) support the mechanical stresses and retain mechanical strength after implantation, providing the correct mechanical environment for the neo-tissue formation [1, 11]; (g) elicit an acceptable degree of inflammation *in vivo* [1, 12, 84]; and h) a cost-effective fabrication [1, 68].

Biodegradable biomaterials, either natural (*e.g.* collagen, alginate, fibrin, chitosan, starch) [85-94] or synthetic (*e.g.* polycaprolactone (PCL), poly-L-lactic acid, poly-lactide-co-glycolide) [75, 78, 95-101], have been processed into scaffolds for tissue engineering. Natural biomaterials can intrinsically provide some positive biochemical cues, although presenting some limitations such as its limited mechanical properties, are prone to batch-to-batch variability, have short shelf life and immunoreactivity. In contrast, synthetic biomaterials can be chemically and mechanically tuned, are easily sterilized, more reproducible and have a longer shelf life [102]. However, current clinically used biomaterials have limited functional capacity to repair the injured tissues [103]. One of the major problems related with implantable

biomaterials is the limited bioactivity and suboptimal integration with the host tissue, thus a biofunctionalization with biomolecules is required to increase the integrative tissue repair.

Among the different polymer processing techniques, electrospinning has been proposed as an efficient technique for the production of non-woven micro- to nano-fibrous meshes [104, 105]. The fiber dimension defines several interesting properties such as area to volume ratio, porosity and mechanical properties. From a biological point of view, almost every extracellular matrix (ECM) of connective tissue is based on nanofibrous structures (e.g. skin, cartilage and bone). This similarity makes electrospun nanofibers great candidates to provide the cells an environment similar to the native structure of the ECM [95, 106]. Most of the desirable properties of tissue engineered scaffolds can be addressed by electrospun nanofibrous meshes, such as porosity, interconnected pores with adjustable pores size, capabilities for effective surface functionalization and adjustable surface morphology [107-110]. Therefore, our research group has been exploring electrospun nanofiber meshes (NFMs) obtained by electrospinning for cartilage and bone tissue engineering applications [95, 108, 111-118]. Aiming to improve the NFMs functionality, different antibodies, proteins and lipidic nanoparticles were been immobilized at the surface of nanofibers [13, 16, 112, 113, 119-121].

### **I-2.3. Bioactive Molecules**

Different signals from the extracellular microenvironment can play significant roles over the cell performance, namely insoluble ECM macromolecules, diffusible/soluble molecules, and cell-cell receptors (**Figure I-1 a**). The insoluble bioactive molecules can be whole proteins, such as ECM proteins or short peptides sequences (cell binding domains) isolated from the ECM proteins [122]. The diffusible/soluble molecules (including the growth factors (GFs)) can have different modes of action over the cellular activity: autocrine (cell secretes molecules that binds to receptors on that same cell, leading to changes in that same cell), paracrine (cell produces a signal to induce changes in nearby cells) and/or endocrine (communicate a molecule over a long distance; the signals are released from a cell into the bloodstream and can travel to other anatomical locations) (**Figure I-1 b**) [122, 123].

The bioactive signals (GFs, cytokines) involved in tissue repair or function restoration also play a fundamental role in TERM strategies. Biomaterials can be loaded with these bioactive molecules, which can be released in a controlled way from the biomaterial substrate by diffusion, being able to interact with the surrounding cells. Indeed, a precise control over these

signaling molecules within a specific location may allow the regulation of the regenerative processes [124]. The most common biomolecules studied in the TERM field can be divided in the following major categories: (i) ECM proteins, (ii) GFs and (iii) extracellular vesicles (EVs).

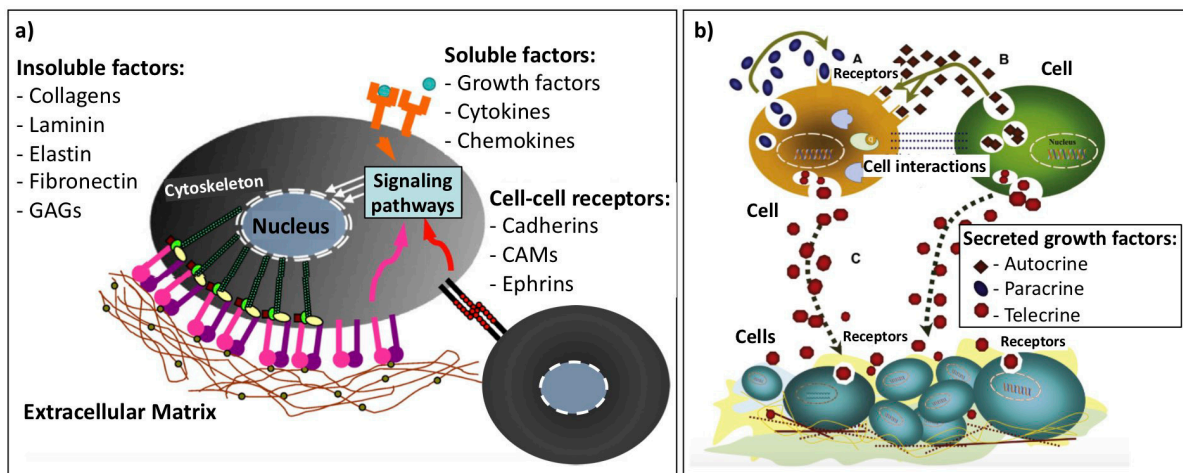


Figure I-1 The extracellular microenvironment (a) and cell signaling by soluble factors (b) [122, 125].

### I-2.3.1. Extracellular Matrix Proteins

The ECM is well recognized as a natural scaffold that supports the cells in the living organisms. It comprises several proteins, proteoglycans and other signaling molecules, important for the modulation of a wide range of cellular behavior such as adhesion, proliferation, migration and differentiation [126]. ECM proteins are typically fibrillar and provide a complex structural and functional network, capable of interacting with several cell surface receptors [127].

#### I-2.3.1.1 *Fibronectin*

Fibronectin is a high molecular weight glycoprotein of the ECM known to promote cell adhesion, growth, migration and differentiation of several cell types, influencing both the cell morphology and physiology [128-131]. It is important in wound healing and embryonic development processes. A altered fibronectin expression, degradation, and organization is associated with a number of pathologies, including cancer and fibrosis [132]. Fibronectin structure and stability are well known both in soluble form (blood and other extracellular fluids) and in an insoluble (interfaces, connective tissues and attached to cell surfaces) [70, 99, 132,

133]. This glycoprotein consists of two subunits of 220 kDa, containing three types of repeating units (I, II, and III), that mediate interactions with other fibronectin molecules, other ECM proteins (e.g. collagen, fibrin, and heparan sulfate proteoglycans), and cell surface receptors (e.g. integrins) (**Figure I-2**) [132]. The occurrence and intensity of these interactions in fibronectin coated biomaterial surfaces has been suggested to play an important role in determining the fibronectin function [134]. Specifically, fibronectin coating strategies were achieved through simple adsorption [135, 136], grafting [137, 138] or layer by layer [90, 139]. Those studies have shown the importance of fibronectin in controlling cell adhesion and survival among different substrates.

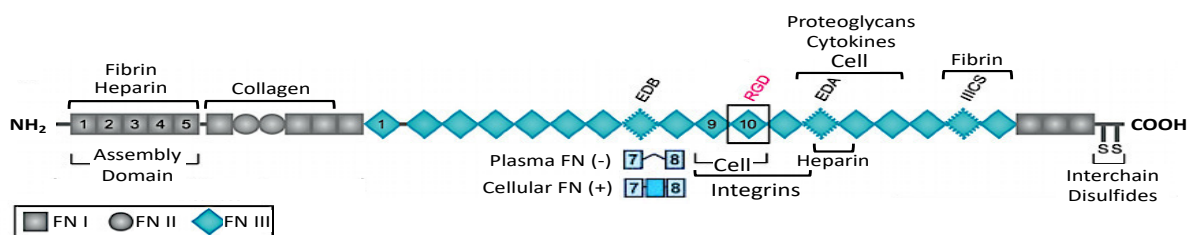


**Figure I-2 Fibronectin primary structure and its binding domains.**

During tissue repair, the fibronectin plays vital roles [140]. Upon tissue injury, plasma form of fibronectin is incorporated into fibrin clots to exert effect on platelet activation and to mediate hemostasis. Soluble form of fibronectin is then synthesized and assembled by cells as they migrate into the clot to reconstitute damage tissue. Different forms of fibronectin play differential and temporally discrete roles during tissue repair.

Fibronectin has a structural role by providing a scaffold with enhanced cell adhesion and differentiation. In adult stem cells, fibronectin can promote differentiation along skeletal lineages while suppressing adipogenic differentiation [141-143]. Studies have shown that chondrogenesis is enhanced when mesenchymal stem cells are cultured with fibronectin [144, 145]. Although fibronectin is not usually considered a principal cartilage protein, it is present throughout differentiation and persists in mature cartilaginous tissue. Furthermore, fibronectin has shown significant migratory and proliferative effects over mesenchymal progenitor cells which relied on chemotactic activity [146]. Nonetheless, the fibronectin osteogenic-inductive ability was also reported [131, 147-149]. Fibronectin immobilized at the surface of nanohydroxyapatite/PCL electrospun nanofibrous scaffolds provided suitable environment for cell attachment, proliferation and enhanced osteogenic differentiation of mesenchymal stem

cells, as demonstrated by the increase calcium deposition and alkaline phosphatase activity [148]. These findings reinforce the idea that the biological response to a biofunctionalized biomaterial can be modulated by the amount and the conformation of immobilized fibronectin.

### **I-2.3.2. Extracellular Vesicles**

Tissue regeneration involving stem cells can be driven by the paracrine activity of released EVs, delivering specific cargoes to the surrounding cells. Proteins, cytokines, RNA and subsequent gene expression orchestrate the regeneration process by promoting cell survival, control inflammation, repair lesions and improve the healing process [150].

Recently, the regenerative potential of cell paracrine effects has increased interest, and focused on EVs and the bioactive molecules they release, namely proteins, lipids, and nucleic acids [151, 152]. Studies have been demonstrated the regenerative potential of the cell-free strategies using conditioned medium [153-156] or EVs [157, 158]. The EVs function applied to tissue regeneration has been demonstrated using disease models, namely chronic wound [159], osteoarthritis [160], myocardial infarction [161] and lung diseases [162, 163]. Furthermore, EVs can be easily stored, and its dosage and potency optimized, reducing the cost and time associated with expanding or harvesting the stem cells [164].

### **I-2.3.3. Growth Factors**

GFs are natural cell-signaling polypeptides which are secreted by the cells and can bind to specific receptors on specific cells. They can be soluble or immobilized in the ECM and they are able to promote cell growth, tissue morphogenesis, wound healing and regeneration [125, 165]. Several GFs with different specific targets and functions are involved in different phases of the healing process, namely Vascular Endothelial Growth Factor (VEGF), Basic Fibroblast Growth Factor (b-FGF), Epidermal Growth Factor (EGF), Transforming Growth Factor Beta (TGF- $\beta$ ) or Platelet derived growth factor (PDGF) [166-168]. Indeed, the GFs have an active role when an injury occurs, by coordinating the healing process, until the wound is completely repaired [169]. Another important aspect related to GFs function is their crucial role in the exchange of information between different cell populations and their microenvironment [125, 167, 170].

Wound healing is a complex biologic process that involves three different phases: inflammation, a proliferation and repair phase (including the angiogenesis, proliferation and synthesis of ECM) and remodeling (**Figure I-3**) [166]. Beginning by platelet activation, the clotting factors, cytokines and GFs are released at the injured site, initiating the healing response. PDGF initiates the chemotaxis of neutrophils, macrophages, smooth muscle cells and fibroblasts, and also promotes the proliferation of fibroblasts. TGF- $\beta$  attracts macrophages, stimulating them to produce additional cytokines like b-FGF, that enhances collagen synthesis, leading to a strong response of the matrix [171, 172]. Therefore, the inflammatory response is characterized by leucocyte extravasion and accumulation at the injury site, and monocyte/macrophage activation [173].

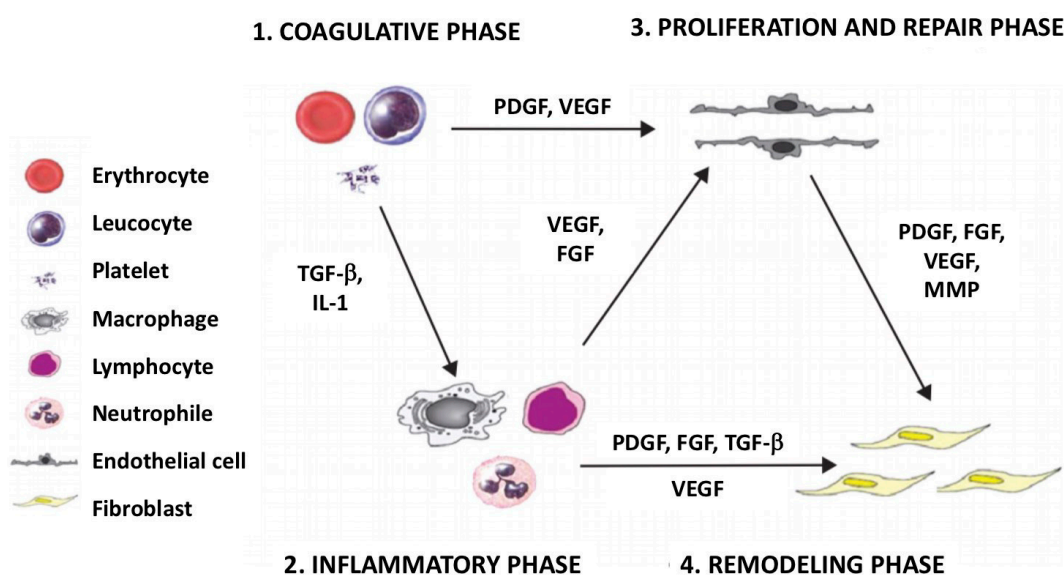


**Figure I-3** Schematic overview of the wound healing process and the biomolecules involved [174].

In the trophic phase, several processes are develop including angiogenesis, collagen deposition, granulation tissue formation, epithelialization, and wound contraction [170, 173]. The activation of endothelial cells by VEGF initiates the angiogenesis process, namely the formation of new blood vessels able to promote blood flow [175]. As the healing progresses, the cells migrate into the injury site, using the fibrin matrix as a scaffold, the cells divide and differentiate, producing collagen, proteoglycans and other components of the natural ECM [166]. The epithelization process is stimulated by the presence of EGF secreted by the activated macrophages, platelets and keratinocytes at the injury site [171, 172]. By the end of healing process, namely in the remodeling stage, there is a decrease in cell density and, therefore, on the metabolic activity of the healed tissue [172, 173]. The duration of each phase and

progression into the next stage are precisely controlled by signaling molecules (i.e. GFs) released in the injury site [166, 167, 170].

The engineering of a microenvironment able to mimic the critical aspects of a natural healing process, namely the wound healing cascade, by providing suitable biochemical and physic-chemical factors is the basis of TERM research [125]. Therefore, it is absolutely necessary to provide the cells an environment that can mimic the natural environment in which they can proliferate and differentiate efficiently. For that, an artificial ECM delivering the appropriate bioactive factors is required. Due to all these aspects, the integration of bioactive molecules into the biomaterials design plays an important role in cellular regulation of adhesion, proliferation, differentiation and gene expression. Accordingly, TERM approaches comprising GFs that play an important role during the wound healing are described in the next sections.

#### I-2.3.3.1 *Properties and Roles of Growth Factors*

As previously stated, GFs play an important role in cellular processes involved in tissue repair and regeneration [167, 169, 176]. However, GFs have different mechanisms of action depending on the concentration, on the half-life, on their state (soluble or immobilized in the ECM), as well as on the phenotype of the target cells [176]. The GFs currently used in different therapeutic applications are presented in **Table I-1** and discussed in the next sections.

**Table I-1 Most relevant growth factors in the TERM field.**

Growth factor	Role	Targets	Critical issues	Ref.
TGF- $\beta$	Promotes the production of extracellular matrix; Modulates and enhances the proliferation of fibroblasts; Increases and stimulates synthesis of collagen type I; Enhances the proliferation of bone/cartilage/vascular smooth muscle cells; Regulates inflammatory processes; Crucial role in stem cell differentiation.	Bone/ Cartilage	Rapid degradation due to the short half-life; High expression often correlated with malignancy; Rapid diffusion;	[16, 76, 177-185]



**Table I 1 Most relevant growth factors in the TERM field (Continued).**

<b>Growth factor</b>	<b>Role</b>	<b>Targets</b>	<b>Critical issues</b>	<b>Ref.</b>
<b>IGF</b>	Chemotactic for fibroblast and stimulates protein synthesis; Enhances bone formation by inducing proliferation and differentiation of osteoblasts.	Bone/ Dermal wound healing/ Pancreatic stem cell differentiation	IGF-I deficiency cause liver cirrhosis, age-related cardiovascular and neurological diseases; Higher circulating IGF-I levels could be a marker or a causal factor of cancer;	[16, 36, 87, 178, 181, 186-192]
<b>BMP</b>	Involved in cartilage development; Induces bone and cartilage formation; Plays a key role in osteoblast differentiation and maturation; Plays a key role in renal development and repair.	Bone/ Cartilage/ Renal	Rapid degradation due to the short half-life; Rapid diffusion, requiring controlled release.	[20, 39, 82, 193-208]
<b>VEGF</b>	Promoter of angiogenesis and vasculogenesis; Controls endothelial cells migration, proliferation and survival; Increases microvascular permeability.	Vascularization/ Stem cell differentiation	Rapid degradation due to the short half-life; Excessive amounts cause vascular leakage.	[37, 83, 89, 201, 209-212]
<b>NGF</b>	Regulates growth, maintenance, proliferation, and survival of certain target neurons; Plays a key role in survival of pancreatic beta cells; Regulates of the immune system.	Nervous system/ Immune system	Short half-life and rapid diffusion; NGF deficiency cause neurodegenerative diseases.	[83, 189, 213-218]
<b>b-FGF</b>	Potent inductor of cell proliferation; Promotes angiogenesis and differentiation; Induces proliferation of endothelial cells and smooth muscle cells; Induces endothelial capillary formation.	Bone/ Cartilage/ Periodontal tissue/ Vascularization	Rapid diffusion, requiring controlled release; Mitogen for a wide variety of cell types.	[215, 219-221]

Table I 1 Most relevant growth factors in the TERM field (Continued).

Growth factor	Role	Targets	Critical issues	Ref.
<b>PDGF</b>	Released from platelets; Stimulates angiogenesis; Induces macrophages activation; Recruitment of smooth muscle cells to endothelial linings; Vessel maturation; Collagen synthesis.	Cartilage/ Bone/ Angiogenesis	Vessel destabilization when at high concentration; Increased activity associated with several diseases.	[222-227]
<b>EGF</b>	Triggers gene expression related to proliferation; Promotes mesenchymal and epithelial cells differentiation; Induces angiogenesis.	Skin/ Cornea Nervous System	Short half-life, rapid diffusion; Large amounts of protein required for response.	[228-231]

#### 1.2.3.3.1.1 Transforming Growth Factor Beta (TGF- $\beta$ )

TGF- $\beta$  is a pleiotropic polypeptide which belong to the TGF- $\beta$  superfamily. Those regulates multiple biological processes, including embryonic development, adult stem cell differentiation, immune regulation, wound healing, and inflammation. [232]. TGF- $\beta$  family members are synthesized as prepropeptide precursors and are then processed and released as homodimers or heterodimers in order to bind to its receptor (transmembrane serine/threonine kinase receptors), regulating cellular functions. Skeletal cells express TGF- $\beta$ 1, TGF- $\beta$ 2, and TGF- $\beta$ 3. Those have shown to play a major role in cartilage development, being the TGF- $\beta$ 3 more effective in the *in vitro* chondrogenesis of MSCs when compared to TGF- $\beta$ 1 and TGF- $\beta$ 2 [233]. The TGF- $\beta$  family members are generally considered potent stimulators of proteoglycans, type II collagen synthesis, being able to induce the chondrogenic differentiation of MSCs *in vitro* [84]. However, the maintenance of a critical threshold concentration of the TGF- $\beta$  for a prolonged time is crucial for the onset and maintenance of chondrogenesis. Therefore, the development of scaffolds which can provide temporal and/or spatial control of TGF- $\beta$  bioavailability has been carried out in order to improve the cartilage repair [76, 177-179, 185]. For example, TGF- $\beta$ 3 immobilized poly-(lactic-co-glycolic acid)-gelatin/chondroitinsulfate/hyaluronic acid (PLGA-GCH) scaffold efficiently induced the chondrogenic differentiation of MSCs, exhibiting chondrocyte morphology and cartilage ECM deposition, *in vitro* [177]. After implantation, cartilage was successfully regenerated to repair chondral defects.

#### *1.2.3.3.1.2 Insulin-like Growth Factor (IGF)*

Insulin-like Growth Factor (IGF) is a protein with high sequence similarity to insulin, having insulin-like actions in some tissues, though they are far less potent than insulin. Those GFs, namely IGF-I and IGF-II play important roles in the regulation of growth and metabolism [234]. The IGF-I stimulates systemic body growth, and has growth-promoting effects on almost every cell in the body, especially skeletal muscle, cartilage, bone, liver, kidney, nerve, skin, hematopoietic, and lung cell. IGF-II is recognized as a major fetal GF, while IGF-I is a major GF in adults [235]. At the injured muscle, it can enhance cell homing, healing and regeneration [191], and its chondrogenic differentiation potential has been also extensively investigated [16, 178]. Indeed, it is involved in cartilage repair and considered an essential mediator of cartilage homeostasis and metabolism, stimulating the proteoglycan synthesis [36, 87, 188, 192, 236]. IGF-I is involved in the chondrogenic differentiation by regulating the synthesis of DNA, *Aggrecan* and *Collagen type II* at the transcription level in rat articular chondrocytes [236].

*In vitro* cultures with IGF-I and TGF- $\beta$ 1 stimulate glycosaminoglycan and collagen synthesis in bovine articular cartilage explants [237]. Furthermore, studies using IGF-1 combined with TGF- $\beta$  show an improvement in chondrogenesis [36, 178, 238-240]. The MSCs cultured in the presence of TGF- $\beta$ 3 and IGF-I, combined in cycling patterns, showed the chondrocyte-like characteristic, namely a strong expression of Sox 9 and cartilage extracellular matrix genes [240].

#### *1.2.3.3.1.3 Nerve Growth Factor (NGF)*

Nerve growth factor (NGF) plays an important role in the process of repair and regeneration of injured nerves, regulating the proliferation and differentiation of cells, and the myelination of neurons, being an important group of GFs that stimulate and promote neurogenesis [213]. This neurotrophic factor is crucial to facilitate the survival and the innervation of autonomic nerves and sensory neurons [189]. Therefore, the NGF was been widely used in nerve tissue engineering strategies to improve neurogenesis at the injury site [83, 214, 215, 217, 218].

#### *1.2.3.3.1.4 Bone Morphogenetic Proteins (BMPs)*

Bone morphogenetic proteins (BMPs) are multi-functional GFs which belong to the TGF- $\beta$  superfamily. The BMPs are involved in the growth and development of several tissues and organs such as bones, heart, kidneys, eyes, skin and teeth [200]. These GFs are physiologically synthesized by mesenchymal cells, osteoprogenitor cells, chondrocytes, osteoblasts and

platelets [205]. Although the name implies that all BMPs members are inducers of bone, some BMPs can act as inhibitors of bone formation. For example, BMP-3 is a negative regulator of bone density, and BMP-13 is a strong inhibitor of bone formation [241, 242]. While, BMP-2, 4, 6, 7, and 9 are commonly referred to as the osteogenic BMPs, based on their potent bone-inducing activity [243]. For instance, BMP-2 is a potent osteogenic factor which plays a key role in the creation of many tissues engineered bone grafts [82, 193-195, 203, 204].

BMPs have also pro-anabolic and anti-catabolic effects in many organ systems. For example, BMP-4 serves to regulate limb development, and BMP-13 has a modulatory role in the development of the eye [244, 245]. BMP-7, important for cartilage development, is a powerful cytokine that induces chondrocyte differentiation [197, 198].

#### *I.2.3.3.1.5 Vascular Endothelial Growth Factor (VEGF)*

Secreted and synthesized by many cell types, VEGF is a dimeric glycoprotein which binds indirectly to the ECM via linker molecules, namely heparin sulfate proteoglycans [246, 247]. VEGF promotes angiogenesis by regulating the formation and maturation of blood vessels, acting mainly on vascular endothelial cells [248]. However, VEGF is not only involved in angiogenesis, but also implicated in the maturation of osteoblasts, ossification, and bone turnover [249, 250]. The incorporation of VEGF into a biomaterial has been carried out in order to improve the TERM strategy in vascularized tissues dependent on the formation of new blood vessels [81, 201, 209, 211, 212].

### **I-2.4. Sources of Bioactive Molecules**

Regenerative medicine holds the promise to repair or replace damaged and injured tissues by therapeutically manipulating its natural ability to heal after injury or disease. In this context, blood components and their blood derivative formulations can provide a wide range of bioactive molecules (i.e. ECM proteins; GFs; cytokines) that are essential in the regulation of wound healing process [251, 252]. Positive clinical effects of the use of different types of blood derivatives has been reported on several fields of TERM, namely in the treatments of cartilage disorders [253], tendon injuries and pathologies [254], as well as in periodontal [255] and soft tissues [256].

Peripheral blood is constituted by different cellular elements like red blood cells, white blood cells and platelets, sub-cellular and molecular components [252]. The separation of blood

components leads to different blood derivatives. Generally, it starts with a whole blood centrifugation in order to separate the blood into three phases: a lower layer rich in red blood cells; an interface layer (buffy coat) rich in white blood cells and platelets; and an upper layer corresponding to the blood plasma with platelets in suspension. When an anticlotting agent (e.g. heparin or citrate) was previously added, the interface layer can be submitted to a further centrifugation step to produce a fraction poor in platelets (platelet-poor plasma (PPP)) and a fraction rich in platelets (PRP) [252, 257, 258]. Since platelets are a source of GFs, there is a growing interest in the use of PRP as a strategy to optimize tissue healing [258], namely in orthopedics and musculoskeletal disorders [166, 259].

The impact of the discoveries regarding the healing potential of blood derivatives has increased the optimism about autologous regenerative medicine. PRP is a cost-effective product, since it is taken from a simple blood sample and, therefore, it is easy to use in the current clinical practice. Due to its autologous source, there are no regulatory concerns about its biosafety, since concerns related with immunogenic reaction and disease transmission are eliminated. However, due to its complex protein composition, GFs and cytokines, some mechanisms involved in its mode of action are still poorly understood [260].

GFs are protected and stabilized via their binding to different ECM components that regulate their availability and signaling [261, 262]. In a biomimetic strategy, blood derivatives (i.e. PRP) were combined with different biomaterials to modulate the delivery of bioactive molecules in order to guide the wound healing process [75, 77, 199, 263-265]. For example, platelet lysate impregnated in collagen/gelatin scaffolds are able to promote wound healing *in vivo*, by enhancing cell proliferation and vessel growth in a granulation tissue of a full-thickness skin defect [264]. While, when PRP is incorporated into gelatin sponges and implanted into alveolar bone defects in rats, PRP was capable to enhance bone regeneration [265]. However, the PRP alone dispersed from the injury site not contributing to the wound healing process. Thus, the incorporation of PRP into biomaterials is relevant to locate the delivery of biomolecules at the injury site.

Studies consistently shown that the use of PRP may be an approach to develop clinically relevant biomaterials able to deliver growth factors and, simultaneously, allow cell culture, and, finally, integration of the *in vivo* formed neo-tissue into the native environment [253, 260, 266]. Some of those therapeutic products are currently undergoing clinical studies for skin, maxillofacial, orthopedic, and wound healing related applications [267, 268].

Commercial products using blood derivatives as a source of bioactive molecules to functionalize biomaterials are already approved and distributed for musculoskeletal disorders. For example, the BST-CarGel® (Smith and Nephew, MA, USA), a chitosan solution that, when mixed with patient's whole blood, create a liquid bioscaffold for cartilage repair [269]. Patients treated with BST-CarGel® showed a significantly superiority of repair tissue quantity and quality over the microfracture alone (standard and first-line surgical treatment) in a randomized controlled clinical trial. Thus, the BST-CarGel® is a safe and effective treatment for symptomatic full-thickness cartilage lesions with clinical benefit significant over baseline levels of pain, stiffness, and function.

In order to fulfill the needs of TERM strategies, the definition of good manufacturing practice protocols to standardize the production method of blood derivatives formulations, together with the continuous understanding of the basic biology of blood derivatives in wound healing modulation will provide robust and reproducible therapeutic results. Furthermore, designed biomaterials incorporating blood derivatives that bind to and sequester bioactive molecules, and the full understanding of the nature of these interactions will enable engineering the wound healing environment towards tissue regeneration.

### **I-3. BIOFUNCTIONALIZATION STRATEGIES**

The bioactive molecules made available in physiological environments are susceptible to inactivation by degradation, prior to the possibility of reaching the desired target cells. Therefore, high doses of biomolecules are typically required to induce cellular response, although the high doses can lead to cells and tissues damage, due to cytotoxic side effects. Thus, biomaterial-based systems can be design to deliver bioactive molecules locally, controlling its effects [125, 270]. The biofunctionalization of biomaterial surfaces with bioactive molecules gained special interest mainly due to the need of optimize the biological performance of implantable medical devices.

The biocompatibility of the biomaterial surface is an important requisite on protein adsorption, as it should not interfere with the native structure of the bioactive molecule [270]. The biomaterial surface chemistry, namely the availability of reactive groups, has to be considered when choosing an appropriate immobilization strategy. Moreover, the use of an aqueous-based chemistry to immobilize the bioactive molecules are generally required, as most of them are either not soluble and/or become denatured in the presence of organic solvents [125,

270, 271]. Surface biofunctionalization is achieved by adsorption or chemical bonding of the bioactive molecules to the polymer surface in order to promote a specific cell response [270, 272]. Accordingly, the immobilization of bioactive molecules, as represented on **Figure I-4**, can be divided in two different main categories: (i) non-covalent immobilization by physical adsorption, owing to protein-protein hydrogen bonding or protein-protein hydrophobic interaction with an intermediate molecule (**Figure I-4 a**), (ii) covalent immobilization of biomolecules (**Figure I-4 b**) and (iii) combined techniques (**Figure I-4 c**). A summary of biofunctionalized biomaterials developed in the last years is presented **Table I-4** and discussed in the next sections.

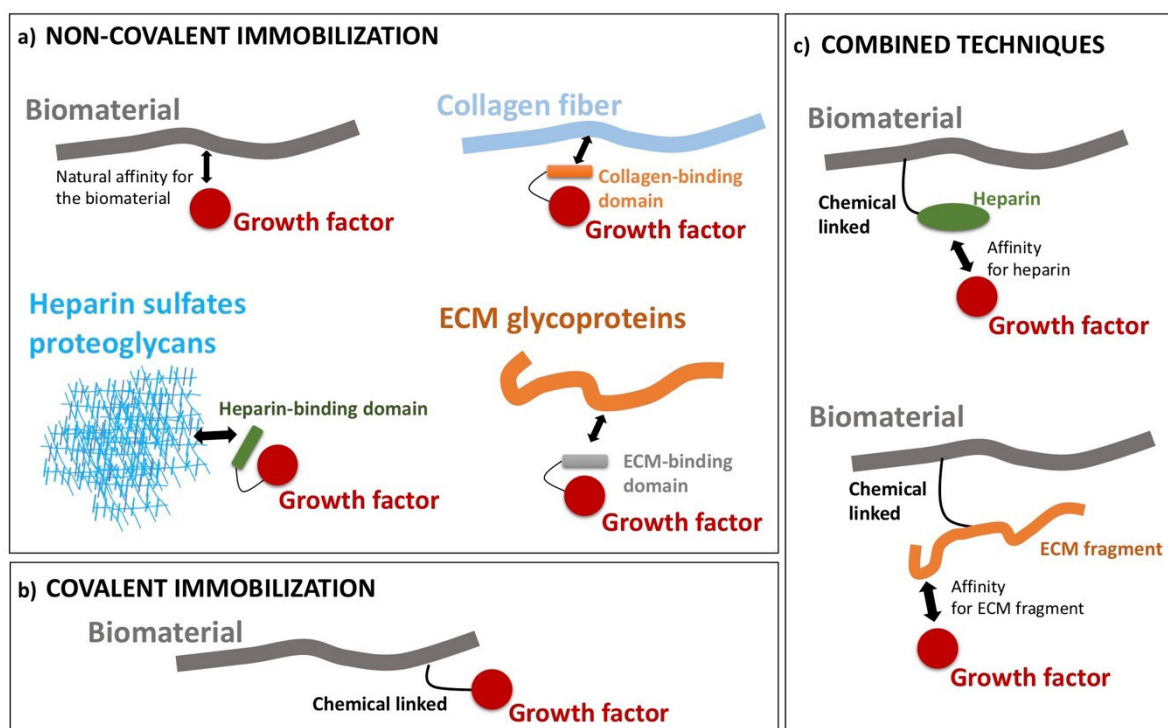


**Figure I-4** Schematic diagram showing different biofunctionalization techniques. (A) Strategies for non-covalent immobilization of the bioactive molecules, leveraging the natural affinity of biomolecules to these biomaterials. (B) Strategies to covalently attach bioactive molecules to biomaterials using chemical or enzymatic tools. (C) Combined strategies to employ endogenous ECM as the delivery biomatrix by engineering fusions of bioactive molecules with ECM binding domains

Table I-2 Biofunctionalization strategies applied in TERM approaches.

Biofunctionalization strategy	Biomaterial (polymer)	Biomolecule	Application	Result	Ref.
<b>Non-covalent immobilization</b>	Collagen I/III scaffolds	Peptides arginine-glycine-aspartic acid (RGD)	Cardiomyogenesis	RGD signaling to integrins was not a rate-limiting event for cardiomyogenesis.	[273]
	Titanium / gelatin	TGF- $\beta$ 1 / IGF-1	Cartilage	Induced proliferation and differentiation of MG63 cells.	[181]
	Poly(lactic-co-glycolic acid)	TGF-beta 1-loaded gelatin microspheres	Cartilage	Increased cell proliferation; High sulfated glycosaminoglycan production; Promoted cartilage regeneration in defective articular cartilage.	[185]
	Bacterial cellulose / gelatin	VEGF-silk fibroin nanoparticles	Vascularization	Improved cell viability and proliferation; Promoted vessel blood formation <i>in vivo</i> .	[211]
	Polycaprolactone / hyaluronic acid	BMP-2	Bone	Induced upregulation of bone markers; Slight newly bone formation.	[195]
	Polycaprolactone / Pluronic F127	VEGF / Laminin	Smooth muscle regeneration	High cell growth; Induced effective smooth muscle cell differentiation.	[37]
	Silk fibroin / poly(ethylene oxide)	Laminin	Peripheral nerve regeneration	Improved the surface hydrophilicity; Increased the cell proliferation.	[274]
	Poly(lactic-co-glycolic acid)	Hydroxyapatite / Collagen	Bone	Accelerated cell spreading; Increased alkaline phosphatase activity; Enhanced expression of osteogenic-related genes.	[275]



Table 1 2 Biofunctionalization strategies applied in TERM approaches (Continued).

Biofunctionalization strategy	Biomaterial (polymer)	Biomolecule	Application	Result	Ref.
<b>Non-covalent immobilization</b>	Poly (L-lactic acid)	NGF / VEGF	Peripheral nerve regeneration	Enhanced the neural differentiation of induced pluripotent stem cells-derived neural crest stem cells; Induced neovascularization and nerve healing <i>in vivo</i> .	[83]
	Nanostructured hydroxyapatite	BMP-2	Bone	Improved osteogenesis; Enhanced bone formation <i>in vivo</i> .	[204]
	Polycaprolactone	VEGF	Tissue-engineered heart valve	Promoted the adhesion and proliferation of endothelial cells.	[212]
	Marine natural sponges / bioactive glass	Gelatin	Bone	Increased <i>in vivo</i> bone formation.	[276]
	Nanocrystalline diamond / submicron crystalline diamond	Fibronectin	Bone	Spread and migration of osteoblast cells.	[135]
	Chitosan	Aptamer / Fibronectin	Tissue engineering	Aptamers contribute to control fibronectin adsorption	[136]
	Mineral microparticles	VEGF	Bone	Improved bone repair by the increment of erythropoietin and Runx-2 expression.	[209]
	Poly(lactic-co-glycolic acid)	BMP-7	Cartilage	High proteoglycan and collagen type II production, and thick hyaline cartilage formation.	[39]
	Poly(lactic-co-glycolic acid)	EGF / Lidocaine	Wound healing	Improve the post-operative pain relief and wound healing.	[229]

Table 1 2 Biofunctionalization strategies applied in TERM approaches (Continued).

Biofunctionalization strategy	Biomaterial (polymer)	Biomolecule	Application	Result	Ref.
Non-covalent immobilization	Elastine-like polypeptides / Polyethylene glycol	Laminin-1 sequences (IKVAV / VKAIV)	Nerve	Sensory neurons are able to formed longer neurite. Absence of detectable inflammation <i>in vivo</i> .	[277]
	Poly (lactic acid) / Poly (vinul alcohol)	BMP-2	Guide Bone Regeneration	Enables the cell attachment and proliferation.	[193]
	Gelatin / Polycaprolactone	TGF- $\beta$ 2	Vasculature	High growth and infiltration of vascular smooth muscle cells; Modulate the cell response by the release of TGF- $\beta$ 2.	[180]
Covalent immobilization	Poly(lactic acid)-co-[(glycolic acid)-alt-(L-lysine)]	RGD peptide / NGF	Peripheral nerve regeneration	High nerve regeneration potential.	[216]
	Polycaprolactone	TGF-beta 1; b-FGF / VEGF	Biomedical applications	Successfully antibodies immobilization in different designs; Bound VEGF remain bioactive.	[13]
	Microposts	Laminin	Cardiac tissue	Increase the beating rate.	[278]
	Lysozyme amyloid-like nanofibrils	Lipase	Biomedical applications	The photo-immobilized lipase has better thermostability and enhanced resistance to non-conventional environment; Morphology compatible with amyloid-like aggregates.	[279]
	Poly(lactide-co-glycolide)/hydroxy apatite	BMP-2	Bone	Induced the osteogenesis of Mouse Adipose-Derived Stem Cells.	[280]

Table 1 2 Biofunctionalization strategies applied in TERM approaches (Continued).

Biofunctionalization strategy	Biomaterial (polymer)	Biomolecule	Application	Result	Ref.
<b>Covalent immobilization</b>	Poly(ethylene glycol)	BMP-2 / TGF- $\beta$ 3	Bone	Significantly influenced hMSCs osteochondral differentiation.	[20]
	Nanoporous anodic alumina and macroporous silicon	Collagen / Fibronectin	Biomedical applications	High cell adhesion and proliferation obtained with fibronectin coatings.	[129]
	Poly-(lactic-co-glycolic acid)-gelatin / chondroitin sulfate / hyaluronic acid	TGF- $\beta$ 3	Cartilage	Induced chondrogenic differentiation of MSCs; Increased chondral defects repair.	[177]
	Polyethylene terephthalate	Chitosan	Biomedical applications	High resistance to bacterial attachment of Escherichia coli and Staphylococcus.	[281]
	Dental implant	Collagen type I	Bone	Improve osseointegration, especially in regions with a low bone quality.	[282]
	Polycaprolactone	Platelet-Rich Plasma	Wound healing	Improved adhesion, early spreading, and growth of human fibroblasts; Prolonged biological activity of immobilized molecules.	[97]
	Polyurethane-type shape memory polymers	Collagen	Tissue engineering	Enhanced the biocompatibility of the scaffold.	[283]
	Polycaprolactone	TGF- $\beta$ 3 / IGF-I	Cartilage	Cartilaginous ECM formation.	[16]

Table I 2 Biofunctionalization strategies applied in TERM approaches (Continued).

Biofunctionalization strategy	Biomaterial (polymer)	Biomolecule	Application	Result	Ref.
<b>Combined techniques</b>	starPEG-heparin hydrogel	matrix metalloprotease / RGD peptides / TGF $\beta$ 1	Wound healing	Supported fibroblast attachment, spreading, proliferation matrix deposition and remodeling; Induced myofibroblast differentiation of fibroblasts.	[179]
	Heparin / poloxamer	b-FGF / NGF	Peripheral Nerve Regeneration	Induced Schwann cell proliferation; Enhanced axonal regeneration and remyelination; Improved recovery of motor function.	[215]
	Silk fibroin	Heparin / TGF- $\beta$ 2 / Growth/differentiation factor 5	Tendon/ligament-to-bone tissue engineering	Enhanced the expression of cartilage markers and collagen II protein content.	[184]
	Titanium	Polydopamine/ Collagen	Integration with soft tissues	High adhesion of human foreskin fibroblasts and human immortal keratinocytes; Improved tissue compatibility.	[19]
	Poly(ethylene glycol) / gelatin	Laminin-derived YIGSR peptide / VEGF	Basement membrane	Enhanced endothelial cell behavior.	[284]
	Gelatin / hydroxyapatite composite	BMP-2 / Avidin-biotin	Bone	Improved osteogenesis.	[206]

### **I-3.1. Non-covalent Immobilization**

Physical entrapment, adsorption or ionic complexation are all strategies applied in non-covalent immobilization [285]. Physical entrapment consists in biomolecules encapsulation/incorporation into the biomaterial scaffold. Adsorption results by incubating the biomaterial in a solution of the bioactive molecules, taking advantage of the direct interactions between the biomolecules and the biomaterial surface, such as polyelectrolyte interaction or other secondary interactions, or of indirect interaction via intermediate proteins or other biological molecules [180, 285-287]. Regarding ion complexation, proteins with different isoelectric points may be used for polyion complexation with charged macromolecules. Due to the desorption or the irreversibility of the immobilized biomolecules, the ionic complexation can cause protein inactivation and denaturation [285].

The bioactive molecules can attach to the material surface owing to surface interactions, such as Van der Waal forces, hydrophobic interactions and hydrogen bonds. For example, ionic complex of gelatin and TGF- $\beta$ 1 are obtained by encapsulating gelatin microparticles loaded with TGF- $\beta$ 1 into oligo[poly(ethylene glycol) fumarate] hydrogels at pH 7.4 [287]. Those interactions occurred, due to the negatively charged gelatin and the positive charged TGF- $\beta$ 1. The release of TGF- $\beta$ 1 can be tuned by the degradation properties of the natural and synthetic polymers.

Surface biofunctionalization via non-covalent immobilization has the advantage of being a simple and gentle procedure accompanied by limited damage of the biomaterial structures and of the bioactive molecules. However, the stability of the protein binding in non-covalent binding is not comparable with covalent immobilization.

### **I-3.2. Covalent Immobilization**

With the intention of solving the previous referred limitations and to improve the stability and sustained delivery of immobilized biomolecules to target cells, covalent immobilization methods emerged as a viable alternative approach. In covalent surface bonding, molecules are chemically bonded to the biomaterial surface exposing the bioactive sites of the molecules. Despite being a more complex processes, covalent immobilization strategies can prolong the GFs availability much more than the one achieved by the non-covalent immobilization

strategies [288]. Furthermore, covalent immobilization allows spatial control of the biomolecule's distribution over the surface of a biomaterial, increasing the efficacy of the biofunctionalized biomaterials [125, 270, 289]. Immobilized bioactive molecules become protected against cellular inactivation and digestion, having a local and prolonged activity when in physiological-like environments [165]. Therefore, the protein immobilization can overcome the diffusion limitations of soluble GFs. While the delivery of GFs elicits responses in the surrounding environment, covalently immobilized GFs may have the additional advantage of confined local and more prolonged effects, avoiding unspecific side effects [125, 165, 289].

To accomplish the covalent immobilization two steps are required: (i) exposure of functional groups and (ii) covalent binding of the bioactive molecules to the surface functional groups. The most common functional groups exploited in surface biofunctionalization are the amines or the carboxyl groups [271]. If the biomaterial substrates do not have any of these chemical groups, some treatments can be performed in order to chemically activate their surface, namely hydrolysis and aminolysis [13, 16, 290] to expose carboxyl [98, 291] and amine groups respectively. Plasma treatment can be also applied to insert functional groups at the surface for further covalent immobilization [292].

In order to achieve a more stable and strong protein binding, the covalent immobilization often requires the use of a linker. A linker molecule is a chemical molecule capable of reacting with both the polymer and the bioactive molecule [270]. Frequently, 1-Ethyl-3-(3-dimethylaminopropyl)carbodiimide (EDC), a crosslinking agent that couples the carboxyl groups to the amine groups, is used to stabilize the amide bond [293]. The EDC reaction with carboxyl groups forms an o-acylisourea intermediate, which then reacts with the amine-containing molecule. Due to the highly unstable intermediate, the sulfo-N-hydroxysuccinimide (sulfo-NHS) or N-hydroxysuccinimide (NHS) may be added to create a more stable amine-reactive sulfo-NHS or NHS ester intermediate, improving the reaction efficiency [293]. This coupling method is very effective and can be performed under mild reaction conditions [270, 293]. After a preliminary chemical treatment, the surface is biofunctionalized by the immobilization of a bioactive molecule via an amide bond between the amine group/carboxylic group of the bioactive molecule and the exposed carboxylic group/amine group on the biomaterial surface, respectively [293]. EDC chemistry has been used to immobilize biomolecules, such as VEGF and fibronectin, at the surface of poly(l-lactic acid) (PLLA) scaffolds, demonstrating improved growth of human umbilical vein endothelial cells *in vitro* [210]. VEGF has been also covalently immobilized in collagen scaffolds [294] and at the

surface of PCL nanofibers [13] using EDC chemistry. The effect of different reaction buffer (Phosphate-Buffered Saline (PBS), distilled water and 2-(N-morpholino)- ethanesulfonic acid (MES)) on the covalent immobilization of VEGF and angiopoietin-1 was investigated using the porous collagen scaffolds [295]. The highest proliferation rates and lactate metabolism were observed when PBS was used to immobilize VEGF and angiopoietin-1. Therefore, the use of an appropriate elution buffer during the covalent bonding procedures may be crucial to obtain a satisfactory biofunctionalization.

Covalent immobilization of GFs to a biomaterial surface can also be achieved by a photo-initiated reaction [207, 279-281, 296, 297]. This method consists on the functionalization of the bioactive molecule with a photo-reactive group and, afterwards, the binding of the modified protein to the biomaterial surface upon exposure radiation (e.g. ultraviolet light (UV)) at a defined wavelength. For example, BMP-2 was photo-immobilized on poly(lactide-co-glycolide)/hydroxyapatite nanocomposites [280]. This strategy allowed the long-term immobilization of proteins on the biomaterial surface, enhancing the osteogenesis potential of adipose-derived stem cells. The spatial defined distribution of the immobilized biomolecule could also be achieved through the use of photomasks or laser scanning light sources [297]. Similar to the coupling method with EDC, the photo-immobilization is very effective, but its use is relatively expensive and the use of radiation may compromise the proteins bioactivity, bioavailability and conformation [270, 272, 297].

Covalent immobilization is a complex process, which may limit the type of biomolecule that can be immobilized owing to the harsh conditions that sometimes are required to obtain a satisfactory biofunctionalization [270]. For instance, large biomolecules such as GFs can be inactivated by the organic solvents used during covalent bonding procedures. Otherwise, combined techniques employing both non-covalent and covalent immobilization methods can be exploited to biofunctionalized the biomaterial surfaces.

### **I-3.3. Combined Techniques**

In order to overcome problems related with inactivation or denaturation of covalently immobilized biomolecules and the weak non-covalent immobilization, the use of intermediate molecules that bind both the biomolecule and the biomaterial surface can be an alternative approach. The glycosaminoglycans, ECM proteins, small oligopeptides mimicking ECM proteins, avidin – biotin molecules and antibodies may be used as an intermediate molecule

[206]. These biomolecules are capable to be chemically or physically deposited at the biomaterial surface, offering biological sites for biomolecules incorporation. It is well established that GFs binding via ECM domains can regulate the cell behaviour [298]. Several GFs, such as IGF, b-FGF, TGF- $\beta$ , EGF, VEGF, PDGF, among others, interact with ECM proteins, heparin or heparan sulfate [179, 183, 184, 298, 299]. This biofunctionalization strategies provides stable and strong covalent bonds between the biomaterial surface and the intermediate molecules, avoiding exposure of the bioactive molecules to the harsh solvents. The presence of the binding domains on the intermediate molecules exhibited at the biomaterial surface leads to a strong charge or hydrophobicity, favoring the attraction of bioactive molecules [300]. Therefore, it is not required substantial incubation time for the biomolecules attachment to the intermediate molecule, being able to use a wider choice of buffer systems in comparison with chemical bonding [301]. The only drawback is that the combined techniques involve more preparation steps.

#### **I-4. APPLICATIONS OF BIOFUNCTIONAL STRATEGIES**

The immobilization of target bioactive molecules improves their stability, which may provide beneficial contributions for different tissue repair strategies. The next sections will focus on the most promising results on the application of immobilized biomolecules at the surface of biomaterial substrates. The effects of immobilized biomolecules have been studied in various areas including neurogenesis, cartilage and bone regeneration, angiogenesis, dermal wound healing, pancreas and liver, and stem cell differentiation.

##### **I-4.1. Cartilage Repair**

Articular cartilage is a flexible connective tissue, which is predominantly avascular, aneural and alymphatic [302], having a limited capacity for repair. Due to the absence of vasculature, the progenitor cells from the blood or the bone marrow are not available to support tissue repair and remodeling [303]. Advanced TERM strategies have been proposed to overcome its limited propensity self-repair, leading to functional replacement. TGF- $\beta$  and IGF-I have been identified as important proteins on the regulation of cartilage development and on the homeostasis of mature articular cartilage [304, 305], as reported above.



Studies demonstrated that TGF- $\beta$  incorporated into a biomaterial can significantly improve the efficacy of a cartilage tissue engineering strategy [16, 177, 181, 185]. For example, the TGF- $\beta$ 1-immobilized PLGA-gelatin scaffold promoted chondrogenic differentiation of ASCs *in vitro*, with a significant increase in sulfated glycosaminoglycan content as compared to ASC-seeded on non-TGF- $\beta$ 1-immobilized PLGA-gelatin scaffolds [185]. As well as, the selectively immobilization of endogenous TGF- $\beta$ 3 derived from human platelet lysates at the surface of a single PCL nanofibrous substrate, was able to induce the chondrogenic differentiation of hBM-MS-C *in vitro*, as confirmed by the typical spherical morphology of chondrocytes and the immunolocalization of collagen type II [16]. Therefore, the immobilization of TGF- $\beta$  have favorable outcomes in cartilage tissue engineering strategies, overcoming the lack of local retention and the need of high amounts of proteins to achieve the desired biological effects.

Among the various BMPs, BMP-7 has demonstrated pro-anabolic and anti-catabolic effects in cartilage tissue restoration [39, 197, 198]. Indeed, the delivery of BMP-7 incorporated into fibrous PLGA scaffolds resulted in enhanced proteoglycan and collagen type II synthesis by synovium-resident mesenchymal stem cells, and the formation of a thick hyaline cartilage when transplanted into osteochondral defects in a rabbit animal model [39].

#### **I-4.2. Nerve Regeneration**

Due to an often-unsatisfactory nerve regeneration, the peripheral nerve injury still remains a major clinical surgical challenge. Despite autologous nerve grafts are considered the gold standard, tissue engineered nerve guidance grafts are valuable, alternatives for this unmet medical need [306].

Tissue engineered nerve guidance grafts comprise a biomaterial-based scaffold and a multitude of cellular and/or molecular components [307-313]. Therefore, the bioactive molecules are usually incorporated into the nerve conduit to improve neurogenesis at the injury site [288, 309, 310, 314, 315]. Among the bioactive molecules, NGF is an important growth factor capable to stimulate and promote neurogenesis, as described above. Hence, it was widely used in nerve tissue engineering strategies [83, 214, 215, 217, 218]. For example, the incorporation of NGF into a hyaluronic acid-based hydrogel could restore erectile function in a rat model of cavernous nerve crush injury [217]. Aiming at a dual-delivery strategy, NGF and VEGF were incorporated into nanofibrous scaffolds, enhancing the neural differentiation of induced pluripotent stem cells-derived neural crest stem cells *in vitro* [83]. Furthermore, this

dual-delivery scaffold significantly improved the neovascularization and nerve healing, in a rat sciatic nerve injury model.

### **I-4.3. Bone Regeneration**

The gold standard treatment of bone fractures relies on the use of autologous bone grafts [316]. However, despite their biocompatibility and exceptional osteoconductive properties, autografts are of limited supply and are associated with donor site morbidity. Allografts and xenografts are valid alternatives to autologous bone grafts, despite the risk of disease transmission, infection and rejection [317, 318]. Advanced TERM strategies emerged as new therapeutic solution to stimulate the natural healing process, namely by the application of biological signals and cells.

The most widely used osteogenic inducing molecules are the BMPs (namely the BMP-2, already approved by the FDA for human use) that induce new bone formation and regeneration at specific sites [319-321]. In products applied in spinal fusions and oral surgery, BMPs are delivered to the site of the fracture by being incorporated into a bone implant, and released gradually to allow bone formation. However, the delivery method of BMPs often shows a lack of local retention and the need of high amounts of proteins to achieve the desired biological effects. The immobilization of such GFs may have favorable outcomes in bone tissue engineering strategies, as well as on the osteointegration of orthopedic implants, with the use of significantly less amounts of GF in order to achieve effective osteogenic outcomes [270].

BMPs have been immobilized in different substrates like PLGA scaffolds [322], chitosan membranes [323] and PCL scaffolds [324], showing that the biological effect of immobilized BMP-2 can significantly increase the expression of osteoblastic differentiation markers, when osteogenic precursor cells are cultured. Biofunctional biomaterials have also been developed by using the covalent binding of biotin and BMP-2 through amino functional groups [196, 202, 206]. The surface immobilization of BMP-2 on gelatin/hydroxyapatite composite scaffold can effectively improve osteogenesis, having a higher alkaline phosphatase activity than that composite film without BMP-2. Importantly, the covalent binding used to biofunctionalized the biomaterial does not affect the BMP-2 bioactivity [206]. Regarding the *in vivo* efficiency, when comparing the soluble BMP-2 and its immobilized form, the former approach showed that bone amount and maturity have increased [31,114–116].

### **I-4.3.1. Angiogenesis**

The lack of a functional and integrated vascular system is one of the major problems in tissue engineered strategies, namely in bone tissue engineering. The vascular system is essential to maintain the viability and function of tissues, by providing nutrients, oxygen and cell metabolites transport. Therefore, the absence of an appropriate vascular system may cause unwanted cellular necrosis [325, 326].

The capillary networks formation (angiogenesis) are highly regulated by soluble molecules such as VEGF, being the endothelial cells the main responsible entities. Both matrix-bound and soluble forms of VEGF can be found in physiological environment, playing an essential role in endothelial cells proliferation and vascular sprouting [327, 328]. Being a successful TERM strategy dependent on the formation of new blood vessels, the incorporation of VEGF into a biomaterial has been carried out [81, 201, 209, 211, 212]. Surface biofunctionalization of decellularized porcine aortic valve with VEGF-loaded PCL nanoparticles was able to accelerate the *in vivo* endothelialization and regeneration of the decellularized valves by increase the blood capillaries formation [212]. The delivery of low doses of BMP-2 and VEGF by a silk fibroin-nanohydroxyapatite scaffold are able to promote angiogenesis in an early bone healing stage and facilitated osteogenic differentiation both *in vitro* and *in vivo* [201]. A dual delivery system, where different ratios of BMP-2 and VEGF were entrapped within polyelectrolyte multilayer (PEM) films, enhanced the mineral density within the *de novo* bone, then those containing BMP-2 only, which suggests a more complete remodeling due to an increase local vascular network [81].

### **I-5. FINAL REMARKS**

The surface biofunctionalization of a biomaterial substrate has gained a growing interest in the TERM field, aiming to develop more effective approaches. Although, the effect of soluble bioactive factors over the behavior and signaling of different cell types is well known, the knowledge of the influence of immobilized bioactive molecules is increasing and major research efforts are needed. Cellular response to an immobilized bioactive molecule cannot always be predicted in the same way as for soluble form, due to their short half-lives. When GFs are immobilized, those biomolecules become protected against cellular inactivation and

digestion, leading to a sustained activity. Consequently, with the immobilization of GFs it is possible to confined local and more prolonged bioactive effect, avoiding unspecific side effects.

This introduction summarized different biofunctionalization strategies applied in TERM field, based on different physical, chemical and biological modification strategies, using a wide range of bioactive molecules. Biofunctionalization strategies are essential to develop highly effective biomolecules delivery systems able to directly promote interactions between the immobilized biomolecules and the resident cells, avoiding the potential side effects caused by their systemic administration. A literature analysis revealed that a combination of different immobilization techniques is often required to achieved optimal results. The biggest challenge of the biofunctionalization relies on finding the appropriate balance between the bioactive molecules and the physicochemical properties of the biomaterial substrate that can regulate cell behaviors. However, the significant progresses and the promising results achieved will attract major research efforts in the future, being the biomaterial surface biofunctionalization an emerging field.

## **I-6. REFERENCES**

- [1] K.L. Christman, Biomaterials for tissue repair, *Science* 363(6425) (2019) 340-341.
- [2] J.R. Fuchs, B.A. Nasser, J.P. Vacanti, Tissue engineering: a 21st century solution to surgical reconstruction, *Ann Thorac Surg* 72(2) (2001) 577-91.
- [3] A.S. Mao, D.J. Mooney, Regenerative medicine: Current therapies and future directions, *Proc Natl Acad Sci U S A* 112(47) (2015) 14452-9.
- [4] W. Zhang, H. Ouyang, C.R. Dass, J. Xu, Current research on pharmacologic and regenerative therapies for osteoarthritis, *Bone Res* 4 (2016) 15040.
- [5] J.Y. Kim, B.M. Kang, J.S. Lee, H.J. Park, H.J. Wi, J.S. Yoon, C. Ahn, S. Shin, K.H. Kim, K.C. Jung, O. Kwon, UVB-induced depletion of donor-derived dendritic cells prevents allograft rejection of immune-privileged hair follicles in humanized mice, *Am J Transplant* 19(5) (2019) 1344-1355.
- [6] S. Kim, Y.S. Han, J.H. Lee, S.H. Lee, Combination of MSC spheroids wrapped within autologous composite sheet dually protects against immune rejection and enhances stem cell transplantation efficacy, *Tissue Cell* 53 (2018) 93-103.
- [7] D.F. Williams, To engineer is to create: the link between engineering and regeneration, *Trends Biotechnol* 24(1) (2006) 4-8.

- [8] E.S. Place, N.D. Evans, M.M. Stevens, Complexity in biomaterials for tissue engineering, *Nat Mater* 8(6) (2009) 457-70.
- [9] K. Sivaraman, K. Muthukumar, C. Shanthi, A potential bioactive peptide candidate for biomaterial and tissue engineering applications, *Life Sci* 226 (2019) 140-148.
- [10] M.R. Simu, E. Pall, T. Radu, M. Miclaus, B. Culic, A.S. Mesaros, A. Muntean, G.A. Filip, Development of a novel biomaterial with an important osteoinductive capacity for hard tissue engineering, *Tissue Cell* 52 (2018) 101-107.
- [11] G. Peng, H. Liu, Y. Fan, Biomaterial Scaffolds for Reproductive Tissue Engineering, *Ann Biomed Eng* 45(7) (2017) 1592-1607.
- [12] S. Zhuo, M. Ni, L. Bi, L. Xia, J. Fan, H.H. Chan, Stem Cell-Biomaterial Interactions for Tissue Engineering, *Stem Cells Int* 2015 (2015) 126710.
- [13] C. Oliveira, A.R. Costa-Pinto, R.L. Reis, A. Martins, N.M. Neves, Biofunctional Nanofibrous Substrate Comprising Immobilized Antibodies and Selective Binding of Autologous Growth Factors, *Biomacromolecules* 15(6) (2014) 2196-2205.
- [14] L.E. Sperling, K.P. Reis, P. Pranke, J.H. Wendorff, Advantages and challenges offered by biofunctional core-shell fiber systems for tissue engineering and drug delivery, *Drug Discov Today* 21(8) (2016) 1243-1256.
- [15] S. Sangkert, S. Kamolmatyakul, W.L. Chai, J. Meesane, A biofunctional-modified silk fibroin scaffold with mimic reconstructed extracellular matrix of decellularized pulp/collagen/fibronectin for bone tissue engineering in alveolar bone resorption (vol 166, pg 30, 2016), *Mater Lett* 229 (2018) 348-348.
- [16] M.R. Casanova, M.A. Da Silva, A.R. Costa-Pinto, R.L. Reis, A. Martins, N.M. Neves, Chondrogenesis-inductive nanofibrous substrate using both biological fluids and mesenchymal stem cells from an autologous source, *Mat Sci Eng C-Mater* 98 (2019) 1169-1178.
- [17] M. Moyo, J.O. Okonkwo, N.M. Agyei, Recent Advances in Immobilization Strategies in Biomaterial Nanotechnology for Biosensors, *Bioengineered Nanomaterials* (2014) 61-92.
- [18] S. Van Vlierberghe, E. Vanderleyden, V. Boterberg, P. Dubrue, Gelatin Functionalization of Biomaterial Surfaces: Strategies for Immobilization and Visualization, *Polymers-Basel* 3(1) (2011) 114-130.
- [19] Y. Zhu, D.D. Liu, X.L. Wang, Y. He, W.J. Luan, F.Z. Qi, J.D. Ding, Polydopamine-mediated covalent functionalization of collagen on a titanium alloy to promote biocompatibility with soft tissues, *J Mater Chem B* 7(12) (2019) 2019-2031.
- [20] A. Di Luca, M. Klein-Gunnewiek, J.G. Vancso, C.A. van Blitterswijk, E.M. Benetti, L. Moroni, Covalent Binding of Bone Morphogenetic Protein-2 and Transforming Growth Factor-3 to 3D Plotted Scaffolds for Osteochondral Tissue Regeneration, *Biotechnol J* 12(12) (2017).
- [21] C.H. Lu, Y.H. Chang, S.Y. Lin, K.C. Li, Y.C. Hu, Recent progresses in gene delivery-based bone tissue engineering, *Biotechnol Adv* 31(8) (2013) 1695-706.

- [22] R. Subbiah, R.E. Guldberg, *Materials Science and Design Principles of Growth Factor Delivery Systems in Tissue Engineering and Regenerative Medicine*, *Adv Healthc Mater* 8(1) (2019) e1801000.
- [23] L.M. Caballero Aguilar, S.M. Silva, S.E. Moulton, Growth factor delivery: Defining the next generation platforms for tissue engineering, *J Control Release* 306 (2019) 40-58.
- [24] J. Kobayashi, A. Kikuchi, T. Aoyagi, T. Okano, Cell sheet tissue engineering: Cell sheet preparation, harvesting/manipulation, and transplantation, *J Biomed Mater Res A* 107(5) (2019) 955-967.
- [25] L. Roseti, A. Bassi, B. Grigolo, P.M. Fornasari, Development of Human Chondrocyte-Based Medicinal Products for Autologous Cell Therapy, *Biomaterials Science and Engineering* (2011) 349-368.
- [26] M.T. Fuller, E. Davies, A. Spence, Regulation of self-renewal, proliferation and differentiation in an adult stem cell lineage, *Mech Develop* 126 (2009) S3-S3.
- [27] J. Motlik, J. Klima, J. Hlucilova, D. Usvald, R. Prochazka, B. Dvorankova, K. Smetana, Mechanisms of self-renewal and differentiation of adult stem cells isolated from bone marrow, brain and epidermis of the miniature pigs, *Reprod Domest Anim* 42 (2007) 68-69.
- [28] U. Lakshmiopathy, C. Verfaillie, Stem cell plasticity, *Blood Rev* 19(1) (2005) 29-38.
- [29] I. Kehat, D. Kenyagin-Karsenti, M. Snir, H. Segev, M. Amit, A. Gepstein, E. Livne, O. Binah, J. Itskovitz-Eldor, L. Gepstein, Human embryonic stem cells can differentiate into myocytes with structural and functional properties of cardiomyocytes, *J Clin Invest* 108(3) (2001) 407-414.
- [30] G. Virt, Ethical aspects of human embryonic stem cell use and commercial umbilical cord blood stem cell banking. Ethical reflections on the occasion of the regulation of the European Council and Parliament on advanced therapy medicinal products, *Bundesgesundheitsbla* 53(1) (2010) 63-67.
- [31] J. Hu, J.M. Wang, From embryonic stem cells to induced pluripotent stem cells-Ready for clinical therapy?, *Clin Transplant* 33(6) (2019).
- [32] K. Takahashi, K. Tanabe, M. Ohnuki, M. Narita, T. Ichisaka, K. Tomoda, S. Yamanaka, Induction of pluripotent stem cells from adult human fibroblasts by defined factors, *Cell* 131(5) (2007) 861-872.
- [33] J.H. Zhang, G.F. Wilson, A.G. Soerens, C.H. Koonce, J.Y. Yu, S.P. Palecek, J.A. Thomson, T.J. Kamp, Functional Cardiomyocytes Derived From Human Induced Pluripotent Stem Cells, *Circ Res* 104(4) (2009) E30-E41.
- [34] R.G. Rowe, G.Q. Daley, Induced pluripotent stem cells in disease modelling and drug discovery, *Nat Rev Genet* 20(7) (2019) 377-388.
- [35] A.K. Kundu, A.J. Putnam, Vitronectin and collagen I differentially regulate osteogenesis in mesenchymal stem cells, *Biochem Bioph Res Co* 347(1) (2006) 347-357.

- [36] L. Uebersax, H.P. Merkle, L. Meinel, Insulin-like growth factor I releasing silk fibroin scaffolds induce chondrogenic differentiation of human mesenchymal stem cells, *Journal of Controlled Release* 127(1) (2008) 12-21.
- [37] S.R. Lee, T.H. Kim, S.H. Oh, S.K. Kwon, J.H. Lee, VEGF/Laminin Co-Immobilized Membrane for Enhanced Differentiation of Muscle-derived Stem Cells into Smooth Muscle Cells, *Polym-Korea* 42(5) (2018) 866-873.
- [38] A. Mohammadpour, S. Arjmand, A.S. Lotfi, H. Tavana, M. Kabir-Salmani, Promoting hepatogenic differentiation of human mesenchymal stem cells using a novel laminin-containing gelatin cryogel scaffold, *Biochem Bioph Res Co* 507(1-4) (2018) 15-21.
- [39] H.J. Kim, M.A. Han, J.Y. Shin, J.H. Jeon, S.J. Lee, M.Y. Yoon, H.J. Kim, E.J. Choi, S.H. Do, V.C. Yang, H.N. He, Y.I. Yang, Intra-articular delivery of synovium-resident mesenchymal stem cells via BMP-7-loaded fibrous PLGA scaffolds for cartilage repair, *Journal of Controlled Release* 302 (2019) 169-180.
- [40] H. Castromalaspina, R.E. Gay, G. Resnick, N. Kapoor, P. Meyers, D. Chiarieri, S. Mckenzie, H.E. Broxmeyer, M.A.S. Moore, Characterization of Human-Bone Marrow Fibroblast Colony-Forming Cells (Cfu-F) and Their Progeny, *Blood* 56(2) (1980) 289-301.
- [41] Y. Shi, J. Su, A.I. Roberts, P. Shou, A.B. Rabson, G. Ren, How mesenchymal stem cells interact with tissue immune responses, *Trends Immunol* 33(3) (2012) 136-43.
- [42] M.J. Hoogduijn, Are mesenchymal stromal cells immune cells?, *Arthritis Res Ther* 17 (2015) 88.
- [43] R.O.C. Oreffo, C. Cooper, C. Mason, M. Clements, Mesenchymal stem cells - Lineage, plasticity, and skeletal therapeutic potential, *Stem Cell Rev* 1(2) (2005) 169-178.
- [44] S. Corrao, G. La Rocca, M. Lo Iacono, T. Corsello, F. Farina, R. Anzalone, Umbilical cord revisited: from Wharton's jelly myofibroblasts to mesenchymal stem cells, *Histol Histopathol* 28(10) (2013) 1235-1244.
- [45] L. Aust, B. Devlin, S.J. Foster, Y.D.C. Halvorsen, K. Hicok, T. du Laney, A. Sen, G.D. Willingmyre, J.M. Gimble, Yield of human adipose-derived adult stem cells from liposuction aspirates, *Cytotherapy* 6(1) (2004) 7-14.
- [46] T. Teramura, K. Fukuda, S. Kurashimo, Y. Hosoi, Y. Miki, S. Asada, C. Hamanishi, Isolation and characterization of side population stem cells in articular synovial tissue, *Bmc Musculoskel Dis* 9 (2008).
- [47] S. Shi, S. Gronthos, Perivascular niche of postnatal mesenchymal stem cells in human bone marrow and dental pulp, *J Bone Miner Res* 18(4) (2003) 696-704.
- [48] W.M. Jackson, L.J. Nesti, R.S. Tuan, Potential therapeutic applications of muscle-derived mesenchymal stem and progenitor cells, *Expert Opin Biol Th* 10(4) (2010) 505-517.
- [49] D.S. Krause, M.J. Fackler, C.I. Civin, W.S. May, CD34: Structure, biology, and clinical utility, *Blood* 87(1) (1996) 1-13.

- [50] P. Bianco, M. Riminucci, S. Gronthos, P.G. Robey, Bone marrow stromal stem cells: Nature, biology, and potential applications, *Stem Cells* 19(3) (2001) 180-192.
- [51] R.E.B. Fitzsimmons, M.S. Mazurek, A. Soos, C.A. Simmons, Mesenchymal Stromal/Stem Cells in Regenerative Medicine and Tissue Engineering, *Stem Cells International* (2018).
- [52] A.I. Caplan, Adult mesenchymal stem cells for tissue engineering versus regenerative medicine, *J Cell Physiol* 213(2) (2007) 341-347.
- [53] P. Godara, R.E. Nordon, C.D. McFarland, Mesenchymal stem cells in tissue engineering, *J Chem Technol Biot* 83(4) (2008) 397-407.
- [54] X. Li, M.J. Wang, X.G. Jing, W.M. Guo, C.X. Hao, Y. Zhang, S. Gao, M.X. Chen, Z.Z. Zhang, X.L. Zhang, S. Shen, B. Zhang, H. Xian, Z.H. Wang, Y. Wang, X. Sui, A.Y. Wang, J. Peng, S.B. Lu, S.Y. Liu, Q.Y. Guo, Bone Marrow- and Adipose Tissue-Derived Mesenchymal Stem Cells: Characterization, Differentiation, and Applications in Cartilage Tissue Engineering, *Crit Rev Eukar Gene* 28(4) (2018) 285-310.
- [55] S. Kern, H. Eichler, J. Stoeve, H. Kluter, K. Bieback, Comparative analysis of mesenchymal stem cells from bone marrow, umbilical cord blood, or adipose tissue, *Stem Cells* 24(5) (2006) 1294-1301.
- [56] R. Izadpanah, C. Trygg, B. Patel, C. Kriedt, J. Dufour, J.M. Gimble, B.A. Bunnell, Biologic properties of mesenchymal stem cells derived from bone marrow and adipose tissue, *J Cell Biochem* 99(5) (2006) 1285-1297.
- [57] G.I. Im, Y.W. Shin, K.B. Lee, Do adipose tissue-derived mesenchymal stem cells have the same osteogenic and chondrogenic potential as bone marrow-derived cells?, *Osteoarthr Cartilage* 13(10) (2005) 845-853.
- [58] S. Wakitani, K. Imoto, T. Yamamoto, M. Saito, N. Murata, M. Yoneda, Human autologous culture expanded bone marrow mesenchymal cell transplantation for repair of cartilage defects in osteoarthritic knees, *Osteoarthritis Cartilage* 10(3) (2002) 199-206.
- [59] M.L. Alves da Silva, A. Martins, A.R. Costa-Pinto, P. Costa, S. Faria, M. Gomes, R.L. Reis, N.M. Neves, Cartilage tissue engineering using electrospun PCL nanofiber meshes and MSCs, *Biomacromolecules* 11(12) (2010) 3228-36.
- [60] L. Rackwitz, F. Djouad, S. Janjanin, U. Noth, R.S. Tuan, Functional cartilage repair capacity of de-differentiated, chondrocyte- and mesenchymal stem cell-laden hydrogels in vitro, *Osteoarthritis Cartilage* 22(8) (2014) 1148-57.
- [61] S. Moeinzadeh, S.R. Pajoum Shariati, E. Jabbari, Comparative effect of physicomechanical and biomolecular cues on zone-specific chondrogenic differentiation of mesenchymal stem cells, *Biomaterials* 92 (2016) 57-70.
- [62] Y.N. Wu, J.B. Law, A.Y. He, H.Y. Low, J.H. Hui, C.T. Lim, Z. Yang, E.H. Lee, Substrate topography determines the fate of chondrogenesis from human mesenchymal stem cells resulting in specific cartilage phenotype formation, *Nanomedicine* 10(7) (2014) 1507-16.



- [63] Q. Hu, B. Ding, X. Yan, L. Peng, J. Duan, S. Yang, L. Cheng, D. Chen, Polyethylene glycol modified PAMAM dendrimer delivery of kartogenin to induce chondrogenic differentiation of mesenchymal stem cells, *Nanomedicine* 13(7) (2017) 2189-2198.
- [64] K. Marupanthorn, C. Tantrawatpan, P. Kheolamai, D. Tantikanlayaporn, S. Manochantr, Bone morphogenetic protein-2 enhances the osteogenic differentiation capacity of mesenchymal stromal cells derived from human bone marrow and umbilical cord, *Int J Mol Med* 39(3) (2017) 654-662.
- [65] K.T. Shalumon, H.T. Liao, C.Y. Kuo, C.B. Wong, C.J. Li, P.A. Mini, J.P. Chen, Rational design of gelatin/nanohydroxyapatite cryogel scaffolds for bone regeneration by introducing chemical and physical cues to enhance osteogenesis of bone marrow mesenchymal stem cells, *Mat Sci Eng C-Mater* 104 (2019).
- [66] S.Q. Zang, L. Zhu, K.F. Luo, R. Mu, F. Chen, X.C. Wei, X.D. Yan, B.Y. Han, X.L. Shi, Q.T. Wang, L. Jin, Chitosan composite scaffold combined with bone marrow-derived mesenchymal stem cells for bone regeneration: in vitro and in vivo evaluation, *Oncotarget* 8(67) (2017) 110890-110903.
- [67] W.M. Saltzman, *Tissue Engineering: Engineering Principles for the Design of Replacement Organs and Tissues*, Oxford University Press, 2004.
- [68] H.J. Mathieu, Bioengineered material surfaces for medical applications, *Surf Interface Anal* 32(1) (2001) 3-9.
- [69] Y. Shibasaki, S. Hirohara, K. Terada, T. Ando, M. Tanihara, Collagen-Like Polypeptide Poly(Pro-Hyp-Gly) Conjugated with Fibronectin-Derived Peptides Enhances the Cell Adhesion, Migration and Stratification, *Ifmbe Proc* 37 (2012) 1086-1089.
- [70] M. Hindie, E. Camand, R. Agniel, F. Carreiras, E. Pauthe, P. Van Tassel, Effects of human fibronectin and human serum albumin sequential adsorption on preosteoblastic cell adhesion, *Biointerphases* 9(2) (2014) 029008.
- [71] E.M. Yazlovitskaya, O.M. Viquez, T.X. Tu, A. De Arcangelis, E. Georges-Labouesse, A. Sonnenberg, A. Pozzi, R. Zent, The laminin binding alpha 3 and alpha 6 integrins cooperate to promote epithelial cell adhesion and growth, *Matrix Biol* 77 (2019) 101-116.
- [72] K.F. Leong, C.M. Cheah, C.K. Chua, Solid freeform fabrication of three-dimensional scaffolds for engineering replacement tissues and organs, *Biomaterials* 24(13) (2003) 2363-2378.
- [73] A. Berdichevski, M.A. Birch, A.E. Markaki, Collagen scaffolds with tailored pore geometry for building three-dimensional vascular networks, *Mater Lett* 248 (2019) 93-96.
- [74] H. Shin, K. Zygourakis, M.C. Farach-Carson, M.J. Yaszemski, A.G. Mikos, Attachment, proliferation, and migration of marrow stromal osteoblasts cultured on biomimetic hydrogels modified with an osteopontin-derived peptide, *Biomaterials* 25(5) (2004) 895-906.
- [75] A. Spreafico, F. Chellini, B. Frediani, S. Niccolini, G. Bernardini, A. Rocchi, R. Marcolongo, M. Galeazzi, A. Santucci, Effect of Human Platelet Rich Plasma Releasates on Proliferation and Matrix Synthesis of Human Articular Chondrocytes Grown on a Polyglycolic

Acid-Based Biomaterial (Pga): Molecular, Proteomical and Immunofluorescence Analysis, *Osteoarthr Cartilage* 18 (2010) S85-S85.

[76] D.C. Ardila, E. Tamimi, F.L. Danford, D.G. Haskett, R.S. Kellar, T. Doetschman, J.P. Vande Geest, TGF beta 2 differentially modulates smooth muscle cell proliferation and migration in electrospun gelatin-fibrinogen constructs, *Biomaterials* 37 (2015) 164-173.

[77] S. Oughlis, S. Changotade, F. Poirier, A.M. Cieutat, G. Rohman, J. Peltzer, V. Migonney, J.J. Lataillade, D. Lutowski, Improved proliferation and osteogenic differentiation of human mesenchymal stem cells on a titanium biomaterial grafted with poly(sodium styrene sulphonate) and coated with a platelet-rich plasma proteins biofilm, *J Bioact Compat Pol* 31(6) (2016) 568-582.

[78] H.S. Shi, S.Y. Yang, S.H. Zeng, X. Liu, J. Zhang, J. Zhangb, T.T. Wu, X.L. Ye, T. Yu, C.R. Zhou, J.D. Ye, Enhanced angiogenesis of biodegradable iron-doped octacalcium phosphate/poly(lactic-co-glycolic acid) scaffold for potential cancerous bone regeneration, *Appl Mater Today* 15 (2019) 100-114.

[79] T. Kanjevac, C. Gustafson, A. Ivanovska, F. Ravanetti, A. Cacchioli, D. Bosnakovski, Inflammatory Cytokines and Biodegradable Scaffolds in Dental Mesenchymal Stem Cells Priming, *Curr Stem Cell Res T* 14(4) (2019) 320-326.

[80] T. Schilling, M. Bauer, C. Biskup, A. Haverich, T. Hassel, Engineering of biodegradable magnesium alloy scaffolds to stabilize biological myocardial grafts, *Biomed Eng-Biomed Te* 62(5) (2017) 493-504.

[81] N.J. Shah, M.L. Macdonald, Y.M. Beben, R.F. Padera, R.E. Samuel, P.T. Hammond, Tunable dual growth factor delivery from polyelectrolyte multilayer films, *Biomaterials* 32(26) (2011) 6183-93.

[82] M. Bouyer, R. Guillot, J. Lavaud, C. Plettinx, C. Olivier, V. Curry, J. Boutonnat, J.L. Coll, F. Peyrin, V. Jossierand, G. Bettega, C. Picart, Surface delivery of tunable doses of BMP-2 from an adaptable polymeric scaffold induces volumetric bone regeneration, *Biomaterials* 104 (2016) 168-81.

[83] B. Xia, Y.G. Lv, Dual-delivery of VEGF and NGF by emulsion electrospun nanofibrous scaffold for peripheral nerve regeneration, *Mat Sci Eng C-Mater* 82 (2018) 253-264.

[84] N. Bhardwaj, D. Devi, B.B. Mandal, Tissue-Engineered Cartilage: The Crossroads of Biomaterials, Cells and Stimulating Factors, *Macromol Biosci* 15(2) (2015) 153-182.

[85] H.C. Lima, J.V. Araujo, N.M. Neves, J.F. Mano, R.L. Reis, Cell encapsulation in thermoresponsive chitosan based hydrogels for cartilage tissue engineering, *Tissue Eng Pt A* 14(5) (2008) 709-710.

[86] G.A. Silva, O.P. Coutinho, P. Ducheyne, I.M. Shapiro, R.L. Reis, Starch-based microparticles as vehicles for the delivery of active platelet-derived growth factor, *Tissue Eng* 13(6) (2007) 1259-1268.

[87] D.M. Yoon, J.P. Fisher, Effects of exogenous IGF-1 delivery on the early expression of IGF-1 signaling molecules by alginate embedded chondrocytes, *Tissue Eng Pt A* 14(7) (2008) 1263-1273.

- [88] N. Nwe, T. Furuike, H. Tamura, Selection of a biopolymer based on attachment, morphology and proliferation of fibroblast NIH/3T3 cells for the development of a biodegradable tissue regeneration template: Alginate, bacterial cellulose and gelatin, *Process Biochem* 45(4) (2010) 457-466.
- [89] T.R. Chan, P.J. Stahl, Y. Li, S.M. Yu, Collagen-gelatin mixtures as wound model, and substrates for VEGF-mimetic peptide binding and endothelial cell activation, *Acta Biomater* 15 (2015) 164-172.
- [90] S. Mauquoy, C. Dupont-Gillain, Combination of collagen and fibronectin to design biomimetic interfaces: Do these proteins form layer-by-layer assemblies?, *Colloid Surface B* 147 (2016) 54-64.
- [91] T.K. Yoo, S.H. Han, J. Han, Protective effects of biodegradable collagen implants on thinned sclera after strabismus surgery: a paired-eye study, *J Aapos* 21(6) (2017) 467-471.
- [92] M. Ansari, S.S. Kordestani, S. Nazralizadeh, H. Eslami, Biodegradable Cell-Seeded Collagen Based Polymer Scaffolds for Wound Healing and Skin Reconstruction, *J Macromol Sci B* 57(2) (2018) 100-109.
- [93] Y.Y. Wei, W. Zeng, R. Wan, J. Wang, Q. Zhou, S.J. Qiu, S.R. Singh, Chondrogenic Differentiation of Induced Pluripotent Stem Cells from Osteoarthritic Chondrocytes in Alginate Matrix, *Eur Cells Mater* 23 (2012) 1-12.
- [94] D.H. Zhang, I.Y. Shadrin, J. Lam, H.Q. Xian, H.R. Snodgrass, N. Bursac, Tissue-engineered cardiac patch for advanced functional maturation of human ESC-derived cardiomyocytes, *Biomaterials* 34(23) (2013) 5813-5820.
- [95] A. Martins, E.D. Pinho, S. Faria, I. Pashkuleva, A.P. Marques, R.L. Reis, N.M. Neves, Surface Modification of Electrospun Polycaprolactone Nanofiber Meshes by Plasma Treatment to Enhance Biological Performance, *Small* 5(10) (2009) 1195-1206.
- [96] Y.C. Liu, T. Nelson, J. Chakroff, B. Cromeens, J. Johnson, J. Lannutti, G.E. Besner, Comparison of polyglycolic acid, polycaprolactone, and collagen as scaffolds for the production of tissue engineered intestine, *J Biomed Mater Res B* 107(3) (2019) 750-760.
- [97] S. Miroshnichenko, V. Timofeeva, E. Permyakova, S. Ershov, P. Kiryukhantsev-Korneev, E. Dvorakova, D.V. Shtansky, L. Zajickova, A. Solovieva, A. Manakhov, Plasma-Coated Polycaprolactone Nanofibers with Covalently Bonded Platelet-Rich Plasma Enhance Adhesion and Growth of Human Fibroblasts, *Nanomaterials-Basel* 9(4) (2019).
- [98] J.L. Chen, B. Chu, B.S. Hsiao, Mineralization of hydroxyapatite in electrospun nanofibrous poly(L-lactic acid) scaffolds, *Journal of Biomedical Materials Research Part A* 79a(2) (2006) 307-317.
- [99] M. Hindie, M.C. Degat, F. Gaudiere, O. Gallet, P.R. Van Tassel, E. Pauthe, Pre-osteoblasts on poly(L-lactic acid) and silicon oxide: Influence of fibronectin and albumin adsorption, *Acta Biomater* 7(1) (2011) 387-394.
- [100] A.E. Swilem, M. Lehocky, P. Humpolicek, Z. Kucekova, I. Junkar, M. Mozetic, A.A. Hamed, I. Novak, Developing a biomaterial interface based on poly(lactic acid) via plasma-

assisted covalent anchorage of D-glucosamine and its potential for tissue regeneration, *Colloid Surface B* 148 (2016) 59-65.

[101] H. Nakao, R.D. Jacquet, M. Shasti, N. Isogai, A.S. Murthy, W.J. Landis, Long-Term Comparison between Human Normal Conchal and Microtia Chondrocytes Regenerated by Tissue Engineering on Nanofiber Polyglycolic Acid Scaffolds, *Plast Reconstr Surg* 139(4) (2017) 911e-921e.

[102] A. Asti, L. Gioglio, Natural and synthetic biodegradable polymers: different scaffolds for cell expansion and tissue formation, *Int J Artif Organs* 37(3) (2014) 187-205.

[103] M.F. Meek, J.H. Coert, US Food and Drug Administration/Conformit Europe-approved absorbable nerve conduits for clinical repair of peripheral and cranial nerves, *Ann Plast Surg* 60(1) (2008) 110-6.

[104] S.R. Baker, S. Banerjee, K. Bonin, M. Guthold, Determining the mechanical properties of electrospun poly-epsilon-caprolactone (PCL) nanofibers using AFM and a novel fiber anchoring technique, *Mat Sci Eng C-Mater* 59 (2016) 203-212.

[105] Q.P. Pham, U. Sharma, A.G. Mikos, Electrospinning of polymeric nanofibers for tissue engineering applications: A review, *Tissue Eng* 12(5) (2006) 1197-1211.

[106] L.A. Smith, P.X. Ma, Nano-fibrous scaffolds for tissue engineering, *Colloid Surface B* 39(3) (2004) 125-131.

[107] C.L. Casper, J.S. Stephens, N.G. Tassi, D.B. Chase, J.F. Rabolt, Controlling surface morphology of electrospun polystyrene fibers: Effect of humidity and molecular weight in the electrospinning process, *Macromolecules* 37(2) (2004) 573-578.

[108] J.V. Araujo, A. Martins, I.B. Leonor, E.D. Pinho, R.L. Reis, N.M. Neves, Surface controlled biomimetic coating of polycaprolactone nanofiber meshes to be used as bone extracellular matrix analogues, *J Biomat Sci-Polym E* 19(10) (2008) 1261-1278.

[109] M.A. da Silva, A. Crawford, J. Mundy, A. Martins, J.V. Araujo, P.V. Hatton, R.L. Reis, N.M. Neves, Evaluation of extracellular matrix formation in polycaprolactone and starch-compounded polycaprolactone nanofiber meshes when seeded with bovine articular chondrocytes, *Tissue Eng Part A* 15(2) (2009) 377-85.

[110] Z. Rezvani, J.R. Venugopal, A.M. Urbanska, D.K. Mills, S. Ramakrishna, M. Mozafari, A bird's eye view on the use of electrospun nanofibrous scaffolds for bone tissue engineering: Current state-of-the-art, emerging directions and future trends, *Nanomedicine* 12(7) (2016) 2181-2200.

[111] M.L.A. da Silva, A. Martins, A.R. Costa-Pinto, P. Costa, S. Faria, M. Gomes, R.L. Reis, N.M. Neves, Cartilage Tissue Engineering Using Electrospun PCL Nanofiber Meshes and MSCs, *Biomacromolecules* 11(12) (2010) 3228-3236.

[112] N. Monteiro, A. Martins, R. Pires, S. Faria, N.A. Fonseca, J.N. Moreira, R.L. Reisa, N.M. Neves, Immobilization of bioactive factor-loaded liposomes on the surface of electrospun nanofibers targeting tissue engineering, *Biomater Sci-Uk* 2(9) (2014) 1195-1209.

- [113] N. Monteiro, D. Ribeiro, A. Martins, S. Faria, N.A. Fonseca, J.N. Moreira, R.L. Reis, N.M. Neves, Instructive Nanofibrous Scaffold Comprising Runt-Related Transcription Factor 2 Gene Delivery for Bone Tissue Engineering, *Acs Nano* 8(8) (2014) 8082-8094.
- [114] J.V. Araujo, C. Cunha-Reis, G. Gogniat, Y. Yang, N. Ashammakhi, R.L. Reis, A.J. El Haj, N.M. Neves, Dynamic studies of biomimetic coated polycaprolactone nanofiber meshes as bone extracellular matrix analogues, *Tissue Eng Pt A* 14(5) (2008) 723-724.
- [115] A. Guimaraes, A. Martins, E.D. Pinho, S. Faria, R.L. Reis, N.M. Neves, Solving cell infiltration limitations of electrospun nanofiber meshes for tissue engineering applications, *Nanomedicine* 5(4) (2010) 539-554.
- [116] A. Martins, A.R.C. Duarte, S. Faria, A.P. Marques, R.L. Reis, N.M. Neves, Osteogenic induction of hBMSCs by electrospun scaffolds with dexamethasone release functionality, *Biomaterials* 31(22) (2010) 5875-5885.
- [117] A. Martins, W. Gang, E.D. Pinho, E. Rebollar, S. Chiussi, R.L. Reis, B. Leon, N.M. Neves, Surface modification of a biodegradable composite by UV laser ablation: in vitro biological performance, *J Tissue Eng Regen M* 4(6) (2010) 444-453.
- [118] N. Monteiro, A. Martins, D. Ribeiro, S. Faria, N.A. Fonseca, J.N. Moreira, R.L. Reis, N.M. Neves, On the use of dexamethasone-loaded liposomes to induce the osteogenic differentiation of human mesenchymal stem cells, *J Tissue Eng Regen M* 9(9) (2015) 1056-1066.
- [119] E. Bacelo, M.A. da Silva, C. Cunha, S. Faria, A. Carvalho, R.L. Reis, A. Martins, N.M. Neves, Biofunctional Nanofibrous Substrate for Local TNF-Capturing as a Strategy to Control Inflammation in Arthritic Joints, *Nanomaterials-Basel* 9(4) (2019).
- [120] J.F. Piai, M.A. da Silva, A. Martins, A.B. Torres, S. Faria, R.L. Reis, E.C. Muniz, N.M. Neves, Chondroitin sulfate immobilization at the surface of electrospun nanofiber meshes for cartilage tissue regeneration approaches, *Appl Surf Sci* 403 (2017) 112-125.
- [121] N. Monteiro, M. Martins, A. Martins, N.A. Fonseca, J.N. Moreira, R.L. Reis, N.M. Neves, Antibacterial activity of chitosan nanofiber meshes with liposomes immobilized releasing gentamicin, *Acta Biomater* 18 (2015) 196-205.
- [122] A. Shekaran, A.J. Garcia, Nanoscale engineering of extracellular matrix-mimetic bioadhesive surfaces and implants for tissue engineering, *Bba-Gen Subjects* 1810(3) (2011) 350-360.
- [123] M.H. Kim, K. Roy, Ligand-Functionalized Biomaterial Surfaces: Controlled Regulation of Signaling Pathways to Direct Stem Cell Differentiation, *Biological Interactions on Materials Surfaces: Understanding and Controlling Protein, Cell, and Tissue Responses* (2009) 157-171.
- [124] C.J. Bishop, J. Kim, J.J. Green, Biomolecule Delivery to Engineer the Cellular Microenvironment for Regenerative Medicine, *Annals of Biomedical Engineering* 42(7) (2014) 1557-1572.
- [125] F.M. Chen, M. Zhang, Z.F. Wu, Toward delivery of multiple growth factors in tissue engineering, *Biomaterials* 31(24) (2010) 6279-6308.

- [126] T. Rozario, D.W. DeSimone, The extracellular matrix in development and morphogenesis: A dynamic view, *Dev Biol* 341(1) (2010) 126-140.
- [127] C. Wai Wong, D.E. Dye, D.R. Coombe, The role of immunoglobulin superfamily cell adhesion molecules in cancer metastasis, *Int J Cell Biol* 2012 (2012) 340296.
- [128] M.M. Mendoza, E. Graham, M. Petroll, Fibronectin as a Regulator of Collective Migration and Clustering of Corneal Fibroblasts in 3D Fibrin Matrices, *Invest Ophth Vis Sci* 56(7) (2015).
- [129] P. Formentin, U. Catalan, L. Pol, S. Fernandez-Castillejo, R. Sola, L.F. Marsal, Collagen and fibronectin surface modification of nanoporous anodic alumina and macroporous silicon for endothelial cell cultures, *J Biol Eng* 12 (2018) 21.
- [130] E. Colombo, F. Calcaterra, M. Cappelletti, D. Mavilio, S. Della Bella, Comparison of Fibronectin and Collagen in Supporting the Isolation and Expansion of Endothelial Progenitor Cells from Human Adult Peripheral Blood, *Plos One* 8(6) (2013) e66734.
- [131] A.B. Faia-Torres, T. Goren, T.O. Ihalainen, S. Guimond-Lischer, M. Charnley, M. Rottmar, K. Maniura-Weber, N.D. Spencer, R.L. Reis, M. Textor, N.M. Neves, Regulation of Human Mesenchymal Stem Cell Osteogenesis by Specific Surface Density of Fibronectin: a Gradient Study, *Acs Appl Mater Inter* 7(4) (2015) 2367-2375.
- [132] R. Pankov, K.M. Yamada, Fibronectin at a glance, *J Cell Sci* 115(20) (2002) 3861-3863.
- [133] G.C. Li, P. Yang, X. Guo, N. Huang, R. Shen, An in vitro evaluation of inflammation response of titanium functionalized with heparin/fibronectin complex, *Cytokine* 56(2) (2011) 208-217.
- [134] L. Baugh, V. Vogel, Structural changes of fibronectin adsorbed to model surfaces probed by fluorescence resonance energy transfer, *Journal of Biomedical Materials Research Part A* 69a(3) (2004) 525-534.
- [135] Y.X. Tian, H.L. Liu, B.W. Sheldon, T.J. Webster, S.C. Yang, H.L. Yang, L. Yang, Surface energy-mediated fibronectin adsorption and osteoblast responses on nanostructured diamond, *J Mater Sci Technol* 35(5) (2019) 817-823.
- [136] L. Parisi, A. Toffoli, M.G. Bianchi, C. Bergonzi, A. Bianchera, R. Bettini, L. Elviri, G.M. Macaluso, Functional Fibronectin Adsorption on Aptamer-Doped Chitosan Modulates Cell Morphology by Integrin-Mediated Pathway, *Materials* 12(5) (2019).
- [137] V. Montano-Machado, L. Hugoni, S. Diaz-Rodriguez, R. Tolouei, P. Chevallier, E. Pauthe, D. Mantovani, A comparison of adsorbed and grafted fibronectin coatings under static and dynamic conditions, *Phys Chem Chem Phys* 18(35) (2016) 24704-24712.
- [138] Y.C. Chang, K.N. Ho, S.W. Feng, H.M. Huang, C.H. Chang, C.T. Lin, N.C. Teng, Y.H. Pan, W.J. Chang, Fibronectin-Grafted Titanium Dental Implants: An In Vivo Study, *Biomed Res Int* 2016 (2016) 2414809.
- [139] K. Bhadriraju, J.S. Hong, S.P. Lund, D.R. Reyes, Fibronectin in Layer-by-Layer Assembled Films Switches Tumor Cells between 2D and 3D Morphology, *Acs Biomater Sci Eng* 3(10) (2017) 2559-2569.

- [140] W.S. To, K.S. Midwood, Plasma and cellular fibronectin: distinct and independent functions during tissue repair, *Fibrogenesis Tissue* 4 (2011).
- [141] M.M. Martino, M. Mochizuki, D.A. Rothenfluh, S.A. Rempel, J.A. Hubbell, T.H. Barker, Controlling integrin specificity and stem cell differentiation in 2D and 3D environments through regulation of fibronectin domain stability, *Biomaterials* 30(6) (2009) 1089-1097.
- [142] N. Ogura, M. Kawada, W.J. Chang, Q. Zhang, S.Y. Lee, T. Kondoh, Y. Abiko, Differentiation of the human mesenchymal stem cells derived from bone marrow and enhancement of cell attachment by fibronectin, *J Oral Sci* 46(4) (2004) 207-13.
- [143] Y. Wang, L. Zhao, C. Smas, H.S. Sul, Pref-1 interacts with fibronectin to inhibit adipocyte differentiation, *Mol Cell Biol* 30(14) (2010) 3480-92.
- [144] C. Jiang, P. Ma, B.P. Ma, Z.H. Wu, G.X. Qiu, X.L. Su, Z.N. Xia, Z.X. Ye, Y.P. Wang, Plasma-Derived Fibronectin Stimulates Chondrogenic Differentiation of Human Subchondral Cortico-Spongious Progenitor Cells in Late-Stage Osteoarthritis, *Int J Mol Sci* 16(8) (2015) 19477-19489.
- [145] P. Singh, J.E. Schwarzbauer, Fibronectin and stem cell differentiation - lessons from chondrogenesis, *J Cell Sci* 125(Pt 16) (2012) 3703-12.
- [146] M.M. Thibault, C.D. Hoemann, M.D. Buschmann, Fibronectin, vitronectin, and collagen I induce chemotaxis and haptotaxis of human and rabbit mesenchymal stem cells in a standardized transmembrane assay, *Stem Cells Dev* 16(3) (2007) 489-502.
- [147] Y. Kang, A.I. Georgiou, R.J. MacFarlane, M.E. Klontzas, M. Heliotis, E. Tsiridis, A. Mantalaris, Fibronectin stimulates the osteogenic differentiation of murine embryonic stem cells, *J Tissue Eng Regen Med* 11(7) (2017) 1929-1940.
- [148] F. Mohamadyar-Toupkanlou, E. Vasheghani-Farahani, H. Hanaee-Ahvaz, M. Soleimani, M. Dodel, P. Havasi, A. Ardeshiryajimi, E.S. Taherzadeh, Osteogenic Differentiation of MSCs on Fibronectin-Coated and nHA-Modified Scaffolds, *ASAIO J* 63(5) (2017) 684-691.
- [149] S. Vogel, S. Arnoldini, S. Moller, M. Schnabelrauch, U. Hempel, Sulfated hyaluronan alters fibronectin matrix assembly and promotes osteogenic differentiation of human bone marrow stromal cells, *Sci Rep* 6 (2016) 36418.
- [150] I.M. Bjorge, S.Y. Kim, J.F. Mano, B. Kalionis, W. Chrzanowski, Extracellular vesicles, exosomes and shedding vesicles in regenerative medicine - a new paradigm for tissue repair, *Biomater Sci-Uk* 6(1) (2017) 60-78.
- [151] M.Z. Ratajczak, M. Kucia, T. Jadczyk, N.J. Greco, W. Wojakowski, M. Tendera, J. Ratajczak, Pivotal role of paracrine effects in stem cell therapies in regenerative medicine: can we translate stem cell-secreted paracrine factors and microvesicles into better therapeutic strategies?, *Leukemia* 26(6) (2012) 1166-1173.
- [152] P.J. Quesenberry, J. Aliotta, M.C. Deregibus, G. Camussi, Role of extracellular RNA-carrying vesicles in cell differentiation and reprogramming, *Stem Cell Res Ther* 6 (2015).

- [153] M. Gnechi, H.M. He, O.D. Liang, L.G. Melo, F. Morello, H. Mu, N. Noiseux, L.N. Zhang, R.E. Pratt, J.S. Ingwall, V.J. Dzau, Paracrine action accounts for marked protection of ischemic heart by Akt-modified mesenchymal stem cells, *Nat Med* 11(4) (2005) 367-368.
- [154] L. Timmers, S.K. Lim, F. Arslan, J.S. Armstrong, I.E. Hofer, P.A. Doevendans, J.J. Piek, R.M. El Oakley, A. Choo, C.N. Lee, G. Pasterkamp, D.P.V. de Kleijn, Reduction of myocardial infarct size by human mesenchymal stem cell conditioned medium, *Stem Cell Res* 1(2) (2008) 129-137.
- [155] X.F. Xia, P.W.Y. Chiu, P.K. Lam, W.C. Chin, E.K.W. Ng, J.Y.W. Lau, Secretome from hypoxia-conditioned adipose-derived mesenchymal stem cells promotes the healing of gastric mucosal injury in a rodent model, *Bba-Mol Basis Dis* 1864(1) (2018) 178-188.
- [156] M.L.A. da Silva, A.R. Costa-Pinto, A. Martins, V.M. Correlo, P. Sol, M. Bhattacharya, S. Faria, R.L. Reis, N.M. Neves, Conditioned medium as a strategy for human stem cells chondrogenic differentiation, *J Tissue Eng Regen M* 9(6) (2015) 714-723.
- [157] Y. Nakamura, S. Miyaki, H. Ishitobi, S. Matsuyama, T. Nakasa, N. Kamei, T. Akimoto, Y. Higashi, M. Ochi, Mesenchymal-stem-cell-derived exosomes accelerate skeletal muscle regeneration, *Febs Lett* 589(11) (2015) 1257-1265.
- [158] M. Martins, D. Ribeiro, A. Martins, R.L. Reis, N.M. Neves, Extracellular Vesicles Derived from Osteogenically Induced Human Bone Marrow Mesenchymal Stem Cells Can Modulate Lineage Commitment, *Stem Cell Rep* 6(3) (2016) 284-291.
- [159] A. Shabbir, A. Cox, L. Rodriguez-Menocal, M. Salgado, E. Van Badiavas, Mesenchymal Stem Cell Exosomes Induce Proliferation and Migration of Normal and Chronic Wound Fibroblasts, and Enhance Angiogenesis In Vitro, *Stem Cells and Development* 24(14) (2015) 1635-1647.
- [160] S. Zhang, W.C. Chu, R.C. Lai, S.K. Lim, J.H.P. Hui, W.S. Toh, Exosomes derived from human embryonic mesenchymal stem cells promote osteochondral regeneration, *Osteoarthr Cartilage* 24(12) (2016) 2135-2140.
- [161] M. Khan, E. Nickoloff, T. Abramova, J. Johnson, S.K. Verma, P. Krishnamurthy, A.R. Mackie, E. Vaughan, V.N.S. Garikipati, C. Benedict, V. Ramirez, E. Lambers, A. Ito, E. Gao, S. Misener, T. Luongo, J. Elrod, G.J. Qin, S.R. Houser, W.J. Koch, R. Kishore, Embryonic Stem Cell-Derived Exosomes Promote Endogenous Repair Mechanisms and Enhance Cardiac Function Following Myocardial Infarction, *Circ Res* 117(1) (2015) 52-64.
- [162] S.Y. Kim, M.V. Joglekar, A.A. Hardikar, T.H. Phan, D. Khanal, P. Tharkar, C. Limantoro, J. Johnson, B. Kalionis, W. Chrzanowski, Placenta stem/stromal cell-derived extracellular vesicles for potential use in lung repair, *Proteomics* (2019) e1800166.
- [163] F.F. Cruz, P.R.M. Rocco, Stem-cell extracellular vesicles and lung repair, *Stem Cell Investig* 4 (2017) 78.
- [164] F.J. Vizoso, N. Eiro, S. Cid, J. Schneider, R. Perez-Fernandez, Mesenchymal Stem Cell Secretome: Toward Cell-Free Therapeutic Strategies in Regenerative Medicine, *Int J Mol Sci* 18(9) (2017).



- [165] Y. Ito, Tissue engineering by immobilized growth factors, *Mat Sci Eng C-Bio S* 6(4) (1998) 267-274.
- [166] I. Andia, M. Sanchez, N. Maffulli, Basic Science: Molecular and Biological Aspects of Platelet-Rich Plasma Therapies, *Oper Tech Orthop* 22(1) (2012) 3-9.
- [167] L. Krishnamoorthy, H.L. Morris, K.G. Harding, Specific growth factors and the healing of chronic wounds, *J Wound Care* 10(5) (2001) 173-8.
- [168] K. Tatsuyama, Y. Maezawa, H. Baba, Y. Imamura, M. Fukuda, Expression of various growth factors for cell proliferation and cytodifferentiation during fracture repair of bone, *Eur J Histochem* 44(3) (2000) 269-78.
- [169] N.T. Bennett, G.S. Schultz, Growth-Factors and Wound-Healing .2. Role in Normal and Chronic Wound-Healing, *Am J Surg* 166(1) (1993) 74-81.
- [170] F. Zarei, M. Soleimanejad, Role of growth factors and biomaterials in wound healing, *Artif Cells Nanomed Biotechnol* 46(sup1) (2018) 906-911.
- [171] T. Velnar, T. Bailey, V. Smrkolj, The wound healing process: an overview of the cellular and molecular mechanisms, *J Int Med Res* 37(5) (2009) 1528-42.
- [172] R.F. Diegelmann, M.C. Evans, Wound healing: an overview of acute, fibrotic and delayed healing, *Front Biosci* 9 (2004) 283-9.
- [173] K. Schmidt-Bleek, H. Schell, N. Schulz, P. Hoff, C. Perka, F. Buttgerit, H.D. Volk, J. Lienau, G.N. Duda, Inflammatory phase of bone healing initiates the regenerative healing cascade, *Cell Tissue Res* 347(3) (2012) 567-73.
- [174] T. Van Bergen, S.V. Van de Velde, E. Vandewalle, L. Moons, I. Stalmans, Improving patient outcomes following glaucoma surgery: state of the art and future perspectives, *Clin Ophthalmol* 8 (2014) 857-867.
- [175] P. Carmeliet, R.K. Jain, Molecular mechanisms and clinical applications of angiogenesis, *Nature* 473(7347) (2011) 298-307.
- [176] A.T. Grazul-Bilska, M.L. Johnson, J.J. Bilski, D.A. Redmer, L.P. Reynolds, A. Abdullah, K.M. Abdullah, Wound healing: the role of growth factors, *Drugs Today (Barc)* 39(10) (2003) 787-800.
- [177] H.B. Fan, H.R. Tao, Y.N. Wu, Y.Y. Hu, Y.N. Yan, Z.J. Luo, TGF-beta 3 immobilized PLGA-gelatin/chondroitin sulfate/hyaluronic acid hybrid scaffold for cartilage regeneration, *Journal of Biomedical Materials Research Part A* 95a(4) (2010) 982-992.
- [178] L. Longobardi, L. O'Rear, S. Aakula, B. Johnstone, K. Shimer, A. Chytil, W.A. Horton, H.L. Moses, A. Spagnoli, Effect of IGF-1 in the chondrogenesis of bone marrow mesenchymal stem cells in the presence or absence of TGF-beta signaling, *J Bone Miner Res* 21(4) (2006) 626-636.
- [179] A. Watarai, L. Schirmer, S. Thones, U. Freudenberg, C. Werner, J.C. Simon, U. Anderegg, TGF beta functionalized starPEG-heparin hydrogels modulate human dermal fibroblast growth and differentiation, *Acta Biomater* 25 (2015) 65-75.

- [180] D.C. Ardila, E. Tamimi, T. Doetschman, W.R. Wagner, J.P.V. Geest, Modulating smooth muscle cell response by the release of TGF beta 2 from tubular scaffolds for vascular tissue engineering, *Journal of Controlled Release* 299 (2019) 44-52.
- [181] L.J. Chen, C. Chen, X.Y. Qiao, K. Yu, L.Z. Xie, J. Cao, B.L. Liu, Y. Yan, Effect of porous titanium coated with IGF-1 and TGF-beta(1) loaded gelatin microsphere on function of MG63 cells, *T Nonferr Metal Soc* 25(9) (2015) 2974-2985.
- [182] D.G.M. Molin, M.C. DeRuiter, T. Doetschman, H.M. Sucov, R.E. Poelmann, A.C. Gittenberger-de Groot, TGF beta 2 does not affect neural crest cell migration but is a key player in vascular remodeling during embryogenesis, *Cardiovascular Development and Congenital Malformations: Molecular and Genetic Mechanisms* (2005) 148-149.
- [183] R. Steer, C. Kielty, Latent TGF-beta-binding protein-1 (LTBP-1) interactions with heparin/heparan sulphate, *Int J Exp Pathol* 94(1) (2013) A40-A41.
- [184] S.F. Tellado, S. Chiera, W. Bonani, P.S.P. Poh, C. Migliaresi, A. Motta, E.R. Balmayor, M. van Griensven, Heparin functionalization increases retention of TGF-beta 2 and GDF5 on biphasic silk fibroin scaffolds for tendon/ligament-to-bone tissue engineering, *Acta Biomater* 72 (2018) 150-166.
- [185] F. Yin, J.F. Cai, W. Zen, Y.H. Wei, W. Zhou, F. Yuan, S.R. Singh, Y.Y. Wei, Cartilage Regeneration of Adipose-Derived Stem Cells in the TGF-beta 1-Immobilized PLGA-Gelatin Scaffold, *Stem Cell Rev Rep* 11(3) (2015) 453-459.
- [186] J.E. Puche, I. Castilla-Cortazar, Human conditions of insulin-like growth factor-I (IGF-I) deficiency, *J Transl Med* 10 (2012) 224.
- [187] K. Bergen, M. Frodin, C. von Gertten, A.C. Sandberg-Nordqvist, M.K. Skold, Neurite Growth and Polarization on Vitronectin Substrate after in Vitro Trauma is not Enhanced after IGF Treatment, *Brain Sci* 8(8) (2018).
- [188] M. Cucchiaroni, H. Madry, Overexpression of human IGF-I via direct rAAV-mediated gene transfer improves the early repair of articular cartilage defects in vivo, *Gene Ther* 21(9) (2014) 811-819.
- [189] T. Geetha, S.D. Rege, S.E. Mathews, S.O. Meakin, M.F. White, J.R. Babu, Nerve growth factor receptor TrkA, a new receptor in insulin signaling pathway in PC12 cells, *J Biol Chem* 288(33) (2013) 23807-13.
- [190] D. Torella, M. Rota, D. Nurzynska, E. Musso, A. Monsen, I. Shiraishi, E. Zias, K. Walsh, A. Rosenzweig, M.A. Sussman, K. Urbanek, B. Nadal-Ginard, J. Kajstura, P. Anversa, A. Leri, Cardiac stem cell and myocyte aging, heart failure, and insulin-like growth factor-1 overexpression, *Circ Res* 94(4) (2004) 514-524.
- [191] N. Winn, A. Paul, A. Musaro, N. Rosenthal, Insulin-like growth factor isoforms in skeletal muscle aging, regeneration, and disease, *Cold Spring Harb Sym* 67 (2002) 507-518.
- [192] Y.H. Yang, G.A. Barabino, Differential Morphology and Homogeneity of Tissue-Engineered Cartilage in Hydrodynamic Cultivation with Transient Exposure to Insulin-Like Growth Factor-1 and Transforming Growth Factor-beta 1, *Tissue Eng Pt A* 19(21-22) (2013) 2349-2360.

- [193] T.N. da Silva, R.P. Goncalves, C.L. Rocha, B.S. Archanjo, C.A.G. Barboza, M.B.R. Pierre, F. Reynaud, P.H.D. Picciani, Controlling burst effect with PLA/PVA coaxial electrospun scaffolds loaded with BMP-2 for bone guided regeneration, *Mat Sci Eng C-Mater* 97 (2019) 602-612.
- [194] S.Y. Hu, H.B. Chen, X.F. Zhou, G. Chen, K. Hu, Y. Cheng, L.L. Wang, F.M. Zhang, Thermally induced self-agglomeration 3D scaffolds with BMP-2-loaded core-shell fibers for enhanced osteogenic differentiation of rat adipose-derived stem cells, *Int J Nanomed* 13 (2018) 4145-4155.
- [195] P.T.S. Kumar, S. Hashimi, S. Saifzadeh, S. Ivanovski, C. Vaquette, Additively manufactured biphasic construct loaded with BMP-2 for vertical bone regeneration: A pilot study in rabbit, *Mat Sci Eng C-Mater* 92 (2018) 554-564.
- [196] C.F. Lai, S.L. Cheng, alpha v beta integrins play an essential role in BMP-2 induction of osteoblast differentiation, *J Bone Miner Res* 20(2) (2005) 330-340.
- [197] R. Nishimura, K. Hata, T. Matsubara, M. Wakabayashi, T. Yoneda, Regulation of bone and cartilage development by network between BMP signalling and transcription factors, *Journal of Biochemistry* 151(3) (2012) 247-254.
- [198] S. Odabas, G. Feichtinger, P. Korkusuz, I. Inci, E. Bilgic, A.S. Yar, T. Cavusoglu, S. Menevse, I. Vargel, E. Piskin, BMP-7 expressing genetically modified primary chondrocytes in cryogel scaffolds for rabbit auricular cartilage repair, *J Tissue Eng Regen M* 6 (2012) 67-67.
- [199] A.G. Sclar, S.P. Best, The Combined Use of rhBMP-2/ACS, Autogenous Bone Graft, a Bovine Bone Mineral Biomaterial, Platelet-Rich Plasma, and Guided Bone Regeneration at Nonsubmerged Implant Placement for Supracrestal Bone Augmentation. A Case Report, *Int J Oral Max Impl* 28(5) (2013) E272-E276.
- [200] G.D. Sierra-Garcia, R. Castro-Rios, A. Gonzalez-Horta, J. Lara-Arias, A. Chavez-Montes, Bone morphogenetic proteins (BMP): clinical application for reconstruction of bone defects, *Gac Med Mex* 152(3) (2016) 381-385.
- [201] Q. Wang, Y.X. Zhang, B. Li, L. Chen, Controlled dual delivery of low doses of BMP-2 and VEGF in a silk fibroin-nanohydroxyapatite scaffold for vascularized bone regeneration, *J Mater Chem B* 5(33) (2017) 6963-6972.
- [202] J.P. Wu, L.L. Li, C. Fu, F. Yang, Z.X. Jiao, X.C. Shi, Y. Ito, Z.L. Wang, Q.Y. Liu, P.B. Zhang, Micro-porous polyetheretherketone implants decorated with BMP-2 via phosphorylated gelatin coating for enhancing cell adhesion and osteogenic differentiation, *Colloid Surface B* 169 (2018) 233-241.
- [203] P.Y. Zhou, J.H. Wu, Y. Xia, Loading BMP-2 on nanostructured hydroxyapatite microspheres for rapid bone regeneration (vol 13, pg 4083, 2018), *Int J Nanomed* 14 (2019) 2753-2753.
- [204] P.Y. Zhou, J.H. Wu, Y. Xia, Y. Yuan, H.Y. Zhang, S.G. Xu, K.L. Lin, Loading BMP-2 on nanostructured hydroxyapatite microspheres for rapid bone regeneration, *Int J Nanomed* 13 (2018) 4083-4092.

- [205] A.C. Carreira, F.H. Lojudice, E. Halcsik, R.D. Navarro, M.C. Sogayar, J.M. Granjeiro, Bone Morphogenetic Proteins Facts, Challenges, and Future Perspectives, *J Dent Res* 93(4) (2014) 335-345.
- [206] C.H. Cheng, Y.H. Lai, Y.W. Chen, C.H. Yao, K.Y. Chen, Immobilization of bone morphogenetic protein-2 to gelatin/avidin-modified hydroxyapatite composite scaffolds for bone regeneration, *J Biomater Appl* 33(9) (2019) 1147-1156.
- [207] D.W. Ham, E.C. Jang, T.I. Son, T.J. Lee, K.S. Song, Photo-immobilization of bone morphogenetic protein-2 using azidophenyl gelatin on a collagen sheet enhances osteogenesis in a rat calvarial defect model, *J Ind Eng Chem* 40 (2016) 177-184.
- [208] A.R. Poynton, J.M. Lane, Safety profile for the clinical use of bone morphogenetic proteins in the spine, *Spine* 27(16) (2002) S40-S48.
- [209] M. Orth, A.K. Shenar, C. Scheuer, B.J. Braun, S.C. Herath, J.H. Holstein, T. Histing, X.H. Yu, W.L. Murphy, T. Pohlemann, M.W. Laschke, M.D. Menger, VEGF-loaded mineral-coated microparticles improve bone repair and are associated with increased expression of epo and RUNX-2 in murine non-unions, *J Orthop Res* 37(4) (2019) 821-831.
- [210] T. Taguchi, A. Kishida, M. Akashi, I. Maruyama, Immobilization of human vascular endothelial growth factor (VEGF165) onto biomaterials: An evaluation of the biological activity of immobilized VEGF165, *J Bioact Compat Pol* 15(4) (2000) 309-320.
- [211] B.X. Wang, X.G. Lv, S.Y. Chen, Z. Li, J.J. Yao, X.F. Peng, C. Feng, Y.M. Xu, H.P. Wang, Bacterial cellulose/gelatin scaffold loaded with VEGF-silk fibroin nanoparticles for improving angiogenesis in tissue regeneration, *Cellulose* 24(11) (2017) 5013-5024.
- [212] J.L. Zhou, J.L. Ding, Z.G. Zhu, J.J. Xu, Y.P. Yi, Y. Li, H.X. Fan, S.H. Bai, J.S. Yang, Y.H. Tang, X. Dong, N.G. Dong, Surface biofunctionalization of the decellularized porcine aortic valve with VEGF-loaded nanoparticles for accelerating endothelialization, *Mat Sci Eng C-Mater* 97 (2019) 632-643.
- [213] Y. Hou, L. Jia, Y. Zhang, W. Ji, H. Li, Activation of the NGF/TrkA signaling pathway attenuates diabetic erectile dysfunction, *Oncotarget* 8(62) (2017) 105692-105702.
- [214] L. Li, G.Y. Li, Y.Y. Dong, Y.L. Ye, Electroacupuncture accelerates peripheral nerve regeneration via enhancement of BDNF, NGF, and GAP43 in rats, *Int J Clin Exp Med* 12(5) (2019) 4904-4911.
- [215] R. Li, Y.Y. Li, Y.Q. Wu, Y.Z. Zhao, H.W. Chen, Y. Yuan, K. Xu, H.Y. Zhang, Y.F. Lu, J. Wang, X.K. Li, X.F. Jia, J. Xiao, Heparin-Poloxamer Thermosensitive Hydrogel Loaded with bFGF and NGF Enhances Peripheral Nerve Regeneration in Diabetic Rats, *Biomaterials* 168 (2018) 24-37.
- [216] Q.J. Yan, Y.X. Yin, B.B. Li, Use new PLGL-RGD-NGF nerve conduits for promoting peripheral nerve regeneration, *Biomed Eng Online* 11 (2012) 36.
- [217] I.G. Kim, S. Piao, J.Y. Lee, S.H. Hong, T.K. Hwang, S.W. Kim, C.S. Kim, J.C. Ra, I. Noh, J.Y. Lee, Effect of an Adipose-Derived Stem Cell and Nerve Growth Factor-Incorporated Hydrogel on Recovery of Erectile Function in a Rat Model of Cavernous Nerve Injury, *Tissue Eng Pt A* 19(1-2) (2013) 14-23.

- [218] H. Zhang, F. Wu, X. Kong, J. Yang, H. Chen, L. Deng, Y. Cheng, L. Ye, S. Zhu, X. Zhang, Z. Wang, H. Shi, X. Fu, X. Li, H. Xu, L. Lin, J. Xiao, Nerve growth factor improves functional recovery by inhibiting endoplasmic reticulum stress-induced neuronal apoptosis in rats with spinal cord injury, *J Transl Med* 12 (2014) 130.
- [219] S. Murakami, Periodontal tissue regeneration by signaling molecule(s): what role does basic fibroblast growth factor (FGF-2) have in periodontal therapy?, *Periodontol* 2000 56(1) (2011) 188-208.
- [220] L.F. Mendes, H. Katagiri, W.L. Tam, Y.C. Chai, L. Geris, S.J. Roberts, F.P. Luyten, Advancing osteochondral tissue engineering: bone morphogenetic protein, transforming growth factor, and fibroblast growth factor signaling drive ordered differentiation of periosteal cells resulting in stable cartilage and bone formation in vivo, *Stem Cell Res Ther* 9(1) (2018) 42.
- [221] H.P. Tan, Y.H. Gong, L.H. Lao, Z.W. Mao, C.Y. Gao, Gelatin/chitosan/hyaluronan ternary complex scaffold containing basic fibroblast growth factor for cartilage tissue engineering, *J Mater Sci-Mater M* 18(10) (2007) 1961-1968.
- [222] A. Matsakas, Establishing the Role of Platelet- Derived Growth Factors in Skeletal Myogenesis, *Heart* 104 (2018) A85-A85.
- [223] L. Ouyang, K. Zhang, J. Chen, J.F. Wang, H. Huang, Roles of platelet-derived growth factor in vascular calcification, *J Cell Physiol* 233(4) (2018) 2804-2814.
- [224] B. Blaauw, Platelet-Derived Growth Factor signaling and the role of cellular crosstalk in functional muscle growth, *Febs Lett* 591(5) (2017) 690-692.
- [225] H.L. Xu, H. Zhang, Y. Ding, Platelet-derived growth factor and stromal cell-derived factor-1 promote the skin wound repairing effect of bone mesenchymal stem cells: a key role of matrix metalloproteinase 1 and collagens, *Int J Clin Exp Pathol* 10(8) (2017) 8253-+.
- [226] J. Andrae, R. Gallini, C. Betsholtz, Role of platelet-derived growth factors in physiology and medicine, *Gene Dev* 22(10) (2008) 1276-1312.
- [227] L. Yuan, S. Lin, W. Ueng, C. Niu, Y. Chan, C. Yang, Synergistic up-regulation of platelet derived growth factor b receptor in cartilage defects regeneration by hyperbaric oxygen and chondrocyte-platelet derived growth factor delivery treatment: An in vitro and in vivo study, *Calcified Tissue Int* 82 (2008) S80-S80.
- [228] G. Scalabrino, D. Veber, G. Tredici, Relationships between cobalamin, epidermal growth factor, and normal prions in the myelin maintenance of central nervous system, *Int J Biochem Cell B* 55 (2014) 232-241.
- [229] C.W. Kao, Y.Y. Tseng, K.S. Liu, Y.W. Liu, J.C. Chen, H.L. He, Y.C. Kau, S.J. Liu, Anesthetics and human epidermal growth factor incorporated into anti-adhesive nanofibers provide sustained pain relief and promote healing of surgical wounds, *Int J Nanomed* 14 (2019) 4007-4016.
- [230] M. Woltje, M. Bobel, M. Bienert, S. Neuss, D. Aibibu, C. Cherif, Functionalized silk fibers from transgenic silkworms for wound healing applications: Surface presentation of

bioactive epidermal growth factor, *Journal of Biomedical Materials Research Part A* 106(10) (2018) 2643-2652.

[231] K. Hori, C. Sotozono, J. Hamuro, K. Yamasaki, Y. Kimura, M. Ozeki, Y. Tabata, S. Kinoshita, Controlled-release of epidermal growth factor from cationized gelatin hydrogel enhances corneal epithelial wound healing, *Journal of Controlled Release* 118(2) (2007) 169-176.

[232] M. Horiguchi, M. Ota, D.B. Rifkin, Matrix control of transforming growth factor-beta function, *J Biochem* 152(4) (2012) 321-9.

[233] C.Q. Chu, X.W. Zhang, Y.K. Chou, S.L. Wu, C. Avenano, T. Caldwell, B. Maniaci, Y. Zhu, Regeneration of Articular Cartilage in Situ with Bone Marrow-Derived Mesenchymal Stem Cells, *Arthritis Rheumatol* 66 (2014) S447-S448.

[234] D. LeRoith, M. McGuinness, J. Shemer, B. Stannard, F. Lanau, T.N. Faria, H. Kato, H. Werner, M. Adamo, C.T. Roberts, Jr., Insulin-like growth factors, *Biol Signals* 1(4) (1992) 173-81.

[235] N.R. Bhakta, A.M. Garcia, E.H. Frank, A.J. Grodzinsky, T.I. Morales, The insulin-like growth factors (IGFs) I and II bind to articular cartilage via the IGF-binding proteins, *J Biol Chem* 275(8) (2000) 5860-6.

[236] H. Messai, Y. Duchossoy, A.M. Khatib, A. Panasyuk, D.R. Mitrovic, Articular chondrocytes from aging rats respond poorly to insulin-like growth factor-1: an altered signaling pathway, *Mech Ageing Dev* 115(1-2) (2000) 21-37.

[237] G.M. Williams, K.J. Dills, C.R. Flores, M.E. Stender, K.M. Stewart, L.M. Nelson, A.C. Chen, K. Masuda, S.J. Hazelwood, S.M. Klisch, R.L. Sah, Differential regulation of immature articular cartilage compressive moduli and Poisson's ratios by in vitro stimulation with IGF-1 and TGF-beta1, *J Biomech* 43(13) (2010) 2501-7.

[238] M. Petrou, P. Niemeyer, M.J. Stoddart, S. Grad, A. Bernstein, H.O. Mayr, G. Bode, N. Sudkamp, M. Alini, G.M. Salzman, Mesenchymal stem cell chondrogenesis: composite growth factor-bioreactor synergism for human stem cell chondrogenesis, *Regen Med* 8(2) (2013) 157-170.

[239] H. Park, J.S. Temenoff, Y. Tabata, A.I. Caplan, R.M. Raphael, J.A. Jansen, A.G. Mikos, Effect of dual growth factor delivery on chondrogenic differentiation of rabbit marrow mesenchymal stem cells encapsulated in injectable hydrogel composites, *Journal of Biomedical Materials Research Part A* 88a(4) (2009) 889-897.

[240] N. Indrawattana, G.P. Chen, M. Tadokoro, L.H. Shann, H. Ohgushi, T. Tateishi, J. Tanaka, A. Bunyaratvej, Growth factor combination for chondrogenic induction from human mesenchymal stem cell, *Biochem Bioph Res Co* 320(3) (2004) 914-919.

[241] A. Daluiski, T. Engstrand, M.E. Bahamonde, L.W. Gamer, E. Agius, S.L. Stevenson, K. Cox, V. Rosen, K.M. Lyons, Bone morphogenetic protein-3 is a negative regulator of bone density, *Nat Genet* 27(1) (2001) 84-88.

[242] B.J. Shen, D. Bhargava, A.Q. Wei, L.A. Williams, H. Tao, D.D.F. Ma, A.D. Diwan, BMP-13 Emerges as a Potential Inhibitor of Bone Formation, *Int J Biol Sci* 5(2) (2009) 192-200.

- [243] H.H. Luu, W.X. Song, X.J. Luo, D. Manning, J.Y. Luo, Z.L. Deng, K.A. Sharffl, A.G. Montag, R.C. Haydon, T.C. He, Distinct roles of bone morphogenetic proteins in osteogenic differentiation of mesenchymal stem cells, *J Orthop Res* 25(5) (2007) 665-677.
- [244] J. Selever, W. Liu, M.F. Lu, R.R. Behringer, J.F. Martin, Bmp4 in limb bud mesoderm regulates digit pattern by controlling AER development, *Dev Biol* 276(2) (2004) 268-279.
- [245] M. Asai-Coakwell, C.R. French, K.M. Berry, M. Ye, R. Koss, M. Somerville, R. Mueller, V. van Heyningen, A.J. Waskiewicz, O.J. Lehmann, GDF6, a novel locus for a spectrum of ocular developmental anomalies, *Am J Hum Genet* 80(2) (2007) 306-315.
- [246] B.R. Olsen, A.D. Berendsen, X.C. Duan, K. Hu, M. Nagao, Roles of Vascular Endothelial Growth Factor in Skeletal Development, Postnatal Homeostasis and Disease, *Faseb J* 31 (2017).
- [247] K. Hu, B.R. Olsen, The roles of vascular endothelial growth factor in bone repair and regeneration, *Bone* 91 (2016) 30-38.
- [248] J.P. Yang, H.J. Liu, X.F. Liu, VEGF promotes angiogenesis and functional recovery in stroke rats, *J Invest Surg* 23(3) (2010) 149-55.
- [249] Y.Q. Yang, Y.Y. Tan, R. Wong, A. Wenden, L.K. Zhang, A.B. Rabie, The role of vascular endothelial growth factor in ossification, *Int J Oral Sci* 4(2) (2012) 64-8.
- [250] J. Street, M. Bao, L. deGuzman, S. Bunting, F.V. Peale, Jr., N. Ferrara, H. Steinmetz, J. Hoeffel, J.L. Cleland, A. Daugherty, N. van Bruggen, H.P. Redmond, R.A. Carano, E.H. Filvaroff, Vascular endothelial growth factor stimulates bone repair by promoting angiogenesis and bone turnover, *Proc Natl Acad Sci U S A* 99(15) (2002) 9656-61.
- [251] S. Padilla, M. Sanchez, G. Orive, E. Anitua, Human-Based Biological and Biomimetic Autologous Therapies for Musculoskeletal Tissue Regeneration, *Trends Biotechnol* 35(3) (2017) 192-202.
- [252] B.B. Mendes, M. Gomez-Florit, P.S. Babo, R.M. Domingues, R.L. Reis, M.E. Gomes, Blood derivatives awaken in regenerative medicine strategies to modulate wound healing, *Adv Drug Deliver Rev* 129 (2018) 376-393.
- [253] E. Kon, R. Buda, G. Filardo, A. Di Martino, A. Timoncini, A. Cenacchi, P. Fornasari, S. Giannini, M. Marcacci, Platelet-rich plasma: intra-articular knee injections produced favorable results on degenerative cartilage lesions, *Knee Surg Sport Tr A* 18(4) (2010) 472-479.
- [254] A. Mishra, J. Woodall, A. Vieira, Treatment of Tendon and Muscle Using Platelet-Rich Plasma, *Clin Sport Med* 28(1) (2009) 113-+.
- [255] P.S. Babo, R.L. Reis, M.E. Gomes, Periodontal tissue engineering: current strategies and the role of platelet rich hemoderivatives, *J Mater Chem B* 5(20) (2017) 3617-3628.
- [256] G. Rohman, C. Langueh, S. Ramtani, J.J. Lataillade, D. Lutomski, K. Senni, S. Changotade, The Use of Platelet-Rich Plasma to Promote Cell Recruitment into Low-Molecular-Weight Fucoidan-Functionalized Poly(Ester-Urea-Urethane) Scaffolds for Soft-Tissue Engineering, *Polymers (Basel)* 11(6) (2019).

- [257] S.P. Arnoczky, D. Delos, S.A. Rodeo, What Is Platelet-Rich Plasma?, *Oper Techn Sport Med* 19(3) (2011) 142-148.
- [258] A.S. Wasterlain, H.J. Braun, J.L. Drago, Contents and Formulations of Platelet-Rich Plasma, *Oper Tech Orthop* 22(1) (2012) 33-42.
- [259] G. Intini, The use of platelet-rich plasma in bone reconstruction therapy, *Biomaterials* 30(28) (2009) 4956-4966.
- [260] B.J. Cole, S.T. Seroyer, G. Filardo, S. Bajaj, L.A. Fortier, Platelet-Rich Plasma: Where Are We Now and Where Are We Going?, *Sports Health* 2(3) (2010) 203-210.
- [261] L. Macri, D. Silverstein, R.A.F. Clark, Growth factor binding to the pericellular matrix and its importance in tissue engineering, *Adv Drug Deliver Rev* 59(13) (2007) 1366-1381.
- [262] I. Capila, R.J. Linhardt, Heparin - Protein interactions, *Angew Chem Int Edit* 41(3) (2002) 391-412.
- [263] G. Intini, S. Andreana, F.E. Intini, R.J. Buhite, L.A. Bobek, Calcium Sulfate and Platelet-Rich Plasma make a novel osteoinductive biomaterial for bone regeneration, *J Transl Med* 5 (2007) 13.
- [264] R. Ito, N. Morimoto, L.H. Pham, T. Taira, K. Kawai, S. Suzuki, Efficacy of the Controlled Release of Concentrated Platelet Lysate from a Collagen/Gelatin Scaffold for Dermis-Like Tissue Regeneration, *Tissue Eng Pt A* 19(11-12) (2013) 1398-1405.
- [265] D. Nakajima, Y. Tabata, S. Sato, Periodontal tissue regeneration with PRP incorporated gelatin hydrogel sponges, *Biomed Mater* 10(5) (2015).
- [266] J.P. Vogel, K. Szalay, F. Geiger, M. Kramer, W. Richter, P. Kasten, Platelet-rich plasma improves expansion of human mesenchymal stem cells and retains differentiation capacity and in vivo bone formation in calcium phosphate ceramics, *Platelets* 17(7) (2006) 462-469.
- [267] S.A. Sell, J.J. Ericksen, T.W. Reis, L.R. Droste, M.B.A. Bhuiyan, D.R. Gater, A case report on the use of sustained release platelet-rich plasma for the treatment of chronic pressure ulcers, *J Spinal Cord Med* 34(1) (2011) 122-127.
- [268] Y. Yamada, S. Nakamura, M. Ueda, K. Ito, Papilla regeneration by injectable stem cell therapy with regenerative medicine: long-term clinical prognosis, *J Tissue Eng Regen M* 9(3) (2015) 305-309.
- [269] M.S. Shive, W.D. Stanish, R. McCormack, F. Forriol, N. Mohtadi, S. Pelet, J. Desnoyers, S. Methot, K. Vehik, A. Restrepo, BST-CarGel (R) Treatment Maintains Cartilage Repair Superiority over Microfracture at 5 Years in a Multicenter Randomized Controlled Trial, *Cartilage* 6(2) (2015) 62-72.
- [270] K.S. Masters, Covalent Growth Factor Immobilization Strategies for Tissue Repair and Regeneration, *Macromol Biosci* 11(9) (2011) 1149-1163.
- [271] D.C.F. Soares, C.M.R. Oda, L.O.F. Monteiro, A.L.B. de Barros, M.L. Tebaldi, Responsive polymer conjugates for drug delivery applications: recent advances in bioconjugation methodologies, *J Drug Target* 27(4) (2019) 355-366.



- [272] Y. Jung, J.Y. Jeong, B.H. Chung, Recent advances in immobilization methods of antibodies on solid supports, *Analyst* 133(6) (2008) 697-701.
- [273] J. Dawson, O. Schussler, A. Al-Madhoun, C. Menard, M. Ruel, I.S. Skerjanc, Collagen scaffolds with or without the addition of RGD peptides support cardiomyogenesis after aggregation of mouse embryonic stem cells, *In Vitro Cell Dev-An* 47(9) (2011) 653-664.
- [274] M. Rajabi, M. Firouzi, Z. Hassannejad, I. Haririan, P. Zahedi, Fabrication and characterization of electrospun laminin-functionalized silk fibroin/poly(ethylene oxide) nanofibrous scaffolds for peripheral nerve regeneration, *J Biomed Mater Res B* 106(4) (2018) 1595-1604.
- [275] X. Yang, Y.Y. Li, W. He, Q.L. Huang, R.R. Zhang, Q.L. Feng, Hydroxyapatite/collagen coating on PLGA electrospun fibers for osteogenic differentiation of bone marrow mesenchymal stem cells, *Journal of Biomedical Materials Research Part A* 106(11) (2018) 2863-2870.
- [276] F. Westhauser, A.S. Senger, D. Obert, F.E. Ciraldo, K. Schuhladen, G. Schmidmaier, A. Moghaddam, A.R. Boccaccini, Gelatin coating increases in vivo bone formation capacity of three-dimensional 45S5 bioactive glass-based crystalline scaffolds, *J Tissue Eng Regen M* 13(2) (2019) 179-190.
- [277] B.P. dos Santos, B. Garbay, M. Pasqua, E. Chevron, Z.S. Chinoy, C. Cullin, K. Bathany, S. Lecommandoux, J. Amedee, H. Oliveira, E. Garanger, Production, purification and characterization of an elastin-like polypeptide containing the Ile-Lys-Val-Ala-Val (IKVAV) peptide for tissue engineering applications, *J Biotechnol* 298 (2019) 35-44.
- [278] A.J.S. Ribeiro, K. Zaleta-Rivera, E.A. Ashley, B.L. Pruitt, Stable, Covalent Attachment of Laminin to Microposts Improves the Contractility of Mouse Neonatal Cardiomyocytes, *Acs Appl Mater Inter* 6(17) (2014) 15516-15526.
- [279] S. Chaves, L.M. Pera, C.L. Avila, C.M. Romero, M. Baigori, F.E.M. Vieyra, C.D. Borsarelli, R.N. Chehin, Towards efficient biocatalysts: photo-immobilization of a lipase on novel lysozyme amyloid-like nanofibrils, *Rsc Adv* 6(11) (2016) 8528-8538.
- [280] T.L. Gao, W.W. Cui, Z.L. Wang, Y. Wang, Y. Liu, P.S. Malliappan, Y. Ito, P.B. Zhang, Photo-immobilization of bone morphogenic protein 2 on PLGA/HA nanocomposites to enhance the osteogenesis of adipose-derived stem cells, *Rsc Adv* 6(24) (2016) 20202-20210.
- [281] J.S. Xv, H.Y. Li, W.R. Zhang, G.C. Lai, H.Y. Xue, J.H. Zhao, M. Tu, R. Zeng, Anti-biofouling and functionalizable bioinspired chitosan-based hydrogel coating via surface photo-immobilization, *J Biomat Sci-Polym E* 30(5) (2019) 398-414.
- [282] A. Scarano, F. Lorusso, T. Orsini, M. Morra, G. Iviglia, L. Valbonetti, Biomimetic Surfaces Coated with Covalently Immobilized Collagen Type I: An X-Ray Photoelectron Spectroscopy, Atomic Force Microscopy, Micro-CT and Histomorphometrical Study in Rabbits, *Int J Mol Sci* 20(3) (2019).
- [283] X.Y. Cheng, J. Fei, A. Kondyurin, K.K. Fu, L. Ye, M.M.M. Bilek, S.S. Bao, Enhanced biocompatibility of polyurethane-type shape memory polymers modified by plasma immersion

ion implantation treatment and collagen coating: An in vivo study, *Mat Sci Eng C-Mater* 99 (2019) 863-874.

[284] J. Su, S.C. Satchell, J.A. Wertheim, R.N. Shah, Poly(ethylene glycol)-crosslinked gelatin hydrogel substrates with conjugated bioactive peptides influence endothelial cell behavior, *Biomaterials* 201 (2019) 99-112.

[285] V. Luginbuehl, L. Meinel, H.P. Merkle, B. Gander, Localized delivery of growth factors for bone repair, *Eur J Pharm Biopharm* 58(2) (2004) 197-208.

[286] K.A. Blackwood, N. Bock, T.R. Dargaville, M.A. Woodruff, Scaffolds for Growth Factor Delivery as Applied to Bone Tissue Engineering, *Int J Polym Sci* (2012).

[287] H. Park, J.S. Temenoff, Y. Tabata, A.I. Caplan, A.G. Mikos, Injectable biodegradable hydrogel composites for rabbit marrow mesenchymal stem cell and growth factor delivery for cartilage tissue engineering, *Biomaterials* 28(21) (2007) 3217-3227.

[288] H.S. Koh, T. Yong, C.K. Chan, S. Ramakrishna, Enhancement of neurite outgrowth using nano-structured scaffolds coupled with laminin, *Biomaterials* 29(26) (2008) 3574-3582.

[289] J. Cabanas-Danes, J. Huskens, P. Jonkheijm, Chemical strategies for the presentation and delivery of growth factors, *J Mater Chem B* 2(17) (2014) 2381-2394.

[290] D.R. Nisbet, L.M.Y. Yu, T. Zahir, J.S. Forsythe, M.S. Shoichet, Characterization of neural stem cells on electrospun poly(epsilon-caprolactone) submicron scaffolds: evaluating their potential in neural tissue engineering, *J Biomat Sci-Polym E* 19(5) (2008) 623-634.

[291] H.S. Yu, J.H. Jang, T.I. Kim, H.H. Lee, H.W. Kim, Apatite-mineralized polycaprolactone nanofibrous web as a bone tissue regeneration substrate, *Journal of Biomedical Materials Research Part A* 88a(3) (2009) 747-754.

[292] Z.W. Ma, W. He, T. Yong, S. Ramakrishna, Grafting of gelatin on electrospun poly(caprolactone) nanofibers to improve endothelial cell spreading and proliferation and to control cell orientation, *Tissue Eng* 11(7-8) (2005) 1149-1158.

[293] J.V. Staros, R.W. Wright, D.M. Swingle, Enhancement by N-Hydroxysulfosuccinimide of Water-Soluble Carbodiimide-Mediated Coupling Reactions, *Anal Biochem* 156(1) (1986) 220-222.

[294] Y.H. Shen, M.S. Shoichet, M. Radisic, Vascular endothelial growth factor immobilized in collagen scaffold promotes penetration and proliferation of endothelial cells, *Acta Biomater* 4(3) (2008) 477-489.

[295] L.L.Y. Chiu, R.D. Weisel, R.K. Li, M. Radisic, Defining conditions for covalent immobilization of angiogenic growth factors onto scaffolds for tissue engineering, *J Tissue Eng Regen M* 5(1) (2011) 69-84.

[296] S. Tsuzuki, A. Wada, Y. Ito, Photo-Immobilization of Biological Components on Gold-Coated Chips for Measurements Using Surface Plasmon Resonance (SPR) and a Quartz Crystal Microbalance (QCM), *Biotechnol Bioeng* 102(3) (2009) 700-707.

- [297] E. Lee, D. Yong, X. Yu, H. Li, C.C. Chan, In-fiber photo-immobilization of a bioactive surface, *J Biomed Opt* 19(12) (2014) 120502.
- [298] J. Taipale, J. KeskiOja, Growth factors in the extracellular matrix, *Faseb J* 11(1) (1997) 51-59.
- [299] A.H. Zisch, M.P. Lutolf, J.A. Hubbell, Biopolymeric delivery matrices for angiogenic growth factors, *Cardiovasc Pathol* 12(6) (2003) 295-310.
- [300] V. Sivagnanam, B. Song, C. Vandevyver, M.A.M. Gijs, On-Chip Immunoassay Using Electrostatic Assembly of Streptavidin-Coated Bead Micropatterns, *Anal Chem* 81(15) (2009) 6509-6515.
- [301] D. Kim, K. Karns, S.Q. Tia, M. He, A.E. Herr, Electrostatic Protein Immobilization Using Charged Polyacrylamide Gels and Cationic Detergent Microfluidic Western Blotting, *Anal Chem* 84(5) (2012) 2533-2540.
- [302] D. Correa, S.A. Lietman, Articular cartilage repair: Current needs, methods and research directions, *Semin Cell Dev Biol* (2016).
- [303] D.J. Huey, J.C. Hu, K.A. Athanasiou, Unlike bone, cartilage regeneration remains elusive, *Science* 338(6109) (2012) 917-21.
- [304] M. Petrou, P. Niemeyer, M.J. Stoddart, S. Grad, A. Bernstein, H.O. Mayr, G. Bode, N. Sudkamp, M. Alini, G.M. Salzman, Mesenchymal stem cell chondrogenesis: composite growth factor-bioreactor synergism for human stem cell chondrogenesis, *Regen Med* 8(2) (2013) 157-70.
- [305] L. Longobardi, L. O'Rear, S. Aakula, B. Johnstone, K. Shimer, A. Chytil, W.A. Horton, H.L. Moses, A. Spagnoli, Effect of IGF-I in the chondrogenesis of bone marrow mesenchymal stem cells in the presence or absence of TGF-beta signaling, *J Bone Miner Res* 21(4) (2006) 626-36.
- [306] V. Chiono, C. Tonda-Turo, Trends in the design of nerve guidance channels in peripheral nerve tissue engineering, *Prog Neurobiol* 131 (2015) 87-104.
- [307] M.D. Sarker, S. Naghieh, A.D. McInnes, D.J. Schreyer, X. Chen, Regeneration of peripheral nerves by nerve guidance conduits: Influence of design, biopolymers, cells, growth factors, and physical stimuli, *Prog Neurobiol* 171 (2018) 125-150.
- [308] M. Moattari, H.M. Kouchesfehiani, G. Kaka, S.H. Sadraie, M. Naghdi, Evaluation of nerve growth factor (NGF) treated mesenchymal stem cells for recovery in neurotmesis model of peripheral nerve injury, *J Cranio Maxill Surg* 46(6) (2018) 898-904.
- [309] G.C. Li, Q.Z. Xiao, L.Z. Zhang, Y.H. Zhao, Y.M. Yang, Nerve growth factor loaded heparin/chitosan scaffolds for accelerating peripheral nerve regeneration, *Carbohydr Polym* 171 (2017) 39-49.
- [310] W. Zeng, M.Y. Rong, X.Y. Hu, W. Xiao, F.Y. Qi, J.H. Huang, Z.J. Luo, Incorporation of Chitosan Microspheres into Collagen-Chitosan Scaffolds for the Controlled Release of Nerve Growth Factor, *Plos One* 9(7) (2014).

- [311] L.M. Marquardt, S.E. Sakiyama-Elbert, Engineering peripheral nerve repair, *Curr Opin Biotechnol* 24(5) (2013) 887-92.
- [312] C. Carvalho, J. Pedro, K.W. Ng, N. Neves, R. Reis, M. Oliveira, Keratin/chitosan as novel grafts for peripheral nerve regeneration, *J Tissue Eng Regen M* 8 (2014) 434-434.
- [313] A.J. Salgado, N. Sousa, N.A. Silva, N.M. Neves, R.L. Reis, Hydrogels for spinal cord injury regeneration, *Woodhead Publ Mater* (2008) 570-594.
- [314] J. Wang, L.L. Tian, L.M. He, N. Chen, S. Ramakrishna, K.F. So, X.M. Mo, Lycium barbarum polysaccharide encapsulated Poly lactic-co-glycolic acid Nanofibers: cost effective herbal medicine for potential application in peripheral nerve tissue engineering, *Sci Rep-Uk* 8 (2018).
- [315] K. Tajdaran, T. Gordon, M.D. Wood, M.S. Shoichet, G.H. Borschel, A glial cell line-derived neurotrophic factor delivery system enhances nerve regeneration across acellular nerve allografts, *Acta Biomater* 29 (2016) 62-70.
- [316] H.C. Pape, A. Evans, P. Kobbe, Autologous Bone Graft: Properties and Techniques, *J Orthop Trauma* 24 (2010) S36-S40.
- [317] T.N. Vo, F.K. Kasper, A.G. Mikos, Strategies for controlled delivery of growth factors and cells for bone regeneration, *Adv Drug Deliver Rev* 64(12) (2012) 1292-1309.
- [318] P.V. Giannoudis, G.M. Calori, T. Begue, G. Schmidmaier, Bone regeneration strategies: Current trends but what the future holds?, *Injury* 44 (2013) S1-S2.
- [319] R.A. Deyo, A. Ching, L. Matsen, B.I. Martin, W. Kreuter, J.G. Jarvik, H. Angier, S.K. Mirza, Use of Bone Morphogenetic Proteins in Spinal Fusion Surgery for Older Adults With Lumbar Stenosis Trends, Complications, Repeat Surgery, and Charges, *Spine* 37(3) (2012) 222-230.
- [320] K.R. Garrison, S. Donell, J. Ryder, I. Shemilt, M. Mugford, I. Harvey, F. Song, Clinical effectiveness and cost-effectiveness of bone morphogenetic proteins in the non-healing of fractures and spinal fusion: a systematic review, *Health Technol Asses* 11(30) (2007) 1-+.
- [321] P.J. Boyne, Application of bone morphogenetic proteins in the treatment of clinical oral and maxillofacial osseous defects, *J Bone Joint Surg Am* 83a (2001) S146-S150.
- [322] H. Shen, X.X. Hu, F. Yang, J.Z. Bei, S.G. Wang, The bioactivity of rhBMP-2 immobilized poly(lactide-co-glycolide) scaffolds, *Biomaterials* 30(18) (2009) 3150-3157.
- [323] Y.J. Park, K.H. Kim, J.Y. Lee, Y. Ku, S.J. Lee, B.M. Min, C.P. Chung, Immobilization of bone morphogenetic protein-2 on a nanofibrous chitosan membrane for enhanced guided bone regeneration, *Biotechnol Appl Bioc* 43 (2006) 17-24.
- [324] H.N. Zhang, F. Migneco, C.Y. Lin, S.J. Hollister, Chemically-Conjugated Bone Morphogenetic Protein-2 on Three-Dimensional Polycaprolactone Scaffolds Stimulates Osteogenic Activity in Bone Marrow Stromal Cells, *Tissue Eng Pt A* 16(11) (2010) 3441-3448.
- [325] J. Rouwkema, N.C. Rivron, C.A. van Blitterswijk, Vascularization in tissue engineering, *Trends Biotechnol* 26(8) (2008) 434-441.

[326] R.K. Jain, P. Au, J. Tam, D.G. Duda, D. Fukumura, Engineering vascularized tissue, *Nat Biotechnol* 23(7) (2005) 821-823.

[327] A. Hoeben, B. Landuyt, M.S. Highley, H. Wildiers, A.T. Van Oosterom, E.A. De Bruijn, Vascular endothelial growth factor and angiogenesis, *Pharmacol Rev* 56(4) (2004) 549-580.

[328] N. Ferrara, H.P. Gerber, J. LeCouter, The biology of VEGF and its receptors, *Nat Med* 9(6) (2003) 669-676.

## **SECTION 2**

# **EXPERIMENTAL DESIGN**

# **Chapter II**

## **Materials & Methods**

## Chapter II

### Materials and Methods

#### OVERVIEW

In this chapter, the different materials, reagents and methodologies used to produce the biofunctional nanofibrous systems are described. The different biofunctional nanofibrous systems developed in this work were obtained using a polycaprolactone electrospun nanofibrous mesh (NFM) biofunctionalized with Fibronectin, Extracellular Vesicles, TGF- $\beta$ 3, IGF-I, NGF, BMP-2 and VEGF. For that, defined antibodies were immobilized at the surface of NFM, taking advantage of the specific and efficient interactions between an antibody and its antigen.

Different characterization methodologies were used to evaluate the physico-chemical and biological performance of the developed biofunctional nanofibrous systems. Moreover, this chapter will provide some insights on the methodological fundamentals aiming to justify the methods selected to answer specific research questions of this experimental work.



## II-1. MATERIALS

### II-1.1. Polycaprolactone (PCL)

Polycaprolactone (PCL) is a biodegradable polyester with a melting point of around 60 °C and a glass transition temperature of about –60 °C. It is a hydrophobic and semicrystalline polymer, whose chemical structure is shown in **Figure II-1**. Derived by chemical synthesis from crude oil, PCL can be synthesized by a ring opening polymerization of a cyclic lactone monomer (i.e. poly-caprolactone), and degraded by hydrolysis of its ester bonds in physiological conditions (i.e. human body) [1, 2].

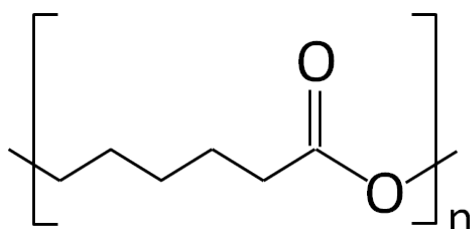


**Figure II-1** Chemical structure of polycaprolactone.

PLC belongs to the aliphatic polyester family, being characterized by good mechanical/elastic properties, low toxicity, biocompatibility and long-term biodegradability [3, 4]. Its potential use as a biomaterial was recognized and approved by Food and Drug Administration (FDA), being used in the human body as a drug delivery device, suture or adhesion preventing barrier [5, 6]. In particular, it is especially interesting for the development of long-term implantable devices, due to its slow degradation (up to 2–4 years, depending of the starting molecular weight of the device or implant) [7]. The limitations of PCL as a biomaterial lies in its poor antimicrobial properties, poor adhesion to cells due to hydrophobic surface and the need to use toxic solvents to dissolve it (when required). The PCL (Mw = 70 000 – 90 000 determined by GPC) used in this work was purchase from Sigma-Aldrich (St. Louis, MO; USA).

### II-1.2. Antibodies

An antibody or immunoglobulin (Ig) is a large Y- shaped protein (**Figure II-2**), mainly produced by B-cells and used by the immune system to identify and neutralize pathogens such

as bacteria and viruses [8]. It recognizes a unique part of the foreign target, namely an antigen, via the fragment antigen-binding variable region [9].

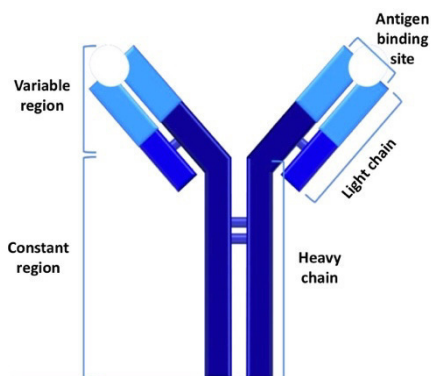


**Figure II-2 Structure of an Antibody.**

Antibodies are glycoproteins typically composed of four basic structural units, namely two identical large heavy chains and two identical small light chains. There are several different types of heavy and light chains; specifically, in mammals; there are five types of Ig heavy chain ( $\alpha$ ,  $\delta$ ,  $\epsilon$ ,  $\gamma$ , and  $\mu$ ) and two types of Ig light chain ( $\lambda$  and  $\kappa$ ) [8, 10]. An antibody is made up of a variable region that is specific, and a constant region that is common for each type of antibody. The variable region is also known as the antigen binding site where only a specific antigen (e.g. growth factors, fibronectin and extracellular vesicles (EVs) in the present case) can be linked. Aptamers are oligonucleotide or peptide molecules which could be considered as alternatives to the use of antibodies, as both have the ability to recognize a specific molecule with high affinity and specificity [11]. In fact, aptamers are nucleotide analogues of antibodies, but aptamer-generation is significantly easier and cheaper than the production of antibodies [12]. The major drawbacks of aptamers are their low affinity and rapid degradation. Moreover, the aptamer generation in most cases requires the availability of purified target molecules [13]. In this sense, the use of aptamers in this work is not feasible.

The antibodies used in this work do not present neutralizing activity, leaving the cell receptor binding domain of the bound proteins free to perform their biological activity. Specifically, Anti-human CD63 monoclonal antibody (clone E-12) and Anti-human VEGF monoclonal antibody (clone JH121) were purchased from Santa Cruz Biotechnology, Inc (Heidelberg, Germany) and kept at 4°C until further use. Anti-human BMP-2 polyclonal antibody was purchased from Merck KGaA (Darmstadt, Germany), and kept at 4°C until further use. Anti-rat NGF monoclonal antibody (clone EP1320Y) and anti-human Fibronectin

monoclonal antibody (clone BC-1) were purchased from Abcam<sup>®</sup> (Cambridge, UK). Anti-human TGF- $\beta$ 3 monoclonal antibody (Clone 44922) and Anti-human IGF-I polyclonal antibody were purchased from Bio-technie/R&D Systems<sup>™</sup> (Minneapolis, MN; USA). Those antibodies were reconstituted in a phosphate buffer solution (PBS) and kept at -20°C until further use. The host specie of the NGF and the BMP-2 antibodies was the rabbit, whereas for the Fibronectin, the CD63, the VEGF and the TGF- $\beta$ 3 antibodies the host was the mouse, and for the IGF-I antibody the host was the goat.

A secondary antibody aids in the detection, sorting or purification of primary antibodies, which directly binds to the target antigen. In this work, Alexa Fluor<sup>®</sup> 594 donkey anti-mouse IgG (H+L) and Alexa Fluor<sup>®</sup> 594 goat anti-mouse IgG (H+L) with red fluorescence were used as secondary antibodies against the anti-TGF- $\beta$ 3 and the anti-VEGF antibodies, respectively. Alexa Fluor<sup>®</sup> 488 donkey anti-rabbit IgG (H+L) with green fluorescence were used as secondary antibody against the anti-BMP-2 and the anti-NGF antibodies. Alexa Fluor<sup>®</sup> 488 rabbit anti-goat IgG (H+L), Alexa Fluor<sup>®</sup> 488 donkey anti-mouse IgG (H+L) and Alexa Fluor<sup>®</sup> 488 rabbit anti-mouse IgG (H+L) with green fluorescence were used as secondary antibodies against the anti-IGF-I, the anti-Fibronectin and the anti-CD63 antibodies, respectively. All secondary antibodies were purchased from Life Technologies (Carlsbad, CA; USA) and kept at 4°C until further use.

### **II-1.3. Bioactive Proteins**

Recombinant proteins provided important breakthroughs in biomedical biotechnology by overcoming the insufficient yields of protein obtained from natural sources [14]. Recombinant proteins are made through genetic engineering, recombinant DNA technology. Basically, the gene is isolated and cloned into an expression system, namely a vector, producing large quantities of recombinant proteins [15]. Several expression systems are used namely prokaryotic and eukaryotic systems such as *Escherichia coli* and mammalian cell lines, respectively, depending on the characteristics and intended application of the recombinant protein. Therefore, although most recombinant proteins in clinical use are from human origin, they were expressed in other organisms such as bacteria, yeast, or animal cells in culture. Actually, more than 130 recombinant proteins were approved by the United States FDA for therapeutic use, while more than 170 recombinant proteins are produced and used in medicine worldwide [16].

In this work, recombinant human Growth Factors (GFs), namely the TGF- $\beta$ 3 (a 25.0 kDa protein composed of two identical 112 amino acid polypeptide chains linked by a single disulfide bond), the IGF-I/IGF-1 (a 7.6 kDa globular protein containing 70 amino acids, and 3 intra-molecular disulfide bonds), the VEGF<sub>121</sub> (a 28.4 kDa disulfide-linked homodimeric protein consisting of two 121 amino acid polypeptide chains), and the basic fibroblast growth factor (bFGF; a 17.2 kDa protein consisting of 154 amino acid residues) were expressed in *Escherichia coli*; whereas the recombinant NGF- $\beta$  from rat (a 13.2 kDa homodimer protein consisting of two 120-amino acid polypeptides) was expressed in Sf21 cells. All GFs were reconstituted in PBS and kept at -20°C until further use. The recombinant human TGF- $\beta$ 3, VEGF<sub>121</sub> and bFGF were purchased from PreproTech Inc. (Rochy Hill, NJ; USA), while the recombinant human IGF-I/IGF-1 and NGF- $\beta$  from rat were purchased from Bio-technie/R&D Systems™ (Minneapolis, MN; USA) and Sigma-Aldrich (St. Louis, MO; USA), respectively.

The human fibronectin used in this work was obtained from a natural source, namely human donor plasma. Human plasma fibronectin protein with 220 kDa was purified (approximately 95%) by affinity chromatography on gelatin agarose, followed by chromatography on heparin-agarose. Those was purchased from Merck KGaA (Darmstadt, Germany) and kept at 4°C until further use.

## II-2. REAGENTS

All the reagents used in this work were purchased from Sigma-Aldrich (St. Louis, MO, USA), unless otherwise specified.

## II-3. BIOMATERIAL SUBSTRATE FABRICATION AND (BIO)FUNCTIONALIZATION

The biomaterial scaffolds developed during the course of this work were produced by electrospinning techniques. Electrospinning is a versatile and cost-effective polymer processing technique for the production of non-woven micro- to nano-fibrous meshes. The fiber dimension defines several interesting properties such as surface area to volume ratio, porosity and mechanical properties. From a biological point of view, almost every extracellular matrix (ECM) of connective tissues is based on nanofibrous structures (e.g. skin, cartilage and bone). These morphological similarities make electrospun nanofibers great candidates to provide the cells an environment similar to the native structure of the ECM [17, 18]. Most of the desirable

properties of tissue engineered scaffolds can be addressed by electrospun nanofibrous meshes (NFMs), such as porosity, interconnected pores with adjustable pores size, capabilities for effective surface functionalization and adjustable surface morphology [19-22]. In this work, the surface of electrospun PCL NFMs were activated and functionalized by the insertion of amine groups, followed by biofunctionalization with different bioactive molecules for various regenerative strategies, illustrating the versatility of this NFM structure for different biomedical applications.

### **II-3.1. The Electrospinning processing technique**

The process of using electrostatic forces to produce fibers has been known for over 100 years. Unlike conventional fiber spinning methods (as dry-spinning or melt-spinning), electrospinning has its roots in electrostatic spraying (electrospraying), making use of electrostatic forces to stretch the solution as it solidifies [23, 24]. Electrospinning has many controllable processing parameters that affect the fibers formation and the resulting structure [19]. Generally, the production of nanofibers using the electrospinning technique is based on uniaxial stretching of a viscoelastic solution, containing a dissolved polar or non-polar polymer solution, caused by electrostatic forces [23, 25].

There are basically three main components in the traditional electrospinning set up: a high voltage power source, a capillary tube with a pipette or a needle, and a metallic collector (**Figure II-3**) [23, 26]. The fiber formation is achieved by forcing the viscous polymeric solution through a spinneret, in most cases the metal tip of a needle, exposed to an electric field, forming initially a droplet. As the intensity of the electric field is increased, the droplet is turned into a conical shape fluid structure called the Taylor cone, which was first described mathematically by Taylor in 1964 [27]. If the viscosity and surface tension of the polymeric solution are suitable, the breaking of the cone is prevented and a stable jet is formed. The increase in the applied high voltage leads to the elongation of the Taylor cone. When the repulsive force within the charged solution is higher than its surface tension, the cone is elongated, becoming a jet. This fluid filament is directed to the grounded collector. At this time, the solvent is evaporated and the nanofibers are formed and deposited at the surface of the collector as a non-woven web of small fibers – the nanofibrous mesh [23, 25, 28]. The obtained non-woven mesh structure consists typically of randomly aligned fibers deposited in successive

layers over a static collector. The fibers are stacked one over another while being deposited, building several interconnections due to the presence of residual solvent.

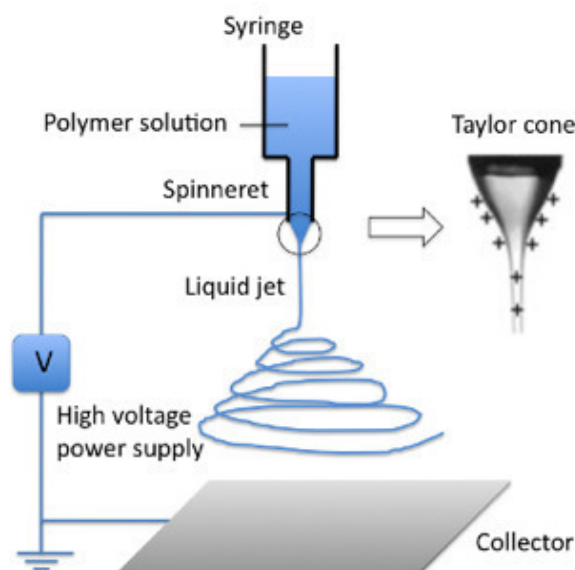


**Figure II-3** The common setup and working principle of electrospinning [26].

The main problems related with the conventional arrangement of the electrospinning apparatus are: 1) the gravitational force, which allows drops to fall down from the needle creating defects on the mesh; 2) the low production efficiency, intrinsically associated with the production of only one nanofiber at a time [29]. This is particularly relevant in industrial applications where a continuous and rapid process is essential.

For the production of the PCL NFMs used in this work, a 5 mL plastic syringe (B-Braun) and a needle with 0.8 mm circular external diameter tip was used to electrospun the PCL solution. A 15% (w/v) PCL solution was prepared with an organic solvent mixture composed of chloroform and dimethylformamide (7:3 ratio), as described previously [30]. The PCL solution was electrospun by applying a voltage of 12.5 kV, a needle tip-to-ground collector distance of 20 cm and a flow rate of 1mL/h. After the complete processing of 1mL of solution, the NFM was left to dry, in order to evaporate all solvent residues. The produced PCL NFMs were composed of nanofibers with diameters in the submicron range, from 0.4 to 1.4  $\mu\text{m}$  with an average pore size of  $72.67 \pm 31.48 \mu\text{m}$  (**Figure II-4**) [31]. The processed NFM was further cut into square smaller samples of  $1\text{cm}^2$  for further use in all the works, except on the experimental study of **Chapter VII**, where NFMs were cut into square samples of  $1.3\text{cm}^2$ .

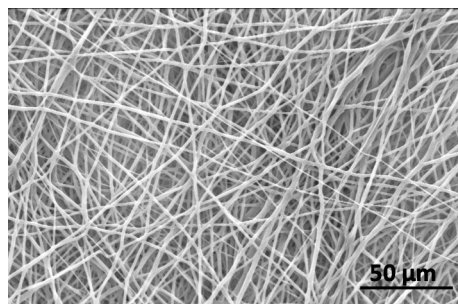


**Figure II-4** Scanning electron microscopy analysis of an electrospun polycaprolactone nanofibrous mesh.

### **II-3.2. Surface Functionalization of Electrospun Nanofibers**

The surfaces of electrospun nanofibrous meshes may be physically or chemically modified to provide biomimetic microenvironments for the surrounding tissues and cells [22, 32]. Physical surface functionalization methods are based on flame, corona discharge, plasma, electron beam, ion beam, X-ray, or  $\gamma$ -ray-induced treatments [33-35]. However, functionalization by chemical means involves immersion of the material in specific solutions or exposure to the vapor of a chemical agent, which results in a change of the molecular arrangement [30, 36, 37]. Hence, the chemical modification method relies on performing graft polymerization to introduce functional groups at the nanofibers' surface. Generally, the surface graft polymerization method begins with a physical method, in order to produce free radicals for the polymerization [30, 38]. This enhances the material surface by altering its charge, chemical group functionality and wettability.

Herein, the activation of the surface of the nanofibers was carried out using an ultraviolet-ozone (UV-O) system [30, 39]. The UV-O method is a photo-sensitized oxidation process in which molecules are excited by the absorption of short-wavelength UV radiation, generating highly reactive free oxygen ( $O\cdot$ ) radicals, which leads to the formation of  $-OH$  and  $-COOH$  groups (**Figure II-5A**) [40]. This happens when the 253.7 nm UV radiation is absorbed by most hydrocarbons and also by ozone, reacting with oxygen to produce volatile molecules. Oxygen is dissociated at 184.9 nm, and once both UV wavelengths – 253.7 nm and 184.9 nm – are present, atomic oxygen is continuously generated, and ozone is continually formed and destroyed. This combination can destroy organic contamination up to the molecular-level of organic contamination, cleaning surfaces and sterilize biomaterials. Nonetheless, polymers degradation is a major concern, thus, for each biomaterial, the optimization of time and intensity of irradiation is required. UV-O treatment parameters for the PCL NFMs were previously

optimized [30]. Activation was performed by the exposure of both sides during 4 minutes to UV-O irradiation (UV-O Cleaner<sup>®</sup>, model ProCleaner 220 from Bioforce Nanoscience, Utah, USA).

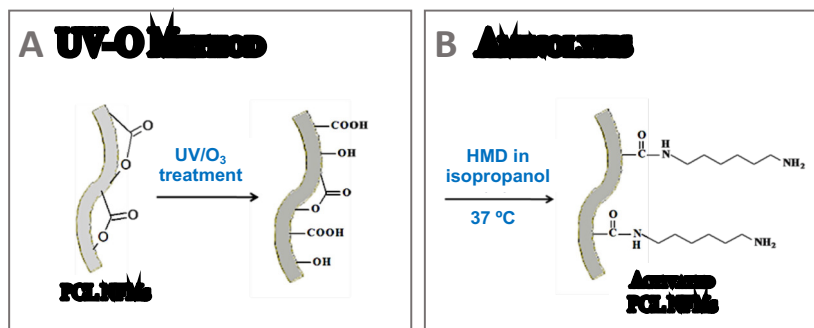


Figure II-5 Surface activation and functionalization of the electrospun PCL nanofibers.

Aminolysis is a straightforward chemical method for the introduction of amino groups at the surface of polyesters, by the cleavage of ester bonds and the simultaneous generation of amide bonds. One of the two  $-NH_2$  groups reacts with the carbonyl carbon while the other amino group remains free at the nanofibers' surface, potentially stable for subsequent chemical reactions [30, 39, 41, 42]. Activated electrospun nanofibers allows the insertion of amine groups onto the PCL surface by a reaction with diamine (e.g. hexamethylenediamine (HMD)), made available amine group ( $-NH_2$ ) at the surface of NFMs (**Figure II-5B**). This reaction will provide two amine bonds – one that binds to PCL through the reaction with  $-COO-$  group forming a covalent bond ( $-CONH-$ ), and a second one, unreactive and free, that will be available to react with the antibody  $-COOH$  group, attaching it to the nanofiber surface through a 1-ethyl-3(3dimethylaminopropyl)carbodiimide/N-Hydroxysuccinimide mediated reaction (EDC/NHS) [43]. The surface functionalization unavoidably causes additional erosion of the PCL nanofibers' surface, thus the procedure parameters must be optimized. The reaction of a diamine solution with the PCL NFM was optimized as described elsewhere [39]. Accordingly, activated NFMs were immersed in a 1 M HMD solution during 1h at 37°C. By the Ellman's reagent method, an indirectly quantification method, an amount of  $2.83 \pm 0.11$  nmol/cm<sup>2</sup> of amine groups were introduced at the surface of PCL electrospun nanofibers [30].

The introduction of stable amino groups at the scaffolds' surface present some advantages for Tissue Engineering and Regenerative Medicine (TERM) approaches, namely i) is nontoxic to cells or tissues; ii) decrease the surface hydrophobicity; iii) neutralize the acid environment (when applicable) generated during the scaffold degradation and, consequently, reducing the



inflammation around the implanted scaffold; and iv) provide free functional groups able to react with biomolecules such as antibodies, recombinant proteins, plasma/platelet lysate-derived proteins or EVs-derived conditioned media, obtaining cytocompatible surfaces.

### II-3.3. Antibodies Immobilization Strategy – Biofunctionalization

The main concept of this work is the development of different systems capable to spatially present biomolecules selectively captured from a pool of different bioactive factors, namely GFs and EVs immobilized at the surface of a NFMs. For that, antibodies were used as an intermediate molecule that bind the biomolecule of interest to the electrospun nanofiber surface. Indeed, antibodies are capable to be chemically or physically deposited onto the biomaterial surface, offering biological sites for GFs incorporation [39].

In the antibody structure, at the end of the constant region, there is a carboxyl group (-COOH) which can react with the amine groups (-NH<sub>2</sub>) previously inserted at the surface of electrospun nanofibers, leading to its covalent immobilization. A coupling agent is required to achieve a more stable and strong binding. In the present works, the EDC/NHS (1-Ethyl-3-[3-dimethylaminopropyl]carbodiimide hydrochloride/ N-hydroxysuccinimide) mixture was used. EDC couples carboxyl groups to primary amines, while NHS greatly enhances the coupling efficiency, leading to a two-step reaction (**Figure II-6**). The EDC/NHS mixture allows amine reactive NHS esters to become available to react with any carboxyl-containing molecule (-COOH).

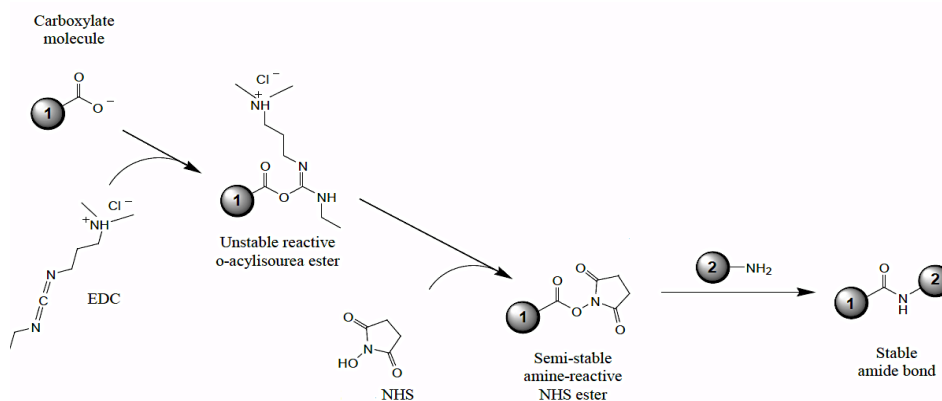


**Figure II-6** EDC reacts preferentially with the carboxyl groups forming O-acylisourea, an unstable reactive ester. In combination with NHS forms a semi-stable amine-reactive ester. This NHS ester can readily react with the available amine groups at the surface of electrospun nanofibers.

**Figure II-7A** shows the antibody immobilization strategy applied in this work. Firstly, the primary antibody was activated by its incubation with EDC/NHS for 15 min at room temperature (RT), for further incubation with activated and functionalized NFMs for 2h at RT or overnight at 4 °C. NFMs were washed twice with PBS, and incubated with a 3% bovine serum albumin (BSA) solution for 30 minutes at RT, in order to block all nonspecific sites. The BSA solution was removed and the secondary antibody or protein solutions (recombinant protein; plasma or platelet lysate samples; and conditioned media) were incubated during 1h at RT.

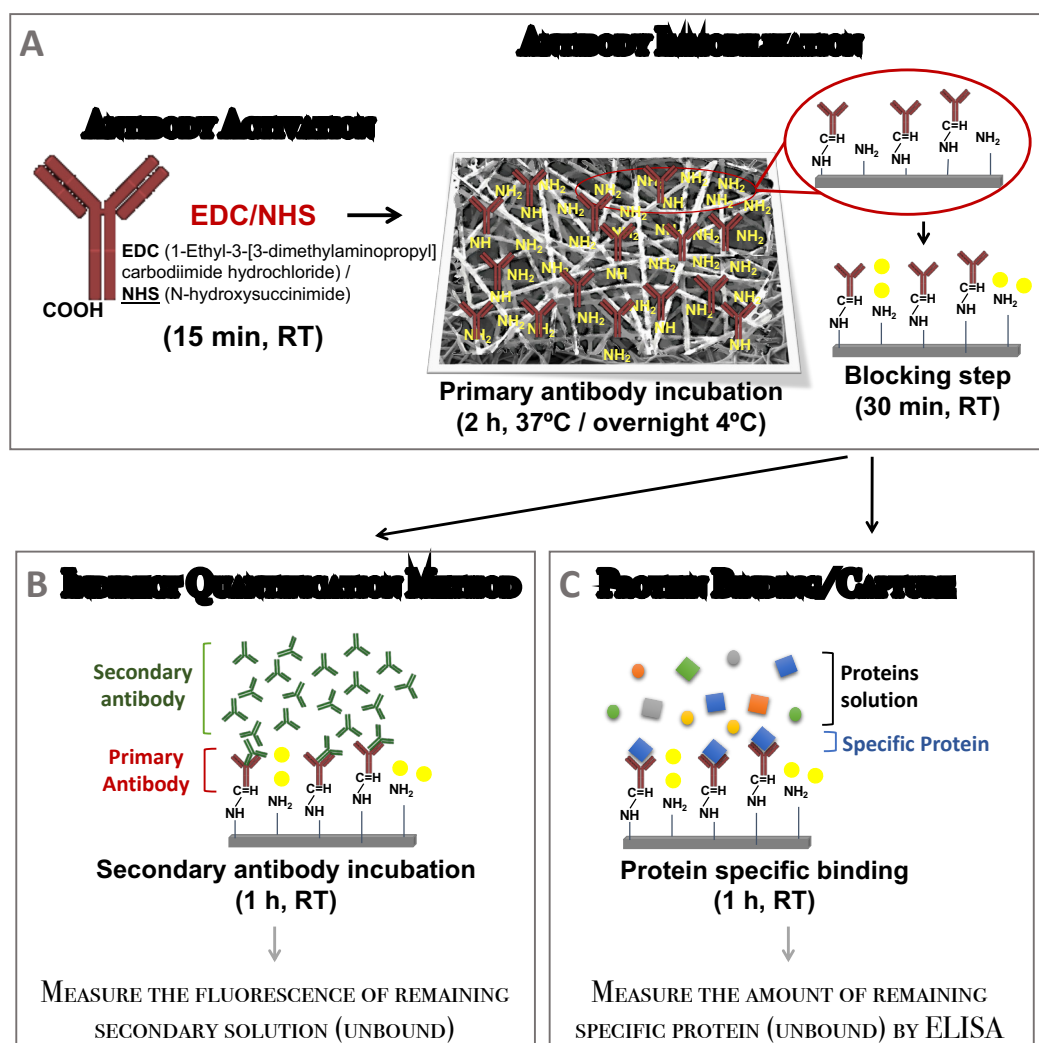


**Figure II-7** Antibody and antigen immobilization strategy implemented to activated and functionalized NFMs.

The degree of antibody immobilization was determined by an indirect method, quantifying the fluorescence of unbound secondary antibody (**Figure II-7B**). After the fluorescent-labeled secondary antibody incubation, the fluorescence of the remaining solution was read out in a

MicroPlate Reader (Synergy HT, BioTek, Vermont, USA). The different specimens of each sample were washed and kept in the dark at 4°C, until fluorescent microscopy observation.

The binding efficiency of biomolecules (i.e. recombinant proteins, plasma/platelet lysate-derived proteins and EVs-derived conditioned media) to antibodies were conducted by incubating them for 1h at RT (**Figure II-7C**). The remaining sample solutions of recombinant proteins, plasma/platelet lysate or conditioned media were kept at -20 °C until ELISA quantification.

### **II-3.3.1. Optimization of Single Antibody Immobilization**

Seven different antibodies (i.e. anti-NGF, anti-Fibronectin, anti-CD63, anti-TGF- $\beta$ 3, anti-IGF-I, anti-BMP-2 and anti-VEGF) were immobilized at the surface of activated and functionalized NFMs. In order to find the maximum immobilization capacity of the system for each antibody, a wide range of concentrations (from 0  $\mu$ g/mL to 14  $\mu$ g/mL) was tested. Activated and functionalized NFM were placed in suspension culture 24 well-plates and 200  $\mu$ l of each primary antibody concentration, previously activated, was added to each well/meshes. The anti-NGF, anti-Fibronectin, anti-CD63, anti-BMP-2 and anti-VEGF were incubated during 2h at RT, while anti-TGF- $\beta$ 3 and anti-IGF-I were incubated overnight at 4 °C. Then, each PCL NFM was washed thrice with 300  $\mu$ l 0.1 M PBS (5 min each time) and a blockage of 300  $\mu$ l 3% BSA was performed for 30 minutes at RT, followed by the secondary antibody (1:200 in PBS) incubation for 1h at RT, as shown in **Figure II-7 A and B**. To quantify the fluorescence of unbound secondary antibody solution (n=3 samples, read in triplicate) a microplate read (Synergy HT-BioTek, Vermont, USA) was used at absorption wavelength of 590 or 495 nm and an emission wavelength of 617 or 519 nm for the AlexaFluor<sup>®</sup> 594 or 488, respectively. The negative control samples were performed by carrying out all antibody immobilization steps, exchanging the primary antibody incubation with PBS.

In further experiments, the following optimized primary antibody concentrations were used: 10  $\mu$ g/mL of anti-NGF, 8  $\mu$ g/mL of anti-Fibronectin and 4  $\mu$ g/mL of anti-CD63, anti-TGF- $\beta$ 3, anti-IGF-I, anti-BMP-2 and anti-VEGF.

### II-3.3.2. Mixed immobilization of two antibodies

In order to have different but complementary antibodies at the surface of the same nanofibrous substrate, a mixed immobilization methodology was established, as depicted in **Figure II-8**. With the immobilization of multiple antibodies at the surface of the same substrate, it is expected that a highly efficient system will be developed, aiming to be applied in tissue engineering and regenerative medicine approaches.

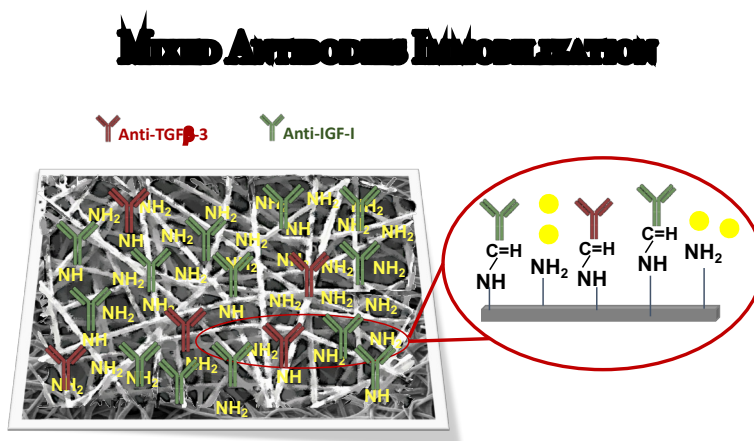


**Figure II-8** Schematic representation of the mixed antibodies immobilized at the surface of activated and functionalized NFMs.

In this work (**Chapter V**), it is hypothesized that the simultaneous immobilization of anti-TGF- $\beta$ 3 and anti-IGF-I at the surface of a single NFMs, able to selectively bound the corresponding GFs, can promote differentiation of human bone marrow-derived mesenchymal stem cells (hBM-MSCs) into the chondrogenic lineage. To achieve this purpose, both antibodies were mixed at a 1:10 proportion at the concentrations optimized before, for a final volume of 200  $\mu\text{l}$  PBS solution per well/NFM and incubated overnight at 4°C. Then the samples were washed and incubated with BSA, as previous described for single antibody immobilization. However, in the secondary antibody step, the NFMs with mixed immobilized antibodies were firstly incubated with Alexa Fluor<sup>®</sup> 594 (for anti-TGF- $\beta$ 3) for 1h at RT, washed twice with 300  $\mu\text{l}$  0.1 M PBS (5 min each time) and incubated with Alexa Fluor<sup>®</sup> 488 (for anti-IGF-I) for 1h at RT. A negative control sample was carried out, without the immobilization of the primary antibodies. The sample were washed and kept in the dark at 4°C, until further analysis by fluorescence microscopy.

### II-3.3.3. Parallel immobilization of two antibodies

The parallel immobilization methodology aimed to immobilize distinct antibodies in different areas of the same nanofibrous substrate (**Figure II-9**). Having the control of spatially immobilized antibodies, we intend to demonstrate the possibility to direct two distinct cell types spatially juxtaposed in physiological environment.

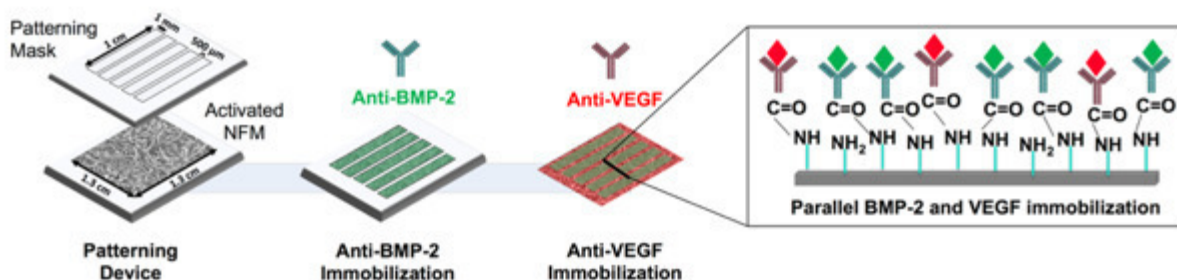


**Figure II-9** Schematic representation of the compartments in the patterning device that allows the immobilization of antibodies in a parallel design of a single NFM.

In this work (**Chapter VII**), it is intended to demonstrate the local differentiation of hBM-MSCs into either osteogenic or endothelial lineage by the immobilization of anti-BMP-2 and anti-VEGF antibodies in a parallel arrangement, capable to selectively bind the corresponding GFs. For that, a patterning device was developed capable of physically divide a single 1.3 cm<sup>2</sup> functionalized electrospun NFM into two distinct juxtaposed areas, avoiding the mixture of different immobilized antibodies. The patterning device consist on a flat acrylic plate at the bottom and an acrylic plate with 5 chambers of 0.1cm x 1cm. The activated and functionalized NFMs were placed between those plates and sealed with screws to makes pressure over the NFM and not allow the solution to diffuse from the exposed to the protected surfaces. The anti-BMP-2 antibody solution, prepared at the concentrations described above, was dropped (30 μl) over each chamber of the patterning device and incubated for 2h at RT, followed by a washing step with PBS. In order to prevent the non-specific binding of the other antibody at the chamber site, a blocking step with 0.3 % BSA solution for 30 min (RT) was performed, followed by a washing step with 0.1 M PBS. Then, the patterning device was disassembled and the anti-VEGF antibody was immobilized on the previously covered areas of the NFMs biofunctionalized with anti-BMP-2. The immobilization of anti-VEGF was performed according to previously described for the single antibody immobilization (washings, BSA blocking and secondary

antibody incubation). The samples were recovered to characterize the spatial distribution of the antibodies by fluorescence microscopy.

#### **II-3.3.4. Fluorescence microscopy**

Fluorescence microscopy allows analyzing the morphological properties of organic and inorganic materials by an optical microscope through fluorescence light. Fluorescence is characterized by a molecular phenomenon in which a substance absorbs light of a specific wavelength and almost instantaneously emits light in another wavelength, designated by excitation and emission [44]. A sample is illuminated with light of an excitation wavelength, the fluoresced light is then imaged through a fluorescence microscopy objective. Many substances naturally exhibit fluorescence, namely autofluorescence. However, bright fluorescence dyes have been developed and applied to selectively stain parts of a specimen. The resolution reaches 200 nm in the  $x$   $y$ - plane and 500 nm in the  $z$ - plane, being the greatest advantage of this technique the possibility of making three-dimensional maps of the samples to within a depth of around 100-200  $\mu\text{m}$ .

Fluorescence Microscopy (Axio Observer, Zeiss; Germany) was conducted in order to characterize the spatial distribution of the antibodies at the surface of electrospun PCL NFMs. Herein, the biological molecules (e.g. antibodies) are labeled with a fluorescence marker (Alexa Fluor<sup>®</sup> 594 or 488) and detected visually by selecting an appropriate wavelength (excitation at 495 nm for Alexa<sup>®</sup> 488 and 590 nm for Alexa<sup>®</sup> 594) accordingly to previously described reading parameters.

#### **II-3.4. Bound bioactive molecules**

Under the scope of this work, different bioactive molecules were bound at the surface of of biofunctional nanofibrous systems. Endogenous bioactive molecules (GFs, Fibronectin, EVs) were obtained from different sources. Considering a possible autologous approach, the blood components and their blood derivatives formulations (i.e plasma and platelet lysates) can be used as a biological fluid. They possess a wide range of bioactive molecules (i.e. GFs and ECM proteins), recognized to play an essential role in the regulation of wound healing [45, 46]. Cell-derived conditioned medium was also considered as a source of bioactive molecules, namely by the recently highlighted EVs content [47, 48].

### II-3.4.1. Blood Plasma

Blood plasma, also named plasma, is the non-cellular fraction of the blood. As a transport system of blood cells or the delivery of nutrients to the cells of the various organs of the body or the transport of waste products derived from cellular metabolism, plasma plays a critical role in maintaining blood and body homeostasis. Blood plasma is obtained by the separation of blood components by the segregation resulting from centrifugation (**Figure II-10**). This process is characterized by the separation of the blood into three phases: a lower phase containing red blood cells; an interface phase (buffy coat) containing white blood cells and platelets; and an upper layer corresponding to the blood plasma with platelets in suspension [46].

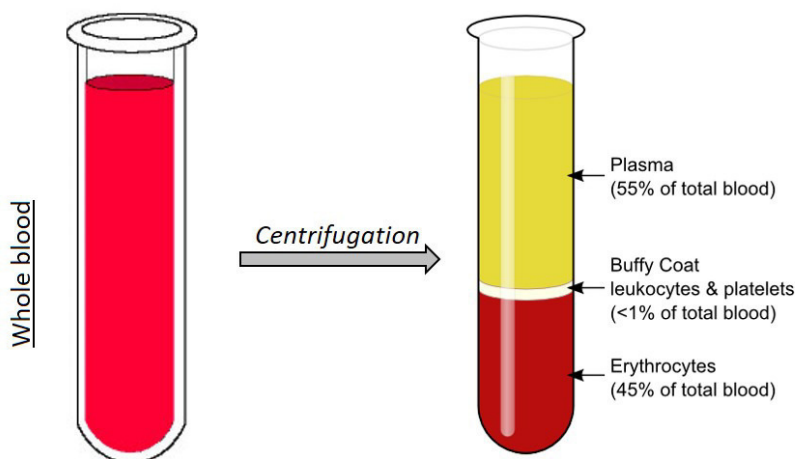


**Figure II-10 Separation of blood components by a whole blood centrifugation [49].**

The plasma used in this work was derived from blood collected from five 10-week-old adult male rats (Sprague Dawley, ENVIGO, Huntingdon, UK), in accordance to the ethical and legal regulations. The whole blood was collected from the abdominal aorta into Anticoagulant Citrate Dextrose-A (3.8%) and centrifugated at  $180 \times g$  for 10 min. Then, the blood plasma samples were coagulated by adding calcium chloride (22 mM) and the clots were allowed to retract for 40 min at  $37 \text{ }^\circ\text{C}$ . Following clot removal, the exudate was centrifuged at  $890 \times g$  for 10 min and the supernatants (i.e., platelet-free plasma) were pooled and stored at  $-80 \text{ }^\circ\text{C}$  until further use in assays to analyze the neurotrophic factor concentration (i.e. NGF $\beta$ ), as described on **Chapter VI**.

### II-3.4.2. Platelet Rich Plasma

Platelet rich plasma (PRP) is known as a volume of autologous plasma containing a platelet concentration above the baseline, namely 1 000 000 platelets/ $\mu\text{L}$  as described by Marx [50]. Platelet concentrates have been explored for tissue engineering applications as a simple and cost-effective source of GFs, cytokines and ECM proteins with key roles in the regeneration of bone and cartilage tissues [51-56]. Those autologous applications reduce the risks of disease transmission and, simultaneously, allows the induction of the “wound healing” cascade in a physiological manner. The endogenous GFs obtained from the platelets can be released through different activation mechanisms as in contact with thrombin [57], thromboplastin [58], calcium salts [57-59] or just by platelets lysis through physical disruption by thermal and osmotic shock, producing the platelet lysate (PL).

The PRP used in this work was originated from outdated collections performed at Hospital de São João (Serviço de Imunohemoterapia do Centro Hospitalar São João, Porto, Portugal), under a previously established protocol approved by the Ethical Committee. The PRP samples with 1 000 000 platelets/ $\mu\text{L}$  were obtained by plasma apheresis and all the lots were biologically qualified according to Portuguese legislation (Decreto-Lei n.º 100/2011) and stored at  $-80\text{ }^{\circ}\text{C}$  until further activation. PRP samples without activation were used in **Chapter III** as a source of endogenous Fibronectin.

#### II-3.4.2.1 *Activation of Platelet Lysate*

Platelet lysate (PL) is obtained by the freeze/thaw process of outdated PRP lots obtained by plasma apheresis [60, 61], holding several advantages over PRP. The process of the freeze/thaw cycles are easy to standardize and the PL obtained can be frozen and stored to be available for further use. The concentration of the GFs and cytokines is reproducible between batches, contributing for more predictable outcomes [61]. Furthermore, PL is rich in TGF- $\beta$ , IGF-I, BMP-2 and VEGF [60, 61].

For the works presented in **Chapters V** and **VII**, the PL was produced by three cycles of freeze/thaw, as previously described [60, 61]. In brief, the collected PRP samples from different donors were subjected to a 3-repeating temperature-shock cycles (frozen with liquid nitrogen at  $-196^{\circ}\text{C}$  and further heated at  $37\text{ }^{\circ}\text{C}$ ), lysing the platelets and releasing their content. The



remaining platelets were eliminated by centrifugation at 1400g for 10 min, followed by filtration with a 0.22  $\mu\text{m}$  filter. A pool of PL was stored at  $-20\text{ }^{\circ}\text{C}$  until further use.

### **II-3.4.3. Conditioned Medium**

The conditioned medium is the medium where cells are cultured, containing metabolites, GFs and ECM proteins secreted by the cultured cells. The secreted factors are known as the secretome, that includes microvesicles, EVs or exosome. Different cell types have the ability to secrete trophic factors that exert beneficial impact on the damaged tissue [62, 63], namely stem cell-derived secreted factors are able to promote tissue repair in tissue/organ damage [64-66]. Chondrocytes are also reported by their ability to secrete factors that may affect the differentiation status of stem cells and can promote chondrogenesis and osteogenesis [67].

In this work, the conditioned medium harvested from cultured human articular chondrocytes (hACs) and hBM-MSCs were used as source of EVs, as described in **Chapter IV**.

### **II-3.4.4. Quantification of Bound Biomolecules**

#### **II-3.4.4.1 Fluorescence-Linked immunosorbent Assay (FLISA)**

After optimizing the maximum concentration of immobilized antibody, the loading capacity of the biofunctional nanofibrous substrate was assessed by quantify the amount of bound biomolecule by using an indirect sandwich method (i.e. FLISA), as described in **Chapter V**. Basically, after all the antibodies immobilization steps, 200  $\mu\text{L}$  of the recombinant protein solutions at different concentrations (ranging from 0  $\mu\text{g}/\text{mL}$  to 6  $\mu\text{g}/\text{mL}$ ) were incubated for 1h at RT. The unbounded recombinant protein solutions were collected and stored at  $-20\text{ }^{\circ}\text{C}$  until further Enzyme-Linked immunosorbent Assay (ELISA) quantification. The biofunctionalized systems were washed with PBS and incubated overnight at  $4\text{ }^{\circ}\text{C}$  with the corresponding primary antibody. Afterwards, the biofunctionalized systems were washed again with PBS, another BSA blocking step was performed and the correspondent secondary antibody was incubated for 1 hour at RT. The fluorescence of unbounded secondary solutions was read in a microplate reader (Synergie HT, Bio- Tek, Vermont, USA), in order to quantify the secondary antibody that was not bound, as previous described for the single antibody immobilization.

#### II-3.4.4.2 *Enzyme-Linked immunosorbent Assay (ELISA)*

In order to assess the amount of unbound biomolecules after its incubation with the biofunctional systems comprising immobilized antibodies, an ELISA was performed. This is another method for the detection and quantification of specific antigens. The principle of this technique relies likewise on antigen-antibody binding, in which the antigen is quantified using a solid-phase immunoassay.

The original recombinant proteins, rat blood plasma, PRP and PL solutions as well as conditioned media, before their incubation with the functional systems, were also stored at -20 °C and used to quantify the initial amount of biomolecules. Under the scope of this thesis (**Chapters III, V and VI**), the human Fibronectin, TGF-beta3 and IGF-I and the rat NGFβ DuoSet® development ELISA kits were purchased from R&D Systems, Inc. (Minneapolis, MN; USA) and stored at -20 °C, whereas the Exosome ELISA Complete Kit (CD63) was purchased from System Biosciences (Mountain View, CA; USA) and kept at 4 °C until further use. The human BMP-2 and VEGF development ELISA kits were purchased from PeptoTech (Rochy Hill, NJ; USA) and stored at -20 °C. The development ELISA kits from R&D Systems, Inc. and PeptoTech were a two-days procedure. Firstly, the primary capture antibodies were incubated overnight in a 96-well plate (Nunc-Immuno MicroWell 96-well solid plates). In the next day, all solutions were prepared according to the manufacturer's protocol and, 100 µL of 3,3',5,5'-Tetramethylbenzidine (TMB) liquid substrate was added to each sample assessed on the R&D Systems, Inc. and System Biosciences ELISA kits. The reaction was stopped by the addition of an equal volume of 1M sulfuric acid and the absorbance read in a microplate (Synergy HT, Bio-TEK, Vermont, USA) at 450 nm, with a wavelength correction set at 540 nm. For the PeptoTech ELISA kits, in the last steps, 100 µL of an 2,2'-azino-bis(3-ethylbenzthiazoline-6-sulphonic acid (ABTS) liquid substrate was added to each well, and a color development was monitored in a microplate (Synergy HT, Bio-TEK, Vermont, USA) at 405 nm, with a wavelength correction set at 650 nm.

#### II-3.4.5. **Scanning Electron Microscopy**

The microarchitecture of EVs bound at the surface of the biofunctionalized system developed in **Chapter IV**, was analyzed by Scanning Electron Microscopy (SEM). SEM is an imaging technique normally used to analyze the surface of a solid specimen. To produce a SEM

image, the SEM generates a beam of electrons and sweeps it over the surface of the specimen instead of using light. The generated electron beam is condensed through a set of lenses before it faces the sample, where the energy of beam electrons is transferred to the electrons in the sample. The secondary collected electrons emitted from the sample are used to produce an image in a set of detections [68]. SEM analyses provides information, such as surface morphology, microstructure, porosity, pore size, and topography. For SEM analysis, samples have to be electrically conductive. A carbon layer is required for a compositional analysis by a couple Energy dispersive X-ray analyzer (EDS), while gold or metal alloys as gold/palladium is used to create conductivity samples and obtain a better image [68]. The microarchitecture of the biofunctionalized systems were analyzed by SEM (AURIGA Compact, Zeiss, Germany) and its composition analysis performed by EDS (INCAx-Act, PentaFET Precision, Oxford Instruments).

### **II-3.5. Biological Assays**

#### **II-3.5.1. Cell Culture**

*In vitro*, the cells are able to be cultured and studied by providing appropriate artificial environments. The cell culture systems are an important research tool, enabling to assess normal cellular processes. Despite different definitions and concepts, cell culture systems can be classified as primary, secondary, or continuous cell culture [69]. Under the scope of this work, continuous and primary cell cultures were used to assess the effectiveness of the different developed biofunctional nanofibrous systems. The different systems were cultured in a humidified incubator at 37°C, in 5% CO<sub>2</sub> atmosphere and the culture medium was changed every 2-3 days.

##### **II-3.5.1.1 Cell Line**

A cell line, known as continuous cell culture system, is a population of cells typically immortalized, presenting the altered-on growth control, but with the absence of virus susceptibility and differentiation capacity [70]. Those cells present a reduced or absent limitation of proliferation, producing a higher cell yield per flask. Continuously growing cell lines are generally easier to maintain and use by commercially available media with increased

growth rate in monolayer or suspension with a population doubling time of 12-24 h [70]. Although the cell lines present greater chromosomal stability, they can diverge from the donor phenotype with culture time, losing the tissue-specific markers. Therefore, for the maintenance of a stable phenotype it is essential the standardization of the culture conditions.

For the work described on **Chapter VI** and conducted under the scope of this PhD work, the rat pheochromocytoma (PC12) cell line was selected to validate the neurogenesis potential of the biofunctional systems. This cell line is derived from a pheochromocytoma of the rat adrenal medulla, having an embryonic origin from the neural crest [71]. Due to its embryological origin, PC12 can easily differentiate into neuron-like cells, having properties similar to neurons. In the presence of NGF, PC12 cells stop dividing and terminally differentiate, making them an useful model system for neuronal differentiation [72].

The rat PC12 cells, kindly provided by the “ICVS - Life and Health Sciences Research Institute”, School of Medicine, University of Minho were maintained in Dulbecco’s modified Eagle’s medium (DMEM) supplemented with 5 % horse serum (HS; Life Technologies, Camarillo, CA; USA), 10 % fetal bovine serum (FBS; Life Technologies, Camarillo, CA; USA) and 1% antibiotic/antimycotic solution (ATB; Life Technologies, Camarillo, CA; USA) in a 75 cm<sup>2</sup> cell culture flask coated with 50 µg/mL collagen type I from rat tail (Santa Cruz Biotechnology, Inc, Heidelberg, Germany). For the assays described in **Chapter VI**, a 50 µL cell suspension containing 20 000 cells was added per each sample and controls, let to adhere for 4h and cultured under basal medium consisting in DMEM medium supplemented with 0.75 % HS, 0.75 % FBS and 1 % ATB. For the differentiation studies, the basal medium was supplemented with or without 100 ng/mL recombinant NGF-β from rat, corresponding to positive or negative controls. The biological parameters, described below, were assessed at predefined culturing times, namely 1, 3 and 7 days.

### **II-3.5.1.2 Primary Cultures**

Primary culture is a cell culture system where the cells were directly obtained from a tissue. The pieces/biopsy (~1 cm<sup>3</sup>) from tissue or organs were removed in aseptic conditions and then the cells can be obtained *via* mechanic, chemical or enzymatic digestion method. The primary cells could display heterogeneous population and a low proliferation rate, but represent the more accurately the host tissues. Moreover, the primary culture cannot maintain their viability for a long culture time, because the cells lose the ability to proliferate and survive, as a result of the

changes that occur physiologically or pathologically [73]. Consequently, the use of high passage has to be avoided and the maintenance regime (i.e. medium formulation, periodic medium change and subculture) should remain consistent throughout all the period of primary cells culture.

Due to the advantages previously described, human articular chondrocytes (hACs) and human bone marrow mesenchymal stem cells (hBM-MSCs) were used under the scope of this work, namely in **Chapters III, IV, V and VII**.

#### *II.3.5.1.2.1 Human articular chondrocytes (hACs)*

Chondrocytes are the only cell type present in cartilage tissue. The use of hACs in regenerative applications have some concerns, since these cells dedifferentiate when expanded *in vitro* using two-dimensional (2D) cultures [74, 75]. In a monolayer culture, hACs acquire a fibroblastic-like morphology after several days in culture [76], while when cultured in biomaterials scaffolds providing a 3D environment they recover the round-shaped morphology by redifferentiation [77].

hACs used in this work, namely in **Chapter IV**, were isolated from human patellae collected under Informed Consent from patients undergoing knee arthroplasty in the Hospital Center of Alto Ave, Guimarães, Portugal, in accordance to the established Protocol (67/CA). The method applied for isolation and expansion of hACs was performed as described elsewhere [78]. This method is based on the enzymatic digestion of ECM cartilage for the release of chondrocytes. Human cartilage samples were dissected in small full-depth pieces and washed twice with PBS, followed its digestion with 0.25% w/v trypsin solution for 30 min at 37°C under agitation. Then, the solution was removed, the cartilage was washed and incubated overnight at 37°C under agitation with a 2 mg/mL collagenase type II solution. In the following day, the cells were washed twice with PBS, counted and plated at a density of  $2 \times 10^6$  cells per 25 cm<sup>2</sup> culture flask. Cells were cultivated with expansion medium consisting of DMEM supplemented with 10 mM Hepes buffer, L-alanyl-L-glutamine, non-essential amino acids, 1 % ATB, 10% FBS and 10 ng/mL b-FGF. For the differentiation studies, a differentiation medium was used consisting of the expansion medium supplemented with 1 mg/mL L-ascorbic acid and 1 mg/mL insulin instead of adding b-FGF.

As described in **Chapter IV**, hACs culture in expansion and differentiation media were used to harvest its conditioned media. Under expansion medium, hACs at passage 3 were seeded in T150 flasks at the density of  $3 \times 10^3$  cells/cm<sup>2</sup> and cultured until reaching the

confluence (7 days). This conditioned medium was harvested, pooled, filtered (pore size 0.22  $\mu\text{m}$ ) and kept at  $-80\text{ }^{\circ}\text{C}$  until further use. Under differentiation medium, a cell suspension containing  $2 \times 10^5$  cells/15 mL centrifuge tubes of hACs at passage 3 were centrifuged at 600g for 5 min, in order to form spherical aggregate or pellet cultures. This conditioned medium was harvested at 21, 24 and 28 days of culture, pooled, filtered (pore size 0.22  $\mu\text{m}$ ) and kept at  $-80\text{ }^{\circ}\text{C}$  until further use. hACs at passage 4 were also seeded on activated and functionalized NFMs at a density of  $2 \times 10^5$  cells/NFM, and cultured under expansion or differentiation media as experimental control conditions to assess the effectiveness of the developed EVs delivery systems (**Chapter IV**).

#### II.3.5.1.2.2 Human bone marrow mesenchymal stem cells (hBM-MSCs)

Mesenchymal stem cells (MSC) have emerged as a strong alternative due to their potential of expansion, namely self-renewal potential, and by the fact that MSC can be obtained from autologous sources [79, 80]. Therefore, the harvest of autologous tissue in a second anatomic location can be avoid by the generation of autologous grafts *in vitro*, achieving one of the goals of tissue engineering and medicine regenerative. Furthermore, MSCs can be isolated from many types of adult tissues, being characterized for its potential to go through multilineage differentiation when cultured with appropriated supplemented culture media and specific environments [81-83].

In this work, Human bone-marrow aspirates were obtained during routine surgical procedures involving knee arthroplasty, under the cooperation agreement established between the 3Bs Research Group, University of Minho and the Hospital Center of Alto Ave, Guimarães, Portugal. A detailed Informed Consent was signed by each patient/donor. Bone marrow contains at least two distinct population of stem cells, namely hematopoietic and non-hematopoietic mesenchymal. The hematopoietic stem cells in adult give rise to all components of the immune and blood system whereas the MSCs can differentiated into bone, cartilage or adipose tissue [79]. The MSCs are characterized by a spindle-shape morphology and colony forming unit capacity (CFUs). Human bone-marrow aspirates were collected into a container with alfa minimum essential medium ( $\alpha$ -MEM; Life Technologies, Carlsbad, CA; USA), supplemented with ATB and 5000 units of heparin, and maintained at  $4\text{ }^{\circ}\text{C}$  until the isolation procedure. The isolation of hBM-MSCs was based on the ability of the cells adhere to plastic as previously described in the literature [84]. The fat was removed and the suspension was centrifuged at 1200 rpm for 15 min at RT. The pellet cells were resuspended in  $\alpha$ -MEM

medium, supplemented with 1 % ATB and 10 % FBS. After culture until confluence, isolated hBM-MSCs were analyzed for their “stemness” by the expression of surface antigens like CD 29, 73, 90 and 105, while negatives for hematopoietic markers such as CD 34 and 45 (assessed by flow cytometry); and by their differentiation potential into the osteogenic, chondrogenic and adipogenic lineages [85].

In the present work we used primary cultures of hBM-MSCs cultured under static conditions to assess the potential of different biofunctional systems, namely their ability to promote chondrogenesis (**Chapters III to V**), osteogenesis or angiogenesis (**Chapter VII**). Confluent hBM-MSCs at passage 4 were harvested, counted and resuspended in basal medium aiming to be seeded at a density of  $2 \times 10^5$  cells/NFM. The constructs were maintained at 37 °C and 5% CO<sub>2</sub> for 4 hours to allow hBM-MSCs attachment. Afterwards, 1mL of basal medium was added to each culture well and left in the incubator overnight. In the next day, the medium was changed to the corresponding condition. The hBM-MSCs were cultured in basal medium, without further supplementation, on the different biofunctional systems. The experimental control conditions comprise hBM-MSCs cultured on activated and functionalized NFMs in basal medium, standard *Chondrogenic differentiation medium* (basal medium supplemented with Insulin-Transferrin-Selenium-G Supplement (ITS; Invitrogen, Carlsbad, CA; USA), 1 mM dexamethasone, 0.1 M sodium pyruvate (Invitrogen, Carlsbad, CA; USA), 17 mM ascorbic acid-2-phosphate, 35 mM L-proline and 10 ng mL<sup>-1</sup> TGF-β3), standard *Osteogenic differentiation medium* (basal medium supplemented with 50 µg/mL ascorbic acid, 10 mM β-glycerophosphate and 10<sup>-7</sup> M dexamethasone) and *Angiogenic differentiation medium* (α-MEM medium supplemented with 2 % FBS and 50 ng/mL VEGF).

For the work described on **Chapter IV**, hBM-MSC culture in basal and chondrogenic differentiation media were also used to harvest its conditioned medium. The collection of those conditioned media was similar to the one described above for hACs.

### II-3.5.2. Cell Viability assay

Viability assays are routinely conducted in order to determine the proportion of viable cells after a potential traumatic procedure, namely disaggregation, cell separation, or cryostorage [86]. The counting of the number of cells (i.e., the growth yield) is labor intensive and time consuming, particularly when a large number of samples is involved, and the duration of each experiment may be anywhere from 1 to 4 weeks. Instead, a number of alternatives have been

developed for assaying cells at higher densities, e.g. in microtitration plates. Indirect measurements of viability are mainly based on its metabolic activity. Indeed, the increase in the number of cells is proportional to the increase in the total amount of protein or DNA, or continued metabolic activity. In these cases, the survival is defined as the metabolic or proliferative capacity of the cell population as a whole.

In the present work (corresponding to **Chapters III to VII**), at each defined culture period, metabolic activity and, consequently, cell viability was determined by a colorimetric assay named CellTiter 96<sup>®</sup> AQueous One Solution Cell Proliferation Assay (Promega, Madison, WI; USA). This assay consisted on the bioreduction of the tetrazolium dye [3-(4,5-dimethylthiazol-2-yl)-5-(3-carboxymethoxyphenyl)-2-(4-sulphophenyl)-2H-tetrazolium, inner salt (MTS)] into a brown formazan product, soluble in culture medium [87]. This conversion is performed by the dehydrogenase enzymes existing in metabolically active cells, accomplished by the production of nicotinamide adenine dinucleotide phosphate (NADPH) or nicotinamide adenine dinucleotide (NADH). The quantity of the reduced brown formazan product is directly proportional to the number of viable cells in culture. The absorbance of the MTS reaction medium from each sample was read in triplicate at 490 nm, after incubation at 37 °C and 5% CO<sub>2</sub> for 3 h. Three specimens per condition and per time point were characterized.

### **II-3.5.3. Cell Proliferation assay**

The amount of cell proliferation can be achieved by the measurements of DNA synthesis [86]. Determination of cell proliferation rate is often performed to determine the cellular response to a particular stimulus, namely physical (e.g. topography of a substrate) or chemical (i.e toxin or growth/differentiation factor). The nucleic acid quantification can be performed by measurement of absorbance at 260 nm, but contaminants (e.g. RNA and single-stranded DNA) commonly found in nucleic acid preparations contributes to the relative insensitivity of this technique. Otherwise, DNA content may be determined by several fluorescence methods, involving reaction with 4,6-diamidino-2-phenylindole (DAPI), PicoGreen or Hoechst 33258. Under the scope of the present work (corresponding to **Chapters III to VII**), the cell proliferation was determined by the total amount of double-stranded DNA (dsDNA) using an ultrasensitive fluorescent nucleic acid stain. The Quant-iT<sup>™</sup>, PicoGreen<sup>®</sup> dsDNA Assay Kit (Invitrogen<sup>™</sup>, Molecular Probes<sup>™</sup>; Oregon, USA) was used, enabling the quantification of minimum amounts (25 µg/mL dsDNA) with a standard spectrofluorometer. Furthermore, using



this method, the presence of RNA and single-stranded DNA did not affect the quantitative results obtained. The samples were collected into sterile Eppendorf tubes containing 1 mL of ultrapure water and kept frozen at -80 °C. Prior to dsDNA quantification, according to the manufacture instructions the various specimens were thawed and sonicated for 15 min. A standard curve was established using pDNA standards prepared at concentrations ranging from 0 to 2 µg/mL. The fluorescence of both the samples and the standards were read in triplicate excitation 485/20 nm and emission 528/20 nm wavelengths. The DNA concentration of each sample was calculated using a standard curve relating the standard DNA concentration and the fluorescence intensity.

#### **II-3.5.4. Total Protein synthesis quantification**

Quantification of the total protein synthesis is a remarkable tool to ascertain about cell status [88]. Indeed, total cellular protein differs regarding cell growth, proliferation and differentiation [89, 90]. The most common procedures for the quantification of total protein synthesis are the colorimetric methods, namely the Lowry method, the bicinchoninic acid assay (BCA) and the biuret method [88].

In this work (corresponding to **Chapters III to VII**), the concentration of total protein was determined for all culture periods, using the same cell lysates as for dsDNA quantification. The Micro BCA™ Protein Assay kit (Thermo Scientific, Pierce, Rockford, USA) was used according to the manufacturer's instructions, in order to quantify the total proteins synthesized by the hBM-MSCs (**Chapters III, IV, V and VII**), hACs (**Chapter IV**) and PC12 cells (**Chapter VI**) in all conditions. This is a colorimetric detection and quantification method which uses the bicinchoninic acid (BCA) reagent for detection of Cu<sup>+1</sup> formed when Cu<sup>+2</sup> is reduced by protein in an alkaline environment. A purple-colored reaction product is formed by the chelation of two molecules of BCA with one cuprous ion (Cu<sup>+1</sup>). This water-soluble complex has a linear absorbance at 562 nm with increasing protein concentration. Triplicates of both samples and standards were incubated at 37 °C for 2 h with working reagent, and the total protein concentration of each sample was calculated based on an albumin standard curve, ranging from 0 to 40 µg/mL.

### II-3.5.5. Glycosaminoglycans quantification

Glycosaminoglycans (GAGs) are a major component of the cartilaginous extracellular matrix and synovial fluid, being a family of highly sulfated, complex, polydisperse linear polysaccharides that display a variety of important biological roles, [91]. Specifically, GAGs comprise the ‘ground substance’ in connective tissues that provides support while allow the cell migration and diffusion of nutrients and soluble signaling molecules within the extracellular matrix. Based on core disaccharide structures, GAGs can be categorized into four main groups: heparin/heparan sulfate, chondroitin sulfate/dermatan sulfate, keratan sulfate, and hyaluronan.

The method of GAGs quantification herein implemented consists, firstly, on the use of proteolytic enzymes capable to degrade cartilaginous ECM, followed by a colorimetric assay to measure the amount of released GAGs [92]. Herein, the GAGs quantification was performed using papain for the digestion of the produced ECM (**Chapters III to V**). After proteoglycans degradation, the released GAGs are able to link the basic dye 1,9 dimethylmethylene blue (DMB) due to its negatively charged, being detected by measuring the absorbance at 530 nm.

DMB assay was performed according to the method described elsewhere [93]. Samples were collected at each time point, frozen overnight and then digested. Digestion solution consisting on 0.05% of papain and 0.096% of N-acetyl cysteine was prepared using a digestion buffer (200 mM of phosphate buffer containing 1 mM ethylenediaminetetraacetic acid, pH 6.8). Samples were incubated with 1mL of this digestion solution, overnight at 60 °C, allowing the newly formed ECM to be separated from the scaffold. Then, the NFMs were centrifuged at 13000 rpm for 10 min and the supernatants were collected and quantified by the DMB assay. DMB stock solution was prepared by dissolving 16 mg of DMB powder in 900 mL of distilled water containing 3.04 g of glycine and 2.73 g of sodium chloride. The pH was adjusted to 3.0 with hydrochloric acid to a final volume of 1 L. The solution was stored at RT covered with aluminum foil. A stock solution of chondroitin sulfate was prepared in water at 5 mg/mL and kept at -20 °C. Dilutions of this solution were performed to obtain a standard curve. 20 µL of water was added to a 96-well plate, as a blank, and the same was performed for all the samples and the chondroitin sulphate diluted solutions. Afterwards, 250 µl of DMB solution was added to each well and the plates were incubated for 10 min at RT. The optical density was measured in a microplate reader (Synergy HT, Bio-TEK; Vermont, USA) at 530 nm.

### II-3.5.6. Alkaline phosphatase quantification

The differentiation of hBM-MSCs into the osteogenic lineage and their mineralization capacity can be achieved by biochemical assays. Typically, it involves the quantification of total calcium content and/or the activity of alkaline phosphatase (ALP), a cell surface protein bound through phosphatidylinositol phospholipid complexes at the plasma membrane [94]. Active formation of mineralized matrix is directly associated with high ALP activity, being the highest levels found in the mineralization front of the bone healing process. ALP is a protein enzyme, which has the physiological role of dephosphorylating compounds, playing an integral role in metabolism within the liver and development within the skeleton.

Under the scope of the work presented in **Chapter VII**, the quantification of ALP was performed according to the method described elsewhere [30], using the same cell lysates as for dsDNA quantification. This method consists on the  $p$ -nitrophenol assay. Nitrophenyl phosphate disodium salt (pnPP; Fluka BioChemika, Austria) is hydrolyzed at pH 10.5 and 37 °C by the ALP presented on the samples to form free yellow-colored  $p$ -nitrophenol. After 1h, a 2M sodium hydroxide (NaOH) solution was added to stop the reaction and the absorbance read at 405 nm in a microplate reader (Synergy HT, Bio-TEK; Vermont, USA). Standards were performed with 10  $\mu\text{mol/mL}$   $p$ -nitrophenol solution, obtaining a standard curve ranging from 0 to 0.3  $\mu\text{mol/mL}$ . Triplicates of each sample and standard were performed, and the ALP synthesis concentrations read off directly from the standard curve.

### II-3.5.7. Cell morphology and distribution

The cell morphology and its distribution over the biofunctionalized systems was assessed by SEM analysis on **Chapters III to VI**. For that, cell fixation is required to obtain biological samples in near natural state. Therefore, the constructs samples (cells-NFMs) were fixed with 2.5 % glutaraldehyde in PBS and keep at 4 °C until further use. Then, the samples were washed in PBS, dehydrated in increasing alcohol concentrations and allowed to dry overnight. As described above, these samples need to be coat with a conductive material such as gold or carbon due to its non-electric conductivity. Finally, they were analyzed by SEM microscopy (Cambridge S360, Leica Cambridge, Cambridge, UK) at x1 000 and x3 000 magnification.

### II-3.5.8. RNA isolation

The RNA isolation is the first and most critical step in performing fundamental molecular biology assays such as real-time polymerase chain reaction (RT-PCR). Under the scope of this work (corresponding to **Chapters III to VII**), the method used for RNA extraction and isolation was based on the Trizol reagent. It is a ready-to-use reagent, which disrupts cells and dissolves their components, maintaining the RNA integrity. Chloroform was added to make the separation of the solution into two distinct phases: aqueous and organic. The aqueous phase contains the RNA, which was recovered by the precipitation with isopropyl alcohol.

At each culturing time, the collected samples were washed with PBS, immersed in Tri reagent<sup>®</sup>, and kept at -80 °C for later RNA extraction. To perform the RNA extraction, samples were defrosted in ice, following the chloroform addition. Samples were vigorously agitated (15 s) and incubated for 15 min in ice. Then, the samples were centrifuged at 13000 rpm for 15 min at 4 °C, the supernatant collected for a sterile 1.5 mL tube, and an equivalent volume of isopropanol was added. The RNA was let to precipitated overnight at -20 °C. Afterwards, samples were centrifuged at 13000 rpm for 15 min at 4 °C, the supernatant discarded and 800 µl of ethanol 70 % was added in order to wash away the isopropanol. Samples were vigorously agitated (15 s) and centrifuged at 9000 rpm for 15 min at 4 °C. The supernatant was carefully removed, and the pellet was left to air dry under sterile conditions. The pellet was then resuspended in 20 µl of DNase free water (Lonza Verviers SPRL, Verviers, Belgium). The concentration and purity of the extracted RNA was determined using the NanoDrop ND-1000 Spectrophotometer (NanoDrop Technologies Inc, USA).

### II-3.5.9. Real-time Polymerase Chain Reaction (RT-PCR)

RT-PCR is a quantitative technique based in the PCR procedure [95]. PCR is a technique to replicate DNA by using a thermal cycling and an enzyme (DNA polymerase). This widely used technique allows the amplification of a copy of a DNA, amplifying it to a detectable quantities (amplicon). The amplicon can only be visualized at the end of the reaction in PCR, while in RT-PCR the amplification and quantification occur in simultaneous, allowing the amplicon visualization through the reaction time. RT-PCR is usually combined with reverse transcription in order to quantify the messenger RNA in cells or tissue. In this work, we used this combination for detecting gene expression of chondrogenic (**Chapter III to V**), neurogenic

(**Chapter VI**), osteogenic or endogenic (**Chapter VII**) related genes. We performed RT-PCR which consist on two steps of fluorogenic assay. Firstly, isolated RNA was reversed transcribed into complementary DNA (cDNA), and then the RT-PCR was performed to detect lineage-related genes.

In the first step, RNA was reverse transcribed into cDNA using the qScript cDNA synthesis kit, Quanta Biosciences, VWR, MA, USA), according to the manufacturer instructions. The reaction was performed using the MiniOpticon real-time PCR detection system (BioRad Laboratories, USA). Subsequently, the obtained cDNA was used as a template for the amplification of the target genes shown in **Table II-1**, according to manufacturer's instructions of the PerfeCta™ SYBR® Green system (Quanta Biosciences, VWR, MA, USA). The number of amplification cycles used for every reaction was 45. Those reactions were carried out in a Mastercycler® ep Gradient S realplex® thermocycler (Eppendorf; Hamburg, Germany).

*Glyceraldehydes-3-phosphate-dehydrogenase (GAPDH)* was used as reference gene, and the expression of all target genes was normalized to the expression of this gene for the same sample. The gene expression quantification was performed according to the Livak method ( $2^{-\Delta\Delta CT}$  method), considering the negative control as calibrator.

#### **II-3.5.10. Alcian Blue Staining**

Alcian blue stain was performed for samples studied in **Chapter III** to **V** to detect cartilage formation. Alcian blue dye stains acid mucopolysaccharides and GAGs. At 28 days of culture, samples were collected, washed with PBS, fixed in a 10% neutral buffered formalin (Bio-Optica Milano S.p.a., Italy), and kept at 4 °C. Afterwards, alcian blue stain was performed by rising the samples in 3 % acetic acid and incubated with 1 % alcian blue solution for 1h at RT. The samples were mounted in aqueous mounting medium and the staining of a cartilaginous ECM observed in an optical microscope (Leica DM750, Leica Cambridge).

Table II-1 Primer sequences used for RT-PCR procedures <sup>a)</sup>.

	gene	forward (5' - 3')	reverse (5' - 3')
Neurogenic (rat)	<i>GAPDH</i>	CAACTCCCTCAAGATTGTCAGCAA	GGCATGGACTGTGGTCATGA
	<i>GAP-43</i>	TTTCCTCTCCTGTCCTGCTC	TGGACTTGGGATCTTTCCTG
	<i>MAP2</i>	GGCACTCCTCCAAGCTACTCT	CTTGACGTTCTTCAGGTCTGG
	<i>NF-160</i>	AGCATTGAGCTCGAGTCGGTG	CTGCTGGATGGTGCCTGGTAG
	<i>NF-200</i>	AAAGTGAACACGGATGCTATGC	GTGCTTTTCAGTGCCTCCAAC
	<i>Syn1</i>	GTGTCAGGGAAGTGGAAAGACC	AGGAGCCCACCACCTCAATA
Chondrogenic	<i>GAPDH</i>	AGCCTCAAGATCATCAGCAA	GTCATGAGTCCTTCCACGAT
	<i>Sox9</i>	TTCATGAAGATGACCGACGC	GTCCAGTCGTAGCCCTTGAG
	<i>Aggrecan</i>	TGAGTCCTCAAGCCTCCTGT	TGGTCTGCAGCAGTTGATTC
	<i>COMP</i>	AGGGATGGAGACGGACATCAG	TCTGCATCAAAGTCGTCCTG
	<i>COL II</i>	CGGTGAGAAGGGAGAAGTTG	GACCGGTCCTCCAGTAGGA
Osteogenic	<i>Runx 2</i>	TTCCAGACCAGCAGCACTC	CAGCGTCAACACCATCATTC
	<i>Osteocalcin</i>	GTGCAGAGTCCAGCAAAGG	TCAGCCACTCGTCACAGC
	<i>Osteopontin</i>	GGGGACAAGTGGAGTGAAAA	CCCACAGACCCTTCCAAGTA
	<i>Oxterix</i>	CCCTTTACAAGCACTAATGG	ACACTGGGCAGACAGTCAG
	<i>BMP-2</i>	TGAATCAGAATGCAAGCAGG	TCTTTTGTGGAGAGGATGCC
	<i>ALP</i>	CTCCTCGGAAGACACTCTG	AGACTGCGCCTGGTAGTTG
	<i>COL I<math>\alpha</math></i>	AAGAACCCCAAGGACAAGAG	GTAGGTGATGTTCTGGGAGG
	<i>COL X</i>	CAGGCATAAAAGGCCCACTA	AGGACTTCCGTAGCCTGGTT
Angiogenic	<i>VEGFR2</i>	AGCGATGGCCTCTTCTGTAA	ACACGACTCCATGTTGGTCA
	<i>PECAM</i>	AAGGCCAGATGCACATCC	TTCTACCCAACATTAAGTTAGCAGG
	<i>VEGF A</i>	GATCCGCAGACGTGTAAATG	CTGGTGAGAGATCTGGTTCC

<sup>a)</sup> *GAPDH* = glyceraldehyde 3-phosphate dehydrogenase; *GAP-43* = growth-associated protein 43; *MAP-2* = microtubule-associated protein 2; *NF-160* = neurofilament 160; *NF-200* = neurofilament 200; *Syn1* = synapsin-1; *Sox9* = Sry-type high mobility group box 9; *COMP* = Cartilage oligomeric matrix protein; *COL II* = collagen type II; *Runx 2* = Runt-related transcription factor 2; *BMP-2* = Bone morphogenetic protein 2; *ALP* = Alkaline phosphatase; *COL I $\alpha$*  = collagen type I alpha; *COL X* = collagen type X; *VEGFR2* = Vascular endothelial growth factor receptor 2; *PECAM* = Platelet and endothelial cell adhesion molecule; *VEGF A* = Vascular endothelial growth factor A.

### II-3.5.11. Immunodetection of lineage-specific proteins

Immunolocalization is routinely used to detect and identify specific protein markers on *in vitro* cultured cells or in tissue sections. In this technique, the biological molecules of interest are labeled with biotin marker and detected visually, usually by adding an avidin-biotinylated enzyme complex and the correspondent enzyme substrate. This indirect observation was used in the present work (corresponding to **Chapters III to VII**) and performed according to the instructions of the manufacture of the R.T.U. VECTASTAIN® Universal ABC Elite® Kit (Vector Laboratories, CA, USA) and DAB Substrate Peroxidase kits. The principle of this method relies on the incubation of the sample with a specific primary antibody to detect the antigen of interest, followed the secondary antibody incubation. The secondary antibody is biotin-labeled, introducing many biotin molecules in the section and in the location of the primary antibody. Then the avidin-biotinylated enzyme complex added are able to bind to the biotin-labeled secondary antibody. Location of the antigen is obtained by adding an enzyme substrate.

The immunodetection of collagen type II was performed in **Chapters III to V**, while collagen type I $\alpha$  was study in **Chapters III, IV and VII**. Immunodetection of the beta III Tubulin, GAP-43, NF200 and Synapsin 1 was carried out in **Chapter VI**. In **Chapter VII**, the immunodetection of bone/vascular-specific proteins were also performed, namely osteopontin, osteocalcin, vWF and CD31 proteins. All the samples were collected at the defined culture time, washed with PBS, fixed in a 10% neutral buffered formalin (Bio-Optica Milano S.p.a., Italy), and kept at 4 °C until further used. Endogenous peroxidase activity was quenched with 0.3% hydrogen peroxide solution for 30 min. This incubation step block tissue intrinsic endogenous peroxidases that could produce a reaction product from the substrate alone. Samples were washed in PBS for 5 min and blocked with R.T.U. Normal Horse Serum from the kit, for 20 min, to avoid non-specific staining. Samples were further incubated with the respective primary antibodies [anti-beta III Tubulin polyclonal antibody (1:100), anti-GAP43 polyclonal antibody (1:200), anti-NF200 monoclonal antibody (1:40), anti-synapsin I polyclonal antibody (1:200), anti-collagen type I $\alpha$ I polyclonal antibody (1:2500), anti-human type II collagen monoclonal antibody (1:500), anti-osteopontin polyclonal antibody (1:1000), anti-osteocalcin monoclonal antibody (1:100), anti-Von Willebrand Factor polyclonal antibody (1:400) and anti-CD31 monoclonal antibody (1:100)] overnight at 4 °C. Afterward, the samples were washed with PBS for 5 min and incubated with the secondary antibody from the kit during 1h at RT. The

secondary antibody was revealed by using the Peroxidase Substrate Kit (DAB) (Vector Laboratories, CA, USA). Samples were washed in water for 5 min and, then, counterstained with hematoxylin for nuclei visualization. By the end, samples were washed in distilled water, mounted in an aqueous mounting medium and observed in an optical microscope (Leica DM750 microscopy).

In **Chapter VI** the beta III Tubulin immunostaining were used to assess the neuronal phenotype of PC12 in response to NGF stimulation. For that, the percentage of neurite-bearing cells was determined by counting more than 200 cells expressing beta III tubulin, in randomly selected fields recorded at 40x lens objective (Leica DM750 microscopy) with a computerized image analyzer (NIH ImageJ software). Neurite-bearing cells are those with neurites lengths greater than or equal to the diameter of the cell body [96, 97].

### **II-3.6. *In vivo* angiogenesis evaluation**

Relevant *in vivo* assays to assess angiogenesis comprise the chorioallantoic membrane (CAM) assay, the Zebrafish, the Subcutaneous and Orthotopic Xenografts or the Matrigel Plug Assay [98]. The ideal angiogenesis model should: (i) responds to human vascular growth factors and small molecules that have angiogenic properties and (ii) depends upon structural proteins, such as integrins, of the plasma membrane of endothelial cells in the assay system that are very comparable to those in human cells. Herein, an *in vivo* model of preclinical research, namely the CAM assay, was implemented as a minimally invasive, short-term *in vivo* alternative. Traditionally used as an angiogenic assay, the CAM of the developing embryo provides a non-innervated, rapidly growing vascular bed that can serve as a surrogate blood supply for organ culture and thus a good platform for biomaterial testing [99].

#### **II-3.6.1. Chick chorioallantoic membrane assay**

Chick chorioallantoic membrane (CAM) is composed by a multilayer epithelium, incorporating the ectoderm at the air interface, mesoderm or stroma and endoderm at the interface with the allantoic sac. The CAM assay is a well-established model for studding angiogenesis and cell invasion, due to its highly-vascularized nature, high reproductivity, simplicity and cost effectiveness [100].



In **Chapter VII**, CAM assay was performed to evaluate the angiogenic potential of the engineered biofunctional system comprising endogenous BMP-2 and VEGF bound in a side-by-side fashion. This method was performed as described in the referred chapter. A total number of 120 white fertilized chicken eggs from Pinto Bar (Amares, Portugal) were incubated at 37°C (model B8420, Termarks; Bergen, Norway) during 3 days for embryonic growth. A window was open into the eggshell to evaluate embryo viability, after puncturing the air chamber, to allowed dissociation of the CAM from the shell membrane. The window was then sealed with transparent tape (~50 x 30 mm, AXTON 50 mm) to prevent dehydration and the eggs were returned to the incubator at 37°C until implantation of the substrates. On the 10<sup>th</sup> day of embryonic development, the engineered biofunctional systems (BMP-2, VEGF and BMP-2|VEGF) and controls (without NFM and with activated NFM) were placed on the CAM. At the 17<sup>th</sup> day, the chicken embryos were sacrificed by adding a paraformaldehyde (Merck, Berlin, Germany) solution at 4% (v/v), followed by its incubation at -80° C for 10 min. The implanted specimens with adjacent CAM portions were cut and fixed with 4% paraformaldehyde. *Ex ovo* images were captured using the AxioVision imaging software (release 4.8; Zeiss, Germany) connected to an AxioCAM ICc1 digital camera (Zeiss, Germany) attached to a stereomicroscope (Stemi 2000- C; Zeiss, Germany), for each condition in both sides (i.e. chorionic and allantoic epithelium). Three independent CAM assays were performed and a minimum of 10 eggs/samples were used for each condition.

### II-3.6.1.1 *Analysis of blood vessel convergence*

A semiquantitative method was used to evaluate the total number of macroscopic blood vessels converging toward the implanted engineered biofunctional systems (BMP-2, VEGF and BMP-2|VEGF) and controls (without NFM and with activated NFM). This semiquantitative method has been previously described by Ribatti, *et al.*, [101] for the quantification of angiogenesis in the CAM of chicken eggs, using gelatin sponges as implanted materials. In this work (**Chapter VII**), the *ex ovo* images of the explants obtained after 17 days of embryonic development were processed using the ImageJ 1.52a software program (National Institutes of Health, USA) to count the total number of blood vessels converging toward the implanted substrates. For quantification purposes, the magnification of the stereomicroscope images was kept constant (0.65 X), as well as the image-processed area (800 x 800 pixels). The total number

of macroscopic microvessels that converged toward the graft was counted blindly for each egg by three independent observers.

An automated angiogenesis quantification method was also conducted by using the *Vessel Analysis* plugin a Fiji (ImageJ 1.52i) to perform in a reliable and repeatable way a sequence of operations leading to a robust segmentation of EC images and a reproducible extraction of the skeleton representing the microvascular network.[102] Measurements of vascular density (i.e. ratio of vasculature area to total selection area) and vascular length density (i.e. ratio of skeletonized vasculature area to total area) are expressed in percentage.

#### **II-4. STATISTICAL ANALYSIS**

Statistical analysis was performed using the SPSS statistic software (release 24.0.0.0 for Mac). First, a Shapiro-Wilk test was used to ascertain about the data normality and Levene test for the homogeneity of variances [103]. When data follow a normal distribution, parametric tests were used (i.e. one-way ANOVA test followed by Tukey's HSD test). The one-way ANOVA (one-way analysis of variance) test is used to compare means of one variable in two or more independent groups of samples, using the F distribution [104]. This parametric statistical test makes assumptions about the parameters of the population distribution; thus, the data normality and homogeneity of variances were firstly assessed to choose the best statistic test. When the normality and variance homogeneity were rejected, non-parametric tests were used (i.e. Kruskal-Wallis test followed by Tukey's HSD test). Kruskal-Wallis test are been used to compare one variable in more than two independent groups of samples, using ranks of observations rather than observation themselves [105]. When the Kruskal-Wallis test indicated significant differences between the independent groups, different multiple comparison test should be performed to find which one or how many are different. Therefore, in this work, the Tukey test was applied to find which pairs of biofunctional system exhibited significant differences. The Tukey multiple comparison procedure is also known as the "honestly significant difference test" or HSD test [106].  $p$  values than 0.01 were considered statistically significant in all parametric tests.

## II-5. REFERENCES

- [1] C.G. Pitt, M.M. Gratzl, G.L. Kimmel, J. Surles, A. Schindler, Aliphatic Polyesters .2. The Degradation of Poly(DL-Lactide), Poly(Epsilon-Caprolactone), and Their Copolymers *In vivo*, *Biomaterials* 2(4) (1981) 215-220.
- [2] R. Anbarasan, V. Kohila, B. Meenarathi, G. Jeyalakshmi, A. Jancirani, Synthesis, characterization and non-isothermal degradation kinetics of poly(epsilon-caprolactone)/Fe<sub>3</sub>O<sub>4</sub>-dye nanocomposites, *Sn Appl Sci* 1(6) (2019).
- [3] F.E. Wiria, K.F. Leong, C.K. Chua, Y. Liu, Poly-epsilon-caprolactone/hydroxyapatite for tissue engineering scaffold fabrication via selective laser sintering, *Acta Biomater* 3(1) (2007) 1-12.
- [4] Y.Z. Zhang, J. Venugopal, Z.M. Huang, C.T. Lim, S. Ramakrishna, Characterization of the surface biocompatibility of the electrospun PCL-collagen nanofibers using fibroblasts, *Biomacromolecules* 6(5) (2005) 2583-9.
- [5] R.S. Bezwada, D.D. Jamiolkowski, I.Y. Lee, V. Agarwal, J. Persivale, S. Trenkabethin, M. Erneta, J. Suryadevara, A. Yang, S. Liu, Monocryl(R) Suture, a New Ultra-Pliable Absorbable Monofilament Suture, *Biomaterials* 16(15) (1995) 1141-1148.
- [6] M.M. Moers-Carpi, S. Sherwood, Polycaprolactone for the Correction of Nasolabial Folds: A 24-Month, Prospective, Randomized, Controlled Clinical Trial, *Dermatol Surg* 39(3) (2013) 457-463.
- [7] P.A. Gunatillake, R. Adhikari, Biodegradable synthetic polymers for tissue engineering, *Eur Cell Mater* 5 (2003) 1-16; discussion 16.
- [8] K. Murphy, C. Weaver, *Janeway's Immunobiology*, 9th Edition, Janeway's Immunobiology, 9th Edition (2017) 1-904.
- [9] G.W. Litman, J.P. Rast, M.J. Shamblott, R.N. Haire, M. Hulst, W. Roess, R.T. Litman, K.R. Hindsfrey, A. Zilch, C.T. Amemiya, Phylogenetic Diversification of Immunoglobulin Genes and the Antibody Repertoire, *Mol Biol Evol* 10(1) (1993) 60-72.
- [10] E. Maverakis, K. Kim, M. Shimoda, M.E. Gershwin, F. Patel, R. Wilken, S. Raychaudhuri, L.R. Ruhaak, C.B. Lebrilla, Glycans in the immune system and The Altered Glycan Theory of Autoimmunity: A critical review, *Journal of Autoimmunity* 57 (2015) 1-13.
- [11] S.D. Jayasena, Aptamers: An emerging class of molecules that rival antibodies in diagnostics, *Clin Chem* 45(9) (1999) 1628-1650.
- [12] R.C. Conrad, L. Giver, Y. Tian, A.D. Ellington, In vitro selection of nucleic acid aptamers that bind proteins, *Combinatorial Chemistry* 267 (1996) 336-367.
- [13] A.V. Lakhin, V.Z. Tarantul, L.V. Gening, Aptamers: Problems, Solutions and Prospects, *Acta Naturae* 5(4) (2013) 34-43.
- [14] L. Gifre, A. Aris, A. Bach, E. Garcia-Fruitos, Trends in recombinant protein use in animal production, *Microb Cell Fact* 16 (2017).

- [15] N. Ferrer-Mirallas, P. Saccardo, J.L. Corchero, Z.K. Xu, E. Garcia-Fruitos, General Introduction: Recombinant Protein Production and Purification of Insoluble Proteins, *Methods Mol Biol* 1258 (2015) 1-24.
- [16] P.V. Pham, *Medical Biotechnology: Techniques and Applications, Omics Technologies and Bio-Engineering: Towards Improving Quality of Life, Vol 1: Emerging Fields, Animal and Medical Biotechnologies* (2018) 449-469.
- [17] L.A. Smith, P.X. Ma, Nano-fibrous scaffolds for tissue engineering, *Colloid Surface B* 39(3) (2004) 125-131.
- [18] A. Martins, E.D. Pinho, S. Faria, I. Pashkuleva, A.P. Marques, R.L. Reis, N.M. Neves, Surface Modification of Electrospun Polycaprolactone Nanofiber Meshes by Plasma Treatment to Enhance Biological Performance, *Small* 5(10) (2009) 1195-1206.
- [19] C.L. Casper, J.S. Stephens, N.G. Tassi, D.B. Chase, J.F. Rabolt, Controlling surface morphology of electrospun polystyrene fibers: Effect of humidity and molecular weight in the electrospinning process, *Macromolecules* 37(2) (2004) 573-578.
- [20] J.V. Araujo, A. Martins, I.B. Leonor, E.D. Pinho, R.L. Reis, N.M. Neves, Surface controlled biomimetic coating of polycaprolactone nanofiber meshes to be used as bone extracellular matrix analogues, *J Biomat Sci-Polym E* 19(10) (2008) 1261-1278.
- [21] M.A. da Silva, A. Crawford, J. Mundy, A. Martins, J.V. Araujo, P.V. Hatton, R.L. Reis, N.M. Neves, Evaluation of extracellular matrix formation in polycaprolactone and starch-compounded polycaprolactone nanofiber meshes when seeded with bovine articular chondrocytes, *Tissue Eng Part A* 15(2) (2009) 377-85.
- [22] Z. Rezvani, J.R. Venugopal, A.M. Urbanska, D.K. Mills, S. Ramakrishna, M. Mozafari, A bird's eye view on the use of electrospun nanofibrous scaffolds for bone tissue engineering: Current state-of-the-art, emerging directions and future trends, *Nanomedicine-Uk* 12(7) (2016) 2181-2200.
- [23] J. Doshi, D.H. Reneker, Electrospinning Process and Applications of Electrospun Fibers, *J Electrostat* 35(2-3) (1995) 151-160.
- [24] A.M. Ganan-Calvo, J. Davila, A. Barrero, Current and droplet size in the electro spraying of liquids. Scaling laws, *J Aerosol Sci* 28(2) (1997) 249-275.
- [25] P. Gibson, H. Schreuder-Gibson, D. Rivin, Transport properties of porous membranes based on electrospun nanofibers, *Colloid Surface A* 187 (2001) 469-481.
- [26] B. Ghorani, N. Tucker, Fundamentals of electrospinning as a novel delivery vehicle for bioactive compounds in food nanotechnology, *Food Hydrocolloid* 51 (2015) 227-240.
- [27] G. Taylor, Disintegration of Water Drops in an Electric Field, *Proceedings of the Royal Society of London. Series A. Mathematical and Physical Sciences* 280(1382) (1964) 383-397.
- [28] F. Dabirian, S.A.H. Ravandi, A.R. Pischevar, R.A. Abuzade, A comparative study of jet formation and nanofiber alignment in electrospinning and electrocentrifugal spinning systems, *J Electrostat* 69(6) (2011) 540-546.

- [29] W.E. Teo, S. Ramakrishna, A review on electrospinning design and nanofibre assemblies, *Nanotechnology* 17(14) (2006) R89-R106.
- [30] N. Monteiro, A. Martins, R. Pires, S. Faria, N.A. Fonseca, J.N. Moreira, R.L. Reisa, N.M. Neves, Immobilization of bioactive factor-loaded liposomes on the surface of electrospun nanofibers targeting tissue engineering, *Biomater Sci-Uk* 2(9) (2014) 1195-1209.
- [31] M.A. da Silva, A. Crawford, J. Mundy, A. Martins, J.V. Araujo, P.V. Hatton, R.L. Reis, N.M. Neves, Evaluation of Extracellular Matrix Formation in Polycaprolactone and Starch-Compounded Polycaprolactone Nanofiber Meshes When Seeded with Bovine Articular Chondrocytes, *Tissue Eng Pt A* 15(2) (2009) 377-385.
- [32] A. Martins, R. Reis, N. Neves, Critical aspects of electrospun meshes for biomedical applications, in: N. Neves (Ed.), *Electrospinning for advanced biomedical applications and therapies* 2012, pp. 69-87.
- [33] N. M., *Plasma Modification of Polymer Surfaces and Plasma Polymerization.*, Springer, Berlin, Heidelberg, *Polymer Surfaces and Interfaces.*, 2008.
- [34] S.G. Wang, W.J. Cui, J.Z. Bei, Bulk and surface modifications of polylactide, *Anal Bioanal Chem* 381(3) (2005) 547-556.
- [35] C.M. Chan, T.M. Ko, H. Hiraoka, Polymer surface modification by plasmas and photons, *Surf Sci Rep* 24(1-2) (1996) 3-54.
- [36] W.G. Qiu, Y.D. Huang, W.B. Teng, C.M. Cohn, J. Cappello, X.Y. Wu, Complete Recombinant Silk-Elastinlike Protein-Based Tissue Scaffold, *Biomacromolecules* 11(12) (2010) 3219-3227.
- [37] O. Suwantong, P. Pavasant, P. Supaphol, Electrospun Zein Fibrous Membranes Using Glyoxal as Cross-Linking Agent: Preparation, Characterization and Potential for Use in Biomedical Applications, *Chiang Mai J Sci* 38(1) (2011) 56-70.
- [38] Y.M. Shin, K.S. Kim, Y.M. Lim, Y.C. Nho, H. Shin, Modulation of spreading, proliferation, and differentiation of human mesenchymal stem cells on gelatin-immobilized poly(L-lactide-co-epsilon-caprolactone) substrates, *Biomacromolecules* 9(7) (2008) 1772-1781.
- [39] C. Oliveira, A.R. Costa-Pinto, R.L. Reis, A. Martins, N.M. Neves, Biofunctional Nanofibrous Substrate Comprising Immobilized Antibodies and Selective Binding of Autologous Growth Factors, *Biomacromolecules* 15(6) (2014) 2196-2205.
- [40] F. Darain, W.Y. Chan, K.S. Chian, Performance of Surface-Modified Polycaprolactone on Growth Factor Binding, Release, and Proliferation of Smooth Muscle Cells, *Soft Mater* 9(1) (2011) 64-78.
- [41] Y. Zhu, Z.W. Mao, C.Y. Gao, Aminolysis-based surface modification of polyesters for biomedical applications, *Rsc Adv* 3(8) (2013) 2509-2519.

- [42] J.F. Piai, M.A. da Silva, A. Martins, A.B. Torres, S. Faria, R.L. Reis, E.C. Muniz, N.M. Neves, Chondroitin sulfate immobilization at the surface of electrospun nanofiber meshes for cartilage tissue regeneration approaches, *Appl Surf Sci* 403 (2017) 112-125.
- [43] Y.B. Zhu, C.Y. Gao, X.Y. Liu, J.C. Shen, Surface modification of polycaprolactone membrane via aminolysis and biomacromolecule immobilization for promoting cytocompatibility of human endothelial cells, *Biomacromolecules* 3(6) (2002) 1312-1319.
- [44] I.J. Cox, Scanning Optical Fluorescence Microscopy, *Journal of Microscopy-Oxford* 133(Feb) (1984) 149-154.
- [45] S. Padilla, M. Sanchez, G. Orive, E. Anitua, Human-Based Biological and Biomimetic Autologous Therapies for Musculoskeletal Tissue Regeneration, *Trends in Biotechnology* 35(3) (2017) 192-202.
- [46] B.B. Mendes, M. Gomez-Florit, P.S. Babo, R.M. Domingues, R.L. Reis, M.E. Gomes, Blood derivatives awaken in regenerative medicine strategies to modulate wound healing, *Adv Drug Deliver Rev* 129 (2018) 376-393.
- [47] F. Collino, M.C. Deregibus, S. Bruno, L. Sterpone, G. Aghemo, L. Viltono, C. Tetta, G. Camussi, Microvesicles Derived from Adult Human Bone Marrow and Tissue Specific Mesenchymal Stem Cells Shuttle Selected Pattern of miRNAs, *Plos One* 5(7) (2010).
- [48] M. Martins, D. Ribeiro, A. Martins, R.L. Reis, N.M. Neves, Extracellular Vesicles Derived from Osteogenically Induced Human Bone Marrow Mesenchymal Stem Cells Can Modulate Lineage Commitment, *Stem Cell Rep* 6(3) (2016) 284-291.
- [49] HORIBA, Blood plasma. <[https://www.horiba.com/en\\_en/technology/measured-and-controlled-objects/liquid/blood-plasma/](https://www.horiba.com/en_en/technology/measured-and-controlled-objects/liquid/blood-plasma/)>, 2019 2019).
- [50] P. Borzini, I. Mazzueco, Platelet-rich plasma (PRP) and platelet derivatives for topical therapy. What is true from the biologic view point?, *Isbt Sci Ser* 2(1) (2007) 272-+.
- [51] D.P. Fang, P. Jin, Q.X. Huang, Y. Yang, J.M. Zhao, L. Zheng, Platelet-rich plasma promotes the regeneration of cartilage engineered by mesenchymal stem cells and collagen hydrogel via the TGF- $\beta$ /SMAD signaling pathway, *J Cell Physiol* 234(9) (2019) 15627-15637.
- [52] R. Burchard, H. Huflage, C. Soost, O. Richter, B. Bouillon, J.A. Graw, Efficiency of platelet-rich plasma therapy in knee osteoarthritis does not depend on level of cartilage damage, *J Orthop Surg Res* 14 (2019).
- [53] M.I. Kennedy, K. Whitney, T. Evans, R.F. LaPrade, Platelet-Rich Plasma and Cartilage Repair, *Curr Rev Musculoske* 11(4) (2018) 573-582.
- [54] P. Gupta, G.N. Hall, L. Geris, F.P. Luyten, I. Papantoniou, Human Platelet Lysate Improves Bone Forming Potential of Human Progenitor Cells Expanded in Microcarrier-Based Dynamic Culture, *Stem Cell Transl Med* 8(8) (2019) 810-821.
- [55] Y.J. Jee, Use of platelet-rich fibrin and natural bone regeneration in regenerative surgery, *J Kor Assoc Oral Max* 45(3) (2019) 121-122.

- [56] R. Shah, T.M. Gowda, R. Thomas, T. Kumar, D.S. Mehta, Biological activation of bone grafts using injectable platelet-rich fibrin, *J Prosthet Dent* 121(3) (2019) 391-393.
- [57] I. Martineau, E. Lacoste, G. Gagnon, Effects of calcium and thrombin on growth factor release from platelet concentrates: Kinetics and regulation of endothelial cell proliferation, *Biomaterials* 25(18) (2004) 4489-4502.
- [58] M.R. Messora, M.J.H. Nagata, R.C.M. Dornelles, S.R.M. Bomfim, F.A.C. Furlaneto, L.G.N. de Melo, T.M. Deliberador, A.F. Bosco, V.G. Garcia, S.E. Fucini, Bone healing in critical-size defects treated with platelet-rich plasma activated by two different methods. A histologic and histometric study in rat calvaria, *J Periodontal Res* 43(6) (2008) 723-729.
- [59] G. Intini, S. Andreana, F.E. Intini, R.J. Buhite, L.A. Bobek, Calcium Sulfate and Platelet-Rich Plasma make a novel osteoinductive biomaterial for bone regeneration, *J Transl Med* 5 (2007).
- [60] N. Fekete, M. Gadelorge, D. Furst, C. Maurer, J. Dausend, S. Fleury-Cappellesso, V. Mailander, R. Lotfi, A. Ignatius, L. Sensebe, P. Bourin, H. Schrezenmeier, M.T. Rojewski, Platelet lysate from whole blood-derived pooled platelet concentrates and apheresis-derived platelet concentrates for the isolation and expansion of human bone marrow mesenchymal stromal cells: production process, content and identification of active components, *Cytotherapy* 14(5) (2012) 540-554.
- [61] R. Crespo-Diaz, A. Behfar, G.W. Butler, D.J. Padley, M.G. Sarr, J. Bartunek, A.B. Dietz, A. Terzic, Platelet Lysate Consisting of a Natural Repair Proteome Supports Human Mesenchymal Stem Cell Proliferation and Chromosomal Stability, *Cell Transplant* 20(6) (2011) 797-811.
- [62] D.Z. Yang, W. Wang, L.P. Li, Y.L. Peng, P. Chen, H.Y. Huang, Y.L. Guo, X.W. Xia, Y.Y. Wang, H.Y. Wang, W.E. Wang, C.Y. Zeng, The Relative Contribution of Paracrine Effect versus Direct Differentiation on Adipose-Derived Stem Cell Transplantation Mediated Cardiac Repair, *Plos One* 8(3) (2013).
- [63] M.J. Lee, J. Kim, K.I. Lee, J.M. Shin, J.I. Chae, H.M. Chung, Enhancement of wound healing by secretory factors of endothelial precursor cells derived from human embryonic stem cells, *Cytotherapy* 13(2) (2011) 165-178.
- [64] H.O. Kim, S.M. Choi, H.S. Kim, Mesenchymal Stem Cell-Derived Secretome and Microvesicles as a Cell-Free Therapeutics for Neurodegenerative Disorders, *Tissue Eng Regen Med* 10(3) (2013) 93-101.
- [65] T. Tarcisia, L. Damayanti, R.D. Antarianto, Y. Moenadjat, J.A. Pawitan, Adipose derived stem cell conditioned medium effect on proliferation phase of wound healing in Sprague Dawley rat, *Med J Indones* 26(4) (2017) 239-245.
- [66] Z.Y. Du, C.F. Wei, K. Cheng, B.S. Han, J.Q. Yan, M.J. Zhang, C.H. Peng, Y.B. Liu, Mesenchymal stem cell-conditioned medium reduces liver injury and enhances regeneration in reduced-size rat liver transplantation, *Journal of Surgical Research* 183(2) (2013) 907-915.

- [67] N.S. Hwang, S. Varghese, C. Puleo, Z.J. Zhang, J. Elisseeff, Morphogenetic signals from chondrocytes promote chondrogenic and osteogenic differentiation of mesenchymal stem cells, *J Cell Physiol* 212(2) (2007) 281-284.
- [68] D.M. Doroski, K.S. Brink, J.S. Temenoff, Techniques for biological characterization of tissue-engineered tendon and ligament, *Biomaterials* 28(2) (2007) 187-202.
- [69] V.Y. Tabakov, Y.V. Schepkina, V.V. Chestkov, Modern Principles of Classification and Development of Nutrient Media for Culturing of Human and Animal Cells, *B Exp Biol Med+* 155(1) (2013) 164-171.
- [70] C. Macdonald, Development of New Cell-Lines for Animal-Cell Biotechnology, *Crit Rev Biotechnol* 10(2) (1990) 155-178.
- [71] L.A. Greene, A.S. Tischler, Establishment of a Noradrenergic Clonal Line of Rat Adrenal Pheochromocytoma Cells Which Respond to Nerve Growth-Factor, *P Natl Acad Sci USA* 73(7) (1976) 2424-2428.
- [72] N. Darbinian, Cultured Cell Line Models of Neuronal Differentiation: NT2, PC12, Neuronal Cell Culture: Methods and Protocols 1078 (2013) 23-33.
- [73] O. Uysal, T. Sevimli, M. Sevimli, S. Gunes, A.E. Sariboyaci, Cell and Tissue Culture: The Base of Biotechnology, Omics Technologies and Bio-Engineering: Towards Improving Quality of Life, Vol 1: Emerging Fields, Animal and Medical Biotechnologies 2018, pp. 391-429.
- [74] M. Schnabel, S. Marlovits, G. Eckhoff, I. Fichtel, L. Gotzen, V. Vecsei, J. Schlegel, Dedifferentiation-associated changes in morphology and gene expression in primary human articular chondrocytes in cell culture, *Osteoarthritis Cartilage* 10(1) (2002) 62-70.
- [75] M. Jakob, O. Demartean, D. Schafer, B. Hintermann, W. Dick, M. Heberer, I. Martin, Specific growth factors during the expansion and redifferentiation of adult human articular chondrocytes enhance chondrogenesis and cartilaginous tissue formation in vitro, *J Cell Biochem* 81(2) (2001) 368-77.
- [76] N. Ahmed, L. Gan, A. Nagy, J. Zheng, C. Wang, R.A. Kandel, Cartilage tissue formation using redifferentiated passaged chondrocytes in vitro, *Tissue Eng Part A* 15(3) (2009) 665-73.
- [77] K. Chaipinyo, B.W. Oakes, M.P. van Damme, Effects of growth factors on cell proliferation and matrix synthesis of low-density, primary bovine chondrocytes cultured in collagen I gels, *J Orthop Res* 20(5) (2002) 1070-8.
- [78] A. Crawford, S.C. Dickinson, Chondrocyte isolation, expansion, and culture on polymer scaffolds, *Methods Mol Biol* 238 (2004) 147-58.
- [79] R.E.B. Fitzsimmons, M.S. Mazurek, A. Soos, C.A. Simmons, Mesenchymal Stromal/Stem Cells in Regenerative Medicine and Tissue Engineering, *Stem Cells Int* (2018).
- [80] A.I. Caplan, Adult mesenchymal stem cells for tissue engineering versus regenerative medicine, *J Cell Physiol* 213(2) (2007) 341-347.
- [81] Y.H. Jiang, B.N. Jahagirdar, R.L. Reinhardt, R.E. Schwartz, C.D. Keene, X.R. Ortiz-Gonzalez, M. Reyes, T. Lenvik, T. Lund, M. Blackstad, J.B. Du, S. Aldrich, A. Lisberg, W.C.



Low, D.A. Largaespada, C.M. Verfaillie, Pluripotency of mesenchymal stem cells derived from adult marrow, *Nature* 418(6893) (2002) 41-49.

[82] M.F. Pittenger, A.M. Mackay, S.C. Beck, R.K. Jaiswal, R. Douglas, J.D. Mosca, M.A. Moorman, D.W. Simonetti, S. Craig, D.R. Marshak, Multilineage potential of adult human mesenchymal stem cells, *Science* 284(5411) (1999) 143-147.

[83] P. Bianco, M. Riminucci, S. Gronthos, P.G. Robey, Bone marrow stromal stem cells: Nature, biology, and potential applications, *Stem Cells* 19(3) (2001) 180-192.

[84] S.A. Kuznetsov, P.H. Krebsbach, K. Satomura, J. Kerr, M. Riminucci, D. Benayahu, P.G. Robey, Single-colony derived strains of human marrow stromal fibroblasts form bone after transplantation in vivo, *J Bone Miner Res* 12(9) (1997) 1335-1347.

[85] M. Dominici, K. Le Blanc, I. Mueller, I. Slaper-Cortenbach, F.C. Marini, D.S. Krause, R.J. Deans, A. Keating, D.J. Prockop, E.M. Horwitz, Minimal criteria for defining multipotent mesenchymal stromal cells. The International Society for Cellular Therapy position statement, *Cytotherapy* 8(4) (2006) 315-317.

[86] R.I. Freshney, Cytotoxicity, in: R.I. FRESHNEY (Ed.), *Culture of Animal Cells: A Manual of Basic Technique and Specialized Applications*, 7th Edition, Wiley-Blackwell 2016.

[87] A.H. Cory, T.C. Owen, J.A. Barltrop, J.G. Cory, Use of an aqueous soluble tetrazolium/formazan assay for cell growth assays in culture, *Cancer Commun* 3(7) (1991) 207-12.

[88] R.I. Krohn, The colorimetric detection and quantitation of total protein, *Curr Protoc Cell Biol Appendix* 3 (2011) 3H.

[89] H.H. Engelhard, 3rd, J.L. Krupka, K.D. Bauer, Simultaneous quantification of c-myc oncoprotein, total cellular protein, and DNA content using multiparameter flow cytometry, *Cytometry* 12(1) (1991) 68-76.

[90] M. Marti, L. Mulero, C. Pardo, C. Morera, M. Carrio, L. Laricchia-Robbio, C.R. Esteban, J.C. Izpisua Belmonte, Characterization of pluripotent stem cells, *Nat Protoc* 8(2) (2013) 223-53.

[91] F.Z. Zhang, Z.; Linhardt R. J., Glycosaminoglycans, in: E.D.P. Cummings, M. (Ed.), *Handbook of Glycomics*, ACADEMIC PRESS 2010.

[92] C.J. Billington, Cartilage proteoglycan release assay, *Methods Mol Biol* 151 (2001) 451-6.

[93] W. Kafienah, T.J. Sims, Biochemical methods for the analysis of tissue-engineered cartilage, *Methods Mol Biol* 238 (2004) 217-30.

[94] S. Hofmann, D. Kaplan, G. Vunjak-Novakovic, L. Meinel, *Tissue Engineering of Bone, Culture of Cells for Tissue Engineering* 2006, pp. 323-373.

[95] S.J. Maddocks, R., Quantitative PCR: Things to Consider, in: S.J. Maddocks, R. (Ed.), *Understanding PCR*, Academic Press 2017, pp. 45-52.

- [96] H. Kawakami, K. Hiraka, S. Nagaoka, Y. Suzuki, M. Iwaki, Neuronal attachment and outgrowth on a micropatterned fluorinated polyimide surface, *J Artif Organs* 7(2) (2004) 83-90.
- [97] Y.M. Yang, W.J. Zhao, J.H. He, Y.H. Zhao, F. Ding, X.S. Gu, Nerve conduits based on immobilization of nerve growth factor onto modified chitosan by using genipin as a crosslinking agent, *Eur J Pharm Biopharm* 79(3) (2011) 519-525.
- [98] S.A. Mousa, M. Yalcin, P.J. Davis, Models for Assessing Anti-Angiogenesis Agents: Appraisal of Current Techniques, *Anti-Angiogenesis Strategies in Cancer Therapies 2017*, pp. 21-38.
- [99] R. Auerbach, L. Kubai, D. Knighton, J. Folkman, A simple procedure for the long-term cultivation of chicken embryos, *Dev Biol* 41(2) (1974) 391-4.
- [100] N.A. Lokman, A.S.F. Elder, C. Ricciardelli, M.K. Oehler, Chick Chorioallantoic Membrane (CAM) Assay as an In Vivo Model to Study the Effect of Newly Identified Molecules on Ovarian Cancer Invasion and Metastasis, *International Journal of Molecular Sciences* 13(8) (2012) 9959-9970.
- [101] D. Ribatti, B. Nico, A. Vacca, M. Presta, The gelatin sponge-chorioallantoic membrane assay, *Nat Protoc* 1(1) (2006) 85-91.
- [102] P. Nowak-Sliwinska, J.P. Ballini, G. Wagnieres, H. van den Bergh, Processing of Fluorescence Angiograms for the Quantification of Vascular Effects Induced by Anti-angiogenic Agents in the CAM model (vol 79, pg 21, 2010), *Microvascular Research* 80(1) (2010) 177-177.
- [103] S.S. Shapiro, M.B. Wilk, An Analysis of Variance Test for Normality (Complete Samples), *Biometrika* 52 (1965) 591-&.
- [104] G.C. Ramseyer, *Statistical-Methods for Psychology - Howell, Dc*, *Contemp Psychol* 39(7) (1994) 727-729.
- [105] H. Mansouri, Analysis of variance based on ranks using computing packages, *American Statistical Association - 1996 Proceedings of the Statistical Computing Section* (1996) 146-149.
- [106] H.J. Keselman, J.C. Rogan, Tukey Multiple Comparison Test - 1953-1976, *Psychol Bull* 84(5) (1977) 1050-1056.

## **SECTION 3**

# **STRATEGIES FOR CARTILAGE REPAIR**

## **CHAPTER III**

# **Fibronectin Bound to a Fibrous Substrate has Chondrogenic-inductive Properties**

## Chapter III

### Fibronectin Bound to a Fibrous Substrate has Chondrogenic-inductive Properties<sup>†</sup>

#### ABSTRACT

Articular cartilage is an avascular tissue with a low self-regeneration potential. Furthermore, this tissue is characterized by a dense and specific extracellular matrix (ECM). Fibronectin (FN) is a key constituent of the pericellular ECM, assembled into a fibrillar matrix through a cell-mediated process. Although FN is essential in chondrocytes condensation during cartilage development, being implicated in chondrogenic events, its potential to induce chondrogenic differentiation of mesenchymal stem cells (MSCs) remains unclear.

In this study, we evaluate the chondrogenic potential of FN bound at the surface of an electrospun nanofibrous mesh (NFM). For that, anti-FN antibody was immobilized at the surface of NFMs, capable of selectively bind endogenous FN (eFN) from blood plasma. The chondrogenic potential of bound eFN was further assessed by culturing human bone marrow-derived MSCs during 28 days, in basal growth medium. The biological results indicate that NFMs biofunctionalized with eFN were able to successfully induce the chondrogenesis of MSCs by the high expression of *SOX9*, *COMP*, *Aggrecan*, *Collagen type II*, as well as glycosaminoglycans synthesis. Therefore, biofunctionalized nanofibrous comprising eFN significantly enhance the efficacy of a cartilage tissue engineering strategy.

---

<sup>†</sup> This chapter is based on the following publication:

Casanova M. R., Reis R. L., Martins A. and Neves N. M., "Fibronectin Bound to a Fibrous Substrate has Chondrogenic-inductive Properties", Submitted for publication.

### III-1. INTRODUCTION

During the cartilage development, a condensed mass of cells is formed by the aggregation of the undifferentiated mesenchyme, which undergo differentiation to form mature chondrocytes and deposit cartilage-specific extracellular matrix (ECM) [1]. The ECM is a fibrillar network of proteins, being a critical regulator of the cell behavior [2]. Cell-ECM binding provides chemical signals, structural support and local cues, organized to promote integration of environmental information in the intracellular pathways. ECM signals are communicated through the cell-surface receptors to regulate cellular functions such as proliferation, migration, survival and differentiation [3, 4].

A temporal change in the composition of the deposited ECM is the key feature of chondrogenesis. It is determinant for differentiated chondrocytes to be able to maintain a cartilaginous structure and function, and not to undergo hypertrophy [5]. The protein composition of the ECM varies among the development stages of chondrogenesis. During condensation, matrix proteins such as FN, collagen I and the proteoglycan versican are prevalent [6, 7]. In contrast, matrix deposited by differentiated chondrocytes is rich in collagens II and IX and the proteoglycan aggrecan [8-10], this matrix might provide the optimal structure and stiffness, which is known to be important for chondrocyte differentiation [11].

FN is a 440KDa glycoprotein, widely distributed in the ECM, plasma and other body fluids [4]. In plasma, FN has a concentration range of 200–400  $\mu\text{g/mL}$  [12, 13]. It is a key constituent of the pericellular ECM, forming essential connections between cell surface integrin receptors and structural components of the ECM (i.e. collagens) [5]. This essential role of FN in chondrocytes condensation during cartilage development is well known [14-16]. Therefore, FN acts as a matrix assembler by promoting cell adhesion and differentiation [5, 14, 16-22], by activating intracellular pathways through integrins signaling, regulate gene expression during chondrogenesis [23, 24].

Articular cartilage degeneration and lesions are considered the most common cause of severe long-term pain and lead to physical disability and significant decrease in the quality of life [25, 26]. Many treatment options have been implemented to repair damaged cartilage, such as microfracture and mosaicplasty [27]. The first tissue engineering strategy proposed for cartilage repair was autologous chondrocyte implantation (ACI), consisting in the implantation of autologous chondrocytes into the patient chondral injury [28]. The procedure was improved into the second generation matrix-induced autologous chondrocyte implantation (MACI),

involving the culturing of autologous chondrocytes onto a three dimensional collagen biocompatible scaffold [29]. Despite the promising results reported by chondrocyte implantation techniques in a large percentage of patients, the properties of healthy, normal articular cartilage are still unmatched by those advanced therapies [27]. Cartilage tissue engineering has emerged as an alternative strategy for the repair or regeneration of damaged cartilage. Within this strategy, mesenchymal stem cells (MSCs) are a promising source of adult cells, which can be induced to differentiated into the chondrogenic lineage under specific conditions. Specifically, chondrogenic differentiation of MSCs could be achieved through their exposure to either cell-adhesion molecules (i.e. chondroitin sulfate) or lineage-specific growth factors, such as transforming growth factor-beta (TGF- $\beta$ ) [30-33].

Envisioning an autologous approach, we herein report on the development of a biofunctionalized electrospun polycaprolactone nanofibrous mesh (PCL NFM) able to specifically bind endogenous FN (eFN) from a pool of blood plasma samples. Herein, the glycoprotein FN was investigated for their role in the chondrogenic differentiation of human bone marrow MSCs (hBM-MSCs). The impact of the bound FN over the cell proliferation, development of the ECM and its composition, as well as the gene expression of hBM-MSCs, were all evaluated.

## **III-2. MATERIALS AND METHODS**

### **III-2.1. Production of activated and functionalized PCL NFMs**

The production of activated and functionalized PCL NFMs was performed as described elsewhere [34]. Briefly, a polymeric solution of 15% (w/v) PCL (Polycaprolactone- Mn 70,000-90,000 by GPC, Sigma-Aldrich, Europe) in chloroform/dimethylformamide (7/3, Sigma-Aldrich, Europe) was electrospun with a voltage of 12kV, a needle tip to ground collector distance of 20cm, and a flow rate of 1mL/h. After the processing of 1mL of the polymeric solution, the NFM was left to dry and cut into samples of 1cm<sup>2</sup>.

The surfaces of the NFMs were activated by UV-ozone irradiation, by exposing both sides to UV light (ProCleaner 220 system, Bioforce Nanoscience) during 2 min. Then, the activated NFMs were immersed in 1M 1,6-hexanediamine (HMD) solution (Sigma-Aldrich Química, S.L., Europe) and incubated for 1h at 37°C, to functionalize the surface of NFMs with amine

groups (-NH<sub>2</sub>). Those activated and functionalized NFMs were further used as control conditions in the biological assays.

### III-2.2. Biofunctionalization of NFMs

A human FN antibody (Mouse monoclonal, Anti-Fibronectin antibody [BC-1] (ab154210), ABCAM, Europe) was immobilized at the surface of the activated and functionalized NFMs by a covalent bond mediated by a coupling agent, namely 1-ethyl-3-(3-(dimethylamino)-propyl)carbodiimide / hydroxysuccinimide mixture (1:4 ratio)(EDC/NHS; Sigma-Aldrich Química, S.L., Europe). Prior to the incubation of a 1 % (v/v) FN antibody solution (PBS, 7.4 pH) for 2h at room temperature (RT), this antibody/EDC/NHS mixture was incubated 15 min at RT for protein activation. The maximum immobilization capacity on the surface of the NFMs was determined by using a wide range of concentrations (from 0 to 14 µg/mL). The non-immobilized FN antibody was removed by washing step with 0.1 M PBS.

After the FN antibody immobilization at the NFMs, a BSA (Sigma-Aldrich Química, S.L., Europe) blocking step was performed (1 h at RT), and the corresponding secondary antibody (1:200 in PBS)(Alexa Fluor<sup>®</sup> 488 donkey anti-mouse IgG (H+L), Life Technologies, USA (~495/517 nm)) was incubated for 1 h at RT. The unbound secondary antibody fluorescence was measured in a microplate reader (Synergy HT, Bio-TEK), as an indirect method to determine the primary antibody immobilization efficiency. The NFMs without primary antibody were used as a negative control to evaluate nonspecific immobilization. The spatial distribution of FN antibody at the surface of the NFM was analyzed by fluorescence microscopy (Axio Observer; Zeiss).

The binding capacity of the biofunctionalized NFMs with FN antibody was assessed by using human blood plasma as an endogenous source of FN. The blood plasma was obtained from plasma apheresis of six healthy donors: three female donors and three male donors. The plasma collections were provided by Hospital de São João (Serviço de Imunohemoterapia do Centro Hospitalar São João, Porto, Portugal) under an established collaboration protocol, approved by the ethical committee. A pool of plasma was performed by mixing the six independent plasma samples. The platelet debris were removed by centrifugation at 1400g during 10 min at 4°C, and supernatants were filtered (0.22 µm filter) and stored at -20°C until further use.



The biofunctionalized NFMs, with the FN antibody at the maximum concentration previously optimized, were incubated with 400  $\mu$ L of plasma (1 h, RT), in order to determine the eFN binding efficiency of the immobilized FN antibody. The unbound protein solutions were collected and stored at -20 °C, until further quantification by *enzyme-linked immunosorbent assay* (ELISA).

The quantification of eFN presented on plasma samples and on the unbound protein solutions were performed by using the human Fibronectin DuoSet<sup>®</sup> development ELISA kits (R&D Systems, Inc., USA). The assay was conducted according to the manufacturer's protocol.

### III-2.3. Biological activity

#### III-2.3.1. hBM-MSCs Isolation, Culture and Seeding

hBM-MSCs were isolated from bone-marrow aspirates collected after obtaining informed consent from patients undergoing knee arthroplasty. Those samples were obtained under the protocol established between the 3B's Research Group, University of Minho and the Hospital Center of Alto Ave, Guimarães, and approved by the ethics committee of this hospital (67/CA). hBM-MSCs were characterized and cultured under static conditions in basal medium ( $\alpha$ -MEM (Sigma-Aldrich, Europe), supplemented with 10% heat-inactivated fetal bovine serum (FBS; Life Technologies, USA) and 1% antibiotic/antimycotic solution (Life Technologies, USA)) at 37 °C and in a humidified atmosphere of 5% CO<sub>2</sub>, using our established standard protocols [35].

Cells were expanded until passage 4 in order to achieve seeding densities of 200 000 cells/50  $\mu$ L/NFM. The conditions assessed were nanofibrous substrates biofunctionalized with eFN bound from a pool of blood plasma (*eFN*) or from commercial FN (*cFN*; Human Plasma Fibronectin Purified Protein, Millipore, USA) under basal medium, without further medium supplementation. The experimental control conditions comprise hBM-MSCs cultured on activated and functionalized NFMs in basal medium (*Basal*), soluble cFN (*cFN soluble*;  $\alpha$ -MEM medium supplemented with 8  $\mu$ g/mL cFibronectin), standard chondrogenic differentiation medium (*Chondro*; basal medium supplemented with Insulin-Transferrin-Selenium-G Supplement (ITS; Invitrogen), 1 mM dexamethasone (Sigma-Aldrich), 0.1 M sodium pyruvate (Invitrogen), 17 mM ascorbic acid-2-phosphate (Wako Pure Chemical Industries, Ltd.), 35 mM L-proline (Sigma-Aldrich) and 10 ng mL<sup>-1</sup> TGF- $\beta$ 3) and standard

osteogenic differentiation medium (**Osteo**; basal medium supplemented with 50 µg/mL ascorbic acid, 10 mM β-glycerophosphate and 10<sup>-7</sup> M dexamethasone). The constructs were retrieved for further analysis at predefined culturing times, namely 0, 7, 14, 21 and 28 days. All experiments were performed in triplicate and repeated at least three times (n=3), independently.

### III-2.3.2. Cellular Biochemistry Analysis

Cell proliferation was evaluated by DNA quantification (Quant-iTPicoGreen dsDNA assay, Invitrogen, Alfacene), metabolic activity by the MTS assay (CellTiter 96 AQueous One Solution, Promega) and protein synthesis by Micro BCA assay (Micro BCA™ Protein Assay Kit, Thermo Fisher Scientific, USA), according to the manufacturer's instructions. Glycosaminoglycans (GAGs) quantification was performed according to a colorimetric assay previously established in our lab, namely the dimethyl methylene blue (DMB) assay [36].

### III-2.3.3. Scanning Electron Microscopy (SEM)

The constructs were dehydrated, sputter coated with Au/Pd and analysed in a scanning electron microscope (Model S360, Leica Cambridge, Europe).

### III-2.3.4. Gene Expression Analysis

At each time point, the constructs were washed with PBS, immersed in Tri reagent® (Life Science, VWR, USA), and kept at -80 °C for later RNA extraction. Total RNA was isolated and reverse transcribed into cDNA (qScript cDNA synthesis kit, Quanta Biosciences, VWR, USA), according to the manufacturer instructions. Afterwards, the obtained cDNA was used as a template for the amplification of target genes (**Table III 1**), according to the manufacturer's instructions of the PerfeCta™ SYBR® Green system (Quanta Biosciences, VWR, USA). The qPCR reactions were carried out in a Mastercycler® ep Gradient S realplex® thermocycler (Eppendorf; Hamburg, Europe) for all genes. The transcript expression data were normalized against the housekeeping gene *Glyceraldehydes-3-phosphate-dehydrogenase* (*GAPDH*) and the quantification performed according to the Livak method (2<sup>-ΔΔCT</sup> method) [37], considering the basal medium testing condition (negative control) as calibrator.

**Table III-1 Primer sequences used for RT-PCR procedures <sup>a)</sup>.**

	gene	forward (5' - 3')	reverse (5' -3')
Ref.	<i>GAPDH</i>	AGCCTCAAGATCATCAGCAA	GTCATGAGTCCTTCCACGAT
Chondrogenic	<i>Sox9</i>	TTCATGAAGATGACCGACGC	GTCCAGTCGTAGCCCTTGAG
	<i>Aggrecan</i>	TGAGTCCTCAAGCCTCCTGT	TGGTCTGCAGCAGTTGATTC
	<i>COMP</i>	AGGGATGGAGACGGACATCAG	TCTGCATCAAAGTCGTCCTG
	<i>COL II</i>	CGGTGAGAAGGGAGAAGTTG	GACCGGTCACTCCAGTAGGA
Hypertrophic	<i>COL I<math>\alpha</math></i>	AAGAACCCCAAGGACAAGAG	GTAGGTGATGTTCTGGGAGG
	<i>COL X</i>	CAGGCATAAAAGGCCCACTA	AGGACTTCCGTAGCCTGGTT
	<i>Runx 2</i>	TTCCAGACCAGCAGCACTC	CAGCGTCAACACCATCATTC
	<i>ALP</i>	CTCCTCGGAAGACACTCTG	AGACTGCGCCTGGTAGTTG

<sup>a)</sup> *GAPDH* = Glyceraldehyde 3-phosphate dehydrogenase; *Sox9* = Sry-type high mobility group box 9; *COMP* = Cartilage oligomeric matrix protein; *COL II* = collagen type II; *COL I $\alpha$*  = collagen type I alpha; *COL X* = collagen type X; *Runx 2* = Runt-related transcription factor 2; *ALP* = Alkaline phosphatase.

### III-2.3.5. Histological Analysis

Samples were collected at 28 days of culture, fixed in a 4% paraformaldehyde solution, and kept at 4 °C until further used for staining procedures. Alcian blue staining, immunocytochemistry for collagens type I (COL1A1 (C-18); Santa Cruz Biotechnology, Europe) and type II (mouse anti-human type II collagen monoclonal antibody; Millipore, USA) were performed as described elsewhere [38]. The samples were counterstained with hematoxylin for nuclei visualization and observed in an optical microscope (Leica DM750 microscope).

### III-2.4. Statistical analysis

Statistical analysis was performed using the SPSS statistic software (release 24.0.0.0 for Mac). First, a Shapiro-Wilk test was used to ascertain the data normality and Levene test for the homogeneity of variances. Parametric tests (one-way ANOVA test followed by Tukey's HSD test) were used on data following a normal distribution (i.e. **Figure III-1a**). For all other data, the normality and variance homogeneity were rejected and non-parametric tests were used (Kruskal-Wallis test followed by Tukey's HSD test). *p* values lower than 0.01 were considered statistically significant in non-parametric tests.

### III-3. RESULTS

#### III-3.1. Biofunctionalization of nanofibrous substrates with human plasma fibronectin

The initial aim of this study was to develop a biofunctional nanofibrous substrate comprising the glycoprotein FN from commercial (*cFN*) or endogenous-origin (*eFN*). An optimized activated and functionalized NFM was used, providing binding sites able to bind FN *via* a non-neutralizing antibody-antigen bond. The immobilized FN antibody allows to bind the corresponding protein from a complex biological fluid (i.e. plasma), envisioning an autologous approach. The FN antibody was successfully immobilized at the maximum concentration of 8  $\mu\text{g/mL}$  (Figure III 1 a) and its uniform distribution over the nanofibrous substrate is shown in Figure III 1 b).

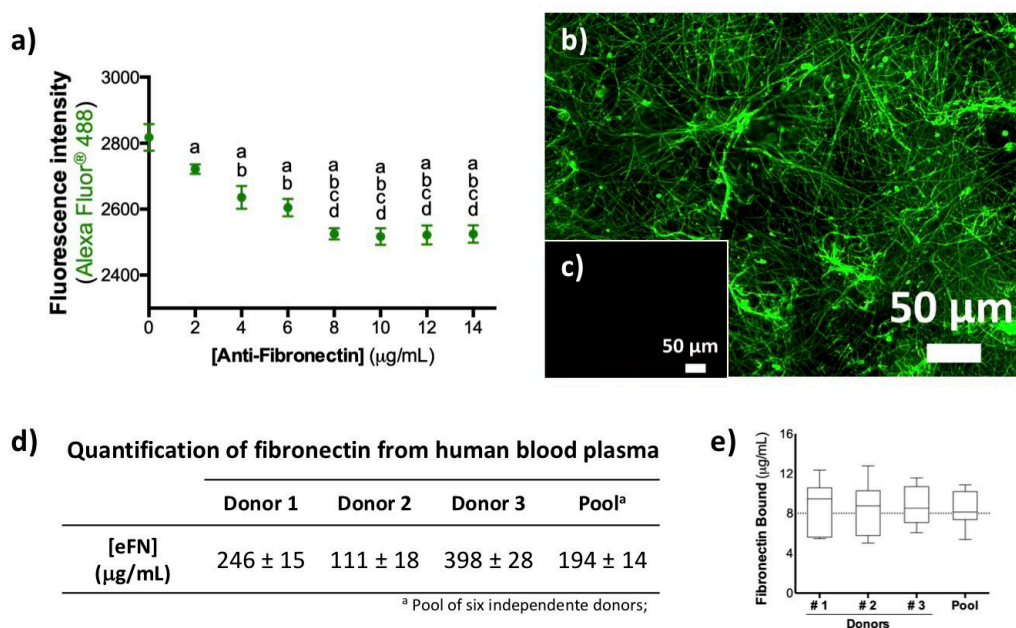


Figure III-1 Top: Maximum immobilization capacity of fibronectin antibody at the surface of activated and functionalized NFM (a). Data were analyzed by the one-way ANOVA test, followed by the Tukey's HSD test ( $p < 0.001$ ): a denotes significant differences compared to concentration 0  $\mu\text{g/mL}$ ; b denotes significant differences compared to concentration 2  $\mu\text{g/mL}$ ; c denotes significant differences compared to concentration 4  $\mu\text{g/mL}$  and d denotes significant differences compared to concentration 6  $\mu\text{g/mL}$ ; Spatial distribution of anti-fibronectin (b) immobilized at the surface of activated and functionalized nanofibrous substrates at 8  $\mu\text{g/mL}$ . The negative control sample (c) was not incubated with the primary antibody. Bottom: Quantification of fibronectin (d) present in 3 independent human blood plasma samples and in a pool of six independent donors. The endogenous fibronectin binding capacity of the biofunctionalized nanofibrous substrate (e).

The binding capacity of the immobilized FN antibody at the nanofibrous substrates was assessed by using eFN from different plasma donors. **Figure III 1 d)** shows the range of concentrations obtained from three different human samples (from 111 to 398  $\mu\text{g}/\text{mL}$ ), and from a pool of six independent donors,  $194 \pm 14 \mu\text{g}/\text{mL}$ . This amount is in line with reported by the literature considering the soluble FN synthesized and secreted by hepatocytes (200–400  $\mu\text{g}/\text{mL}$  in human plasma [12, 13]). Those eFN was successfully bound at the biofunctionalized nanofibrous substrate comprising immobilized FN antibody at the maximum concentration of 8  $\mu\text{g}/\text{mL}$  (**Figure III 1 e**).

### III-3.2. Biological activity of fibronectin over hBM-MSCs

To assess the role of the FN in the chondrogenic differentiation of MSCs, hBM-MSCs were cultured over biofunctionalized nanofibrous substrates comprising bound FN from different sources (i.e. *cFN bound* and *eFN bound*), under basal culture conditions. hBM-MSCs were also cultured over non-biofunctionalized nanofibrous substrates in basal medium (*Basal*), basal medium supplemented with cFN (*cFN soluble*) and standard chondrogenic differentiation medium (*Chondro*).

The influence of soluble or bound FN over hBM-MSCs viability, proliferation and total protein synthesis was assessed using standard cell biology protocols. In terms of cell viability, (**Figure III 2 a**) on the 28<sup>th</sup> day of hBM-MSCs culture on the NFM in chondrogenic differentiation medium (*Chondro*) displayed significantly lower viability than the hBM-MSCs culture on the NFM in basal medium (*Basal*) ( $p < 0.001$ ). However, the biofunctionalized nanofibrous substrates with *eFN bound* presented significantly higher hBM-MSCs viability than non-biofunctionalized NFMs cultured in basal medium (*Basal*) ( $p < 0.01$ ). It is also notable that the conditions comprising cFN (*cFN soluble*; *cFN bound*) have cell viability at the level of the NFMs cultured in basal medium (*Basal*). The biochemical performance, namely cell proliferation and total protein synthesis (**Figure III 2 b and c**), of the hBM-MSCs under biofunctionalized nanofibrous substrates comprising human FN is comparable to that observed in non-biofunctionalized NFMs (*Basal*; *Chondo*) along the culturing time. Likewise, the supplementation of the basal medium with cFN (*cFN soluble*) seems to not induce significant changes over hBM-MSCs proliferation and protein synthesis along the culturing time.

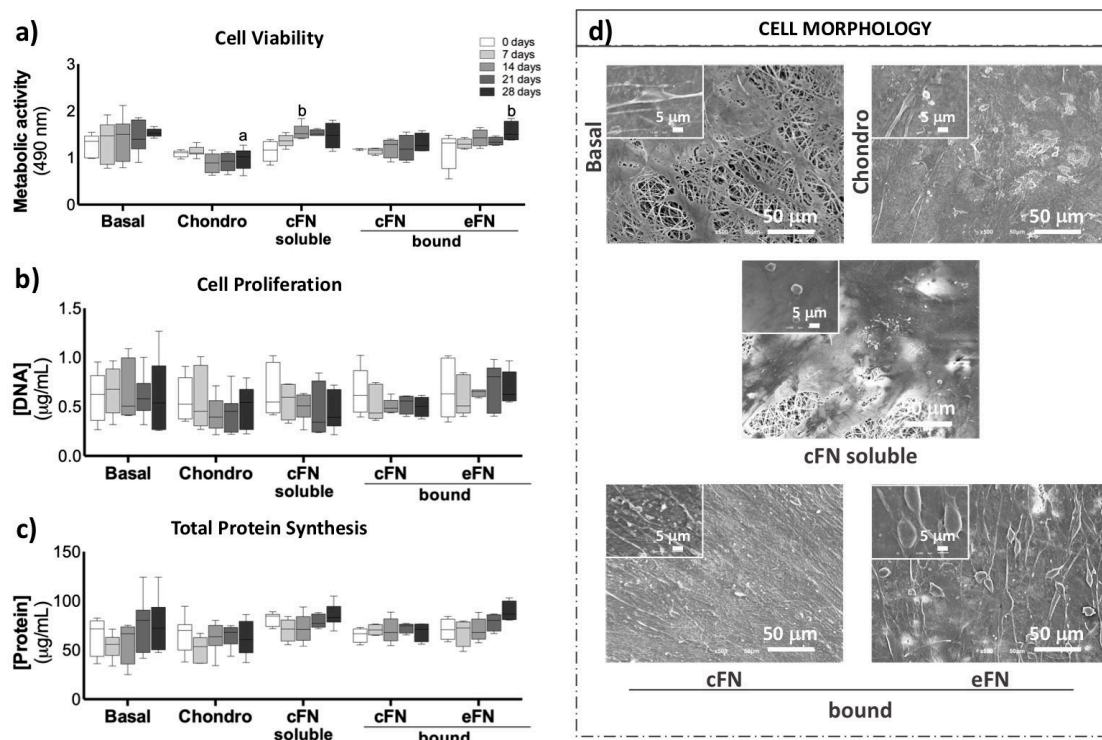


**Figure III-2** Biochemical performance (i.e. cell viability (a) and proliferation (b), total protein synthesis(c) and cell morphology (d) of the hBM-MSCs cultured over biofunctionalized nanofibrous substrates comprising bound fibronectin from different sources (i.e. commercial [*cFN bound*] and endogenous [*eFN bound*]), under basal culture conditions. Non-biofunctionalized nanofibrous substrates in basal medium (*Basal*), basal medium supplemented with commercial fibronectin (*cFN soluble*) and standard chondrogenic differentiation medium (*Chondro*) were used as controls. Data were analyzed by the Kruskal-Wallis test, followed by the Tukey's HSD test ( $p < 0.001$ ): *a* denotes significant differences compared to *Basal*; *b* denotes significant differences compared to *Chondro*;

The morphology of hBM-MSCs culture on the non-biofunctionalized and biofunctionalized nanofibrous substrates was analyzed by SEM at 28 days (**Figure III 2 c**). The hBM-MSCs cultured on biofunctionalized nanofibrous substrates comprising human FN (*cFN bound* and *eFN bound*) showed a round-shaped morphology, whereas the cells on the non-biofunctionalized NFMs cultured in basal medium (*Basal*) presented a fibroblast-like morphology. A less evident round-shaped morphology of the cells was presented by the hBM-MSCs culture on the non-biofunctionalized NFMs under standard chondrogenic differentiation medium (*Chondro*) and basal medium supplemented with cFN (*cFN soluble*).

To assess the onset of the chondrogenic activity of the cultured hBM-MSCs, the GAGs content was quantified and stained by alcian blue (**Figure III 3**). Along the culturing time, the hBM-MSCs culture on the non-biofunctionalized NFMs under standard chondrogenic differentiation medium (*Chondro*) or basal medium supplemented with cFN (*cFN soluble*) and

biofunctionalized nanofibrous substrates comprised human FN (*cFN bound* and *eFN bound*) displayed a significantly higher GAGs synthesis than the non-biofunctionalized NFMs under basal medium (*Basal*) ( $p < 0.001$ ) (**Figure III 3 a**). On the 28<sup>th</sup> day of hBM-MSCs culture, the biofunctionalized NFMs (*cFN bound* and *eFN bound*) displayed a significantly higher GAGs synthesis than the non-biofunctionalized NFMs under standard chondrogenic differentiation medium (*Chondro*) ( $p < 0.0001$ ) or basal medium supplemented with cFN (*cFN soluble*) ( $p < 0.01$ ). Alcian blue staining (**Figure III 3 b**) confirms the presence of GAGs on the cartilaginous ECM of the hBM-MSCs cultured on the non-biofunctionalized NFMs under standard chondrogenic differentiation medium (*Chondro*) or basal medium supplemented with cFibronectin (*cFN soluble*) and biofunctionalized nanofibrous substrates (*cFN bound* and *eFN bound*). It is also possible to observe the absence of the staining on the non-biofunctionalized NFMs under basal medium (*Basal*).

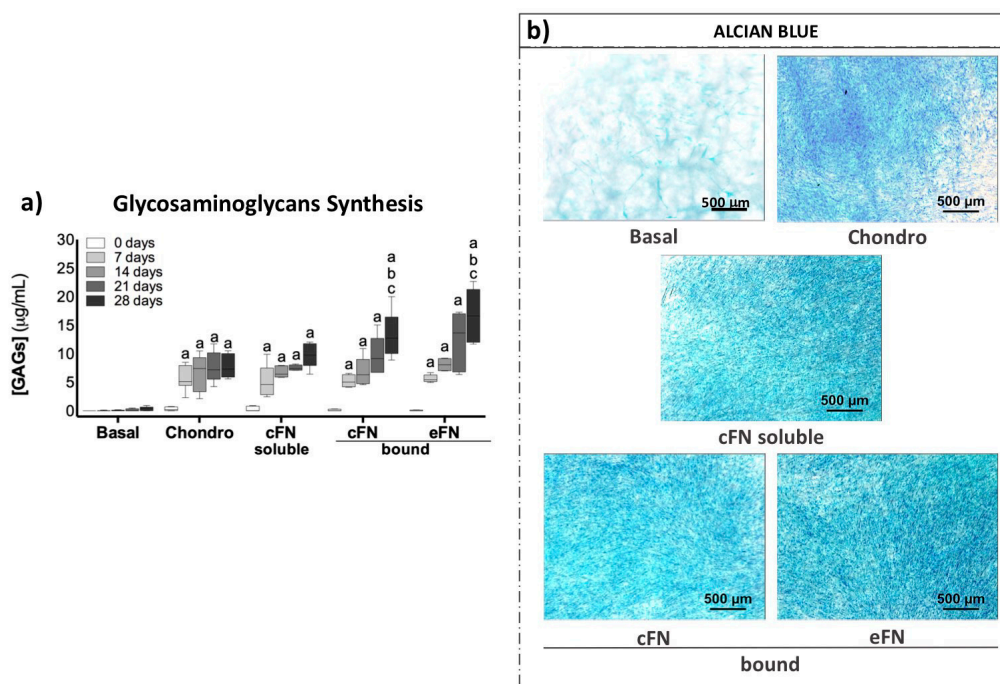


**Figure III-3** Analysis of the sulfated glycosaminoglycans content (a) and staining by Alcian blue (b) of the hBM-MSCs cultured over biofunctionalized nanofibrous substrates comprising bound fibronectin from different sources (i.e. commercial [*cFN bound*] and endogenous [*eFN bound*]), under basal culture conditions. Non-biofunctionalized nanofibrous substrates in basal medium (*Basal*), basal medium supplemented with commercial fibronectin (*cFN soluble*) and standard chondrogenic differentiation medium (*Chondro*) were used as controls. Data were analyzed by the Kruskal-Wallis test, followed by the Tukey's HSD test ( $p < 0.001$ ): *a* denotes significant differences compared to *Basal*; *b* denotes significant differences compared to *Chondro*; *c* denotes significant differences compared to *cFN soluble*;

The expression level of several cartilage-related genes, namely *Sox 9*, *Collagen type II*, *COMP* and *Aggrecan*, was quantified by real-time PCR considering the basal medium condition (*Basal*) as calibrator (**Figure III 4 a, b, c and d**). All these genes are expressed in all testing conditions, except on the non-biofunctionalized NFMs under standard osteogenic differentiation medium (*Osteo*). On the 7<sup>th</sup> day of hBM-MSCs culture, a significantly higher *Aggrecan* and *Collagen type II* expression was observed at the biofunctionalized NFMs with bound eFN (*eFN bound*) ( $p < 0.01$ ). On the 21<sup>th</sup> day of hBM-MSCs culture, a significantly higher *Sox 9* expression was observed in the biofunctionalized nanofibrous substrate with bound eFN (*eFN bound*) when compared to the non-biofunctionalized NFMs under standard chondrogenic differentiation medium (*Chondro*) ( $p < 0.01$ ). On the 28<sup>th</sup> day of hBM-MSCs culture, the biofunctionalized NFMs with bound eFN (*eFN bound*) presented a significantly higher *Sox 9*, *Aggrecan* and *Collagen type II* expression than the non-biofunctionalized NFMs under standard chondrogenic differentiation medium (*Chondro*) and the soluble cFN condition (*cFN soluble*) ( $p < 0.01$ ). Moreover, the expression of *COMP* showed significant differences between the biofunctionalized NFMs with bound eFN (*eFN bound*) and the *Chondro* condition.

Histological sections of the NFMs cultured with hBM-MSCs for 28 days were immunostained for collagen type II (**Figure III 4 e**). The expression of Collagen type II confirms the deposition of a cartilaginous ECM on the biofunctionalized nanofibrous substrates comprising human FN (*cFN bound* and *eFN bound*), on the non-biofunctionalized NFMs under standard chondrogenic differentiation medium (*Chondro*) and on the soluble cFN condition (*cFN soluble*). It was also possible to observe an intense immunodetection of collagen type II on the biofunctionalized NFMs with eFN (*eFN bound*) when compared with the non-biofunctionalized NFMs under standard chondrogenic differentiation medium (*Chondro*), corroborating the previous gene expression data.



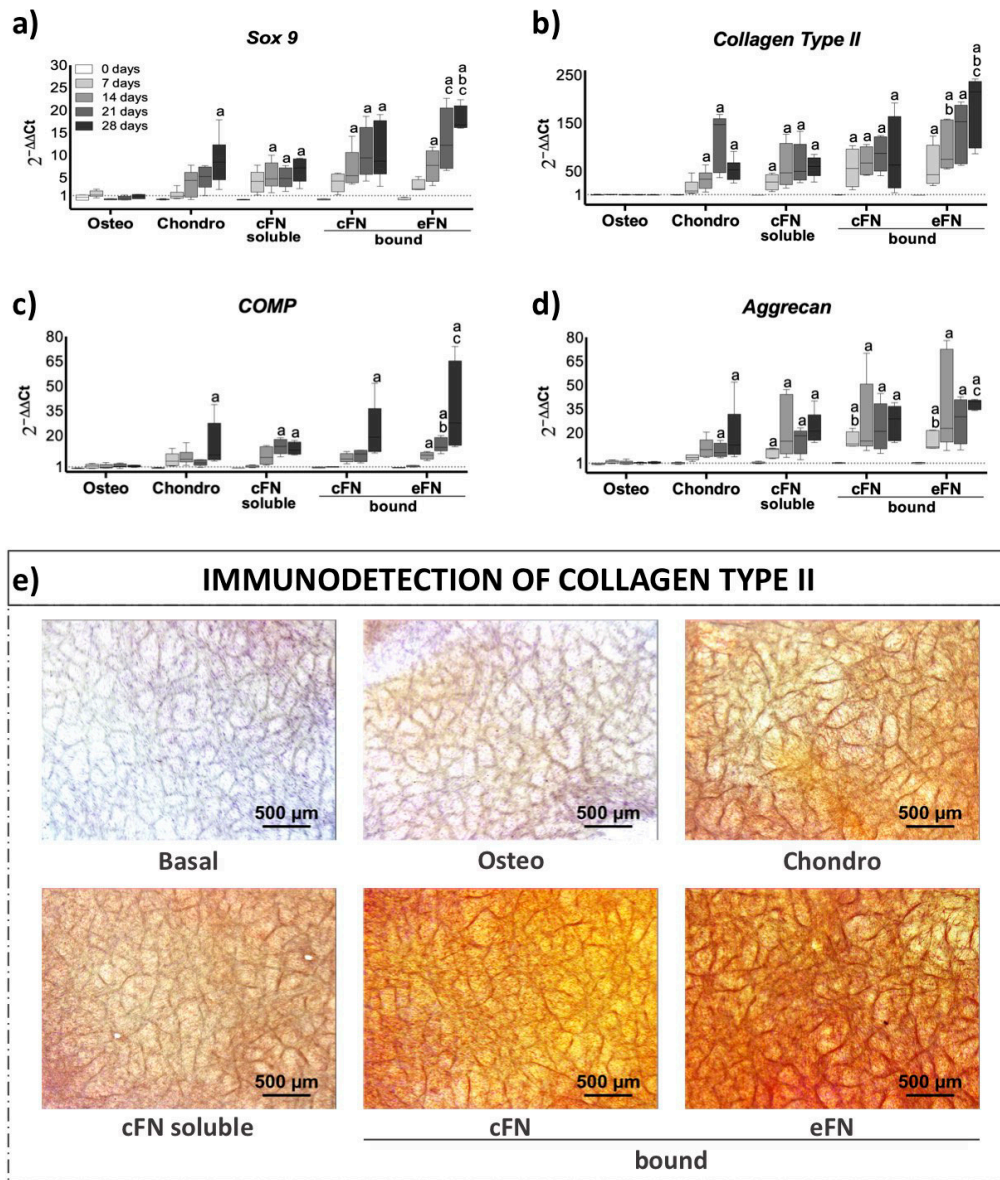


**Figure III-4 Top:** Relative expression of chondrogenic markers (i.e. *Sox 9* (a), *Collagen type II* (b), *COMP* (c) and *Aggrecan* (d)) by hBM-MSCs cultured on biofunctionalized nanofibrous substrates comprising bond fibronectin from different sources (i.e. commercial [*cFN bound*] and endogenous [*eFN bound*]), under basal culture conditions. Non-biofunctionalized nanofibrous substrates in basal medium (*Basal*), basal medium supplemented with commercial fibronectin (*cFN soluble*) and standard chondrogenic differentiation medium (*Chondro*) and standard osteogenic differentiation medium (*Osteo*) were used as controls. The expression was normalized against the GAPDH gene and the quantification was performed according to the Livak method. Data were analyzed by the Kruskal-Wallis test, followed by the Tukey's HSD test ( $p < 0.001$ ): *a* denotes significant differences compared to *Osteo*; *b* denotes significant differences compared to *Chondro*; *c* denotes significant differences compared to *cFN soluble*; **Bottom:** Immunolocalization of collagen type II (e) of the hBM-MSCs cultured over biofunctionalized or non-biofunctionalized nanofibrous substrates.

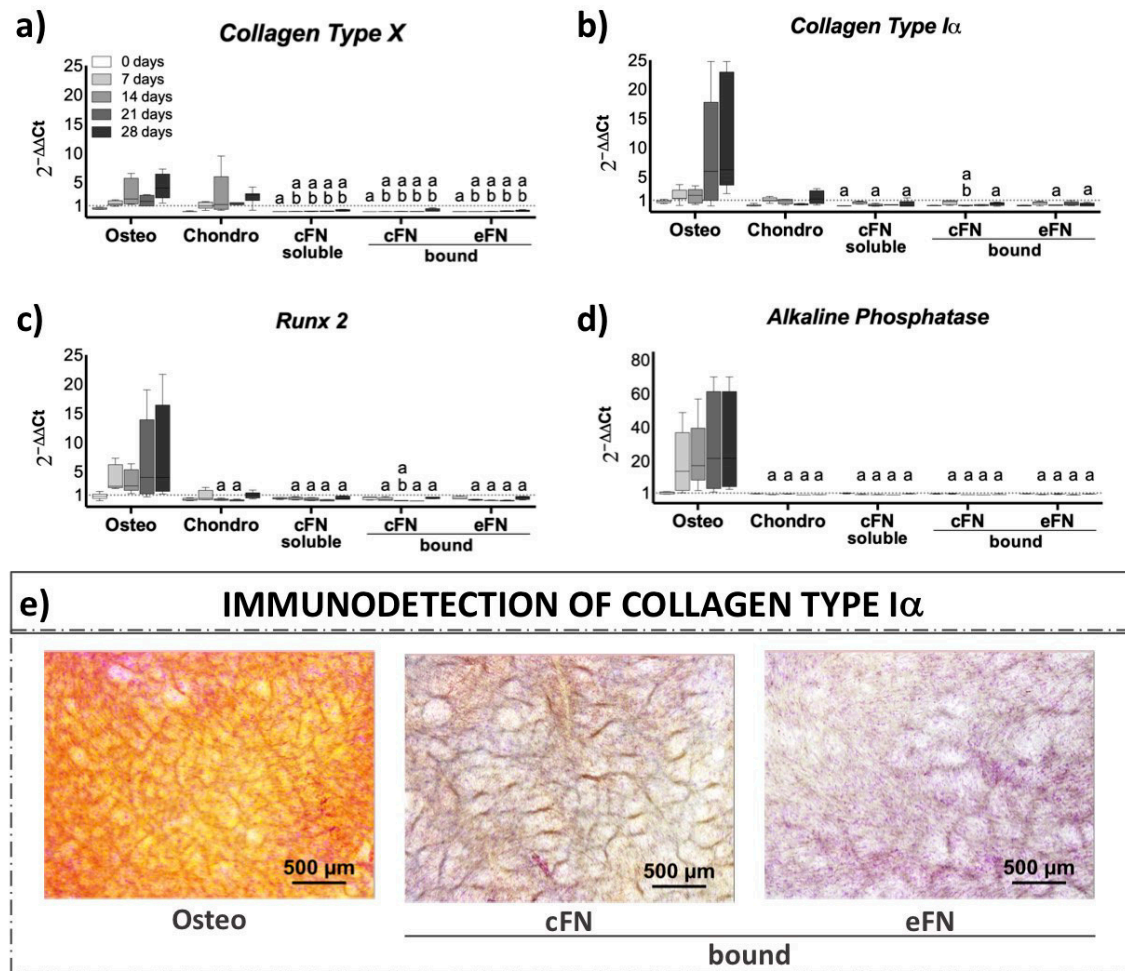


**Figure III-5 Top:** Relative expression of hypertrophic markers (i.e. *Collagen type X* (a), *Collagen type Iα* (b), *Runx 2* (c) and *Alkaline Phosphatase* (d)) by hBM-MSCs cultured on biofunctionalized nanofibrous substrates comprising bound fibronectin from different sources (i.e. commercial [*cFN bound*] and endogenous [*eFN bound*]), under basal culture conditions. Non-biofunctionalized nanofibrous substrates in basal medium (*Basal*), basal medium supplemented with commercial fibronectin (*cFN soluble*), standard chondrogenic differentiation medium (*Chondro*) and standard osteogenic differentiation medium (*Osteo*) were used as controls. The expression was normalized against the GAPDH gene and the quantification was performed according to the Livak method. Data were analyzed by the Kruskal-Wallis test, followed by the Tukey's HSD test ( $p < 0.001$ ): *a* denotes significant differences compared to *Osteo*; *b* denotes significant differences compared to *Chondro*; *c* denotes significant differences compared to *cFN soluble*; **Bottom:** Immunolocalization of collagen type Iα (e) of the hBM-MSCs cultured over biofunctionalized or non-biofunctionalized nanofibrous substrates.

Genotypic data also confirms that only in the non-biofunctionalized NFMs under standard osteogenic differentiation medium (*Osteo*), osteoblastic-related genes were expressed (**Figure III 5 a, b, c, and d**). The lower gene expression patterns were considerably similar on the biofunctionalized nanofibrous substrates comprising human FN (*cFN bound* and *eFN bound*)

and on the non-biofunctionalized NFMs under basal medium supplemented with cFN (*cFN soluble*), indicating that those hBM-MSCs did not differentiate into the osteogenic lineage. Moreover, all the FN conditions (*cFN soluble*; *cFN bound* and *eFN bound*) had significantly lower expression of the hypertrophy-related genes (i.e. *Collagen type X*, *Collagen type I $\alpha$* , *Runx 2*) when compared with the non-biofunctionalized NFMs under standard osteogenic or/and chondrogenic differentiation medium (*Osteo*; *Chondro*) over the culture time ( $p < 0.0001$ ). Furthermore, the absence of a bone ECM was clearly observed by the non-immunodetection of collagen type I $\alpha$  on the FN conditions (*cFN bound* and *eFN bound*) (**Figure III 5 e**).

#### III-4. DISCUSSION

Interactions between cells and ECM provide important cues for the differentiation and development of several tissues, including cartilage. FN is a cell-surface and ECM glycoprotein required for precartilaginous condensation of limb bud cells by integrin-mediated adhesion [15], and the presence of specific FN isoforms influences the extent of condensation [16]. Human FN is a dimeric glycoprotein composed of two polypeptides ( $\alpha$  and  $\beta$  chains) with a molecular weight of 220-250 kDa linked by a single disulfide bond. Each chain contains three different repeating modules (types I, II, and III), which mediate the interaction with other FN modules (FNI<sub>1-5</sub> and FNIII<sub>1-2</sub>) and other ECM components, namely integrins (FNIII<sub>9-10</sub>) and growth factors (FNIII<sub>12-14</sub>) [39]. Physiologically, FN maintains a globular conformation, but it can unfold into an extended conformation *via* cellular stimuli, exposing domains responsible for matrix assembly, cell or growth factors binding [19, 40, 41]. Numerous studies have reported these essential roles of cell-matrix interactions of FN during embryonic development [42-45]. It is suggested that FN has a pivotal role in cartilage formation *in vivo*. Despite the recognized role of FN in chondrogenic events, its capability to induce chondrogenic differentiation of mesenchymal stem cells (MSCs) is not fully understood.

Herein, we report a chondrogenic-inductive nanofibrous substrate biofunctionalized with human FN. For that, functional groups (i.e. amine groups) were generated at the surface of electrospun NFMs, which allow the immobilization of an antibody by its carboxyl group. This immobilization strategy guarantees the efficacy/availability of the FN antibody binding epitopes, extending the half-life of the protein when compared to its free form. Furthermore, the antibody against plasma-derived FN used in this study recognizes the FN type III repeat 7

(FnIII<sub>7</sub>). This antibody does not block the cell receptor binding domains allowing the bound fibronectin to perform its biological activity. The biological activity of the bound FN from different sources (*cFN* and *eFN*) was confirmed by culturing directly hBM-MSCs over the biofunctionalized nanofibrous substrates, reaching a more effective chondrogenic differentiation than the one observed in the standard chondrogenic differentiation medium. Furthermore, it could be demonstrated that soluble cFN (*cFN soluble*) does not appear to have similar potential to differentiate hBM-MSCs towards chondrogenic lineage as compared to its immobilization at the surface of electrospun nanofibrous substrate. Indeed, previous studies have reported that FN conjugation to a surface of a material can change the protein orientation/conformation, determining the FN bioactivity, by changing the integrin binding domain presented to the cells [23, 46]. Therefore, although speculative, soluble FN may maintain a globular conformation, reducing the exposure of the domains responsible to induce the chondrogenic differentiation of hBM-MSCs. Further research will be required to study the exact molecular interactions between cellular surface receptors and the specific domain of FN.

FN was already recognized as a key factor in human serum to enhance mesenchymal progenitor cell migration and proliferation among a wide range of cell types [47-49], including subchondral mesenchymal progenitor cells [18, 20, 21]. This is in line with our current results that show that human plasma-derived FN increased the proliferation of hBM-MSCs and collagen type II synthesis. Regarding differentiation, some previous studies reported that plasma-derived FN had no effect on the chondrogenic differentiation *in vitro* [21], while others demonstrated its involvement in the chondrogenic differentiation of mesenchymal progenitor cells from the subchondral bone [5, 22]. Furthermore, FN has been studied by its osteogenic-inductive ability on FN-coated substrates [50-53]. However, we clearly demonstrate the chondrogenic-inductive capability of the biofunctionalized nanofibrous substrates comprising human FN from different sources (*cFN bound* and *eFN bound*). Specifically, hBM-MSCs cultured on biofunctionalized nanofibrous substrates (*cFN bound* and *eFN bound*) began expressing ECM biomolecules, such as GAG and type II collagen, as well as the chondrogenic differentiation-related genes *Sox-9*, *Aggrecan*, *COMP* and *Collagen type II*, while osteogenic differentiation-related genes were not expressed, namely *Collagen type I $\alpha$*  and *type X*, *Runx-2* and *ALP*. The discriminative differentiation potential of FN reported by several studies could be induced by several reasons. Different MSCs were used with different proliferative, chondrogenic osteogenic and adipogenic differentiation capacities. The concentration of FN used in the currently study was 8  $\mu\text{g/mL}$ , being different from the previous study [21, 22, 50-

53]. Moreover, these could also be partially related with various FN isoforms, which could have an impact over the selected type of molecule and the proper concentration.

The current study clearly demonstrated that FN plays a structural role by providing a scaffold for cell adhesion and differentiation. Intracellular pathways that regulate changes in gene expression during chondrogenesis are activated through integrin-FN interaction [17], which was also demonstrated by our mRNA results, being significantly higher expressed on the biofunctionalized NFMs comprising eFN (*eFN bound*). The FN matrix was shown to support deposition of collagens, latent TGF- $\beta$  binding proteins and other ECM proteins [5]. In line with this study, our results showed that the biofunctionalized NFMs with human FN (*cFN bound* and *eFN bound*) increased the glycosaminoglycans and collagen type II synthesis compared with the positive control (*Chondro*).

Our biofunctional nanofibrous substrate, capable of selectively bound endogenous FN, could have a potential application in cartilage regeneration, particularly as a “one-step repair technique” in conjugation to the microfracture technique. In microfracture, the subchondral stem and progenitor cells form a clot in the defect by the bone marrow and actively by recruiting biomolecules like growth factors or chemokines released from the cartilage or the synovial fluid [54, 55]. Therefore, FN being a component of the synovial fluid can be selectively bound by this biofunctional nanofibrous substrate, and it may play a stimulation-mediated cartilage repair by driving the chondrogenic differentiation of the MSCs.

### **III-5. CONCLUSIONS**

This study shows evidence, for the first time, that biofunctionalized nanofibrous substrates comprising human plasma-derived fibronectin is able to successfully induce the chondrogenic differentiation of hBM-MSCs, displaying typical phenotypic and genotypic of articular chondrocytes. Moreover, the FN bound at the electrospun nanofibrous substrate is more effective than both the stimulation with soluble fibronectin or by the standard chondrogenic differentiation medium. Our envisioning autologous approach (FN biofunctionalized NFMs) is more effective in promoting the chondrogenic differentiation, avoiding the use of medium supplementation. The application of the biofunctionalized nanofibrous substrate may be advantageous for bone marrow-stimulating techniques, such as the microfracture, for the

treatment of focal articular cartilage lesions. Therefore, we suggest fibronectin as an effective bioactive factor in substrates to be used in cartilage repair procedures.

### III-6. ACKNOWLEDGEMENTS

The authors would like to acknowledge the Portuguese Foundation for Science and Technology (FCT) for the PhD grant of M.R.C. (PD/BD/113797/2015) financed by the FCT Doctoral Program on Advanced Therapies for Health (PATH) (FSE/POCH/PD/169/2013), the IF grant of A.M. (IF/00376/2014), and the projects SPARTAN (PTDC/CTM-BIO/4388/2014) and FRONthera (NORTE-01-0145-FEDER-0000232).

### III-7. REFERENCES

- [1] P. Singh, J.E. Schwarzbauer, Fibronectin matrix assembly is essential for cell condensation during chondrogenesis, *J Cell Sci* 127(Pt 20) (2014) 4420-8.
- [2] R.O. Hynes, The extracellular matrix: not just pretty fibrils, *Science* 326(5957) (2009) 1216-9.
- [3] B. Geiger, A. Bershadsky, R. Pankov, K.M. Yamada, Transmembrane crosstalk between the extracellular matrix--cytoskeleton crosstalk, *Nat Rev Mol Cell Biol* 2(11) (2001) 793-805.
- [4] R.M. Wyrce, S. Downes, The role of protein adsorption on chondrocyte adhesion to a heterocyclic methacrylate polymer system, *Biomaterials* 23(2) (2002) 357-364.
- [5] P. Singh, J.E. Schwarzbauer, Fibronectin and stem cell differentiation - lessons from chondrogenesis, *J Cell Sci* 125(Pt 16) (2012) 3703-12.
- [6] W. Dessau, H. von der Mark, K. von der Mark, S. Fischer, Changes in the patterns of collagens and fibronectin during limb-bud chondrogenesis, *J Embryol Exp Morphol* 57 (1980) 51-60.
- [7] N. Kamiya, H. Watanabe, H. Habuchi, H. Takagi, T. Shinomura, K. Shimizu, K. Kimata, Versican/Pg-M regulates chondrogenesis as an extracellular matrix molecule crucial for mesenchymal condensation, *J Biol Chem* 281(4) (2006) 2390-400.
- [8] K. Choocheep, S. Hatano, H. Takagi, H. Watanabe, K. Kimata, P. Kongtawelert, H. Watanabe, Versican facilitates chondrocyte differentiation and regulates joint morphogenesis, *J Biol Chem* 285(27) (2010) 21114-25.
- [9] C.B. Knudson, W. Knudson, Cartilage proteoglycans, *Semin Cell Dev Biol* 12(2) (2001) 69-78.

- [10] W.M. Kulyk, W.B. Upholt, R.A. Kosher, Fibronectin gene expression during limb cartilage differentiation, *Development* 106(3) (1989) 449-55.
- [11] J.L. Allen, M.E. Cooke, T. Alliston, ECM stiffness primes the TGFbeta pathway to promote chondrocyte differentiation, *Mol Biol Cell* 23(18) (2012) 3731-42.
- [12] S. Lucena, C.L. Arocha Pinango, B. Guerrero, [Fibronectin. Structure and functions associated to hemostasis. Review], *Invest Clin* 48(2) (2007) 249-62.
- [13] A. Moroz, E. Deffune, Platelet-rich plasma and chronic wounds: remaining fibronectin may influence matrix remodeling and regeneration success, *Cytotherapy* 15(11) (2013) 1436-9.
- [14] P. Singh, J.E. Schwarzbauer, Fibronectin matrix assembly is essential for cell condensation during chondrogenesis, *Journal of Cell Science* 127(20) (2014) 4420-4428.
- [15] O.S. Bang, E.J. Kim, J.G. Chung, S.R. Lee, T.K. Park, S.S. Kang, Association of focal adhesion kinase with fibronectin and paxillin is required for precartilag condensation of chick mesenchymal cells, *Biochem Biophys Res Commun* 278(3) (2000) 522-9.
- [16] D.G. White, H.P. Hershey, J.J. Moss, H. Daniels, R.S. Tuan, V.D. Bennett, Functional analysis of fibronectin isoforms in chondrogenesis: Full-length recombinant mesenchymal fibronectin reduces spreading and promotes condensation and chondrogenesis of limb mesenchymal cells, *Differentiation* 71(4-5) (2003) 251-61.
- [17] M.E. Vega, J.E. Schwarzbauer, Collaboration of fibronectin matrix with other extracellular signals in morphogenesis and differentiation, *Curr Opin Cell Biol* 42 (2016) 1-6.
- [18] M.M. Thibault, C.D. Hoemann, M.D. Buschmann, Fibronectin, vitronectin, and collagen I induce chemotaxis and haptotaxis of human and rabbit mesenchymal stem cells in a standardized transmembrane assay, *Stem Cells Dev* 16(3) (2007) 489-502.
- [19] P. Singh, C. Carraher, J.E. Schwarzbauer, Assembly of Fibronectin Extracellular Matrix, *Annu Rev Cell Dev Bi* 26 (2010) 397-419.
- [20] R. Kulawig, J.P. Kruger, O. Klein, Z. Konthur, H. Schutte, J. Klose, C. Kaps, M. Endres, Identification of fibronectin as a major factor in human serum to recruit subchondral mesenchymal progenitor cells, *Int J Biochem Cell Biol* 45(7) (2013) 1410-8.
- [21] R.H. Kalkreuth, J.P. Kruger, S. Lau, P. Niemeyer, M. Endres, P.C. Kreuz, C. Kaps, Fibronectin stimulates migration and proliferation, but not chondrogenic differentiation of human subchondral progenitor cells, *Regen Med* 9(6) (2014) 759-773.
- [22] C. Jiang, P. Ma, B.P. Ma, Z.H. Wu, G.X. Qiu, X.L. Su, Z.N. Xia, Z.X. Ye, Y.P. Wang, Plasma-Derived Fibronectin Stimulates Chondrogenic Differentiation of Human Subchondral Cortico-Spongious Progenitor Cells in Late-Stage Osteoarthritis, *Int J Mol Sci* 16(8) (2015) 19477-19489.
- [23] B.G. Keselowsky, D.M. Collard, A.J. Garcia, Surface chemistry modulates fibronectin conformation and directs integrin binding and specificity to control cell adhesion, *J Biomed Mater Res A* 66a(2) (2003) 247-259.

- [24] T. Kutsuna, H. Inoue, H. Takeda, T. Takahashi, H. Yamamoto, H. Miura, S. Higashiyama, Fibronectin regulates proteoglycan production balance in transforming growth factor-beta 1-induced chondrogenesis, *Int J Mol Med* 28(5) (2011) 829-834.
- [25] A.M. Briggs, M.J. Cross, D.G. Hoy, L. Sanchez-Riera, F.M. Blyth, A.D. Woolf, L. March, Musculoskeletal Health Conditions Represent a Global Threat to Healthy Aging: A Report for the 2015 World Health Organization World Report on Ageing and Health, *Gerontologist* 56 Suppl 2 (2016) S243-55.
- [26] A.M. Briggs, A.D. Woolf, K. Dreinhofer, N. Homb, D.G. Hoy, D. Kopansky-Giles, K. Akesson, L. March, Reducing the global burden of musculoskeletal conditions, *Bull World Health Organ* 96(5) (2018) 366-368.
- [27] B.J. Huang, J.C. Hu, K.A. Athanasiou, Cell-based tissue engineering strategies used in the clinical repair of articular cartilage, *Biomaterials* 98 (2016) 1-22.
- [28] T. Welch, B. Mandelbaum, M. Tom, Autologous Chondrocyte Implantation: Past, Present, and Future, *Sports Med Arthrosc* 24(2) (2016) 85-91.
- [29] B.S. Dunkin, C. Lattermann, New and Emerging Techniques in Cartilage Repair: MACI, *Oper Tech Sports Med* 21(2) (2013) 100-107.
- [30] J.F. Piai, M.A. da Silva, A. Martins, A.B. Torres, S. Faria, R.L. Reis, E.C. Muniz, N.M. Neves, Chondroitin sulfate immobilization at the surface of electrospun nanofiber meshes for cartilage tissue regeneration approaches, *Appl Surf Sci* 403 (2017) 112-125.
- [31] M.L.A. da Silva, A. Martins, A.R. Costa-Pinto, V.M. Correlo, P. Sol, M. Bhattacharya, S. Faria, R.L. Reis, N.M. Neves, Chondrogenic differentiation of human bone marrow mesenchymal stem cells in chitosan-based scaffolds using a flow-perfusion bioreactor, *J Tissue Eng Regen M* 5(9) (2011) 722-732.
- [32] C. Vinatier, D. Mrugala, C. Jorgensen, J. Guicheux, D. Noel, Cartilage engineering: a crucial combination of cells, biomaterials and biofactors, *Trends Biotechnol* 27(5) (2009) 307-314.
- [33] D. Magne, C. Vinatier, M. Julien, P. Weiss, J. Guicheux, Mesenchymal stem cell therapy to rebuild cartilage, *Trends Mol Med* 11(11) (2005) 519-526.
- [34] M.R. Casanova, M.A. da Silva, A.R. Costa-Pinto, R.L. Reis, A. Martins, N.M. Neves, Chondrogenesis-inductive nanofibrous substrate using both biological fluids and mesenchymal stem cells from an autologous source, *Mat Sci Eng C-Mater* 98 (2019) 1169-1178.
- [35] M.L.A. da Silva, A. Martins, A.R. Costa-Pinto, P. Costa, S. Faria, M. Gomes, R.L. Reis, N.M. Neves, Cartilage Tissue Engineering Using Electrospun PCL Nanofiber Meshes and MSCs, *Biomacromolecules* 11(12) (2010) 3228-3236.
- [36] M.L. Alves da Silva, A. Martins, A.R. Costa-Pinto, P. Costa, S. Faria, M. Gomes, R.L. Reis, N.M. Neves, Cartilage tissue engineering using electrospun PCL nanofiber meshes and MSCs, *Biomacromolecules* 11(12) (2010) 3228-36.



- [37] K.J. Livak, T.D. Schmittgen, Analysis of relative gene expression data using real-time quantitative PCR and the 2(T)(-Delta Delta C) method, *Methods* 25(4) (2001) 402-408.
- [38] M.A. da Silva, A. Martins, A.A. Teixeira, R.L. Reis, N.M. Neves, Impact of biological agents and tissue engineering approaches on the treatment of rheumatic diseases, *Tissue Eng Part B Rev* 16(3) (2010) 331-9.
- [39] R. Pankov, K.M. Yamada, Fibronectin at a glance, *Journal of Cell Science* 115(20) (2002) 3861-3863.
- [40] M. Cantini, C. Gonzalez-Garcia, V. Llopis-Hernandez, M. Salmeron-Sanchez, Material-Driven Fibronectin Fibrillogenesis, *Acs Sym Ser* 1120 (2012) 471-496.
- [41] J. Ballester-Beltran, M. Cantini, M. Lebourg, P. Rico, D. Moratal, A.J. Garcia, M. Salmeron-Sanchez, Effect of topological cues on material-driven fibronectin fibrillogenesis and cell differentiation, *J Mater Sci-Mater M* 23(1) (2012) 195-204.
- [42] T. Shirai, S. Miyagi, D. Horiuchi, T. Okuda-Katayanagi, M. Nishimoto, M. Muramatsu, Y. Sakamoto, M. Nagata, K. Hagiwara, A. Okuda, Identification of an enhancer that controls up-regulation of fibronectin during differentiation of embryonic stem cells into extraembryonic endoderm, *Journal of Biological Chemistry* 280(8) (2005) 7244-7252.
- [43] H. Fujiwara, Y. Hayashi, N. Sanzen, R. Kobayashi, C.N. Weber, T. Emoto, S. Futaki, H. Niwa, P. Murray, D. Edgar, K. Sekiguchi, Regulation of mesodermal differentiation of mouse embryonic stem cells by basement membranes, *Journal of Biological Chemistry* 282(40) (2007) 29701-29711.
- [44] S. Maretto, P.S. Muller, A.R. Aricescu, K.W.Y. Cho, E.K. Bikoff, E.J. Robertson, Ventral closure, headfold fusion and definitive endoderm migration defects in mouse embryos lacking the fibronectin leucine-rich transmembrane protein FLRT3, *Dev Biol* 318(1) (2008) 184-193.
- [45] J. Liu, X. He, S.A. Corbett, S.F. Lowry, A.M. Graham, R. Fassler, S. Li, Integrins are required for the differentiation of visceral endoderm, *J Cell Sci* 122(Pt 2) (2009) 233-42.
- [46] K. Vallieres, P. Chevallier, C. Sarra-Bournet, S. Turgeon, G. Laroche, AFM imaging of immobilized fibronectin: does the surface conjugation scheme affect the protein orientation/conformation?, *Langmuir* 23(19) (2007) 9745-51.
- [47] E.L. George, E.N. Georges-Labouesse, R.S. Patel-King, H. Rayburn, R.O. Hynes, Defects in mesoderm, neural tube and vascular development in mouse embryos lacking fibronectin, *Development* 119(4) (1993) 1079-91.
- [48] D. Greiling, R.A. Clark, Fibronectin provides a conduit for fibroblast transmigration from collagenous stroma into fibrin clot provisional matrix, *J Cell Sci* 110 ( Pt 7) (1997) 861-70.
- [49] J.E. Schwarzbauer, D.W. DeSimone, Fibronectins, their fibrillogenesis, and in vivo functions, *Cold Spring Harb Perspect Biol* 3(7) (2011).
- [50] Y. Kang, A.I. Georgiou, R.J. MacFarlane, M.E. Klontzas, M. Heliotis, E. Tsiridis, A. Mantalaris, Fibronectin stimulates the osteogenic differentiation of murine embryonic stem cells, *J Tissue Eng Regen Med* 11(7) (2017) 1929-1940.

- [51] F. Mohamadyar-Toupkanlou, E. Vasheghani-Farahani, H. Hanaee-Ahvaz, M. Soleimani, M. Dodel, P. Havasi, A. Ardeshiryajimi, E.S. Taherzadeh, Osteogenic Differentiation of MSCs on Fibronectin-Coated and nHA-Modified Scaffolds, *ASAIO J* 63(5) (2017) 684-691.
- [52] S. Vogel, S. Arnoldini, S. Moller, M. Schnabelrauch, U. Hempel, Sulfated hyaluronan alters fibronectin matrix assembly and promotes osteogenic differentiation of human bone marrow stromal cells, *Sci Rep* 6 (2016) 36418.
- [53] A.B. Faia-Torres, T. Goren, T.O. Ihalainen, S. Guimond-Lischer, M. Charnley, M. Rottmar, K. Maniura-Weber, N.D. Spencer, R.L. Reis, M. Textor, N.M. Neves, Regulation of Human Mesenchymal Stem Cell Osteogenesis by Specific Surface Density of Fibronectin: a Gradient Study, *Acs Appl Mater Inter* 7(4) (2015) 2367-2375.
- [54] M. Endres, K. Neumann, T. Haupl, C. Erggelet, J. Ringe, M. Sittinger, C. Kaps, Synovial fluid recruits human mesenchymal progenitors from subchondral spongy bone marrow, *J Orthop Res* 25(10) (2007) 1299-1307.
- [55] M. Endres, K. Andreas, G. Kalwitz, U. Freymann, K. Neumann, J. Ringe, M. Sittinger, T. Haupl, C. Kaps, Chemokine profile of synovial fluid from normal, osteoarthritis and rheumatoid arthritis patients: CCL25, CXCL10 and XCL1 recruit human subchondral mesenchymal progenitor cells, *Osteoarthr Cartilage* 18(11) (2010) 1458-1466.

# **Chapter IV**

## **Extracellular Vesicles Delivery Systems Capable of Inducing the Chondrogenic Differentiation**

## Chapter IV

### Extracellular Vesicles Delivery Systems Capable of Inducing the Chondrogenic Differentiation ‡

#### ABSTRACT

Extracellular vesicles (EVs) are being increasingly studied by its regenerative potential, namely EVs derived from human bone marrow mesenchymal stem cells (hBM-MSCs) can be used for controlling inflammation, repairing injury and enhancing tissue regeneration. This work aims to develop an EVs delivery system capable of selectively binding EVs present in conditioned medium obtained from human articular chondrocytes (hACs) or chondrogenically induced hBM-MSC. For that, we immobilized CD63 antibody at the surface of an activated and functionalized electrospun nanofibrous substrate. The chondrogenic potential of bound EVs was further assessed by culturing hBM-MSCs during 28 days under basal conditions. EVs-derived from hACs under differentiation medium induced a chondrogenic phenotype characterized by marked induction of SOX9, COMP, Aggrecan, Collagen type II, and glycosaminoglycans content. Both EVs delivery system, namely EVs derived from hACs or chondrogenically committed hBM-MSCs, outperformed the currently used chondroinductive strategies. These data show that naturally secreted EVs can guide the chondrogenic commitment of hBM-MSCs in the absence of other chemical or genetic chondroinductors.

---

‡ This chapter is based on the following patent:

Casanova M. R., Reis R. L., Martins A. and Neves N. M., “Extracellular Vesicles Delivery Systems Capable of Inducing the Chondrogenic Differentiation”, Submitted for publication.

## IV-1. INTRODUCTION

Human articular cartilage is composed by only one cell type, the chondrocyte. The chondrocytes are responsible to maintain the cartilage matrix structure, composition, and properties. In adults, articular cartilage has limited or no potential of self-repair; thus, damaged cartilage needs surgical interventions for either repair or replacement of the joint [1]. The available treatments are based on the transplantation of autologous cells (*e.g.* autologous chondrocytes implantation (ACI)) [2, 3] and *ex vivo* engineered tissue implants (Matrix-induced ACI (MACI)) [4, 5].

Human bone marrow mesenchymal stem cells (hBM-MSCs) are attractive candidates for advanced cell therapies, including cartilage regeneration [6]. hBM-MSCs can be induced to differentiate into the chondrogenic lineage when exposed to specific cocktails of growth factors [6-8]. The difficulty in obtaining a well-defined population and maintaining a stable cartilage phenotype of the differentiated MSCs, preventing them from progressing towards osteogenesis [9] leads to the investigation of approaches beyond the standard chondrogenic medium.

Extracellular vesicles (EVs) are lipidic particles (exosomes, 30-100 nm; microvesicles 50-2000 nm) secreted by cells to deliver biological signals, namely proteins, lipids and nucleic acids (DNA, mRNA and microRNA and tRNAs), which travel protected between the releasing and target cell [10, 11]. EVs can be isolated from virtually all biological fluids including blood, saliva, urine, synovial fluid, pleural effusions, ocular effluent and aqueous humor, nasal secretions, breast milk, amniotic fluid, cerebrospinal fluid, bile and semen [12].

The regenerative potential of EVs has been described for a wide range of tissues, including the heart and blood vessels, kidney, liver, lung, skin, neural and reproductive tissue [13-15]. Among the different types, MSCs are one of the most widely used cells source for generating EVs [16-18]. It is thought that the MSC-derived EVs share the same anti-inflammatory and trophic proprieties as the parental MSCs to exert their therapeutic effects [16, 18]. Indeed, EVs are being recognized by its regenerative potential for controlling inflammation, repairing injury and enhancing tissue regeneration [13]. However, their potential in promoting cartilage repair and slowing degeneration has not been thoroughly investigated [19]. Herein, we hypothesized that EVs derived from human articular chondrocytes (hACs) or chondrogenically differentiated hBM-MSCs will induce the chondrogenic commitment of homotypic cells without further supplementation. Indeed, we have recently demonstrated that hBM-MSCs undergo osteogenic differentiation induced by EVs derived from osteogenically induced hBM-MSCs [18].

Furthermore, the knowledge on the cartilage regenerative potential of EVs derived from hBM-MSCs or even from hACs is scarce. Envisioning an EVs delivery system, we herein report the development of a biofunctionalized electrospun polycaprolactone nanofibrous mesh (PCL NFM) able to specifically bind EVs derived from hACs or chondrogenically committed hBM-MSCs. The regenerative potential of these EVs delivery systems were investigated by assessing their capability to induce the chondrogenic differentiation of hBM-MSCs *in vitro*.

## **IV-2. MATERIALS AND METHODS**

### **IV-2.1. Isolation and expansion of hACs**

Human cartilage samples were collected under Informed Consent from patients undergoing knee arthroplasty in the Hospital Center of Alto Ave, Guimarães, Portugal, in accordance to the established Protocol (67/CA). The isolation of hACs was performed as described elsewhere [20]. Briefly, collected cartilage samples were dissected in small full-depth pieces, washed and digested with 0.25% w/v trypsin solution (Sigma-Aldrich) for 30 min at 37°C under agitation. Then, the solution was removed, the cartilage was washed and incubated overnight at 37°C with a 2 mg ml<sup>-1</sup> collagenase type II solution (Sigma-Aldrich). In the following day, the cells were washed, counted and plated at a density of 2 × 10<sup>6</sup> cells. Cells were expanded in expansion medium [**EM**; Dulbecco's modified Eagle's medium (DMEM; Sigma-Aldrich) containing 10 mM Hepes buffer (Sigma-Aldrich), L-alanyl-L-glutamine (Sigma-Aldrich), non-essential amino acids (Sigma-Aldrich), 1 % antibiotic–antimycotic solution, 10% FBS and 10 ng/ml basic fibroblast growth factor (b-FGF; PeproTech)] at 37 °C in a humidified atmosphere of 5% CO<sub>2</sub>.

### **IV-2.2. Isolation and expansion of hBM-MSCs**

Human bone-marrow aspirates were collected, after obtaining informed consent from patients undergoing knee arthroplasty, under the cooperation agreement established between the 3Bs Research Group, University of Minho and the Hospital Center of Alto Ave, Guimarães, Portugal. hBM-MSCs were isolated and characterized using our established standard protocols [21]. Cells were expanded in basal medium [**BM**; MEM alpha medium ( $\alpha$ -MEM; Sigma-Aldrich) supplemented with 10% heat-inactivated fetal bovine serum (FBS; Life Technologies)

and 1% antibiotic/antimycotic solution (final concentration of penicillin 100 units mL<sup>-1</sup> and streptomycin 100 mg mL<sup>-1</sup>; Life Technologies)] at 37 °C in a humidified atmosphere of 5% CO<sub>2</sub>.

### IV-2.3. Extracellular Vesicles

EVs were obtained using conditioned medium harvested from the hACs and hBM-MSCs in culture. First, the hACs and hBM-MSCs were expanded at passage 3 and a cell suspension containing of  $3 \times 10^3$  cells/cm<sup>2</sup> were subcultured in T150 flasks and cultured in EM and BM, respectively, at 37 °C in a humidified atmosphere of 5% CO<sub>2</sub>. The conditioned media were harvested when the cells reach the confluence (in 7 days), pooled, filtered (pore size 0.22 µm) and used as the starting material, as EVs derived from hACs under expansion medium (*EV<sup>EM</sup>*) or EVs derived from hBM-MSCs under basal medium (*EV<sup>BM</sup>*). A cell suspension containing  $2 \times 10^5$  cells/15 mL centrifuge tubes of hACs or hBM-MSCs were also prepared, to assure obtaining conditioned medium of chondrogenic lineage commitment. In order to form a spherical aggregate or pellet cultures, the cell aliquots were centrifuged at 600g for 5 min and incubated at 37 °C in a humidified atmosphere of 5% CO<sub>2</sub> for 24h incubation. The hACs and hBM-MSCs were culture under differentiation medium [*DM*; expansion medium – instead of adding bFGF, 1 mg ml<sup>-1</sup> L-ascorbic acid (Sigma-Aldrich) and 1 mg ml<sup>-1</sup> insulin (Sigma-Aldrich) were added] or standard chondrogenic differentiation medium [*CM*; basal medium supplemented with Insulin-Transferrin-Selenium-G Supplement (ITS; Invitrogen), 1 mM dexamethasone (Sigma-Aldrich), 0.1 M sodium pyruvate (Invitrogen), 17 mM ascorbic acid-2-phosphate (Sigma-Aldrich), 35 mM L-proline (Sigma-Aldrich) and 10 ng mL<sup>-1</sup> TGF-β3 (Peprotech)], respectively. Those conditioned media (*DM*; *CM*) were harvested at 21, 24 and 28 days of culture, pooled, filtered (pore size 0.22 µm) and used as starting material, as EVs derived from hACs under differentiation medium (*EV<sup>DM</sup>*) or EVs derived from hBM-MSCs under chondrogenic medium (*EV<sup>CM</sup>*).

The amount of EVs presented on each conditioned medium (*i.e.* EM, DM, BM, CM) was quantified by the Exosome ELISA Complete Kit (CD63) (System Biosciences) after EVs isolation using a polymeric precipitation solution (ExoQuick-TC; System Biosciences, BioCat GmbH). Those assays were performed according to the manufacturer's instructions.

#### **IV-2.4. Preparation of activated and functionalized PCL NFMs**

The production of electrospun PCL NFMs was performed as described in detail elsewhere [6]. In brief, a polymeric solution of 15% (w/v) Polycaprolactone (PCL - Mn 70,000-90,000 by GPC, Sigma-Aldrich) in chloroform (Sigma-Aldrich) and N,N-dimethylformamide (7 : 3 volume ratio; Sigma-Aldrich) was electrospun at 12 kV, using a needle-to-ground collector distance of 20 cm, and a flow rate of 1.0 mL h<sup>-1</sup>.

Samples of electrospun PCL NFM (1cm<sup>2</sup>) were activated in an ultraviolet–ozone system (ProCleaner 220, Bioforce Nanoscience) by exposing both sides for 2 minutes each. Incubation in 1M 1,6-hexanediamine solution (Sigma-Aldrich) for 1 h at 37 °C were performed, in order to graft amine groups (-NH<sub>2</sub>) at the NFMs surface. Those NFMs were further used as control conditions in the biological assays.

#### **IV-2.5. Engineered EVs delivery systems**

##### **IV-2.5.1. Antibody immobilization**

The human CD63 antibody (Santa Cruz Biotechnology, Inc.) was immobilized at the surface of NFMs by a covalent bond mediated by a coupling agent, namely 1-ethyl-3-(3-(dimethylamino)-propyl)carbodiimide / hydroxysuccinimide mixture (1:4 ratio; EDC/NHS; Sigma-Aldrich, S.L.). The antibody solution (1 % (v/v)) was mixed for 15 min at room temperature (RT), for the antibody activation, and incubated 2 h at RT on the activated and functionalized nanofibrous substrate.

The maximum immobilization capacity of the antibody over the nanofibrous substrate was determined by using a wide range of concentrations (from 0 to 8 µg mL<sup>-1</sup>). After the CD63 antibody immobilization, a blocking step was performed by a 3 % bovine serum albumin (BSA; Sigma) for 1 h at RT, followed by the secondary antibody (1:200 in PBS) incubation (1 h at RT). Alexa Fluor<sup>®</sup> 488 rabbit anti-mouse (~495/517 nm; Life Technologies) was used as secondary antibody against CD63 antibody. The unbound secondary antibody fluorescence was measured in a microplate reader (Synergy HT, Bio-TEK), as an indirect method to determine the primary antibody immobilization efficiency. In order to evaluate nonspecific immobilization, the activated and functionalized NFM without primary antibody was used as a negative control. The samples were further analyzed by fluorescence microscopy (Axio



Observer; Zeiss) to detect the distribution of the CD63 antibody at the surface of the nanofibrous substrate.

#### IV-2.5.2. EVs binding

Biofunctionalization of NFMs with EVs was achieved by using an antibody-antigen strategy, as described in detail elsewhere [22]. The nanofibrous substrate with immobilized CD63 antibody, at the maximum concentration previously optimized, was incubated with the different conditioned medium previously harvested for 2 h at RT. The unbound EVs solutions were collected and quantified by ELISA (Exosome ELISA Complete Kit (CD63)), in order to define the binding capacity of the engineered EVs delivery system.

The morphology of EVs bound at the surface of biofunctional electrospun PCL NFM (*i.e.*  $EV^{EM}$ ;  $EV^{DM}$ ;  $EV^{BM}$ ;  $EV^{CM}$ ) was analyzed by scanning electron microscopy (SEM; AURIGA Compact, Zeiss, Germany). By energy dispersive spectroscope (EDS; INCAx-Act, PentaFET Precision, Oxford Instruments), an elemental analysis of the EVs delivery systems was performed to further confirm the presence of the EVs at the surface of the NFMs.

The distribution of EVs bound to the NFM biofunctionalized with CD63 antibody was performed by immunofluorescence staining. Firstly, a blocking step (3% BSA for 30 min) was performed. In between each step, the samples were rinsed three times in PBS buffer. For EVs' surface markers staining, samples were incubated with the primary antibodies CD63 (E-12; 1:500; Santa Cruz Biotechnology, Inc.), CD81 (1.3.3.22; 1:500; Santa Cruz Biotechnology, Inc.) and CD9 (C-4; 1:500; Santa Cruz Biotechnology, Inc.) overnight, and then with the corresponding secondary antibody [Alexa Fluor<sup>®</sup> 488 rabbit anti-mouse (~495/517 nm; Life Technologies)] for 1h at RT. The samples were further analysed by fluorescence microscopy (Axio Observer; Zeiss).

### IV-2.6. Biological activity of EVs delivery systems into uncommitted Homotypic cells

#### IV-2.6.1. Cell seeding and culture conditions

The effectiveness of the developed EVs delivery systems (**Table IV-1**), as chondrogenic lineage inducible systems, was assessed using hBM-MSCs. Confluent hBM-MSCs at passage 4 were harvested for seeding onto the EVs delivery systems ( $EV^{EM}$ ;  $EV^{DM}$ ;  $EV^{BM}$ ;  $EV^{CM}$ ) at a

density of  $2 \times 10^5$  cells per sample. These constructs were cultured under basal medium, without further medium supplementation. The experimental control conditions comprise hBM-MSCs cultured on activated and functionalized NFMs in basal medium (*BM*) and standard chondrogenic differentiation medium (*CM*). hACs were also seeded on activated and functionalized NFMs at a density of  $2 \times 10^5$  cells per sample, and cultured under expansion (*EM*) or differentiation (*DM*) medium. The constructs were retrieved for further analysis at predefined culturing times, namely 0, 7, 14, 21 and 28 days. All experiments were performed in triplicate and repeated at least three times ( $n=3$ ), independently.

**Table IV-1 Experimental conditions used in the Cell Biology assays.**

Cells	Condition	Description
hACs	EM	Activated and functionalized NFMs in EM
	DM	Activated and functionalized NFMs in DM
hBM-MSCs	BM	Activated and functionalized NFMs in BM
	CM	Activated and functionalized NFMs in CM
	EV <sup>EM</sup>	Biofunctional NFMs with EVs-derived from hACs under EM
	EV <sup>DM</sup>	Biofunctional NFMs with EVs-derived from hACs under DM
	EV <sup>BM</sup>	Biofunctional NFMs with EVs-derived from hBM-MSCs under BM
	EV <sup>CM</sup>	Biofunctional NFMs with EVs-derived from hBM-MSCs under CM

EM = Expansion Medium; DM = Differentiation Medium; BM = Basal Medium; CM = Chondrogenic Medium;

#### IV-2.6.2. Cellular Biochemistry Analysis

Metabolic activity was evaluated by the MTS assay (CellTiter 96 AQueous One Solution, Promega); the cell proliferation by DNA quantification (Quant-iTPicoGreen dsDNA assay, Invitrogen, Alfacene), and the protein synthesis by the Micro BCA assay (Micro BCA<sup>TM</sup> Protein Assay Kit, Thermo Fisher Scientific), according to the manufacturer's instructions. Glycosaminoglycans (GAGs) quantification was performed according to our established standard colorimetric assay [6].

### IV-2.6.3. Scanning Electron Microscopy (SEM)

The constructs were collected after 28 days of culture and fixed with 2.5 % glutaraldehyde. By increasing alcohol concentrations, samples were dehydrated, followed by sputter coating with Au/Pd. A scanning electron microscope (JSM-6010 LV, JEOL, Japan) was used to observe the distribution and morphology of the cells at x3000 magnification.

### IV-2.6.4. Gene Expression Analysis

At each time point, the constructs were washed, immersed in Tri reagent® (Life Science, VWR), and kept at -80 °C. Total RNA was isolated and reverse transcribed into cDNA (qScript cDNA synthesis kit, Quanta Biosciences), followed by qPCR (PerfeCta™ SYBR® Green system; Quanta Biosciences), according to the manufacturer's instructions. The qPCR reactions were carried out in a Mastercycler® ep Gradient S realplex® thermocycler (Eppendorf; Hamburg) for the target genes described in **Table IV-2**. The transcript expression data were normalized against the housekeeping gene *Glyceraldehydes-3-phosphate-dehydrogenase* (*GAPDH*) and the quantification performed according to the Livak method (2<sup>-ΔΔCT</sup> method). For hACs samples, the expansion medium condition was used as calibrator, while the basal medium condition was used as calibrator of the hBM-MSCs samples.

**Table IV-2 Primer sequences used for RT-PCR procedures <sup>a)</sup>.**

	gene	forward (5' - 3')	reverse (5' - 3')
Ref.	<i>GAPDH</i>	AGCCTCAAGATCATCAGCAA	GTCATGAGTCCTTCCACGAT
Chondrogenic	<i>Sox9</i>	TTCATGAAGATGACCGACGC	GTCCAGTCGTAGCCCTTGAG
	<i>Aggrecan</i>	TGAGTCCTCAAGCCTCCTGT	TGGTCTGCAGCAGTTGATTC
	<i>COMP</i>	AGGGATGGAGACGGACATCAG	TCTGCATCAAAGTCGTCCTG
	<i>COL II</i>	CGGTGAGAAGGGAGAAGTTG	GACCGGTCCTCCAGTAGGA
Hypertrophic	<i>COL Iα</i>	AAGAACCCCAAGGACAAGAG	GTAGGTGATGTTCTGGGAGG
	<i>COL X</i>	CAGGCATAAAAGGCCCACTA	AGGACTTCCGTAGCCTGGTT

<sup>a)</sup> *GAPDH* = Glyceraldehyde 3-phosphate dehydrogenase; *Sox9* = Sry-type high mobility group box 9; *COMP* = Cartilage oligomeric matrix protein; *COL II* = collagen type II; *COL Iα* = collagen type I alpha; *COL X* = collagen type X.

#### IV-2.6.5. Histological Analysis

For constructs were collected after 28 days of culture, fixed in a 10% neutral buffered formalin (Bio-Optica Milano S.p.a.), and kept at 4 °C until further used. Alcian blue staining, immunocytochemistry for collagens type I (COL1A1, clone C-18; Santa Cruz Biotechnology) and type II (mouse anti-human type II collagen monoclonal antibody; Millipore) were performed as described elsewhere [23]. The immunocytochemistry samples were counterstained with hematoxylin for nuclei visualization and observed in an optical microscope (Leica DM750 microscope).

#### IV-2.7. Statistical analysis

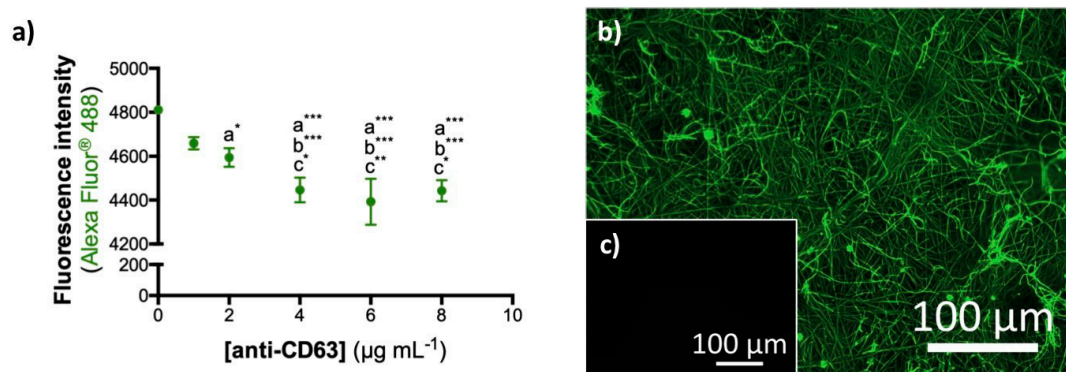
Statistical analysis was performed using the SPSS statistic software (release 24.0.0.0 for Mac). First, the Shapiro-Wilk test was used to ascertain the data normality and the Levene test for the homogeneity of variances. Observing this the normality and variance homogeneity were rejected; non-parametric tests were used (Kruskal-Wallis test followed by Tukey's HSD test). The confidence interval used was 99% and  $p \leq 0.01$  were regarded as statistically significant.

### IV-3. RESULTS

#### IV-3.1. Development and characterization of the EVs delivery systems

To develop a delivery system capable to selectively bind EVs from conditioned medium, a method to generate functional groups at the surface of electrospun PCL NFMs was implemented, which provide binding sites for the biomolecules immobilization. Specifically, the CD63 antibody was immobilized at the surface of activated and functionalized nanofibrous substrates capable to covalently and effectively bind. In order to ensure that the nanofibrous substrate is used at its maximum immobilization capacity, a wide range of concentrations (0 - 8  $\mu\text{g mL}^{-1}$ ) of CD63 antibody were used. According to an indirect quantification method, the maximum immobilization was achieved at the concentration of 4  $\mu\text{g mL}^{-1}$  (**Figure IV-1 a**). By fluorescence microscopy can be observed a uniform distribution of immobilized CD63 antibody over the nanofibrous substrate (**Figure IV-1 b**).

## ANTIBODY IMMOBILIZATION CAPACITY



## QUANTITY OF EXTRACELLULAR VESICLES

d)

	Conditioned Medium derived EVs			
	hACs		hBM-MSCs	
	EM	DM	BM	CM
<b>Total EVs</b> (10 <sup>8</sup> EVs mL <sup>-1</sup> )	11.2 ± 1.3	6.8 ± 2.5	8.2 ± 2.6	7.1 ± 3.1
<b>Bound</b> (10 <sup>8</sup> EVs mL <sup>-1</sup> )	6.9 ± 3.8	5.7 ± 2.5	5.6 ± 2.7	6.1 ± 3.1

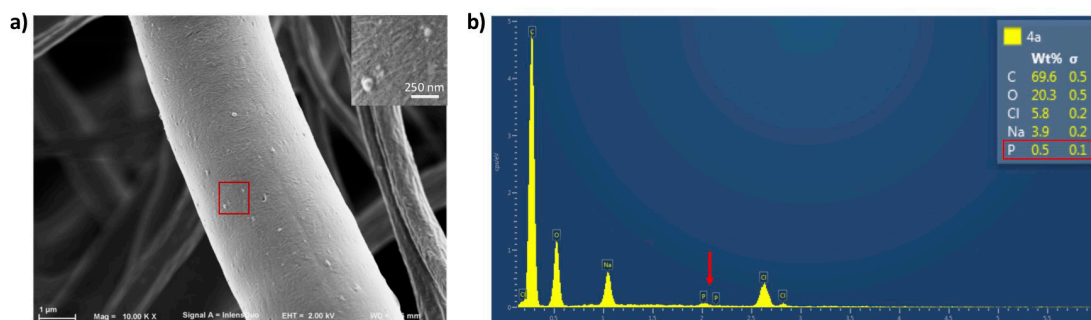
Figure IV-1 Maximum immobilization capacity of CD63 antibody at the surface of activated and functionalized NFM (a). Data were analyzed by the one-way ANOVA test, followed by the Tukey's HSD test (\* $p < 0.01$ ; \*\* $p < 0.001$ ; \*\*\* $p < 0.0001$ ): *a* denotes significant differences compared to concentration 0 µg mL<sup>-1</sup>; *b* denotes significant differences compared to concentration 1 µg mL<sup>-1</sup> and *c* denotes significant differences compared to concentration 2 µg mL<sup>-1</sup>. Spatial distribution of anti-CD63 immobilized at the surface of activated and functionalized nanofibrous substrates at 4 µg mL<sup>-1</sup> (b). The negative control sample was not incubated with the primary antibody (c). Quantification of extracellular vesicles derived from hACs and hBM-MSCs, and bound to the biofunctional nanofibrous system (d).

The binding capacity of the immobilized CD63 antibody was assessed by using conditioned media harvested from hACs cultured under expansion or differentiation media, as well as for hBM-MSCs cultured under basal or chondrogenic media (i.e. *EM*, *DM*, *BM* and *CM*, respectively). The biological status of those EVs-donor cells was reported in **Supplementary Figure IV-1**. **Figure IV-1 d** shows the range of EVs' concentrations obtained from the four different conditioned media (from 6.8 to 11.2 10<sup>8</sup> particles mL<sup>-1</sup>). Those EVs were successfully bound at the surface of biofunctional nanofibrous substrate at the range of 5.6 – 6.9 10<sup>8</sup> particles mL<sup>-1</sup>.

**Figure IV-2** presents the distribution of EVs bind at the surface of the nanofibrous substrate. In the SEM micrograph (**Figure IV-2 a**) can be identified bound EVs with diameters

of 120 nm. Their presence can be also confirmed by the EDS spectrum, namely by the presence of the P element of the phospholipids of EVs (**Figure IV-2 b**). To ascertain about the phenotypic profile of bound EVs, the expression of the tetraspanins CD63/CD81/CD9 was analysed by fluorescence microscopy (**Figure IV-2 c**). These observations showed bound EVs labeled for each of the surface markers, as well as their uniform distribution at the surface of the biofunctional electrospun NFMs.

#### EVs-DELIVERY SYSTEM MORPHOLOGY



#### EVs' SURFACE MARKERS

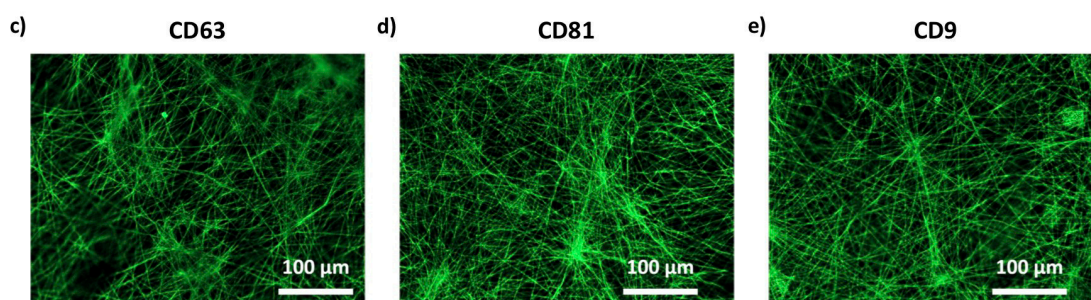


**Figure IV-2** Distribution of EVs bound at the surface of the biofunctional nanofibrous system (a); EDS spectrum of the EVs-delivery system surface (b); Fluorescence micrographs of the EVs markers CD63 (c), CD81 (d) and CD9 (e).

#### IV-3.2. EVs delivery systems elicit hBM-MSCs chondrogenic commitment

The ability of the EVs delivery systems ( $EV^{EM}$ ;  $EV^{DM}$ ;  $EV^{BM}$ ;  $EV^{CM}$ ) to promote the onset of chondrogenesis of uncommitted homotypic cells was examined. The differentiation process is known to impair cell proliferation, due to an increase in the length of the cell cycle [24], and to induce changes in the protein synthesis rate [25]. Therefore, we evaluated the biochemical profile of recipient hACs and hBM-MSCs viability, proliferation and total protein synthesis. In terms of cell viability (**Figure IV-3 a**), on the 14<sup>th</sup> day of culture, the hBM-MSCs cultured on the EVs delivery systems ( $EV^{EM}$ ;  $EV^{DM}$ ;  $EV^{BM}$ ;  $EV^{CM}$ ) displayed significantly higher viability

than the hACs conditions (*EM* and *DM*) or even than the hBM-MSCs control conditions (*BM* and *CM*) ( $p < 0.0001$ ). On the 28<sup>th</sup> day of culture, the hBM-MSCs culture on  $EV^{EM}$  and  $EV^{BM}$  delivery systems presented significantly higher cell viability than hACs cultured in *EM* and hBM-MSCs cultured in *CM* ( $p < 0.01$ ). The EVs delivery systems were favorable for cell proliferation (**Figure IV-3 b**) and protein synthesis (**Figure IV-3 c**), since their levels are comparable to those observed on the control culture conditions (*EM*; *DM*; *BM*; *CM*) over the time. Moreover, the  $EV^{DM}$  delivery system displayed significantly higher proliferation levels and protein synthesis than hACs cultured in *EM* at 28 days of culture ( $p < 0.01$ ). Likewise, the  $EV^{CM}$  delivery system significantly increase protein synthesis of hBM-MSCs when compared to the hACs cultured in *EM* ( $p < 0.01$ ).

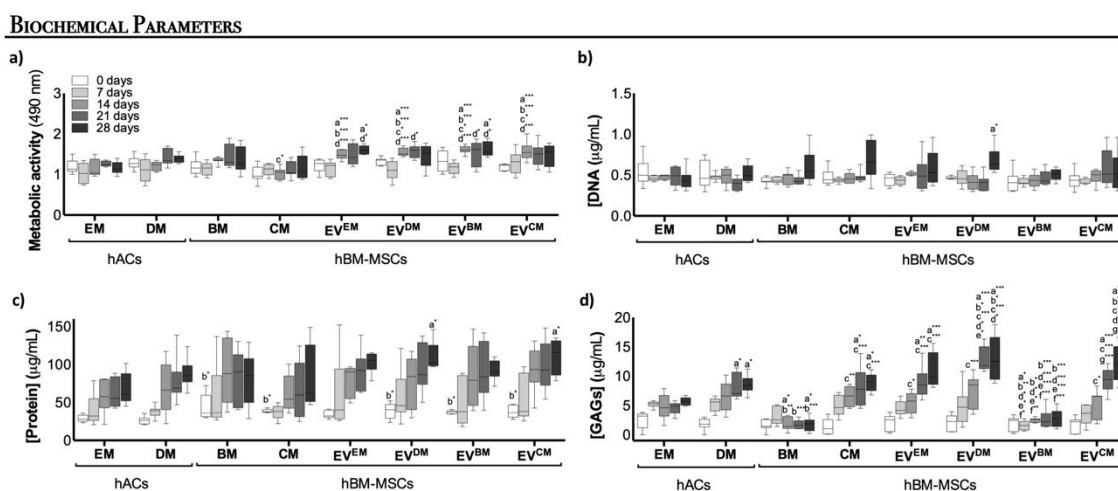


**Figure IV-3** Biochemical performance (i.e. cell viability (a), proliferation (DNA content) (b), total protein synthesis(c) and sulfated glycosaminoglycans (GAGs) content (d) of hBM-MSCs cultured on biofunctional nanofibrous systems comprising EVs derived from different sources (i.e. hACs under expansion medium [ $EV^{EM}$ ], hACs under differentiation medium [ $EV^{DM}$ ], hBM-MSCs under basal medium [ $EV^{DM}$ ] and hBM-MSCs under chondrogenic medium [ $EV^{CM}$ ]), under basal culture conditions. hACs cultured on non-biofunctionalized nanofibrous substrates under expansion medium (*EM*) or differentiation medium (*DM*), and hBM-MSCs cultured on non-biofunctionalized nanofibrous substrates under basal medium (*BM*) or chondrogenic medium (*CM*) were used as controls. Data were analyzed by the Kruskal-Wallis test, followed by the Tukey's HSD test ( $*p < 0.01$ ;  $**p < 0.001$ ;  $***p < 0.0001$ ): *a* denotes significant differences compared to *EM*; *b* denotes significant differences compared to *DM*; *c* denotes significant differences compared to *BM*; *d* denotes significant differences compared to *CM*; *e* denotes significant differences compared to  $EV^{EM}$ ; *f* denotes significant differences compared to  $EV^{DM}$ ; *g* denotes significant differences compared to  $EV^{BM}$ .

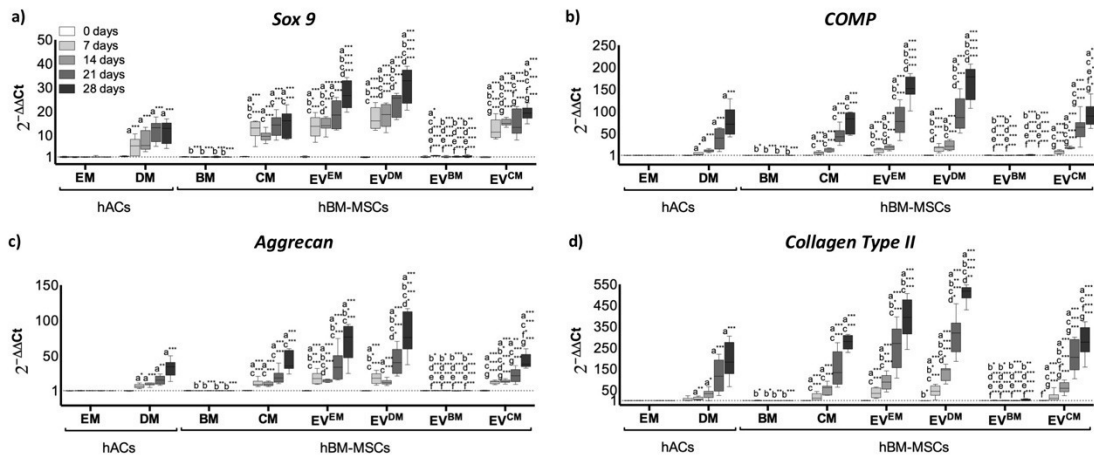
The chondrogenic inductive potential of bound EVs was then evaluated in terms of the extracellular matrix glycosaminoglycans (GAGs) content (**Figure IV-3 d**). Along the culturing time, the hACs (*EM*; *DM*) and the hBM-MSCs cultured under standard chondrogenic medium

(*CM*) and EVs delivery systems, namely the  $EV^{EM}$ ,  $EV^{DM}$  and  $EV^{CM}$ , displayed a significantly higher protein synthesis than the hBM-MSCs cultured under basal medium (*BM*) and the  $EV^{BM}$  delivery system. On the 21<sup>th</sup> day of hBM-MSCs culture, the  $EV^{DM}$  delivery system presented significantly high GAGs content when compared to the  $EV^{EM}$  delivery system ( $p < 0.01$ ). Furthermore, the  $EV^{DM}$  and  $EV^{CM}$  delivery systems displayed a significantly higher synthesis than the positive condition (*CM*) ( $p < 0.01$ ).

To better define the chondrogenic commitment of the hBM-MSCs induced by the EVs delivery systems, the temporal gene expression of chondrogenic markers was investigated (**Figure IV-4**). The cartilage-related genes, namely *Sox 9*, *COMP*, *Aggrecan* and *Collagen type II*, are all expressed in all testing conditions, except on the  $EV^{BM}$  delivery system. Along culture time, a significantly higher cartilage-related gene expression was observed on the EVs delivery systems ( $EV^{EM}$ ;  $EV^{DM}$ ;  $EV^{CM}$ ) ( $p < 0.01$ ). On the 28<sup>th</sup> day of culture, a significantly higher *Sox 9* and *COMP* expression was observed in  $EV^{EM}$  and  $EV^{DM}$  delivery systems when compared to the non-biofunctionalized NFMs under standard chondrogenic differentiation medium (*CM*) ( $p < 0.0001$ ). Likewise, the  $EV^{DM}$  delivery system induced a significantly higher *Aggrecan* and *Collagen type II* expression than hBM-MSCs under standard chondrogenic differentiation medium (*CM*) and the  $EV^{CM}$  delivery system condition ( $p < 0.01$ ). Although, these results show that bound EVs, obtained during hBM-MSCs chondrogenic differentiation and from hACs cultured under differentiation medium, provides guidance for chondrogenic lineage progression of homotypic cells. Therefore, it is also crucial to confirm that the hBM-MSCs were not undergoing hypertrophy and further differentiating into the osteogenic lineage. The lower hypertrophy-related genes (i.e. *Collagen type X*, *Collagen type I $\alpha$* .) expression patterns were considerably similar on all the EVs delivery systems, inversely to the standard chondrogenic differentiation medium (**Figure IV-4 e f**). Moreover, those systems had significantly lower expression of the hypertrophy-related genes when compared with the non-biofunctionalized NFMs under differentiation or chondrogenic media (*EM*; *CM*) along the culture time.



## CHONDROGENIC TRANSCRIPTS EXPRESSION



## HYPERTROPHIC TRANSCRIPTS EXPRESSION

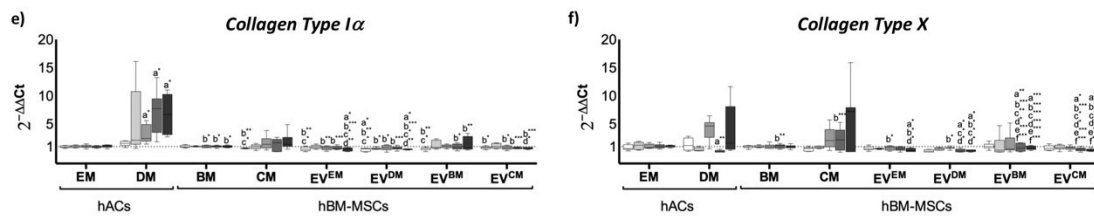


**Figure IV-4** Relative expression of chondrogenic (i.e. *Sox 9* (a), *COMP* (b), *Aggrecan* (c) and *Collagen type II* (d)) and hypertrophic transcripts (i.e. *Collagen type I $\alpha$*  (e), *Collagen type X* (f)) by hBM-MSCs cultured on biofunctional nanofibrous systems comprising EVs derived from different sources (i.e. hACs under expansion medium [EV<sup>EM</sup>], hACs under differentiation medium [EV<sup>DM</sup>], hBM-MSCs under basal medium [EV<sup>DM</sup>] and hBM-MSCs under chondrogenic medium [EV<sup>CM</sup>]), under basal culture conditions. hACs cultured on non-biofunctionalized nanofibrous substrates under expansion medium (EM) or differentiation medium (DM), and hBM-MSCs cultured on non-biofunctionalized nanofibrous substrates under basal medium (BM) or chondrogenic medium (CM) were used as controls. Data were analyzed by the Kruskal-Wallis test, followed by the Tukey's HSD test (\* $p < 0.01$ ; \*\* $p < 0.001$ ; \*\*\* $p < 0.0001$ ): a denotes significant differences compared to EM; b denotes significant differences compared to DM; c denotes significant differences compared to BM; d denotes significant differences compared to CM; e denotes significant differences compared to EV<sup>EM</sup>; f denotes significant differences compared to EV<sup>DM</sup>; g denotes significant differences compared to EV<sup>BM</sup>.

The morphological changes of hBM-MSCs cultured on the different EVs delivery systems, reflect their differentiation stage. SEM observations of the hBM-MSCs cultured for 28 days showed the acquisition of a round-shaped morphology (Figure IV-5 a) typically of chondrocyte cells. Alcian blue staining (Figure IV-5 b) confirms the presence of sulfated extracellular proteoglycans synthesized by hBM-MSCs cultured for 28 days on the EVs delivery systems (EV<sup>EM</sup>; EV<sup>DM</sup>; EV<sup>CM</sup>), being more evident in the EV<sup>DM</sup> delivery system. It is also possible to observe the absence of proteoglycans staining on the EV<sup>BM</sup> delivery system. Those results are corroborated by the immunolocalization of Collagen type II, which confirms the deposition of

a cartilaginous ECM on the EVs delivery systems ( $EV^{EM}$ ;  $EV^{DM}$ ;  $EV^{CM}$ ), accompanied by the absence of Collagen type I $\alpha$  expression. These phenotypic observations were consistent with previously obtained results for glycosaminoglycans production, as well as by the expression of cartilage-related genes.

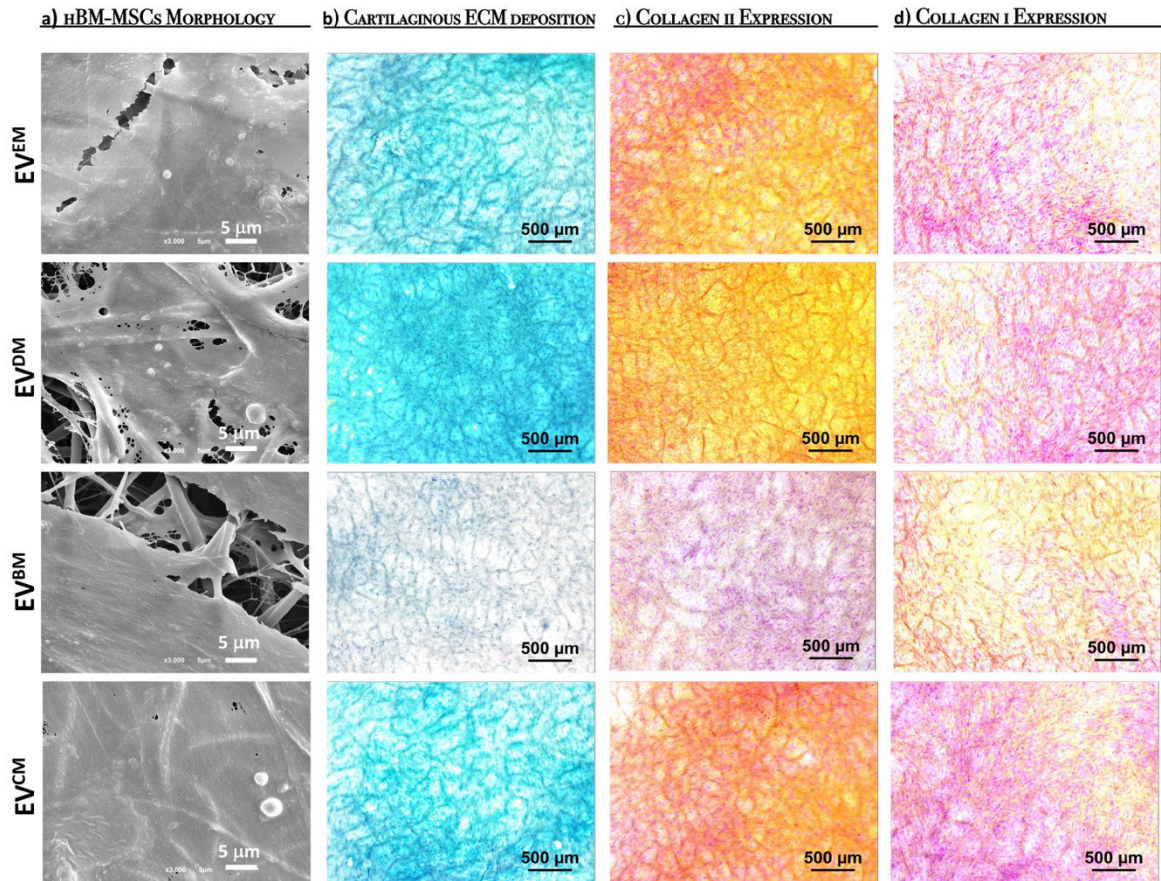


**Figure IV-5** Morphology of hBM-MSCs cultured during 28 days on biofunctional nanofibrous systems comprising EVs derived from different sources (i.e. hACs under expansion medium [ $EV^{EM}$ ], hACs under differentiation medium [ $EV^{DM}$ ], hBM-MSCs under basal medium [ $EV^{DM}$ ] and hBM-MSCs under chondrogenic medium [ $EV^{CM}$ ]), under basal conditions, analyzed by scanning electron microscopy (SEM) (a); stained with alcian blue for sulfated glycosaminoglycans (b); and immunolocalized collagen type II (c) and type I $\alpha$  (d).

#### IV-4. DISCUSSION

EVs are small membrane-enclosed particles actively released by many cell types, including immune cells (T-cells, B-cells, dendritic cells, neutrophils, platelets), connective tissue cells (epithelial cells, fibroblasts) and other specialized cells (endothelial cells, neuronal cells, chondrocyte cells), and stem cells, and are presented in synovial fluid and cartilage extracellular

matrix [26, 27]. Their prominent role in joint development and in the regulation of intra-articular homeostasis leads to recognize EVs as potential biomarkers of joint disease [13, 15, 28]. Therefore, they have been seen as a new tool to restore joint homeostasis and enhance articular cartilage regeneration, since they provide a simpler and safer alternative to current cell-based therapeutic options. MSCs are one of the most prominent cell sources of EVs, and it is thought that the MSC-derived EVs share the parental MSCs phenotype and genotype. Furthermore, EVs derived from MSC have been demonstrated to have positive effects over cell viability and proliferation [29, 30], angiogenesis [16, 31], and immunomodulation [32, 33] in a wide range of physiological systems. For example, in a clinical trial using MSC-derived EVs as treatment, symptoms were considerably mitigated in a patient with therapy-refractory graft-versus-host disease [34].

Our experimental data showed that the culture conditions may affect the yield of EVs (**Figure IV-1 d**). Furthermore, we showed that hACs and hBM-MSCs secrete a population of EVs within the size range reported for hBM-MSC-EVs, 47-180 nm [16, 17]. Our biofunctional nanofibrous substrate with immobilized CD63 antibody was able to bound those cell-derived EVs at the range of  $5.6 - 6.9 \times 10^8$  EVs mL<sup>-1</sup>. Consistent with MSCs expressing CD63 [35], CD81 [36], and CD9 [37], bound EVs also showed the presence of these surface markers, suggesting that they originated at the parent cell plasma membrane lipid rafts [38]. Therefore, the parent cell source could affect the EVs' surface proteins, their glycosylation or lipid composition, and their cargo.

The role of MSC-derived EVs as modulators of joint homeostasis, suggested that an EVs delivery system may be interesting therapeutic alternative in cartilage repair. The developed EVs delivery systems comprising EVs derived from differentiated hACs or chondrogenic differentiated hBM-MSCs outperformed the effect of current chondroinductive strategies, in terms of the type and/or intensity of the signals. Specifically, the early activation of key chondrogenic commitment genes such as *Sox 9* and *Aggrecan*, are considered necessary and sufficient to induce cartilage formation [39-42]. In addition, EVs delivery systems (*EV<sup>EM</sup>*; *EV<sup>DM</sup>*; *EV<sup>CM</sup>*) induced a transient upregulation of downstream matrix-associated genes and proteins that may be required to promote cell-cell and cell-matrix interactions and support long-term differentiation, maintaining a stable cartilage phenotype of the differentiated MSCs [9].

Notably, slight differences were noted between the three EVs delivery systems (*EV<sup>EM</sup>*; *EV<sup>DM</sup>*; *EV<sup>CM</sup>*) tested, suggesting that the inherent cargo of EVs-derived from hACs under

differentiation medium ( $EV^{DM}$ ) may also contributed to the stronger effect. This is in line with articular cartilage vesicles RNA can be transferred to chondrocytes with resultant phenotypic alterations [43]. Indeed, it is reported that EVs are constitutively released into conditioned medium by normal articular chondrocytes [44], participating in non-classical protein secretion, intercellular communication, and pathologic calcification [45, 46]. In order to protect nearby chondrocytes from damage, articular chondrocyte vesicles provide extracellular matrix repair in pericellular cartilage, act to sequester substances such as ATP, calcium and phosphate in toxic concentrations [43, 45, 47].

Cell-derived EVs have similar biological functions to the parent cells, but offer significant advantages over cells such as their small size, low immunogenicity, and depletion of the common issues associated with direct cell injection. However, achieving an effective and controlled delivery of EVs at the target sites is challenging, but is paramount to the efficient restoration of joint homeostasis and sustained effect on the regenerative process. Therefore, the use of our EVs delivery system is expected to be more effective than currently available therapeutics that use soluble proteins or RNA molecules, which are usually prone to fast degradation after injection. Using the herein presented strategy, we can promote a local delivery of bioactive molecules to control over cellular activity, with more prolonged effect due to the bind of EVs at the surface of biofunctional nanofibrous substrates, avoiding degradation. In the microfactory approach, the EVs delivery system can be implanted into the defect site, where uncommitted homotypic cells migrating from microperforations could be induced to differentiate into the chondrogenic lineage by bound the EVs, envisioning a cartilage regeneration approach.

#### **IV-5. CONCLUSIONS**

Our results show the beneficial effects of cell-secreted factors, namely EVs secreted by hACs and hBM-MSCs playing an important role in the modulation of cell fate. Those EVs were successfully bound at the surface of biofunctional nanofibrous substrates, immobilizing the CD63 antibody. The EVs delivery systems comprising EVs derived from differentiated hACs and chondrogenically induced hBM-MSCs successfully induce the chondrogenic commitment of homotypic cells more efficiently than the current chondroinductive strategies. Therefore, EVs delivery systems are potential highly effective cell-free/secretome-based therapies for cartilage repair.

## IV-6. ACKNOWLEDGMENTS

The authors would like to acknowledge the Portuguese Foundation for Science and Technology (FCT) for the PhD grant of M.R.C. (PD/BD/113797/2015) financed by the FCT Doctoral Program on Advanced Therapies for Health (PATH) (FSE/POCH/PD/169/2013), the IF grant of A.M. (IF/00376/2014), and the projects SPARTAN (PTDC/CTM-BIO/4388/2014) and FRONthera (NORTE-01-0145-FEDER-0000232).

## IV-7. REFERENCES

- [1] O. Urbanek, D. Kolbuk, M. Wrobel, Articular cartilage: New directions and barriers of scaffolds development - review, *Int J Polym Mater Po* 68(7) (2019) 396-410.
- [2] X. Armoiry, E. Cummins, M. Connockl, A. Metcalfe, P. Roylel, R. Johnston, J. Rodrigues, N. Waugh, H. Mistry, Autologous Chondrocyte Implantation with Chondrosphere for Treating Articular Cartilage Defects in the Knee: An Evidence Review Group Perspective of a NICE Single Technology Appraisal, *Pharmacoeconomics* 37(7) (2019) 879-886.
- [3] S. Choi, G.M. Kim, Y.H. Maeng, H. Kang, C.T. Teongi, E.E. Lee, S.J. Yoo, D.D. Dlima, M.K. Kim, Autologous Bone Marrow Cell Stimulation and Allogenic Chondrocyte Implantation for the Repair of Full-Thickness Articular Cartilage Defects in a Rabbit Model, *Cartilage* 9(4) (2018) 402-409.
- [4] P. Behrens, T. Bitter, B. Kurz, M. Russlies, Matrix-associated autologous chondrocyte transplantation/implantation (MACT/MACI) - 5-year follow-up, *Knee* 13(3) (2006) 194-202.
- [5] I. Akgun, M. Unlu, O. Erdal, T. Ogut, M. Erturk, E. Ovali, F. Kantarci, G. Caliskan, Y. Akgun, Matrix-induced autologous mesenchymal stem cell implantation versus matrix-induced autologous chondrocyte implantation in the treatment of chondral defects of the knee: a 2-year randomized study, *Arch Orthop Traum Su* 135(2) (2015) 251-263.
- [6] M.R. Casanova, M.A. Da Silva, A.R. Costa-Pinto, R.L. Reis, A. Martins, N.M. Neves, Chondrogenesis-inductive nanofibrous substrate using both biological fluids and mesenchymal stem cells from an autologous source, *Mat Sci Eng C-Mater* 98 (2019) 1169-1178.
- [7] G. Kaul, M. Cucchiaroni, D. Arntzen, D. Zurakowski, M.D. Menger, D. Kohn, S.B. Trippel, H. Madry, Local stimulation of articular cartilage repair by transplantation of encapsulated chondrocytes overexpressing human fibroblast growth factor 2 (FGF-2) in vivo, *J Gene Med* 8(1) (2006) 100-111.
- [8] R.C. Pereira, M. Scaranari, P. Castagnola, M. Grandizio, H.S. Azevedo, R.L. Reis, R. Cancedda, C. Gentili, Novel injectable gel (system) as a vehicle for human articular chondrocytes in cartilage tissue regeneration, *J Tissue Eng Regen M* 3(2) (2009) 97-106.

- [9] A. Dickhut, K. Pelttari, P. Janicki, W. Wagner, V. Eckstein, M. Egermann, W. Richter, Calcification or Dedifferentiation: Requirement to Lock Mesenchymal Stem Cells in a Desired Differentiation Stage, *J Cell Physiol* 219(1) (2009) 219-226.
- [10] S.L.N. Maas, X.O. Breakefield, A.M. Weaver, Extracellular Vesicles: Unique Intercellular Delivery Vehicles, *Trends Cell Biol* 27(3) (2017) 172-188.
- [11] G. Raposo, W. Stoorvogel, Extracellular vesicles: Exosomes, microvesicles, and friends, *J Cell Biol* 200(4) (2013) 373-383.
- [12] K.W. Witwer, E.I. Buzas, L.T. Bemis, A. Bora, C. Lasser, J. Lotvall, E.N.N. Hoen, M.G. Piper, S. Sivaraman, J. Skog, C. Thery, M.H. Wauben, F. Hochberg, Standardization of sample collection, isolation and analysis methods in extracellular vesicle research, *J Extracell Vesicles* 2(1) (2013).
- [13] I.M. Bjorge, S.Y. Kim, J.F. Mano, B. Kalionis, W. Chrzanowski, Extracellular vesicles, exosomes and shedding vesicles in regenerative medicine - a new paradigm for tissue repair, *Biomater Sci-Uk* 6(1) (2017) 60-78.
- [14] S.M. Jay, G. Vunjak-Novakovic, Extracellular Vesicles and Their Versatile Roles in Tissue Engineering, *Tissue Eng Pt A* 23(21-22) (2017) 1210-1211.
- [15] T.N. Lamichhane, S. Sokic, J.S. Schardt, R.S. Raiker, J.W. Lin, S.M. Jay, Emerging Roles for Extracellular Vesicles in Tissue Engineering and Regenerative Medicine, *Tissue Eng Part B-Re* 21(1) (2015) 45-54.
- [16] S.Y. Bian, L.P. Zhang, L.F. Duan, X. Wang, Y. Min, H.P. Yu, Extracellular vesicles derived from human bone marrow mesenchymal stem cells promote angiogenesis in a rat myocardial infarction model, *J Mol Med* 92(4) (2014) 387-397.
- [17] S. Bruno, F. Collino, M.C. Deregibus, C. Grange, C. Tetta, G. Camussi, Microvesicles Derived from Human Bone Marrow Mesenchymal Stem Cells Inhibit Tumor Growth, *Stem Cells Dev* 22(5) (2013).
- [18] M. Martins, D. Ribeiro, A. Martins, R.L. Reis, N.M. Neves, Extracellular Vesicles Derived from Osteogenically Induced Human Bone Marrow Mesenchymal Stem Cells Can Modulate Lineage Commitment, *Stem Cell Rep* 6(3) (2016) 284-291.
- [19] J. Malda, J. Boere, C.H.A. van de Lest, P.R. van Weeren, A.H.M. Wauben, Extracellular vesicles - new tool for joint repair and regeneration, *Nat Rev Rheumatol* 12(4) (2016) 243-249.
- [20] M.L.A. da Silva, A.R. Costa-Pinto, A. Martins, V.M. Correlo, P. Sol, M. Bhattacharya, S. Faria, R.L. Reis, N.M. Neves, Conditioned medium as a strategy for human stem cells chondrogenic differentiation, *J Tissue Eng Regen M* 9(6) (2015) 714-723.
- [21] M.L.A. da Silva, A. Martins, A.R. Costa-Pinto, P. Costa, S. Faria, M. Gomes, R.L. Reis, N.M. Neves, Cartilage Tissue Engineering Using Electrospun PCL Nanofiber Meshes and MSCs, *Biomacromolecules* 11(12) (2010) 3228-3236.

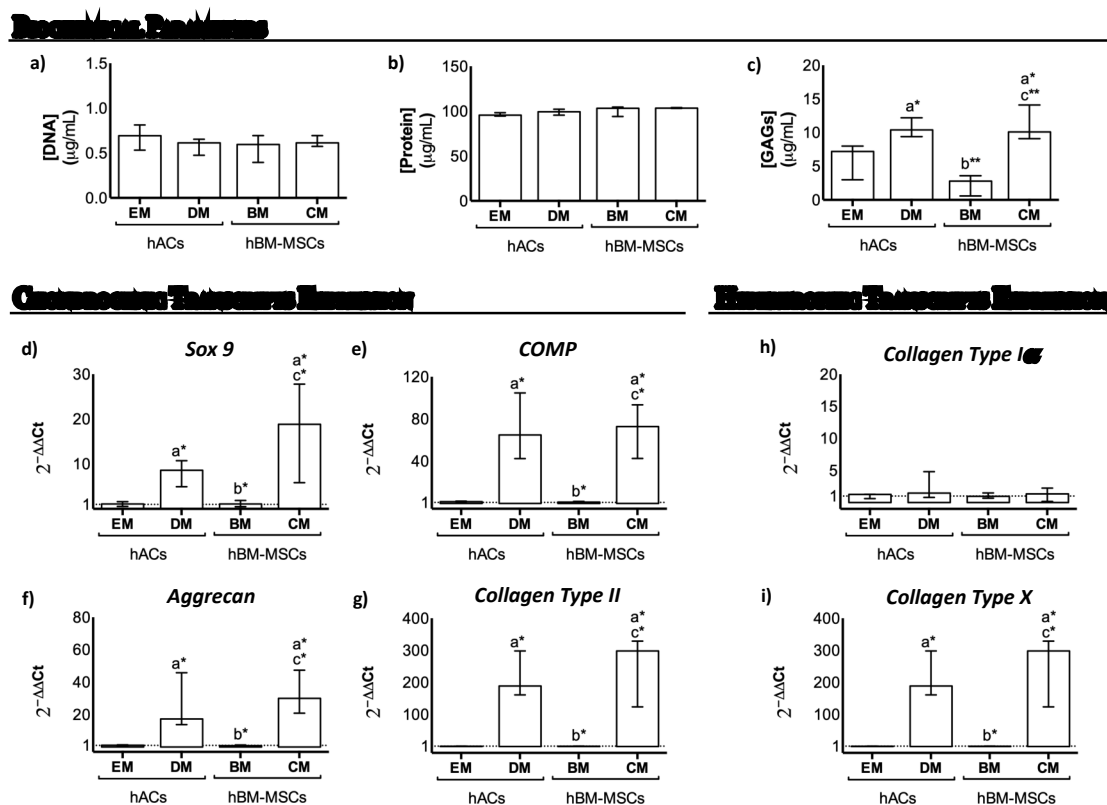
- [22] C. Oliveira, A.R. Costa-Pinto, R.L. Reis, A. Martins, N.M. Neves, Biofunctional Nanofibrous Substrate Comprising Immobilized Antibodies and Selective Binding of Autologous Growth Factors, *Biomacromolecules* 15(6) (2014) 2196-2205.
- [23] M.A. da Silva, A. Martins, A.A. Teixeira, R.L. Reis, N.M. Neves, Impact of biological agents and tissue engineering approaches on the treatment of rheumatic diseases, *Tissue Eng Part B Rev* 16(3) (2010) 331-9.
- [24] M. Roccio, D. Schmitter, M. Knobloch, Y. Okawa, D. Sage, M.P. Lutolf, Predicting stem cell fate changes by differential cell cycle progression patterns, *Development* 140(2) (2013) 459-470.
- [25] A.R. Kristensen, J. Gsponer, L.J. Foster, Protein synthesis rate is the predominant regulator of protein expression during differentiation, *Mol Syst Biol* 9 (2013).
- [26] R.J. Berckmans, R. Nieuwland, P.P. Tak, A.N. Boing, F.P.H.T.M. Romijn, M.C. Kraan, F.C. Breedveld, C.E. Hack, A. Sturk, Cell-derived microparticles in synovial fluid from inflamed arthritic joints support coagulation exclusively via a factor VII-dependent mechanism, *Arthritis Rheum* 46(11) (2002) 2857-2866.
- [27] S. Rani, A.E. Ryan, M.D. Griffin, T. Ritter, Mesenchymal Stem Cell-derived Extracellular Vesicles: Toward Cell-free Therapeutic Applications, *Mol Ther* 23(5) (2015) 812-823.
- [28] E.I. Buzas, B. Gyorgy, G. Nagy, A. Falus, S. Gay, Emerging role of extracellular vesicles in inflammatory diseases, *Nat Rev Rheumatol* 10(6) (2014) 356-364.
- [29] R.C. Lai, F. Arslan, M.M. Lee, N.S.K. Sze, A. Choo, T.S. Chen, M. Salto-Tellez, L. Timmers, C.N. Lee, R.M. El Oakley, G. Pasterkamp, D.P.V. de Kleijn, S.K. Lim, Exosome secreted by MSC reduces myocardial ischemia/reperfusion injury, *Stem Cell Res* 4(3) (2010) 214-222.
- [30] Y. Zhou, H.T. Xu, W.R. Xu, B.Y. Wang, H.Y. Wu, Y. Tao, B. Zhang, M. Wang, F. Mao, Y.M. Yan, S. Gao, H.B. Gu, W. Zhu, H. Qian, Exosomes released by human umbilical cord mesenchymal stem cells protect against cisplatin-induced renal oxidative stress and apoptosis in vivo and in vitro, *Stem Cell Res Ther* 4 (2013).
- [31] H.C. Zhang, X.B. Liu, S. Huang, X.Y. Bi, H.X. Wang, L.X. Xie, Y.Q. Wang, X.F. Cao, J. Lv, F.J. Xiao, Y. Yang, Z.K. Guo, Microvesicles Derived from Human Umbilical Cord Mesenchymal Stem Cells Stimulated by Hypoxia Promote Angiogenesis Both In Vitro and In Vivo, *Stem Cells Dev* 21(18) (2012) 3289-3297.
- [32] B. Zhang, Y.J. Yin, R.C. Lai, S.S. Tan, A.B.H. Choo, S.K. Lim, Mesenchymal Stem Cells Secrete Immunologically Active Exosomes, *Stem Cells Dev* 23(11) (2014) 1233-1244.
- [33] C. Lee, S.A. Mitsialis, M. Aslam, S.H. Vitali, E. Vergadi, G. Konstantinou, K. Sdrimas, A. Fernandez-Gonzalez, S. Kourembanas, Exosomes Mediate the Cytoprotective Action of Mesenchymal Stromal Cells on Hypoxia-Induced Pulmonary Hypertension, *Circulation* 126(22) (2012) 2601-+.

- [34] L. Kordelas, V. Rebmann, A.K. Ludwig, S. Radtke, J. Ruesing, T.R. Doeppner, M. Epple, P.A. Horn, D.W. Beelen, B. Giebel, MSC-derived exosomes: a novel tool to treat therapy-refractory graft-versus-host disease, *Leukemia* 28(4) (2014) 970-973.
- [35] K. Stewart, P. Monk, S. Walsh, C.M. Jefferiss, J. Letchford, J.N. Beresford, STRO-1, HOP-26 (CD63), CD49a and SB-10 (CD166) as markers of primitive human marrow stromal cells and their more differentiated progeny: a comparative investigation in vitro, *Cell Tissue Res* 313(3) (2003) 281-290.
- [36] H.J. Lee, B.H. Choi, B.H. Min, S.R. Park, Changes in Surface Markers of Human Mesenchymal Stem Cells During the Chondrogenic Differentiation and Dedifferentiation Processes In Vitro, *Arthritis Rheum* 60(8) (2009) 2325-2332.
- [37] T.S. Chen, R.C. Lai, M.M. Lee, A.B.H. Choo, C.N. Lee, S.K. Lim, Mesenchymal stem cell secretes microparticles enriched in pre-microRNAs, *Nucleic Acids Res* 38(1) (2010) 215-224.
- [38] S.S. Tan, Y.J. Yin, T. Lee, R.C. Lai, R.W.Y. Yeo, B. Zhang, B. Zhang, S.K. Lim, Therapeutic MSC exosomes are derived from lipid raft microdomains in the plasma membrane, *J Extracell Vesicles* 2(1) (2013).
- [39] C. Wang, T. Zhang, W. Liu, H. Meng, Y. Song, W. Wang, Sox9-induced chondrogenesis in mesenchymal stem cells was mediated by ERK5 signal pathway, *Cell Mol Biol* 62(2) (2016) 1-7.
- [40] Q.H. Pan, Y.C. Yu, Q.Y. Chen, C.S. Li, H. Wu, Y. Wan, J. Ma, F.Y. Sun, Sox9, a key transcription factor of bone morphogenetic protein-2-induced chondrogenesis, is activated through BMP pathway and a CCAAT box in the proximal promoter, *J Cell Physiol* 217(1) (2008) 228-241.
- [41] T.E. Hardingham, R.A. Oldershaw, S.R. Tew, Cartilage, SOX9 and notch signals in chondrogenesis, *J Anat* 209(4) (2006) 469-480.
- [42] M.L. Gutierrez, J.M. Guevara, O.Y. Echeverri, D. Garzon-Alvarado, L.A. Barrera, Aggrecan catabolism during mesenchymal stromal cell in vitro chondrogenesis, *Anim Cells Syst* 17(4) (2013) 243-249.
- [43] E. Mitton, C.M. Gohr, M.T. McNally, A.K. Rosenthal, Articular cartilage vesicles contain RNA, *Biochem Biophys Res Commun* 388(3) (2009) 533-538.
- [44] B.A. Derfus, N.P. Camacho, U. Olmez, V.M. Kushnaryov, P.R. Westfall, L.M. Ryan, A.K. Rosenthal, Transforming growth factor beta-1 stimulates articular chondrocyte elaboration of matrix vesicles capable of greater calcium pyrophosphate precipitation, *Osteoarthritis Cartilage* 9(3) (2001) 189-94.
- [45] A.K. Rosenthal, C.M. Gohr, J. Ninomiya, B.T. Wakim, Proteomic Analysis of Articular Cartilage Vesicles From Normal and Osteoarthritic Cartilage, *Arthritis Rheum* 63(2) (2011) 401-411.
- [46] M. Zhang, R. Schekman, Cell biology. Unconventional secretion, unconventional solutions, *Science* 340(6132) (2013) 559-61.



[47] A.K. Rosenthal, C.M. Gohr, E. Mitton-Fitzgerald, R. Grewal, J. Ninomiya, C.B. Coyne, W.T. Jackson, Autophagy Modulates Articular Cartilage Vesicle Formation in Primary Articular Chondrocytes, *J Biol Chem* 290(21) (2015) 13028-13038.

#### IV-8. SUPPLEMENTARY MATERIAL



**Supplementary Figure IV-1 Biochemical performance (i.e. proliferation (DNA content) (a), total protein synthesis(b)), sulfated glycosaminoglycans (GAGs) content (c) and relative expression of chondrogenic (i.e. *Sox 9* (d), *COMP* (e), *Aggrecan* (f) and *Collagen type II* (g) and hypertrophic transcripts (i.e. *Collagen type Iα* (h), *Collagen type X* (i)) by hACs cultured on non-biofunctionalized nanofibrous substrates under expansion medium (EM) or differentiation medium (DM), and hBM-MSCs cultured on non-biofunctionalized nanofibrous substrates under basal medium (BM) or chondrogenic medium (CM). Data were analyzed by the Kruskal-Wallis test, followed by the Tukey's HSD test (\* $p < 0.01$ ; \*\* $p < 0.001$ ): a denotes significant differences compared to EM; b denotes significant differences compared to DM; c denotes significant differences compared to BM.**

## **Chapter V**

# **Chondrogenesis- inductive Nanofibrous Substrate using both Biological Fluids and Mesenchymal Stem Cells from an Endogenous Source**

## Chapter V

### **Chondrogenesis-inductive Nanofibrous Substrate using both Biological fluids and Mesenchymal Stem Cells from an Endogenous Source<sup>§</sup>**

#### **ABSTRACT**

During the last decade, many cartilage tissue engineering strategies have been developed, being the stem cell-based approach one of the most promising. Transforming Growth Factor- $\beta$ 3 (TGF- $\beta$ 3) and Insulin-like Growth Factor-I (IGF-I) are key proteins involved in the regulation of chondrogenic differentiation. Therefore, these two growth factors (GFs) were immobilized at the surface of a single electrospun nanofibrous mesh (NFM) aiming to differentiate human Bone Marrow-derived Mesenchymal Stem Cells (hBM-MSCs). The immobilization of defined antibodies (i.e. anti-TGF- $\beta$ 3 and anti-IGF-I) allows the selective retrieval of the abovementioned GFs from human platelet lysates (PL). Biochemical assays, involving hBM-MSCs cultured on biofunctional nanofibrous substrates under basal culture medium during 28 days, confirm the biological activity of bound TGF- $\beta$ 3 and IGF-I. Specifically, the typical spherical morphology of chondrocytes and the immunolocalization of collagen type II confirmed the formation of a cartilaginous ECM. Therefore, the proposed biofunctional nanofibrous substrate are able to promote chondrogenesis.

---

<sup>§</sup> This chapter is based on the following publication:

Casanova M. R., Alves da Silva M., Costa-Pinto A. R., Reis R. L., Martins A., Neves N. M., “Chondrogenesis-inductive nanofibrous substrate using both biological fluids and mesenchymal stem cells from an autologous source”, *Materials Science and Engineering: C*, vol. 98, issue 2019, pp. 1169-1178, doi: 10.1016/j.msec.2019.01.069.

## V-1. INTRODUCTION

Articular cartilage is a connective tissue with low repair potential due to its avascular nature and lack of progenitor cells.[1] Therefore, articular cartilage injuries present a challenging problem for the musculoskeletal physicians. Many treatment options have been developed during the last several decades to repair damaged cartilage, such as microfracture and mosaicplasty.[2] However, an adequate therapy for the long-term repair of cartilage lesions and which recover totally the function of this tissue is still to be developed. Tissue engineering and regenerative medicine (TERM) strategies hold the promise to recover injury in cartilage to its native state by combining cells, growth factors (GFs) and scaffolds with appropriate environmental stimulation.[3-5]

Despite the promising result reported by chondrocyte implantation techniques namely autologous chondrocyte implantation (ACI) and matrix-induced autologous chondrocyte implantation (MACI) in a large percentage of patients, they present many drawbacks such as the low yield of autologous chondrocytes during harvesting, loss of cellular differentiation potential when cultured *in vitro*, and decreased capacity to produce extracellular matrix (ECM).[2, 6] Mesenchymal stem cells (MSCs) present advantages over chondrocytes, since they can be obtained from an autologous source, in a less invasive procedure, and have a higher proliferation capacity and chondrogenic differentiation potential.[7, 8]

Bone marrow-derived MSCs (hBM-MSC) have been extensively studied in cartilage engineering and regeneration.[4, 9-14] Conventionally, these MSCs are induced to differentiate into a certain lineage by the supplementation of culture medium with defined exogenous bioactive factors. The culture medium for the *in vitro* chondrogenesis of hBM-MSCs was first described by Johnstone et al. in 1998.[15] The chondrogenic differentiation medium may contain different combinations of the following bioactive factors: dexamethasone, ascorbic acid, Transforming Growth Factor- $\beta$  (TGF- $\beta$ ), Bone Morphogenetic Proteins (BMP), Fibroblast Growth Factors (FGF) and Insulin-like Growth Factor-1 (IGF-I).[6, 7, 10, 16-24] Among these factors, TGF- $\beta$ 3 and IGF-I have been the most effective and commonly used GFs and are able to induce the chondrogenic differentiation of hBM-MSCs; however, IGF-I has been replaced by insulin-transferrin-selenious acid (ITS) or insulin.[10, 16, 17, 21, 25-27] Therefore, we hypothesize that the availability of TGF-  $\beta$ 3 and IGF-I on a biomaterial substrate would lead to the stable chondrogenic differentiation of hBM-MSCs.

Autologous regeneration of tissues, where both cells and bioactive factors are from the same patient, is an attractive approach because it minimizes the risk of an the immune response.[28-30] Much of the current research in cartilage tissue engineering is based on mesenchymal stem cells differentiated into the chondrogenic lineage by recombinant GFs in combination with biomaterials.[10, 18-21, 31] More recently, platelet lysate (PL), which contains a cocktail of different GFs (e.g. bFGF, VEGF, TGF-  $\beta$ , BMPs, PDGF- $\beta\beta$ , EGF, and IGF-I), has been used as an autologous complex mixture of bioactive factors for cells at an injury site.[30, 32]

Electrospun nanofibrous meshes are promising substrates to create biomimetic-engineered cartilage tissue.[33-35] Indeed, electrospinning is a versatile scaffold-synthesis method to produce highly porous structures mimics the morphology of the native extracellular matrix of many connective tissues.[36] The leading goal of this study is to develop a biofunctionalized electrospun nanofibrous mesh (NFM) with chondrogenic induction capacity through the immobilization of endogenous TGF-  $\beta$ 3 and IGF-I retrieved from platelet lysates. For that, we will take advantage of the specific and efficient interactions between specific antibody and its antigen. Based on this biological strategy, it will be possible to selectively bind the GFs of interest (TGF- $\beta$ 3 and IGF-I) from a pool of highly concentrated GFs present in PL. The chondrogenic potential of electrospun NFMs with immobilized TGF- $\beta$ 3 and IGF-I will be validated by culturing hBM-MSCs.

## **V-2. MATERIALS AND METHODS**

### **V-2.1. Production and Characterization**

#### **V-2.1.1. Electrospinning of nanofibrous substrate**

The production of polycaprolactone (PCL) NFMs were performed as described previously.[37] Briefly, a polymeric solution of 15% (w/v) PCL was prepared using an organic solvent mixture of chloroform/dimethylformamide (7:3 ratio). This solution was electrospun at 12.5 kV, using a needle-to-ground collector distance of 20 cm and a flow rate of 1 mL/h. After drying, the electrospun NFMs were cut in to 1 cm<sup>2</sup> squares for further assays. NFMs were

composed of nanofibers with diameters in the submicron range, from 0.4 to 1.4  $\mu\text{m}$  with an average pore size of  $72.67 \pm 31.48 \mu\text{m}$ . [38]

### **V-2.1.2. Functionalization of the nanofibrous substrate surface**

The surface activation and functionalization of the PCL NFMs were performed as described elsewhere.[39] The nanofiber surfaces were activated in an ultraviolet–ozone (UV–ozone) system (ProCleaner 220, Bioforce Nanoscience) by exposing both sides of the NFM during 4 minutes to UV-ozone irradiation. The activated NFMs were immersed in 1 M hexamethylenediamine (Sigma-Aldrich) solution and incubated 1 h at 37 °C, in order to graft amine groups (-NH<sub>2</sub>) on the mesh surfaces.

### **V-2.1.3. Antibody immobilization**

The antibody immobilization at the surface of activated and functionalized nanofibrous substrate was performed as described previously.[40] Briefly, a defined antibody (ie. mouse anti-TGF- $\beta$ 3 and/or goat anti-IGF-I) were immobilized at the surface of NFMs by a covalent bond mediated by a coupling agent, 1-ethyl-3-(3-(dimethylamino)-propyl)carbodiimide (EDC) / hydroxysuccinimide (NHS) mixture (1:4 ratio). An antibody solution of 1 % (v/v) was prepared using an EDC/NHS mixture dissolved in 0.1 M 2-(N-morpholino)-ethanesulfonic acid (MES) buffer containing 0.9% (w/w) sodium chloride (NaCl) at 4.7 pH. 200  $\mu\text{l}$  of antibody solution was mixed for 15 min at room temperature (RT), for the antibody activation, and incubated overnight at 4 °C on the activated and functionalized NFM.

#### **V-2.1.3.1 Single Antibody Immobilization**

The maximum immobilization capacity of a single antibody (Mouse anti-human TGF- $\beta$ 3 monoclonal antibody (Clone 44922), goat anti-human IGF-I polyclonal antibody [Biotechne/R&D Systems<sup>TM</sup>]) on the nanofibrous substrate was determined by using a wide range of concentrations (from 0 to 10  $\mu\text{g}/\text{mL}$ ). After primary antibody immobilization at the surface of the nanofibrous substrate, a blocking step was performed with a 3 % bovine serum albumin (BSA; Sigma-Aldrich) incubation step (1 h at RT), followed by a secondary antibody (1:200 in PBS) incubation (1 h at RT). Alexa Fluor 594<sup>®</sup> donkey anti-mouse IgG (H+L) and Alexa Fluor<sup>®</sup>

488 rabbit anti-goat IgG (H+L) (Life Technologies) were used as secondary antibodies. The unbound secondary antibody fluorescence was measured by a microplate reader (Synergy HT, Bio-TEK) as an indirect method to determine the primary antibody immobilization efficiency. The nanofibrous substrate without primary antibody was used as a negative control to evaluate nonspecific immobilization.

#### **V-2.1.3.2 Mixed Antibodies Immobilization**

The TGF- $\beta$ 3 and IGF-I antibodies were mixed in a PBS solution at a proportion of 1:10, taking into consideration that the TGF- $\beta$ 3 and IGF-1 ratio supplementation on the standard chondrogenic differentiation medium is 1:10. Mixed antibody immobilization was performed as previously described for single antibody immobilization. In order to determine the degree of immobilization, the fluorescence of unbound secondary antibodies was measured. Nanofibrous substrate with mixed antibodies immobilization was firstly incubated with Alexa Fluor<sup>®</sup> 594 (1 h at RT) followed by Alexa Fluor<sup>®</sup> 488 (1 h at RT). A washing step was performed between the secondary antibody incubation. The samples were further analyzed by laser scanning confocal (LSCM; Leica TCS SP8; Leica Microsystems CMS GmbH) microscopy to detect their distribution at the surface of the NFM.

#### **V-2.1.4. Platelet lysates**

Platelet concentrates were obtained from three O Pos female donors at the Immunohemotherapy Service of the Hospital de São João in Porto, under an established cooperation protocol in accordance with ethical and legal regulations. The number of platelets was counted and the sample volume was adjusted to  $10^6$  platelets/ $\mu$ L using the donor's own plasma. Platelet lysate (PL) was prepared as a pool of platelet concentrates according as previously reported.[40] The amount of each growth factor of interest (TGF- $\beta$ 3 and IGF-I) was quantified by *Enzyme-Linked Immunosorbent Assay* (ELISA). Assays (human TGF-beta3 and IGF-I DuoSet<sup>®</sup> development ELISA [R&D Systems, Inc.]) were performed according to the manufacturer's instructions.

### **V-2.1.5. Growth factor binding**

The growth factor binding capacity of the biofunctionalized nanofibrous substrate was performed as described elsewhere,[40] by using a mixture of TGF- $\beta$ 3 and IGF-I from recombinant-origin (TGF- $\beta$ 3 [PeproTech Inc.] and IGF-I [Bio-technne/R&D Systems<sup>TM</sup>]) or from the PL. The unbound protein solutions (from recombinant or PL-origin) were collected and stored at -20 °C until further quantification by ELISA. For the quantification of bound growth factors, a *fluorescence-linked immunosorbent assay* (FLISA) was performed as an indirect method. The biofunctionalized nanofibrous substrate with bound growth factors were incubated overnight at 4 °C with the corresponding primary antibodies, followed by PBS washing and BSA blocking steps. The corresponding secondary antibodies were incubated and the unbound secondary antibody fluorescence was measured as previous described.

### **V-2.2. Biological Assay**

#### **V-2.2.1. Expansion, Seeding, and Chondrogenic Differentiation of Human Bone Marrow Mesenchymal Stem Cells**

hBM-MSCs were obtained from a 95-year-old female donor undergoing knee arthroplasty at the Hospital Center of Alto Ave, Guimarães, in accordance with a protocol established between the 3B's Research Group, University of Minho, and the Hospital Center of Alto Ave, and approved by the ethics committee of this hospital (67/CA). hBM-MSCs were obtained from the patient with informed consent. hBM-MSCs were characterized and cultured using our standard protocols.[10] hBM-MSCs were expanded in basal medium consisting of  $\alpha$ -MEM (Life Technologies) supplemented with 10% heat-inactivated fetal bovine serum (FBS) and 1% antibiotic/antimycotic solution and cultured at 37 °C in a humidified atmosphere of 5% CO<sub>2</sub>. Cells were expanded in the basal medium until passage 4 and then were harvested and counted, and a cell suspension of 200 000 cells/50  $\mu$ L was seeded over each NFM. The conditions assessed were nanofibrous substrates biofunctionalized with antibodies against IGF-I and TGF- $\beta$ 3 in a mixed or single fashion. The corresponding growth factors were bound from recombinant or PL -origin. The hBM-MSCs seeded on the biofunctionalized nanofibrous substrate were cultured under basal medium without further supplementation. The experimental positive control was comprised of hBM-MSCs cultured on functionalized NFM without



antibody immobilization in a standard chondrogenic differentiation medium (basal medium supplemented with Insulin-Transferrin-Selenium-G Supplement (ITS; Invitrogen), 1 mM dexamethasone (Sigma-Aldrich), 0.1 M sodium pyruvate (Invitrogen), 17 mM ascorbic acid-2-phosphate (Wako Pure Chemical Industries, Ltd.), 35 mM L-proline (Sigma-Aldrich), 10 ng mL<sup>-1</sup> TGF-β3 and 100 ng mL<sup>-1</sup> IGF-I). The hBM-MSCs cultured under basal medium on functionalized NFM without antibodies immobilization were used as negative control. The nanofibrous substrates were retrieved at predefined culturing times, namely 7, 14, and 28 days. All experiments were performed in triplicates and repeated at least three times independently.

### V-2.2.2. Cellular Biochemistry Analyses

Cell proliferation was evaluated by DNA quantification (Quant-iTPicoGreen dsDNA assay, Invitrogen, Alfacene), metabolic activity by the MTS assay (CellTiter 96 AQueous One Solution, Promega) and cellular protein by Micro BCA assay (Micro BCA™ Protein Assay Kit, Thermo Fisher Scientific, USA), according to the manufacturer's instructions;

### V-2.2.3. Glycosaminoglycans Quantification

Dimethylmethylene blue (DMB) assay for glycosaminoglycans quantification was performed according to the method described by Kafienah and Sims (2004). [41] Briefly, samples were collected at each time point, washed twice with sterile PBS, transferred into sterile Eppendorf tubes and frozen at -80 °C. Digestion solution consisting on 0.05% of papain and 0.096% of N-acetyl cysteine was prepared using a digestion buffer (200 mM of phosphate buffer containing 1 mM ethylenediaminetetraacetic acid, pH 6.8). Samples were incubated with 1mL of this digestion solution, overnight at 60 °C, allowing the newly formed cartilaginous ECM to be separated from the scaffold. Then, the samples were centrifuged at 13000 rpm for 10 min and the supernatants were collected and quantified by the DMB assay. DMB stock solution was prepared by dissolving 16 mg of DMB powder in 900 mL of distilled water containing 3.04 g of glycine and 2.73 g of sodium chloride. The pH was adjusted to 3.0 with hydrochloric acid to a final volume of 1 L. The solution was stored at room temperature covered with aluminum foil. A stock solution of chondroitin sulfate was prepared in water at 5 mg/mL and kept at -20 °C. Dilutions of this solution were performed to obtain a standard curve. 20 μL water was added to a 96-well plate, as a blank, and the same was performed with all the samples

and with chondroitin sulphate diluted solutions. Afterwards, 250 µl of DMB solution was added to each well and the plates were incubated for 10 min at RT. The optical density was measured in a microplate reader (Synergy HT, Bio-TEK) at 530 nm.

#### V-2.2.4. Scanning Electron Microscopy (SEM)

The samples were collected at each defined time point and analyzed in a scanning electron microscope (Model S360, Leica Cambridge, U.K.) as previously reported.[10] Briefly, samples were collected at each defined time point, washed twice with sterile PBS, transferred into a sterile 24-well plate, immersed in 2.5% glutaraldehyde and kept at 4 °C until further use. The samples were washed in PBS, dehydrated in increasing alcohol concentrations and allowed to dry overnight, then sputter-coated with gold and observed in the SEM. A scanning electron microscope (Cambridge S360, Leica Cambridge, Cambridge, UK) was used to observe the distribution and morphology of the cells at x1 000 and x3 000 magnification.

#### V-2.2.5. RNA Isolation and Real-Time Quantitative Polymerase Chain

At each culturing time, the hBM-MSCs were washed with PBS, immersed in Tri reagent<sup>®</sup>, and stored at -80 °C for later RNA extraction. The extraction was performed as described elsewhere.[10] Briefly, proteins were removed with chloroform extraction, and the RNA pellets were washed once with 2-propanol and once with 70% ethanol. The total RNA pellets were resuspended in RNase-free water. The RNA concentration for each replica (triplicates of each condition per time point) was evaluated using micro-spectrophotometry (NanoDrop 1000, Thermo Scientific; USA).

RNA was reversed-transcribed into cDNA according to the protocol from qScript cDNA Synthesis Kit (Quanta BioSciences; VWR, USA). Afterwards, the obtained cDNA was used as a template for the amplification of the target genes shown in **Table V-1**, according to manufacturer's instructions of the PerfeCta<sup>™</sup> SYBR<sup>®</sup> Green system (Quanta Biosciences, VWR, USA). Forty-five cycles of denaturation (95 °C, 10 s), annealing (temperature-dependent on the gene; **Table V-1**; 30 s), and extension (72 °C, 30 s) were carried out in a Mastercycler<sup>®</sup> ep Gradient S realplex<sup>®</sup> thermocycler (Eppendorf; Hamburg, Germany) for all genes. The transcript expression data were normalized to the housekeeping gene *glyceraldehydes-3-phosphate-dehydrogenase (GAPDH)*, and the quantification was performed according to the

Livak method ( $2^{-\Delta\Delta CT}$  method), with the basal medium condition (negative control) serving as a calibrator.

**Table V-1 Primer sequences used for RT-PCR procedures <sup>a)</sup>.**

gene	forward (5' - 3')	reverse (5' -3')
<i>GAPDH</i>	AGCCTCAAGATCATCAGCAA	GTCATGAGTCCTTCCACGAT
<i>Sox9</i>	TTCATGAAGATGACCGACGC	GTCCAGTCGTAGCCCTTGAG
<i>AGC</i>	TGAGTCCTCAAGCCTCCTGT	TGGTCTGCAGCAGTTGATTC
<i>COL II</i>	CGGTGAGAAGGGAGAAGTTG	GACCGGTCACTCCAGTAGGA
<i>COL I<math>\alpha</math></i>	AAGAACCCCAAGGACAAGAG	GTAGGTGATGTTCTGGGAGG
<i>COL X</i>	CAGGCATAAAAGGCCCACTA	AGGACTTCCGTAGCCTGGTT

<sup>a)</sup> *GAPDH* = glyceraldehyde 3-phosphate dehydrogenase; *Sox9* = Sry-type high mobility group box 9; *AGC* = Agreccan; *COL II* = collagen type II; *COL I $\alpha$*  = collagen type I; *COL X* = collagen type X.

#### V-2.2.6. Histological Analysis

Samples were collected after 28 days of culture, washed twice with sterile PBS, transferred into a sterile 24-well plate, fixed in a 4% paraformaldehyde solution in PBS, and kept at 4 °C until further use for staining procedures. Prior to staining procedures, the fixed samples were washed twice with distilled water. Alcian blue staining was performed by incubating the samples in 1% acetic acid for 1 min, followed by their immersion in 1% Alcian blue solution in 3 % acetic acid for 1h. After that, the stain was poured off, and the samples were counter stained with hematoxylin for 1 min. Samples were washed with water, and mounted in an aqueous mounting medium. The optical microscope (Leica DM750, Leica Cambridge) was used to observe the staining of a cartilaginous ECM.

#### V-2.2.7. Immunolocalization of Type II Collagen

Immunolocalization of type II collagen was also performed in fixed samples. Endogenous peroxidase activity was quenched with 0.3% hydrogen peroxide solution for 30 min. Briefly, samples were incubated with mouse anti-human type II collagen monoclonal antibody (Millipore S.A.S.; France), overnight at 4 °C, in a humidified atmosphere. R.T.U. VECTASTAIN<sup>®</sup> Universal ABC Elite<sup>®</sup> Kit (Vector Laboratories; USA) was used for

secondary antibody according to the manufacturer instructions. Incubation was revealed by using the Peroxidase Substrate Kit (DAB) (Vector Laboratories; USA). Samples were washed in water for 5 min and then counterstained with hematoxylin for nuclei visualization. By the end, samples were washed in distillate water, mounted in an aqueous mounting medium and observed in an optical microscope (Leica DM750 microscope).

### V-2.3. Statistical analysis

Statistical analysis was performed using the SPSS statistical software (release 24.0.0.0 for Mac). First, a Shapiro-Wilk test was used to ascertain the data normality and Levene test for test the homogeneity of variances. For the data that followed a normal distribution, parametric tests were used, namely one-way ANOVA test followed by Tukey's HSD test. When the normality and variance homogeneity were rejected, non-parametric tests were used, namely a Kruskal-Wallis test followed by Tukey's HSD test. A  $p < 0.01$  was considered statistically significant in the analysis of the results.

## V-3. RESULTS

### V-3.1. Single Immobilization

The antibodies against TGF- $\beta$ 3 and IGF-I were immobilized at the surface of activated and functionalized NFM in a wide range of concentrations (0–10  $\mu\text{g mL}^{-1}$ ) to determine the maximum immobilization capacity for each antibody by using an indirect quantification method (**Figure V-1ab**). The maximum concentration of immobilized primary antibody was achieved at 4  $\mu\text{g mL}^{-1}$  for both TGF- $\beta$ 3 and IGF-I antibodies assessed, representing the saturation point of the nanofibrous substrate.

The spatial distribution of the TGF- $\beta$ 3 and IGF-I antibodies immobilized at the surface of the nanofibrous substrate at the 4  $\mu\text{g mL}^{-1}$  concentration and in a single way, is shown in **Figure V-1 d)** and **e)**, respectively. The immobilized antibodies uniformly cover the nanofibers surface, resembling the typical morphology of electrospun NFMs.

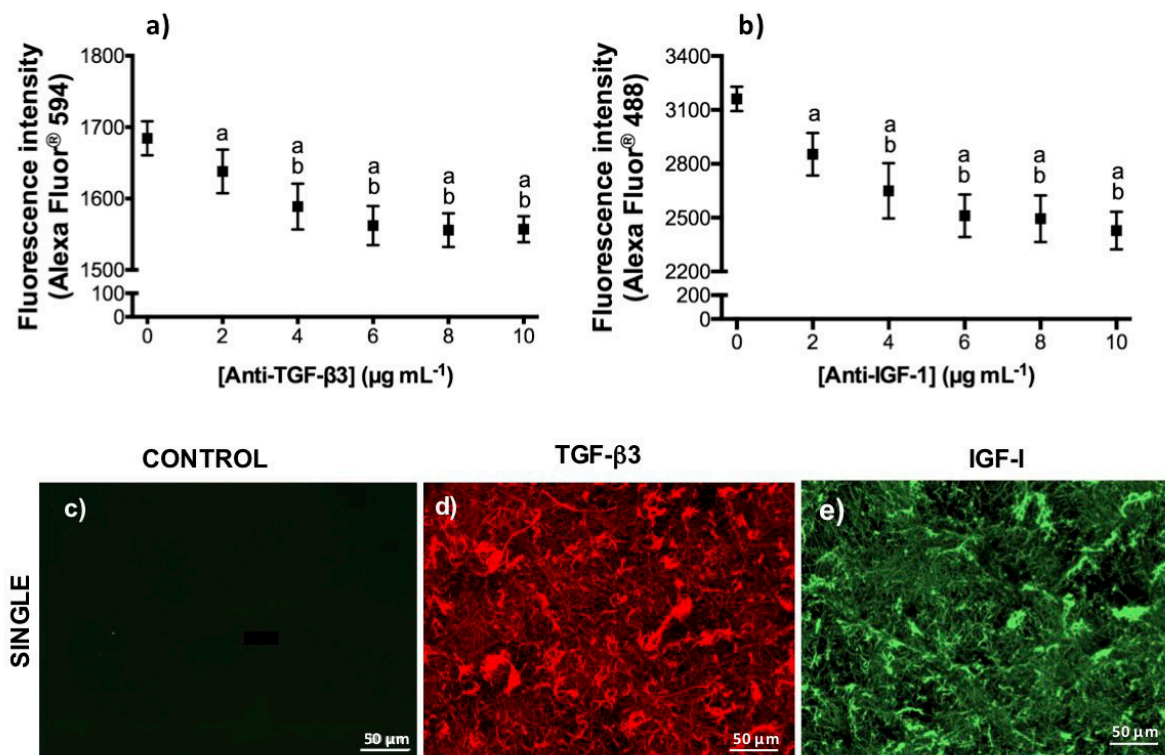


**Figure V-1 Top:** Maximum immobilization capacity of a single antibody at the surface of activated and functionalized NFM: immobilization of anti-TGF- $\beta$ 3 (a) and immobilization of anti-IGF-I (b). Data were analyzed by the one-way ANOVA test, followed by the Tukey's HSD test ( $p < 0.006$ ): a denotes significant differences compared to concentration  $0 \mu\text{g mL}^{-1}$ ; b denotes significant differences compared to concentration  $2 \mu\text{g mL}^{-1}$ . **Bottom:** Spatial distribution of anti-TGF- $\beta$ 3 (d) or anti-IGF-I (e) immobilized at the surface of activated and functionalized nanofibrous substrates at  $4 \mu\text{g mL}^{-1}$ . The negative control sample (c) was not incubated with the primary antibody.

The binding capacity of the biofunctionalized nanofibrous substrate, with an immobilized single primary antibody at  $4 \mu\text{g mL}^{-1}$ , was assessed by quantification of the total amount of recombinant protein that could be bound by the biofunctionalized nanofibrous substrate, by means the indirect of sandwich method (i.e. FLISA) and by the quantification of unbound protein with commercially available ELISAs. For FLISA (**Figure V-2**), an increase of the total amount of recombinant protein leads to a decrease in the fluorescence signal of the secondary antibody, indicating that less secondary antibody is unbound. On the other hand, in ELISAs, an increase on the amount of bound recombinant protein occurs due to an increase in the total amount of recombinant protein used. The recombinant human GF binding capacity of the biofunctionalized nanofibrous substrate reaches its maximum at a concentration from which no statistically significant differences were observed. **Figure V-2** shows that the recombinant human GF binding capacity of the biofunctionalized nanofibrous substrates reached a

maximum at  $4 \mu\text{g mL}^{-1}$  both for rTGF- $\beta$ 3 and for rIGF-I. At this concentration, the binding efficiency of the biofunctionalized nanofibrous surface is  $37 \pm 11 \%$  for rTGF- $\beta$ 3 and  $42 \pm 21 \%$  for rIGF-I.

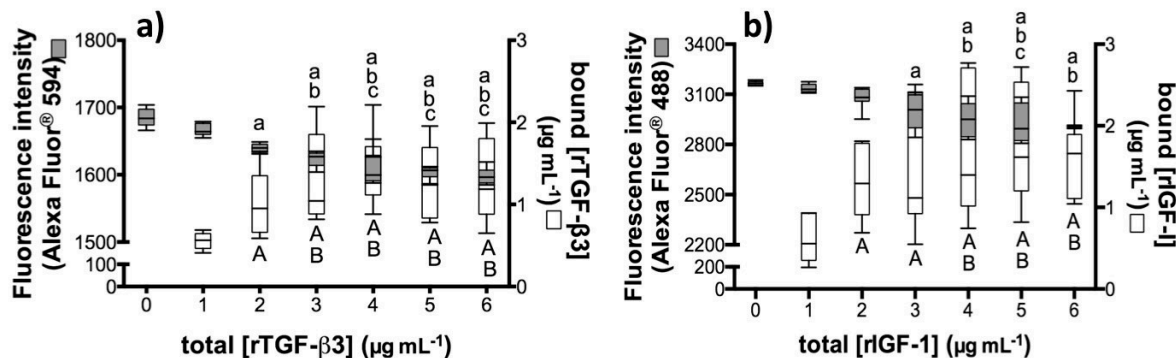


**Figure V-2** Capability of the biofunctionalized nanofibrous substrate to bind different concentrations of recombinant proteins from TGF- $\beta$  3 (a) and IGF-I (b). Data were analyzed by the Kruskal-Wallis test, followed by the Tukey's HSD test ( $p < 0.01$ ): in the FLISA, a denotes significant differences compared to concentration  $0 \mu\text{g mL}^{-1}$ ; b denotes significant differences compared to concentration  $1 \mu\text{g mL}^{-1}$ ; c denotes significant differences compared to concentration  $2 \mu\text{g mL}^{-1}$ ; in the ELISA, A denotes significant differences compared to concentration  $0 \mu\text{g mL}^{-1}$ ; B denotes significant differences compared to concentration  $1 \mu\text{g mL}^{-1}$ .

### V-3.2. Mixed Immobilization

Mixed immobilization of these two different but complementary chondrogenic GF at the surface of the same nanofibrous substrate was performed. To successfully implement this strategy, the single antibody concentration previously optimized (i.e.  $4 \mu\text{g mL}^{-1}$ ) was considered, and the antibodies were mixed at a 1:10 proportion and incubated over the same nanofibrous substrate. Single and mixed immobilization strategies were applied in order to assess the competition for the  $\text{NH}_2$  groups available at the surface of an activated and functionalized NFM (Figure V-3ab). No statistically significant differences were observed between the single and mixed immobilization strategies, which have similar immobilization efficiencies. The results show that no competition occurred between these two antibodies (anti-TGF- $\beta$ 3 and anti-IGF-I) for the same amount of  $\text{NH}_2$  groups available at nanofibrous substrate once no statistically significant differences were observed.

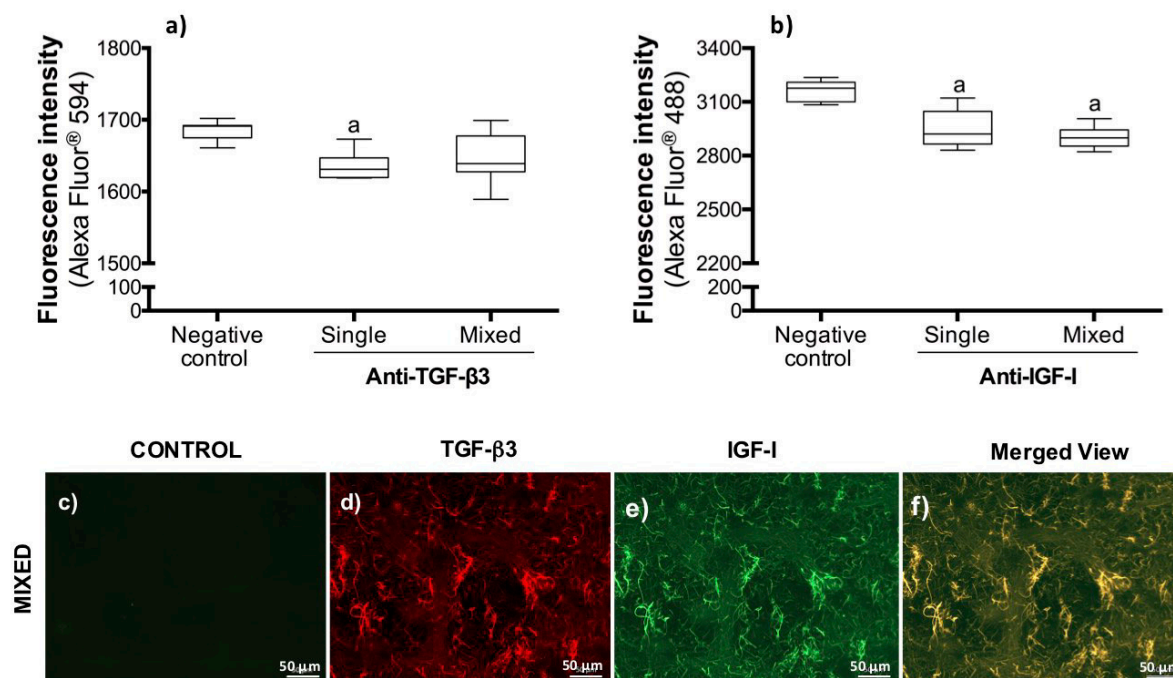


**Figure V-3 Top:** Single or mixed immobilization capacity of anti-TGF-β3 (a) and anti-IGF-I (b) at the surface of activated and functionalized electrospun nanofibers. Data were analyzed by the Kruskal-Wallis test, followed by the Tukey's HSD test ( $p < 0.01$ ): a denotes significant differences compared to negative control. **Bottom:** Spatial distribution of the simultaneously immobilization of TGF-β3 and IGF-I antibodies over the same substrate, in a mixed fashion, at the 1:10 proportion: anti-TGF-β3 (d); anti-IGF-I (e); and merged view (f). Activated and functionalized nanofibrous substrates without primary antibodies immobilization (c).

A uniform spatial distribution of both antibodies immobilized over the same nanofibrous substrate in a mixed fashion (Figure V-3 d) and e)) was confirmed. The yellow color of the merged image (Figure V-3 f) demonstrates the colocalization of both antibodies in a mixed fashion over the same nanofibrous substrate.

Following the immobilization of the antibodies (i.e. anti-TGF-β3 and anti-IGF-I) in a mixed fashion on the nanofibrous substrate, the corresponding recombinant protein solutions (single or mixed) were incubated at concentration previously optimized ( $4 \mu\text{g mL}^{-1}$ ) for single substrates. The results were analyzed by FLISA (Figure V-4 a) and b) and were further confirmed with commercially available ELISAs (Figure V-4 c). No competition between the TGF-β3 and IGF-I recombinant human proteins was observed since the bioactivity of the immobilized mixed antibodies, using single or mixed recombinant GFs solution, was similar. When single recombinant protein solutions were used, the binding capacity of the biofunctional nanofibrous substrate was  $2.0 \pm 0.2 \mu\text{g mL}^{-1}$  for rTGF-β3 and  $2.5 \pm 0.6 \mu\text{g mL}^{-1}$  for rIGF-I. A binding capacity of  $1.9 \pm 0.4 \mu\text{g mL}^{-1}$  for rTGF-β3 and  $2.6 \pm 0.6 \mu\text{g mL}^{-1}$  for rIGF-I was

achieved when a mixed recombinant protein solution was used. This result showed the specificity of the antibody-antigen bond.

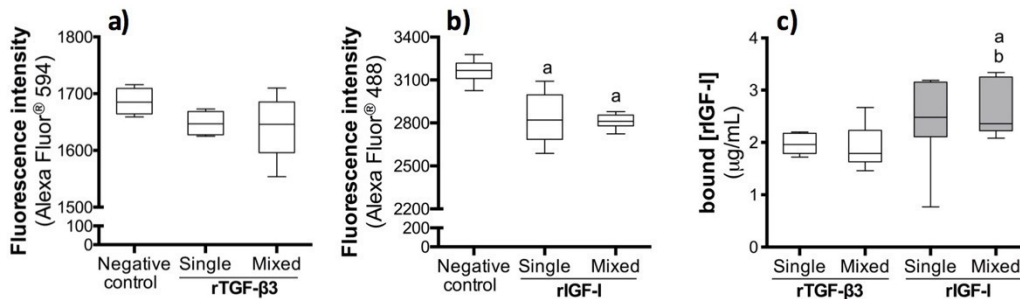


**Figure V-4** Single or mixed immobilization capacity of recombinant TGF- $\beta$ 3 (a) and IGF-I (b) at the surface of activated and functionalized electrospun nanofibers, assessed by the FLISA or the ELISA (c). Data were analyzed by the Kruskal-Wallis test, followed by the Tukey's HSD test ( $p < 0.01$ ): a denotes significant differences compared to negative control.

The amount of each endogenous GF derived from PL of three independent donors was quantified by ELISA, as well as its binding capacity of the biofunctionalized nanofibrous substrates (Table V-2). A wide range of concentrations was obtained from the different donors.

**Table V-2** Quantification of TGF- $\beta$ 3 and IGF-I present in 3 independent human PL samples and in a PL pool. The GFs binding capacity of the biofunctionalized nanofibrous substrate.

		Donor 1	Donor 2	Donor 3	Pool
TGF- $\beta$ 3	[PL] ( $\mu$ g/mL)	179 $\pm$ 39	677 $\pm$ 44 <sup>a</sup>	97 $\pm$ 78 <sup>b</sup>	269 $\pm$ 27
	Bound ( $\mu$ g/mL)	169 $\pm$ 2	669 $\pm$ 1 <sup>a</sup>	92 $\pm$ 1 <sup>b</sup>	267 $\pm$ 1
IGF-I	[PL] (ng/mL)	1.7 $\pm$ 0.1	11.3 $\pm$ 4.3	4.6 $\pm$ 2.1	6.9 $\pm$ 1.1
	Bound (ng/mL)	0.86 $\pm$ 0.32	8.8 $\pm$ 0.3	3.0 $\pm$ 0.3	4.7 $\pm$ 0.3

Data were analyzed by the one-way ANOVA test, followed by the Tukey's HSD test ( $p < 0.01$ ): <sup>a</sup> denotes significant differences compared to donor 1, <sup>b</sup> denotes significant differences compared to donor 2.

However, the binding efficiency of GFs derived from PL samples is similar across the different PL samples, showing the consistency of the immobilization strategy in capturing the GFs. A PL-pool of the three donors, containing 269  $\pm$  27  $\mu$ g mL<sup>-1</sup> of TGF- $\beta$ 3 and 6.9  $\pm$  1.1 ng mL<sup>-1</sup> of IGF-I, and achieving a binding capacity of 267  $\pm$  1  $\mu$ g mL<sup>-1</sup> for TGF- $\beta$ 3 and 4.7  $\pm$  0.3 ng mL<sup>-1</sup> for IGF-I, was used as endogenous source of GF in the subsequent biological assays.



### V-3.3. Biological Activity

The biological activity of biofunctionalized NFM, in single or mixed fashion, was assessed by seeding and culturing hBM-MSCs for 28 days. The hBM-MSCs were cultured on eight different nanofibrous substrate conditions: (i) activated NFM without GFs (Basal medium), (ii) activated NFM without GFs (Chondro medium) (iii) NFM with immobilized TGF- $\beta$ 3 from recombinant-origin (TGF- $\beta$ 3\_rGF), (iv) NFM with immobilized TGF- $\beta$ 3 from PL (TGF- $\beta$ 3\_PL), (v) NFM with immobilized IGF-I from recombinant-origin (IGF-I\_rGF), (vi) NFM with immobilized IGF-I from PL (IGF-I\_PL), (vii) NFM with immobilized TGF- $\beta$ 3 and IGF-I from recombinant-origin (TGF- $\beta$ 3 & IGF-I\_rGF), (viii) NFM with immobilized TGF- $\beta$ 3 and IGF-I from PL (TGF- $\beta$ 3 & IGF-I\_PL). In condition *i*, the hBM-MSCs were cultured in basal medium without chondrogenic factors as a negative control. In condition *ii*, the hBM-MSCs were cultured in standard chondrogenic differentiation medium, with the goal of achieving the differentiation of hBM-MSCs into the chondrogenic lineage. In conditions *iii–viii*, the hBM-MSCs were cultured in basal culture medium in order to evaluate the action of the immobilized GFs from recombinant or PL-origin.

Biological data (**Figure V-5**) confirms the bioactivity of bound TGF- $\beta$ 3 and IGF-I, since the biofunctional nanofibrous substrates did not induce significant changes in hBM-MSCs' viability and proliferation (**Figure V-5ab**) during the different culture times (7, 14 and 28 days) when compared to the controls (condition *i-ii*). Although no statistically significant differences were observed for the nanofibrous substrates functionalized with TGF- $\beta$ 3 and IGF-I, in a single or mixed fashion, they seem to have higher viability and proliferation than the positive control condition (chondro medium). Likewise, the substrates where the GFs were bound from PL performed slightly better, although not statistically different. Concerning the hBM-MSCs' total protein synthesis (**Figure V-5c**), no statistically significant differences were observed between the biofunctional nanofibrous substrates and the controls. On the 28th day, the controls displayed a lower protein concentration than the nanofibrous substrates biofunctionalized with single or mixed TGF- $\beta$ 3 and IGF-I bound from PL.

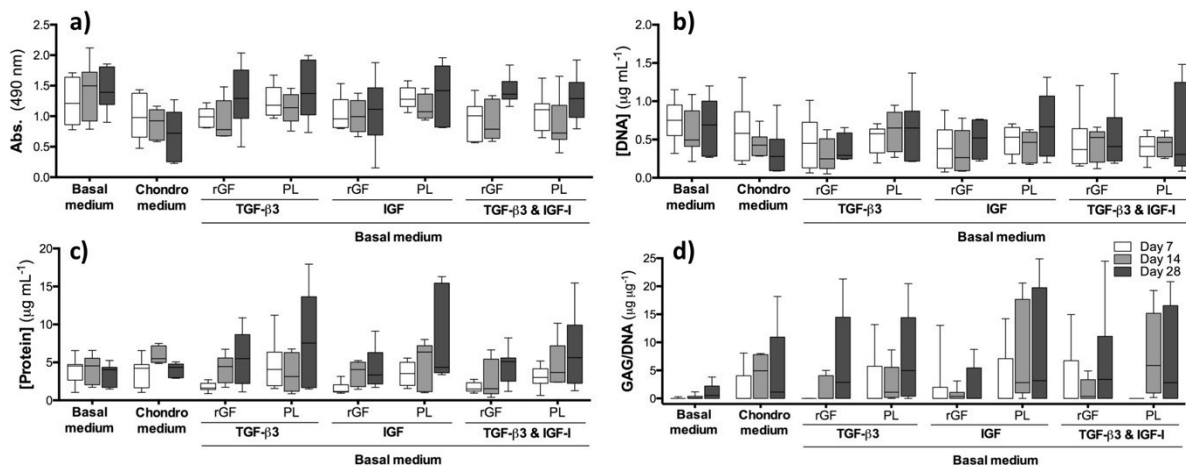


**Figure V-5 Biochemical performance (i.e. metabolic activity (a) and proliferation (b), total protein (c) and GAG/DNA ratio (d) synthesis) of the hBM-MSCs cultured on biofunctionalized biomaterial system. Data were analyzed by the Kruskal-Wallis test, followed by the Tukey's HSD test ( $p < 0.01$ ). No significant differences were observed between culturing conditions.**

Glycosaminoglycan (GAG) production (**Figure V-5d**) was detected in all testing conditions except in the negative condition. In the biofunctionalized nanofibrous substrates there was a tendency to obtain increased accumulation of GAG across time. Although no significant differences were observed between the conditions, the single immobilized TGF-β3 and IGF-I (PL-derived) tendentially display higher GAG concentration after 28 days when compared to the other conditions.

Further analysis of gene expression revealed that in all condition hBM-MSCs expressed cartilage-related genes, indicating that chondrogenic differentiation was induced (**Figure V-6**). A similar expression pattern of *Aggrecan* and *Sox9* was observed in all conditions, and the expression of these genes was maintained throughout the experiment. Furthermore, *Collagen II* expression in biofunctional nanofibrous substrates was significantly higher than in the positive condition (chondro medium) for the 14<sup>th</sup> day of culture. Interestingly, the *Collagen Iα* was expressed at low levels in biofunctional nanofibrous substrates conditions and showed a decreasing trend of expression towards longer culturing times. Furthermore, *Collagen X* expression in the positive condition (chondro medium) was significantly higher than in biofunctional nanofibrous substrates for the last times points of culture. This result confirmed that the hBM-MSCs cultured on the biofunctional nanofibrous substrates were not differentiating into the osteogenic lineage.

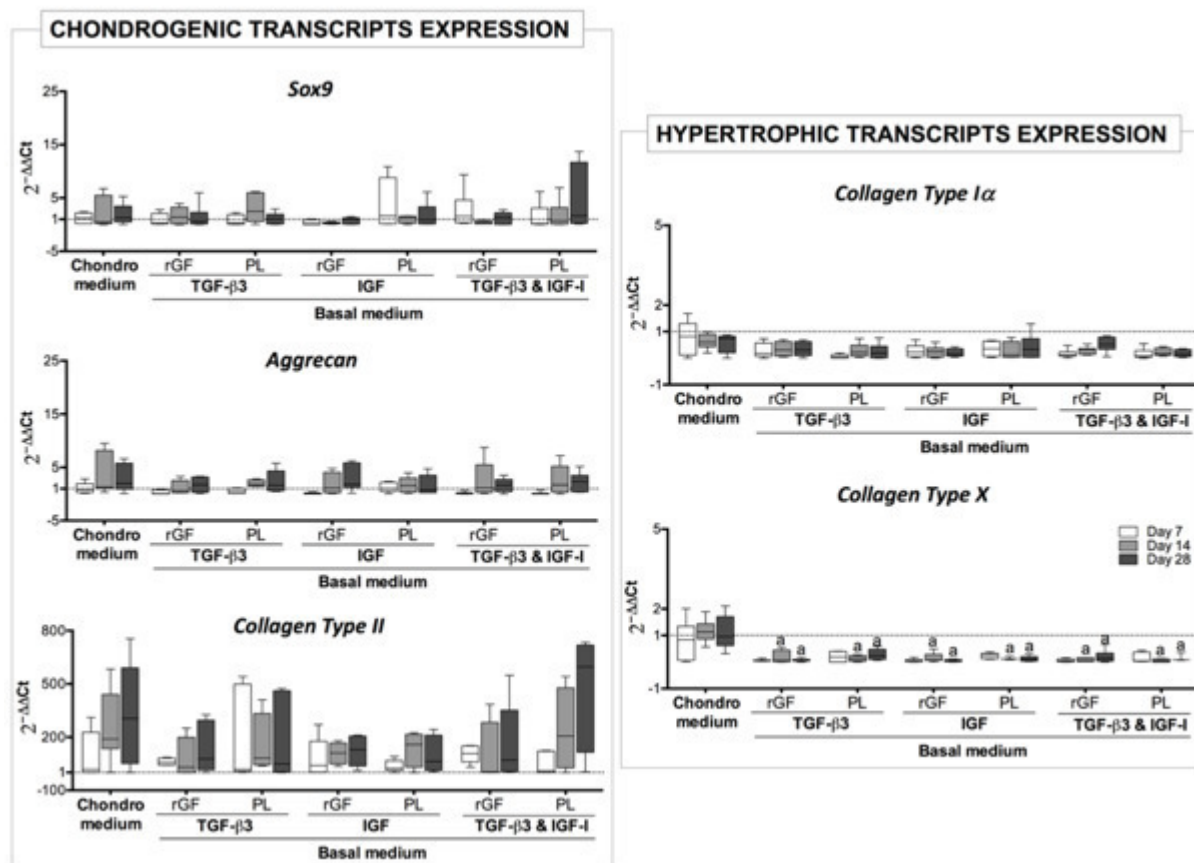


Figure V-6 Relative expression of chondrogenic and hypertrophic markers by hBM-MSCs cultured on biofunctionalized biomaterial system. The expression was normalized against the *GAPDH* gene and the quantification was performed according to the Livak method. Data were analyzed by the Kruskal-Wallis test, followed by the Tukey's HSD test ( $p < 0.01$ ): a denotes significant differences compared to the positive condition (Chondro medium).

SEM analysis of the hBM-MSCs cultured for 28 days on the seven different conditions, shows that the cells began to acquire a round-shaped morphology; this was more evident in the biofunctionalized nanofibrous substrates (Figure V-7).

For the detection of ECM sulfated proteoglycans (Figure V-7), all culture conditions at 28 days were stained with alcian blue. In the conditions *ii-viii*, the cells positively stain to Alcian blue, demonstrating the presence of cartilaginous ECM components. Immunolocalization of collagen type II confirms the deposition of a cartilaginous ECM on the conditions *ii-viii* as observed by the small spots of collagen type II spread across the scaffolds (Figure V-7). These observations were consistent with the previously obtained results for GAG production, as well as by the expression of cartilage-related genes.

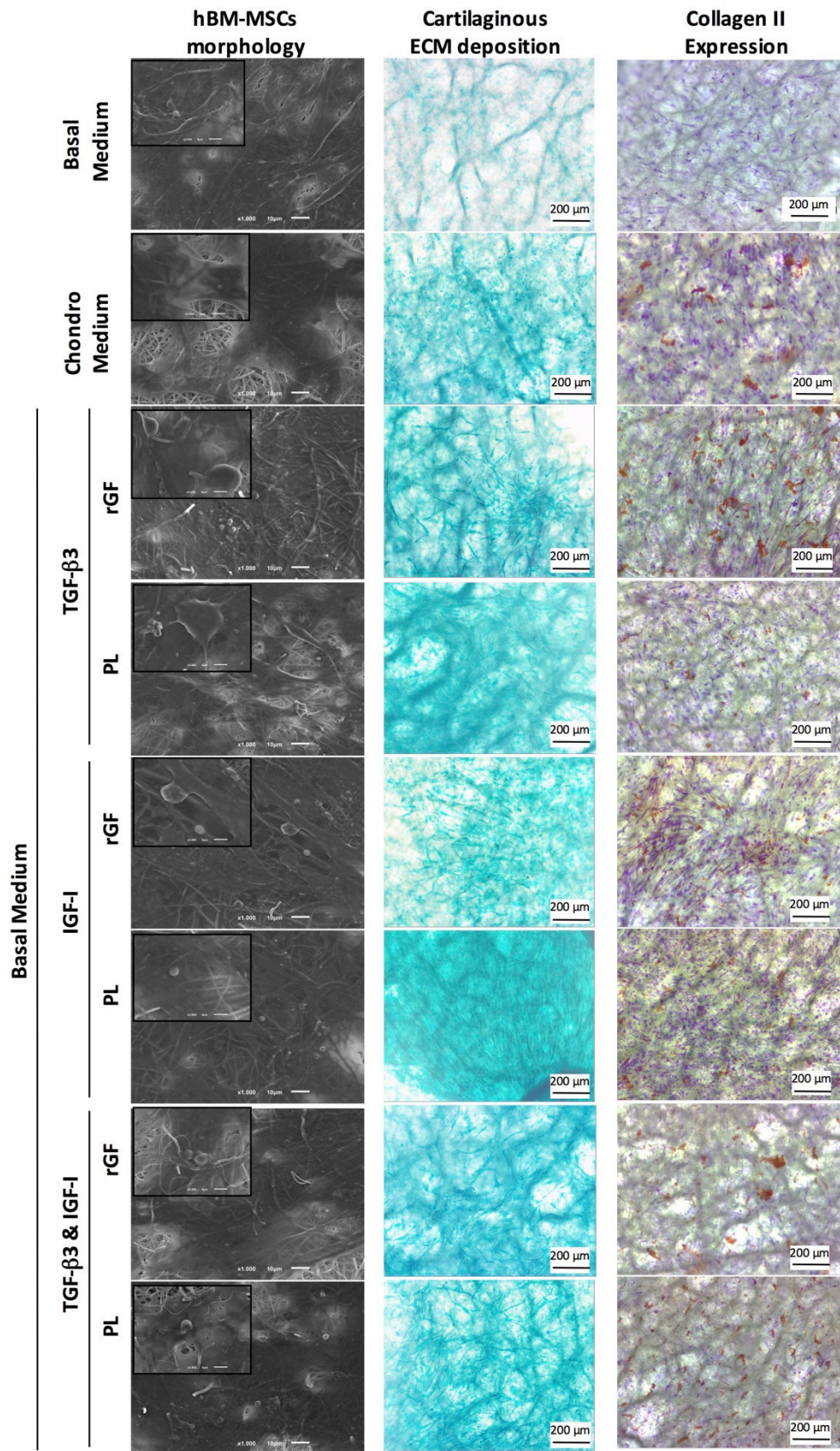


Figure V-7 Morphological analysis of the hBM-MSCs cultured for 28 days by scanning electron microscopy (SEM); staining of sulfated glycosaminoglycans by Alcian blue; immunolocalization of collagen type II (brown staining).

#### V-4. DISCUSSION

Growth factors are stimulatory molecules which help in the regulation of cartilage development and maintenance of the chondrocyte phenotype of the stem cells.[6, 22, 25] The TGF- $\beta$ 3 and IGF-I have significant and complementary activities to induce, accelerate, and/or enhance cartilage tissue formation, and they are commonly used to supplement the chondrogenic-inducing culture medium at concentrations of 10 ng mL<sup>-1</sup> and 100 ng mL<sup>-1</sup>, respectively.[18-21, 26, 27, 42-45] This proportion (1:10) was taken into consideration in our biofunctionalized nanofibrous substrate when both antibodies were immobilized in a mixed fashion. The maximum amount of recombinant growth factors bound at the biofunctionalized nanofibrous substrate was approximately 2  $\mu$ g mL<sup>-1</sup> of TGF- $\beta$ 3 and 2.5  $\mu$ g mL<sup>-1</sup> of IGF-I (**Figure V-4**). Accordingly, our biofunctional nanofibrous substrate enables the immobilization of high concentrations of growth factors (on the  $\mu$ g mL<sup>-1</sup> order), whereas others similar approaches report values that are on the ng mL<sup>-1</sup> order,[46-48] reflecting the positive effect of the high specific surface area of electrospun nanofibers to maximize the potential to immobilize GFs.

The use of platelet-rich plasma (PRP) to stimulate tissue regeneration is growing at the research and clinical levels, especially in orthopedics surgery.[30, 40, 49-53] Different bioactive factors are released from activation, [54] including TGF- $\beta$ 3 and IGF-I. The amount of these two growth factors, in the three-independent human PL' samples, varies between 97 - 269  $\mu$ g mL<sup>-1</sup> of TGF- $\beta$ 3 and 1.66 - 11.31 ng mL<sup>-1</sup> of IGF-I. The differences among the quantified GFs and their variability are related to intrinsic differences between the platelets obtained from the different donors. Comparing this data to values reported in the literature, i.e. TGF- $\beta$ 3 (no data reporting), TGF- $\beta$ 1 (79.7 ng mL<sup>-1</sup>) and IGF-I (69.5 ng mL<sup>-1</sup>), [55] we obtained lower amounts of these factors. The amount of bound endogenous GFs varies according to their concentration in the PL samples. For PL-derived TGF- $\beta$ 3, the binding efficiency (between 95–99%) was high as in the case of the recombinant protein, which is expected, since the concentration present in PL is very low (on the  $\mu$ g mL<sup>-1</sup> order). For IGF-I, only around 52–78% of PL-derived GF was bound to the biofunctionalized nanofibrous substrate. Furthermore, the binding efficiency of the GFs are in the same range for the three independent donors, showing the reproducibility of this approach (**Table V-2**). Despite the differences in the concentration of GFs present in the PL (ranging from  $\mu$ g mL<sup>-1</sup> for TGF- $\beta$ 3 to ng mL<sup>-1</sup> for IGF-I), these concentrations are much lower than the maximum binding capacity of the biofunctionalized

nanofibrous substrate, where recombinant proteins were used at micrograms per milliliter concentration. Herein, a chondrogenesis-inductive nanofibrous substrate was developed by the immobilization of defined antibodies at the surface of electrospun nanofiber, enabling the binding of TGF- $\beta$ 3 ( $267 \pm 1 \mu\text{g mL}^{-1}$ ) and/or IGF-I ( $4.7 \pm 1.1 \text{ ng mL}^{-1}$ ) from a PL' pool or from a recombinant-origin.

TGF- $\beta$ 3 is the essential growth factor for promoting chondrogenesis both *in vivo* and *in vitro*. [15, 17, 22, 42, 56, 57] Attisano and Wrana [58] reported that TGF- $\beta$  signal was transmitted into the nucleus via the smad pathway, which is involved in the activation of *Sox 9*, a transcription factor that induces the expression of other cartilage-specific genes, including *Collagen type II* and *Aggrecan*. [59] We also found that bound TGF- $\beta$ 3 induced *Sox 9* expression by culturing hBM-MSCs, with concomitant expression of cartilaginous extracellular matrix genes, namely *Collagen type II* and *Aggrecan*. Meanwhile, IGF-I is involved in cartilage repair and is considered an essential mediator of cartilage homeostasis and metabolism, primarily due to its capacity to promote chondrocyte survival and proliferation, induce chondrogenic differentiation and stimulate proteoglycan synthesis. [60-63] Messai *et al.* [64] reported that IGF-I is involved in chondrogenic differentiation by regulating the synthesis of *Aggrecan* and *Collagen type II* at the transcription level in rat articular chondrocytes. Our real-time PCR data also showed that hBM-MSCs cultured on biofunctionalized nanofibrous substrate with bound IGF-I expressed cartilaginous genes, namely *Sox 9*, *Aggrecan* and *Collagen type II*.

Many *in vitro* studies have used TGF- $\beta$  and IGF-I in combination, showing enhanced chondrogenesis. [19, 43-45, 63] Indrawattana *et al.* [18] reported that MSCs cultured in the presence of TGF- $\beta$ 3 and IGF-I, combined and in cycling patterns, showed enhanced expression of *Sox 9* and cartilage extracellular matrix genes. Similarly, Matsuda *et al.* [31] reported that the combination of TGF- $\beta$ 3, dexamethasone and IGF-I was the most effective cocktail to stimulate chondrogenic differentiation of MSCs. Conversely, our results showed that hBM-MSCs cultured in the presence of TGF- $\beta$ 3 and IGF-I did not have a higher expression of cartilaginous markers, showing a chondrogenic gene expression profile similar to hBM-MSCs cultured on biofunctionalized nanofibrous substrates with individually bound TGF- $\beta$ 3 or IGF-I. We also found that both endogenous and recombinant growth factors bound at the surface of biofunctionalized nanofibrous substrates were able to regulate the hBM-MSCs' chondrogenesis. Our results showed that the bound IGF-I, similarly to the bound TGF- $\beta$ 3, induced chondrogenic differentiation of hBM-MSCs, stimulating proliferation, protein

synthesis, GAG production, and expression of chondrogenic markers. Furthermore, we showed that the combined action of the two GFs induced the chondrogenic differentiation of BM-MSCs, presenting a chondrogenic gene expression profile similar to BM-MSCs cultured in standard chondrogenic differentiation medium. Interestingly, the results show a trend to have stronger chondrogenic induction by the endogenous PL-derived GFs as compared to the recombinant-GFs. Based on these results, the competitive advantage of this approach relies on sustained and local exposure of endogenous GFs at high concentrations from a man-made extracellular matrix equivalent, capable to induce the chondrogenic differentiation of MSCs, without the need of continuous supply of exogenous recombinant GFs.

Envisioning the clinical translation of the chondrogenesis-inductive nanofibrous substrate herein reported, we foreseen its potential use as an autologous cartilage regeneration strategy or as a substrate in MACI or microfracture approaches. In the MACI approach, MSCs can be cultured on a biofunctional nanofibrous substrate, where both cells and bioactive factors are from the same patient, and then implanted into the defect site. In the microfracture approach, the biofunctional nanofibrous substrate can be implanted into the defect site, where hBM-MSCs migrating from the microperforations are induced to properly differentiate into the chondrogenic lineage by the bound GFs. Both approaches could lead to the regeneration of cartilage, envisioning a personalized therapy for cartilage repair.

## V-5. CONCLUSIONS

This study shows the successful development of a unique chondrogenesis-inductive nanofibrous substrate, which is able to spatially present endogenous GFs immobilized at the surface of a biomaterial scaffold. Cell culture assays with hBM-MSCs demonstrate that the developed biofunctional nanofibrous substrates are able to promote chondrogenesis as effectively as the standard differentiation condition, without the need of continuous supply of exogenous recombinant GFs. The present manuscript describes a new autologous regeneration strategy in which both cells and the bioactive agents, namely TGF- $\beta$ 3 and/or IGF-I, can be obtained from the same patient, providing a personalized therapy for cartilage regeneration.

## V-6. ACKNOWLEDGMENTS

The authors would like to acknowledge the Portuguese Foundation for Science and Technology (FCT) for the PhD grant of MC (PD/BD/113797/2015) financed by the FCT Doctoral Program on Advanced Therapies for Health (PATH) (FSE/POCH/PD/169/2013), the Post-doc fellowships of MAS and ARP (SFRH/BPD/73322/2010 and SFRH/BPD/90332/2012), the IF grant of AM (IF/00376/2014), and the projects SPARTAN (PTDC/CTM-BIO/4388/2014) and FRONthera (NORTE-01-0145-FEDER-0000232).

## V-7. REFERENCES

- [1] C.A. Taylor, D. Braza, J.B. Rice, T. Dillingham, The incidence of peripheral nerve injury in extremity trauma, *Am J Phys Med Rehabil* 87(5) (2008) 381-5.
- [2] W. Wang, J. Gao, L. Na, H. Jiang, J. Xue, Z. Yang, P. Wang, Craniocerebral injury promotes the repair of peripheral nerve injury, *Neural Regen Res* 9(18) (2014) 1703-8.
- [3] M.P. Coleman, M.R. Freeman, Wallerian degeneration, wld(s), and nmnat, *Annu Rev Neurosci* 33 (2010) 245-67.
- [4] B. Chang, Q. Quan, S. Lu, Y. Wang, J. Peng, Molecular mechanisms in the initiation phase of Wallerian degeneration, *Eur J Neurosci* 44(4) (2016) 2040-8.
- [5] R. Deumens, A. Bozkurt, M.F. Meek, M.A. Marcus, E.A. Joosten, J. Weis, G.A. Brook, Repairing injured peripheral nerves: Bridging the gap, *Prog Neurobiol* 92(3) (2010) 245-76.
- [6] J.W. Griffin, M.V. Hogan, A.B. Chhabra, D.N. Deal, Peripheral nerve repair and reconstruction, *J Bone Joint Surg Am* 95(23) (2013) 2144-51.
- [7] L.F. Bulstra, N. Rbia, M.F. Kircher, R.J. Spinner, A.T. Bishop, A.Y. Shin, Spinal accessory nerve to triceps muscle transfer using long autologous nerve grafts for recovery of elbow extension in traumatic brachial plexus injuries, *J Neurosurg* 129(4) (2018) 1041-1047.
- [8] S. Geuna, I. Papalia, G. Ronchi, F.S. d'Alcontres, K. Natsis, N.A. Papadopoulos, M.R. Colonna, The reasons for end-to-side coaptation: how does lateral axon sprouting work?, *Neural Regen Res* 12(4) (2017) 529-533.
- [9] H. Millesi, Bridging defects: autologous nerve grafts, *Acta Neurochir Suppl* 100 (2007) 37-8.
- [10] M.D. Sarker, S. Naghieh, A.D. McInnes, D.J. Schreyer, X. Chen, Regeneration of peripheral nerves by nerve guidance conduits: Influence of design, biopolymers, cells, growth factors, and physical stimuli, *Prog Neurobiol* 171 (2018) 125-150.



- [11] S.J. Forbes, N. Rosenthal, Preparing the ground for tissue regeneration: from mechanism to therapy, *Nat Med* 20(8) (2014) 857-869.
- [12] L.M. Marquardt, S.E. Sakiyama-Elbert, Engineering peripheral nerve repair, *Curr Opin Biotechnol* 24(5) (2013) 887-92.
- [13] F. May, A. Buchner, K. Matiasek, B. Schlenker, C. Stief, N. Weidner, Recovery of erectile function comparing autologous nerve grafts, unseeded conduits, Schwann-cell-seeded guidance tubes and GDNF-overexpressing Schwann cell grafts, *Dis Model Mech* 9(12) (2016) 1507-1511.
- [14] D. Grinsell, C.P. Keating, Peripheral Nerve Reconstruction after Injury: A Review of Clinical and Experimental Therapies, *Biomed Research International* (2014).
- [15] M.L. Wang, M. Rivlin, J.G. Graham, P.K. Beredjiklian, Peripheral nerve injury, scarring, and recovery, *Connect Tissue Res* 60(1) (2019) 3-9.
- [16] M. Moattari, H.M. Kouchesfehiani, G. Kaka, S.H. Sadraie, M. Naghdi, Evaluation of nerve growth factor (NGF) treated mesenchymal stem cells for recovery in neurotmesis model of peripheral nerve injury, *J Cranio Maxill Surg* 46(6) (2018) 898-904.
- [17] G.C. Li, Q.Z. Xiao, L.Z. Zhang, Y.H. Zhao, Y.M. Yang, Nerve growth factor loaded heparin/chitosan scaffolds for accelerating peripheral nerve regeneration, *Carbohydr Polym* 171 (2017) 39-49.
- [18] W. Zeng, M.Y. Rong, X.Y. Hu, W. Xiao, F.Y. Qi, J.H. Huang, Z.J. Luo, Incorporation of Chitosan Microspheres into Collagen-Chitosan Scaffolds for the Controlled Release of Nerve Growth Factor, *Plos One* 9(7) (2014).
- [19] C. Carvalho, J. Pedro, K.W. Ng, N. Neves, R. Reis, M. Oliveira, Keratin/chitosan as novel grafts for peripheral nerve regeneration, *J Tissue Eng Regen M* 8 (2014) 434-434.
- [20] A.J. Salgado, N. Sousa, N.A. Silva, N.M. Neves, R.L. Reis, Hydrogels for spinal cord injury regeneration, *Woodhead Publ Mater* (2008) 570-594.
- [21] H.S. Koh, T. Yong, C.K. Chan, S. Ramakrishna, Enhancement of neurite outgrowth using nano-structured scaffolds coupled with laminin, *Biomaterials* 29(26) (2008) 3574-3582.
- [22] Q. Quan, H.Y. Meng, B. Chang, G.B. Liu, X.Q. Cheng, H. Tang, Y. Wang, J. Peng, Q. Zhao, S.B. Lu, Aligned fibers enhance nerve guide conduits when bridging peripheral nerve defects focused on early repair stage, *Neural Regeneration Research* 14(5) (2019) 903-912.
- [23] J. Wang, L.L. Tian, L.M. He, N. Chen, S. Ramakrishna, K.F. So, X.M. Mo, Lycium barbarum polysaccharide encapsulated Poly lactic-co-glycolic acid Nanofibers: cost effective herbal medicine for potential application in peripheral nerve tissue engineering, *Sci Rep-Uk* 8 (2018).
- [24] K. Tajdaran, T. Gordon, M.D. Wood, M.S. Shoichet, G.H. Borschel, A glial cell line-derived neurotrophic factor delivery system enhances nerve regeneration across acellular nerve allografts, *Acta Biomater* 29 (2016) 62-70.

- [25] G. Terenghi, Peripheral nerve regeneration and neurotrophic factors, *Journal of Anatomy* 194 (1999) 1-14.
- [26] C.A. Ribeiro, J.S. Fraga, M. Graos, N.M. Neves, R.L. Reis, J.M. Gimble, N. Sousa, A.J. Salgado, The secretome of stem cells isolated from the adipose tissue and Wharton jelly acts differently on central nervous system derived cell populations, *Stem Cell Research & Therapy* 3 (2012).
- [27] R.R. Zhang, Y. Zhang, S. Yi, Identification of critical growth factors for peripheral nerve regeneration, *Rsc Adv* 9(19) (2019) 10760-10765.
- [28] T. Geetha, S.D. Rege, S.E. Mathews, S.O. Meakin, M.F. White, J.R. Babu, Nerve Growth Factor Receptor TrkA, a New Receptor in Insulin Signaling Pathway in PC12 Cells, *J Biol Chem* 288(33) (2013) 23807-23813.
- [29] K.B. Santosa, N.J. Jesuraj, A. Viader, M. MacEwan, P. Newton, D.A. Hunter, S.E. Mackinnon, P.J. Johnson, Nerve allografts supplemented with schwann cells overexpressing glial-cell-line-derived neurotrophic factor, *Muscle & Nerve* 47(2) (2013) 213-223.
- [30] J. Etulain, H.A. Mena, R.P. Meiss, G. Frechtel, S. Gutt, S. Negrotto, M. Schattner, An optimised protocol for platelet-rich plasma preparation to improve its angiogenic and regenerative properties, *Sci Rep-Uk* 8 (2018).
- [31] M.R. Casanova, M.A. Da Silva, A.R. Costa-Pinto, R.L. Reis, A. Martins, N.M. Neves, Chondrogenesis-inductive nanofibrous substrate using both biological fluids and mesenchymal stem cells from an autologous source, *Mat Sci Eng C-Mater* 98 (2019) 1169-1178.
- [32] C. Oliveira, A.R. Costa-Pinto, R.L. Reis, A. Martins, N.M. Neves, Biofunctional Nanofibrous Substrate Comprising Immobilized Antibodies and Selective Binding of Autologous Growth Factors, *Biomacromolecules* 15(6) (2014) 2196-2205.
- [33] S.F. Chang, C.P. Yang, C.C. Tai, H. Tseng, Gene Expression and Behavior Analysis of PC12 Cells Grown on Biodegradable Nano-fibrous Membranes, *Curr Nanosci* 7(6) (2011) 886-892.
- [34] L. Shang, Z.B. Huang, X.M. Pu, G.F. Yin, X.C. Chen, Preparation of Graphene Oxide-Doped Polypyrrole Composite Films with Stable Conductivity and Their Effect on the Elongation and Alignment of Neurite, *Acs Biomater Sci Eng* 5(3) (2019) 1268-1278.
- [35] H. Kawakami, K. Hiraka, S. Nagaoka, Y. Suzuki, M. Iwaki, Neuronal attachment and outgrowth on a micropatterned fluorinated polyimide surface, *J Artif Organs* 7(2) (2004) 83-90.
- [36] Y.M. Yang, W.J. Zhao, J.H. He, Y.H. Zhao, F. Ding, X.S. Gu, Nerve conduits based on immobilization of nerve growth factor onto modified chitosan by using genipin as a crosslinking agent, *Eur J Pharm Biopharm* 79(3) (2011) 519-525.
- [37] X. Gu, F. Ding, D.F. Williams, Neural tissue engineering options for peripheral nerve regeneration, *Biomaterials* 35(24) (2014) 6143-56.
- [38] E. Schnell, K. Klinkhammer, S. Balzer, G. Brook, D. Klee, P. Dalton, J. Mey, Guidance of glial cell migration and axonal growth on electrospun nanofibers of poly-epsilon-

caprolactone and a collagen/poly-epsilon-caprolactone blend, *Biomaterials* 28(19) (2007) 3012-25.

[39] H. Saito, L.B. Dahlin, Expression of ATF3 and axonal outgrowth are impaired after delayed nerve repair, *BMC Neurosci* 9 (2008) 88.

[40] Y. Tsuda, M. Kanje, L.B. Dahlin, Axonal outgrowth is associated with increased ERK 1/2 activation but decreased caspase 3 linked cell death in Schwann cells after immediate nerve repair in rats, *BMC Neurosci* 12 (2011) 12.

[41] R.T. Uren, A.M. Turnley, Regulation of neurotrophin receptor (Trk) signaling: suppressor of cytokine signaling 2 (SOCS2) is a new player, *Front Mol Neurosci* 7 (2014) 39.

[42] T.L. Nguyen, C.K. Kim, J.H. Cho, K.H. Lee, J.Y. Ahn, Neuroprotection signaling pathway of nerve growth factor and brain-derived neurotrophic factor against staurosporine induced apoptosis in hippocampal H19-7/IGF-IR [corrected], *Exp Mol Med* 42(8) (2010) 583-95.

[43] M.R. Casanova, M. Alves da Silva, A.R. Costa-Pinto, R.L. Reis, A. Martins, N.M. Neves, Chondrogenesis-inductive nanofibrous substrate using both biological fluids and mesenchymal stem cells from an autologous source, *Mater Sci Eng C Mater Biol Appl* 98 (2019) 1169-1178.

[44] E. Bacelo, M.A. da Silva, C. Cunha, S. Faria, A. Carvalho, R.L. Reis, A. Martins, N.M. Neves, Biofunctional Nanofibrous Substrate for Local TNF-Capturing as a Strategy to Control Inflammation in Arthritic Joints, *Nanomaterials-Basel* 9(4) (2019).

[45] F. Bastami, P. Vares, A. Khojasteh, Healing Effects of Platelet-Rich Plasma on Peripheral Nerve Injuries, *J Craniofac Surg* 28(1) (2017) e49-e57.

[46] M. Sanchez, A. Garate, D. Delgado, S. Padilla, Platelet-rich plasma, an adjuvant biological therapy to assist peripheral nerve repair, *Neural Regen Res* 12(1) (2017) 47-52.

[47] N.P. Patel, K.A. Lyon, J.H. Huang, An update-tissue engineered nerve grafts for the repair of peripheral nerve injuries, *Neural Regen Res* 13(5) (2018) 764-774.

[48] M. Sanchez, E. Anitua, D. Delgado, P. Sanchez, R. Prado, G. Orive, S. Padilla, Platelet-rich plasma, a source of autologous growth factors and biomimetic scaffold for peripheral nerve regeneration, *Expert Opin Biol Ther* 17(2) (2017) 197-212.

[49] M. Hadjiconstantinou, L. McGuire, A.M. Duchemin, B. Laskowski, J. Kiecolt-Glaser, R. Glaser, Changes in plasma nerve growth factor levels in older adults associated with chronic stress, *J Neuroimmunol* 116(1) (2001) 102-6.

[50] B.C. Lee, I.G. Choi, Y.K. Kim, B.J. Ham, B.H. Yang, S. Roh, J. Choi, J.S. Lee, D.Y. Oh, Y.G. Chai, Relation between plasma brain-derived neurotrophic factor and nerve growth factor in the male patients with alcohol dependence, *Alcohol* 43(4) (2009) 265-9.

[51] E. Emanuele, P. Politi, M. Bianchi, P. Minoretti, M. Bertona, D. Geroldi, Raised plasma nerve growth factor levels associated with early-stage romantic love, *Psychoneuroendocrinology* 31(3) (2006) 288-94.

[52] M.B. Levanti, A. Germana, F. de Carlos, E. Ciriaco, J.A. Vega, G. Germana, Effects of increased nerve growth factor plasma levels on the expression of TrkA and p75 in rat testicles, *J Anat* 208(3) (2006) 373-9.

[53] L. Aloe, S. Rossi, L. Manni, Altered expression of nerve growth factor and its receptors in the kidneys of diabetic rats, *J Nephrol* 24(6) (2011) 798-805.

[54] J. Liu, J.D. Li, J. Lu, J. Xing, J. Li, Contribution of nerve growth factor to upregulation of P2X(3) expression in DRG neurons of rats with femoral artery occlusion, *Am J Physiol Heart Circ Physiol* 301(3) (2011) H1070-9.

## **SECTION 4**

# **STRATEGIES FOR NERVE REGENERATION**

# **Chapter VI**

## **Guided Nerve Regeneration Mediated by Endogenous NGF bound at the surface of an Electrospun Fibrous**

## Chapter VI

### **Guided Nerve Regeneration Mediated by Endogenous NGF bound at the surface of an Electrospun Fibrous Mesh\*\***

#### **ABSTRACT**

Peripheral nerve injury still remaining a major clinical challenge, since the available solutions lead to a dysfunctional nerve regeneration. Despite autologous nerve grafts being considered the gold standard, tissue engineered nerve guidance grafts are valuable alternatives to overcome this unmet medical need. Nerve growth factor (NGF) is the most prominent neurotrophic factor, being recognized to facilitate the survival and the innervation of autonomic nerves and sensory neurons. Therefore, the development of a nerve guidance graft able to potentiate the interaction between injured neurons and endogenous NGF, would be a safer and more effective alternative to grafts that release NGF at the injury site. In this work, we demonstrated the selective retrieval of endogenous NGF, derived from rat blood plasma, by a biofunctional electrospun nanofibrous mesh (NFM). The neurogenesis potential of the NFM-NGF systems was evaluated by culturing rat pheochromocytoma (PC12) cells during 7 days, without further induction. The biological results indicate that this NGF delivery system promotes neuronal differentiation, being more effective than the control condition or even the bound recombinant NGF. Therefore, endogenous NGF bind to the surface of NFM might be able to promote functional peripheral nerve regeneration.

---

\*\* This chapter is based on the following publication:

Casanova M. R., Reis R. L., Martins A. and Neves N. M., "Guided Nerve Regeneration Mediated by Endogenous NGF bound at the surface of an Electrospun Fibrous Mesh", Submitted for publication.

## VI-1. INTRODUCTION

Nerve regeneration remains an enormous clinical challenge, following peripheral nerve injury [1], which can significantly affect the patients' quality of life. With the rise of the number of accidents, peripheral nerve injury is becoming an increasingly common clinical problem. Although the peripheral nervous system has greater regeneration capacity than the central nervous system [2, 3], the axonal reconnection and functional recovery by spontaneous peripheral nerve repair is limited by the size and severity of the lesion [4].

Many treatment options were used to repair nerve lesions, such as surgical reconnection and nerve allografts (autologous and alloplastic nerve conduits) [5-11], although the optimal treatment for large nerve defects remains elusive. The surgical reconnection by sutured end-to-end is normally used to bridge small peripheral nerve injury gaps [6, 8]. However, when there is a large defect (>10 mm in rats, or >30 mm in humans) [12], the required graft needs to bridge the gap and support axonal regrowth. Currently, autografts are used to bridge the peripheral nerve gap, which can lead to permanent donor site morbidity and inadequate functional repair [7, 9, 13]. Despite the best treatment techniques used in the clinic, the functional motor and sensory regeneration is often unsatisfactory because of neuroma and scar formation at the suture site, axonal loss, or failure of target reinnervation [14, 15]. Therefore, the recent advances in neural tissue engineering might be an alternative to conventional grafts transplantation.

Tissue Engineered Nerve guidance grafts comprise a biomaterial-based scaffold and a multitude of cellular and/or molecular components [10, 12, 16-20]. Generally, the scaffolds are capable of guiding the axonal and functional regeneration, as a bridge to restore the gap. Electrospun nanofibers were extensively used as potential scaffold in neural tissue engineering, owing to the high specific surface area, physical structure mimicking the morphology of the native neural extracellular matrix, and as a carrier to deliver clinically relevant proteins like growth factors [21-23].

In order to improve neurogenesis at the injury site, bioactive molecules are usually incorporated into the nerve conduit [17, 18, 21, 23, 24]. Among the bioactive molecules, neurotrophic factors are an important group of growth factors that stimulate and promote neurogenesis [25]. Nerve growth factor (NGF) is the most prominent and the commonly used neurotrophic factor for peripheral nerve regeneration [16, 18, 24, 26]. It acts as a chemoattractant, which may regulate the proliferation and differentiation of cells, and the myelination of neurons [27]. This neurotrophic factor is crucial to facilitate the survival and the



innervation of autonomic nerves and sensory neurons [28]. Therefore, the development of nerve guidance grafts incorporating NGF is an emerging approach in the field of peripheral nerve regeneration [12, 17, 18, 24, 29]. Although encouraging, the expensive and instable clinic efficacy of the NGF, and the uncontrolled delivery of the growth factor [18, 24] to avoid presenting cells exposing to supraphysiological doses [29], has limited the clinical translation of these approaches. An alternative choice is the use of autologous bioactive factors which always avoid the immune response, having less side effects [11], combined with local treatment, without affecting off-site tissues, maintaining the efficacy of the NGF by having it concentrated at the surface of a biomaterial.

Taking advantage of this statement, the immobilization of autologous bioactive molecules at the surface of biomedical systems has attracted increasing interest, in order to enhance their biological functionality at the cellular level. Accordingly, a herein we demonstrated, for the first time, the selective retrieval of endogenous NGF, derived from rat blood plasma, bind at the surface of an electrospun nanofibrous meshes (NFMs). The neurogenic potential of the NFM functionalized with endogenous NGF (NFM-NGF) was evaluated to assess its potential efficacy on guided nerve regeneration.

## **VI-2. MATERIALS AND METHODS**

### **VI-2.1. Rat blood plasma**

Plasma derived from rat blood were collected from five 10-week-old adult male rats (Sprague Dawley, ENVIGO), in accordance to the ethical and legal regulations. Blood samples were collected directly from the heart and the plasma preparation was adapted from previously described methods [30]. Briefly, rat blood samples with anti-coagulant (3.8% Citrate-dextrose solution; Sigma) were incubated at 4 °C for 30 min. Then, blood samples were coagulated by adding calcium chloride (22 mM; Sigma) and the clots were allowed to retract for 40 min at 37 °C. Following clot removal, the exudate was centrifuged at  $890 \times g$  for 10 min and the supernatant containing the platelet-derived growth factors (plasma) was stored at -80°C until further use. A pool of rat blood plasma was performed and the neurotrophic factor concentration (i.e. NGF $\beta$ ) determined by the Rat beta-NGF DuoSet<sup>®</sup> *Enzyme- Linked Immunosorbent Assay* (ELISA) (R&D Systems, Inc.), according to the manufacturer's protocol. The pool of rat blood plasma was stored at -20 °C until further use.

## **VI-2.2. Production of amine functionalized electrospun fibrous meshes (NFM)**

The NFM were obtained by electrospinning a polymeric solution of 15% (w/v) Polycaprolactone (PCL - Mn 70,000-90,000 by GPC, Sigma-Aldrich, Europe) in chloroform/dimethylformamide (7/3, Sigma-Aldrich, Europe), by applying a voltage of 12kV, a needle tip to ground collector distance of 20 cm, and a flow rate of 1mL/h as described elsewhere [31]. After the processing of 1mL of the polymeric solution, the NFM was left to dry and cut into samples of 1cm<sup>2</sup>.

The surfaces of the NFM were activated by exposing both sides to UV-ozone irradiation (2 min; ProCleaner 220 system, Bioforce Nanoscience) and functionalized with amine groups (-NH<sub>2</sub>) by incubating in 1M 1,6-hexanediamine solution (Sigma) for 1h at 37°C.

## **VI-2.3. Nerve growth factor functionalized electrospun fibrous meshes**

The endogenous NGF immobilization at the surface of NFM was performed using an antibody-antigen strategy [32].

### **VI-2.3.1. Antibody Immobilization**

To determine the maximum immobilization capacity of the system, a wide range of the anti-NGF antibody concentrations (from 0 to 12 µg/mL) were used. The immobilization of the anti-NGF antibody (EP1320Y; Abcam) at the surface of the NFM was achieved using a covalent bond mediated by a coupling agent (1-ethyl-3-(3-(dimethylamino)-propyl)carbodiimide / hydroxysuccinimide mixture; Sigma). After incubation for 2h at room temperature (RT), a bovine serum albumin (BSA; Sigma) blocking step was performed (1h; RT), and the corresponding secondary antibody (1:200)(Alexa Fluor<sup>®</sup> 488 donkey anti-rabbit IgG (H+L), Life Technologies, USA (~495/517 nm)) was incubated for 1 h (RT). To determine the degree of immobilization, the fluorescence of unbound secondary antibody solution was quantified ( $n = 3$  samples, read in triplicate) in a microplate reader (Synergy HT, Bio-TEK). Negative control samples consist in the substitutes of the primary antibody immobilization step by 0.1 M phosphate buffered saline (PBS; Sigma). The samples were recovered to characterize the spatial distribution of the anti-NGF antibody by fluorescence microscopy (Axio Observer; Zeiss).

### VI-2.3.2. NGF binding

The NFM functionalized with anti-NGF antibody at the maximum concentration were incubated (1h; RT) with 200  $\mu$ L of NGF from recombinant-origin (*NFM-rNGF*; 100 ng/mL; NGF- $\beta$  from rat recombinant; Sigma) or from the rat blood plasma (*NFM-pNGF*) as an autologous approach. In order to assess the binding efficacy of the proposed delivery system, the unbound protein solutions were collected and stored at -20 °C, until further quantification by using the Rat beta-NGF DuoSet<sup>®</sup> ELISA kit (R&D Systems, Inc.). Physico-chemical characterization of the indirect printed hierarchical SF scaffolds

### VI-2.4. Biological *in vitro* assays

The effectiveness of the developed NFM functionalized with NGF $\beta$  (**Table VI-1**), as nerve regeneration guided system, was assessed using rat PC12 cells derived from a pheochromocytoma of rat adrenal medulla. This cell line is a useful model system to study neuronal differentiation, because the PC12 cells undergo differentiation when exposed to NGF. This cell line has been extensively used to evaluate biomaterials for nerve regeneration applications [22, 23, 33, 34].

**Table VI-1** Experimental conditions used in the Cell Biology assays

Condition	Description
NFM	- NFM in <i>BM</i> <sup>a)</sup> without rNGF
	+ NFM in <i>BM</i> supplemented with 100 ng/mL of rNGF
NFM-rNGF	NFM functionalized with rNGF in <i>BM</i>
NFM-pNGF	NFM functionalized with plasma-derived NGF in <i>BM</i>

<sup>a)</sup> *BM* \_ DMEM supplemented with 0.75% horse serum (HS), 0.75% fetal bovine serum (FBS), 1% antibiotic/antimycotic (ATB);

#### VI-2.4.1. PC12 cell culture

The rat PC12 cells were kindly provided by the “ICVS - Life and Health Sciences Research Institute”, school of medicine, University of Minho. Cells were cultured in expansion medium composed of DMEM medium (Sigma) supplemented with 5 % horse serum (HS; Sigma), 10 % fetal bovine serum (FBS; Life Technologies) and 1% antibiotic/antimycotic solution (ATB;

Life Technologies) in a 75 cm<sup>2</sup> cell culture flask coated with 50 µg/mL collagen type I from rat tail (Santa Cruz Biotechnology, Inc). Cells were maintained at 37°C in a humidified incubator with 5% CO<sub>2</sub>, and the culture medium was changed twice a week. For the assays, subconfluent cells, were harvested with TrypLE Express (1X) (Invitrogen), seeded at a density of 20 000/NFM and cultured in basal medium (BM; DMEM medium supplemented with 0.75 % HS, 0.75 % FBS and 1 % ATB). For the differentiation studies, PC12 cultured on NFM in BM supplemented with or without 100 ng/mL NGF-β from rat recombinant (Sigma) were carried out as positive or negative controls, respectively (**Table VI-1**). Cultures were incubated in a humid atmosphere at 37 °C and 5% CO<sub>2</sub>, and retrieved for further analysis at predefined culturing times, namely 1, 3 and 7 days. All experiments were performed in triplicate and repeated at least three times ( $n=3$ ), independently.

#### **VI-2.4.2. Cellular Biochemistry Analysis**

The cellular performance of PC12 on the different culture conditions was evaluated for metabolic activity by the MTS assay (CellTiter 96 AQueous One Solution, Promega), DNA quantification (Quant-iTPicoGreen dsDNA assay, Invitrogen) and protein synthesis by Micro BCA assay (Micro BCA™ Protein Assay Kit, Thermo Fisher Scientific), according to the manufacturer instructions.

#### **VI-2.4.3. Scanning Electron Microscopy (SEM)**

The morphology of PC12 cells on the different culture condition were analyzed by SEM (JSM-6010 LV, JEOL, Japan). The specimens were prepared for SEM analysis, all culture conditions were dehydrated and sputter coated with Au/Pd.

#### **VI-2.4.4. Gene Expression Analysis**

For the gene expression analysis, PC12 on different culture condition, at each time point, were washed with PBS, immersed in Tri reagent® (Life Science, VWR, USA) and kept at -80 °C until further use. Total RNA was extracted according to the Tri reagent® manufacturer's instructions. The cDNA was amplified from 100 ng of total RNA using qScript cDNA synthesis kit (Quanta Biosciences, VWR). The qPCR reactions were carried out in a Mastercycler® ep

Gradient S realplex<sup>®</sup> thermocycler (Eppendorf; Hamburg, Europe) for neurogenic genes (**Table VI-2**), according to the manufacturer's instructions of the PerfeCta<sup>™</sup> SYBR<sup>®</sup> Green system (Quanta Biosciences, VWR, USA).

**Table VI-2 Primer sequences used for RT-PCR procedures <sup>a)</sup>.**

gene	forward (5' - 3')	reverse (5' - 3')
<i>GAPDH</i>	CAACTCCCTCAAGATTGTCAGCAA	GGCATGGACTGTGGTCATGA
<i>GAP-43</i>	TTTCCTCTCCTGTCCTGCTC	TGGACTTGGGATCTTTCCTG
<i>MAP2</i>	GGCACTCCTCCAAGCTACTCT	CTTGACGTTCTTCAGGTCTGG
<i>NF-160</i>	AGCATTGAGCTCGAGTCGGTG	CTGCTGGATGGTGTCTCTGGTAG
<i>NF-200</i>	AAAGTGAACACGGATGCTATGC	GTGCTTTTCAGTGCCTCCAAC
<i>Syn1</i>	GTGTCAGGGAAGTGGAAAGACC	AGGAGCCCACCACCTCAATA

<sup>a)</sup> *GAPDH* = glyceraldehyde 3-phosphate dehydrogenase; *GAP-43* = growth-associated protein 43; *MAP-2* = microtubule-associated protein 2; *NF-160* = neurofilament 160; *NF-200* = neurofilament 200; *Syn1* = synapsin-1.

The housekeeping gene *Glyceraldehydes-3-phosphate-dehydrogenase (GAPDH)* was used to normalize the transcript expression data, and the quantification performed according to the Livak method ( $2^{-\Delta\Delta CT}$  method), considering the negative control as calibrator.

#### VI-2.4.5. Immunocytochemistry

Following the previous described cell culture conditions, samples were collected at 7 days fixed in a 10% formalin solution and kept at 4 °C until further used for staining procedures. Samples were incubated with beta III Tubulin (anti-beta III Tubulin polyclonal antibody, 1:100 dilution; Abcam), GAP-43 (rabbit GAP43 polyclonal antibody, 1:200 dilution; Thermo Fisher Scientific), NF200 (mouse anti-neurofilament 200 monoclonal antibody, 1:40 dilution, Sigma) and Synapsin 1 (rabbit anti-synapsin I polyclonal antibody, 1:200 dilution; Abcam) overnight at 4 °C, in a humidified atmosphere after the quenching of endogenous peroxidase activity (0.3% hydrogen peroxide solution; 30 min). R.T.U. VECTASTAIN<sup>®</sup> Universal ABC Elite<sup>®</sup> Kit (Vector Laboratories; USA) was used for secondary antibody detection and incubation revealed by using the Peroxidase Substrate Kit (DAB) (Vector Laboratories; USA), according to the manufacturer instructions. The samples were counterstained with hematoxylin for nuclei visualization, mounted in aqueous mounting medium (Sigma) and observed in an optical microscope (Leica DM750 microscope).

#### **VI-2.4.6. Neurite outgrowth**

Since PC12 cells differentiate towards the neuronal phenotype in response to NGF stimulation, the bioactivity of NGF from recombinant- (rNGF) or from rat blood plasma (pNGF) origin immobilized at the surface of NFM was quantified by counting the neurite outgrowth from PC12 cells. For different cell culture conditions (**Table VI-1**) at the different times points, the percentage of neurite-bearing cells was determined by counting more than 200 cells in randomly selected fields of beta III Tubulin immunostaining recorded at 40x lens objective (Leica DM750 microscope) with a computerized image analyzer (NIH ImageJ software). Neurite-bearing cells are those with neurites lengths greater than or equal to the diameter of the cell body [35, 36].

#### **VI-2.5. Statistical analysis**

All statistical analysis was performed using the SPSS statistic software (release 24.0.0.0 for Mac). The Shapiro-Wilk test was used to ascertain the data normality, and the Levene test for the homogeneity of variances. As for all data, the normality and variance homogeneity were rejected, thus non-parametric tests were used (Kruskal-Wallis test followed by Tukey's HSD test). *P* values lower than 0.01 were considered statistically significant in non-parametric tests. The confidence interval used was 99% and  $p \leq 0.01$  were regarded as statistically significant.

### **VI-3. RESULTS**

#### **VI-3.1. Physicochemical properties of the NFM functionalized with NGF**

An optimized activated and functionalized NFM with anti-NGF antibody was developed, providing binding sites to NGF *via* a non-neutralizing antibody, envisioning an autologous approach. The maximum antibody immobilization capacity was determined using an indirect quantification method (**Figure VI-1 a**). The maximum concentration of immobilized anti-NGF antibody was achieved at 10  $\mu\text{g/mL}$ , corresponding to a lower fluorescence signal of the free secondary antibody.

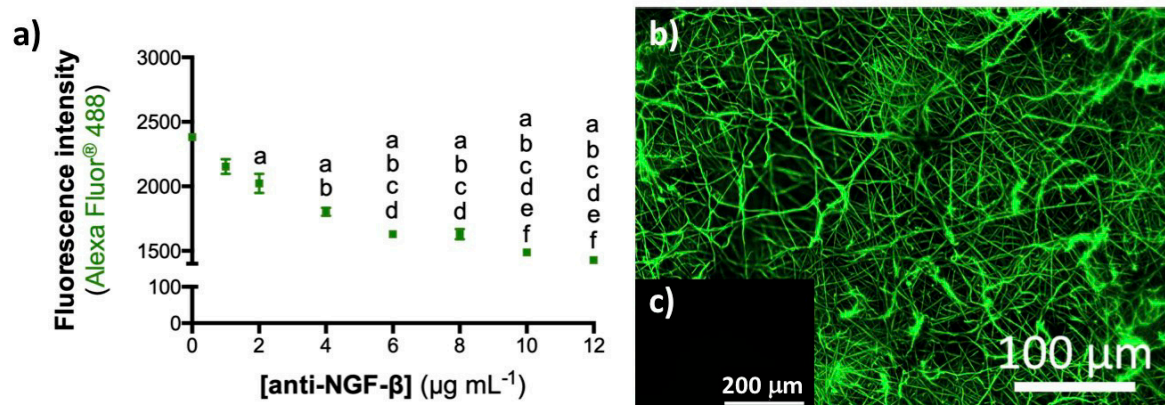


**Figure VI-1** Maximum immobilization capacity of anti-NGF- $\beta$  antibody at the surface of activated and functionalized NFM (a). Data were analyzed by the one-way ANOVA test, followed by the Tukey's HSD test ( $p < 0.01$ ): a denotes significant differences compared to concentration 0  $\mu\text{g/mL}$ ; b denotes significant differences compared to concentration 1  $\mu\text{g/mL}$ ; c denotes significant differences compared to concentration 2  $\mu\text{g/mL}$ ; d denotes significant differences compared to concentration 4  $\mu\text{g/mL}$ ; e denotes significant differences compared to concentration 6  $\mu\text{g/mL}$  and f denotes significant differences compared to concentration 8  $\mu\text{g/mL}$ . Spatial distribution of anti-NGF immobilized at the NFM at 10  $\mu\text{g/mL}$  (b). The negative control sample was not incubated with the primary antibody (c).

Fluorescence micrograph (**Figure VI-1 b**) showed a uniform distribution of anti-NGF antibody immobilized at the nanofibers surface. The binding capacity of the immobilized anti-NGF antibody was assessed by using NGF from recombinant-origin (rNGF) or from a pool of rat blood plasma (pNGF). **Table VI-3** showed that NGF from different origins were bound to the surface of NFM. Despite the different NGF concentrations, the binding efficiency stayed in the same range for the two different origins (approximately 95%), being  $98\,700 \pm 200$   $\mu\text{g/mL}$  of rNGF or  $567 \pm 23$   $\mu\text{g/mL}$  of pNGF bound to the NFM biofunctionalized with anti-NGF.

**Table VI-3** Quantification of NGF recombinant or derived from rat blood plasma) and the binding capacity of the NFM-NGF system

	Recombinant ( $\mu\text{g/mL}$ )	Plasma ( $\mu\text{g/mL}$ )
[NGF]	$99\,990 \pm 10$	$597 \pm 40$
<b>bound</b>	$98\,700 \pm 200$	$567 \pm 23$

### VI-3.2. Performance of PC12 cells cultured on NFM-NGF

PC12 cells were cultured over NFM functionalized with NGF from different sources (i.e. rNGF and pNGF), under basal conditions, in order to determine the effectiveness of these biofunctionalized systems.

In terms of cell viability (**Figure VI-2 a**), the PC12 cells cultured on the NFM comprising endogenous NGF (*NFM-pNGF*) displayed significantly higher viability than the control conditions (*NFM-* and *NFM+*) at days 1 and 3 ( $p < 0.001$ ). However, on the 7<sup>th</sup> day of PC12 culture, all cultured conditions have similarly high cell viability. The NFM-NGF systems were favorable for cell proliferation and protein synthesis, since the levels of DNA content (**Figure VI-2 b**) and the protein synthesis (**Figure VI-2 c**) are comparable to those observed on the culture control conditions (*NFM-* and *NFM+*) along the time. As shown in **Figure VI-2 d**), PC12 cells attach, spread, and proliferate on all the NFM conditions. The morphology changes of PC12 cells culture on the different culture conditions along the culturing time, reflect their differentiation stage. In the negative control condition (*NFM-*), the PC12 cells displayed the morphology of undifferentiated PC12 cells, being smaller and spherical on all culturing times. Although, in the presence of NGF (*NFM+*; *NFM-rNGF*; *NFM-pNGF*), the PC12 cells start to differentiate showing an elongated morphology. Indeed, a few cells grown on NFM without NGF treatment (*NFM-*) showed elongated shape, while on the *NFM-pNGF* system the elongated cell morphologies is consistently observed.



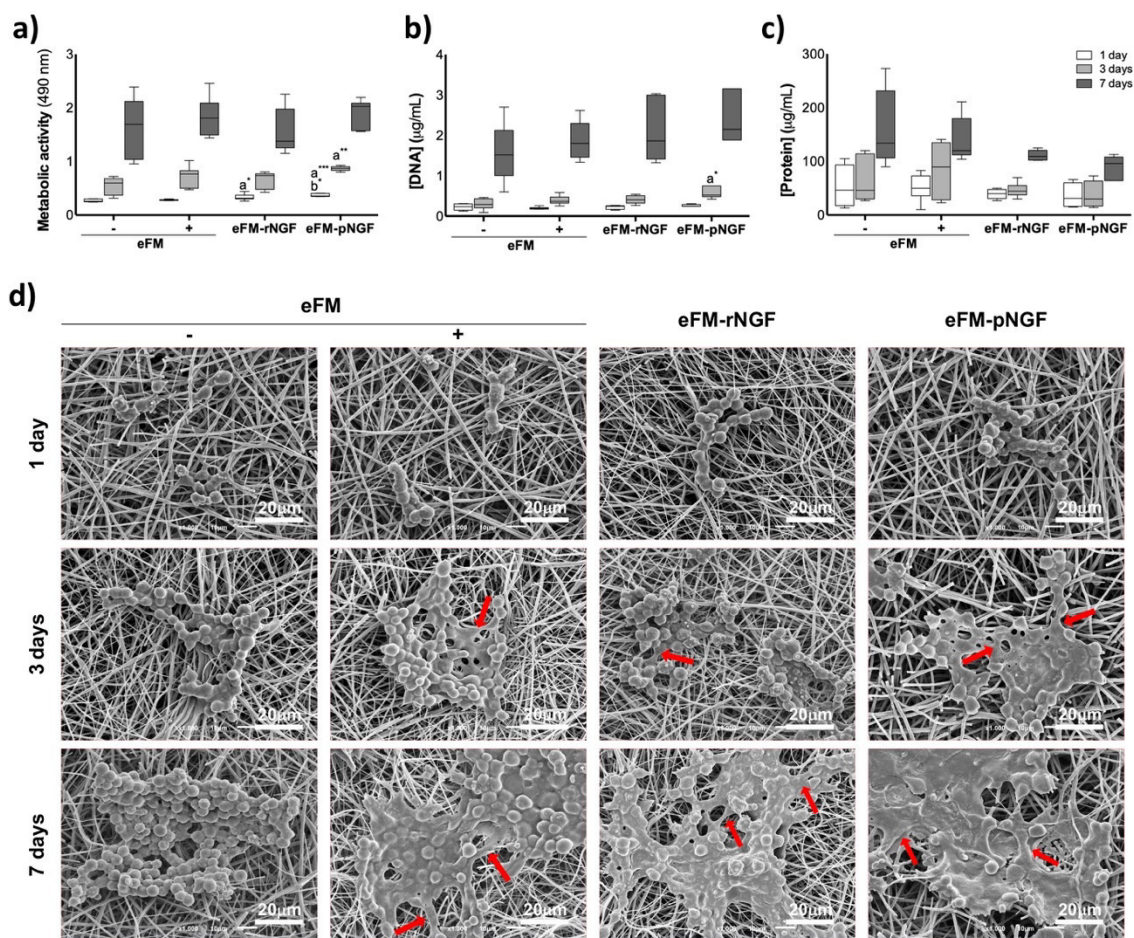


**Figure VI-2 Top:** Biochemical performance (i.e. metabolic activity (a), proliferation (b) and protein synthesis (c)) of the PC12 cells cultured on NFM functionalized with NGF $\beta$  from different sources, under basal medium. NFMs cultured with PC12 cells under basal (NFM-) or neuronal differentiation media (NFM+) were used as controls. Data were analysed by the Kruskal-Wallis test, followed by the Tukey's HSD test ( $p < 0.01$ ): a denotes significant differences compared to NFM- and b denotes significant differences compared to NFM+; \* $p < 0.01$ ; \*\* $p < 0.001$ ; \*\*\* $p < 0.0001$ ; **Bottom:** Morphological analysis of the PC12 cells on different culture condition, along culturing time, by scanning electron microscopy (SEM) (d).

PC12 cell differentiation was studied by analyzing the number of neurite-bearing cells (differentiated PC12 cells), along the culturing time. After the 7<sup>th</sup> day of culture, the neurite outgrowth in the *NFM-rNGF* condition was a little higher than that observed in the positive control condition (*NFM+*) (**Figure VI-3 a**). But, the neurite outgrowth in *NFM-pNGF* condition was significantly higher than that observed in either the positive or negative controls (*NFM+*; *NFM-*). The result suggested that the NGF bound to the surface of NFM kept its bioactive, i.e., its ability to promote neurite outgrowth from PC12 cells (**Figure VI-3 b**).

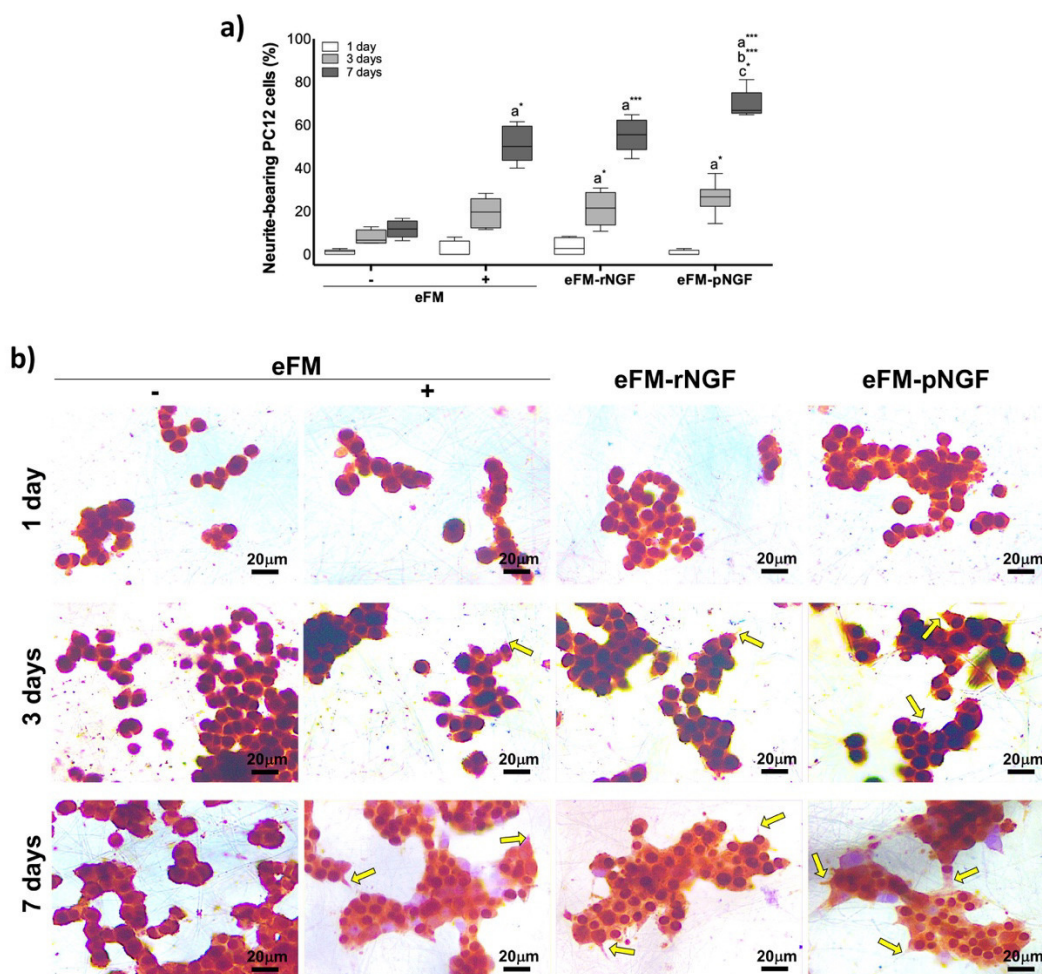


**Figure VI-3 Top: Percentage of neurite-bearing PC12 cells on different culture condition along culturing time (a). Data were analysed by the Kruskal-Wallis test, followed by the Tukey's HSD test ( $p < 0.01$ ): a denotes significant differences compared to NFM-; b denotes significant differences compared to NFM+ and c denotes significant differences compared to NFM-rNGF; \* $p < 0.01$ ; \*\* $p < 0.001$ ; \*\*\* $p < 0.0001$ ; Bottom: Immunocytochemistry with beta-III Tubulin (brown) of PC12 cells on different culture condition along culturing time (b).**

In order to evaluate the impact of NFM-NGF systems on neuronal-related gene expression by PC12 cells, qPCR was used to analyze the expression levels of the *growth-associated protein 43* regulation gene (*GAP-43*), the *microtubule-associated protein 2* regulation gene (*MAP2*), the *medium-molecular-weight neurofilament protein* regulation gene (*NF160*), the *high-molecular-weight neurofilament protein* regulation gene (*NF200*) and *synapsin 1* regulation gene (*Syn1*). Quantitative results, considering the negative control condition (NFM-) as calibrator are shown in **Figure VI-4**. Except for *GAP-43*, all other genes are not expressed on the 1<sup>th</sup> day of PC12 cells culture, in all testing conditions. On the 3<sup>th</sup> day, PC12 cells cultured on the NFM-pNGF condition present significantly higher *GAP-43*, *NF160*, *NF200* and *Syn1* expression when compared to positive control condition (NFM+) ( $p < 0.01$ ). Likewise, the

*NFM-pNGF* condition shown a significantly higher *GAP-43*, *NF160*, *NF200* and *MAP2* expression than the *NFM+* condition at 7 days of PC12 cell culture ( $p < 0.0001$ ). Moreover, the *NFM-pNGF* condition showed significantly higher expression of *GAP-43*, *MAP2* and *NF160* genes when compared to the *NFM-rNGF* condition ( $p < 0.01$ ). These results indicate that the *NFM-pNGF* system may provide a stronger stimulation for the PC12 cell differentiation than the other conditions.

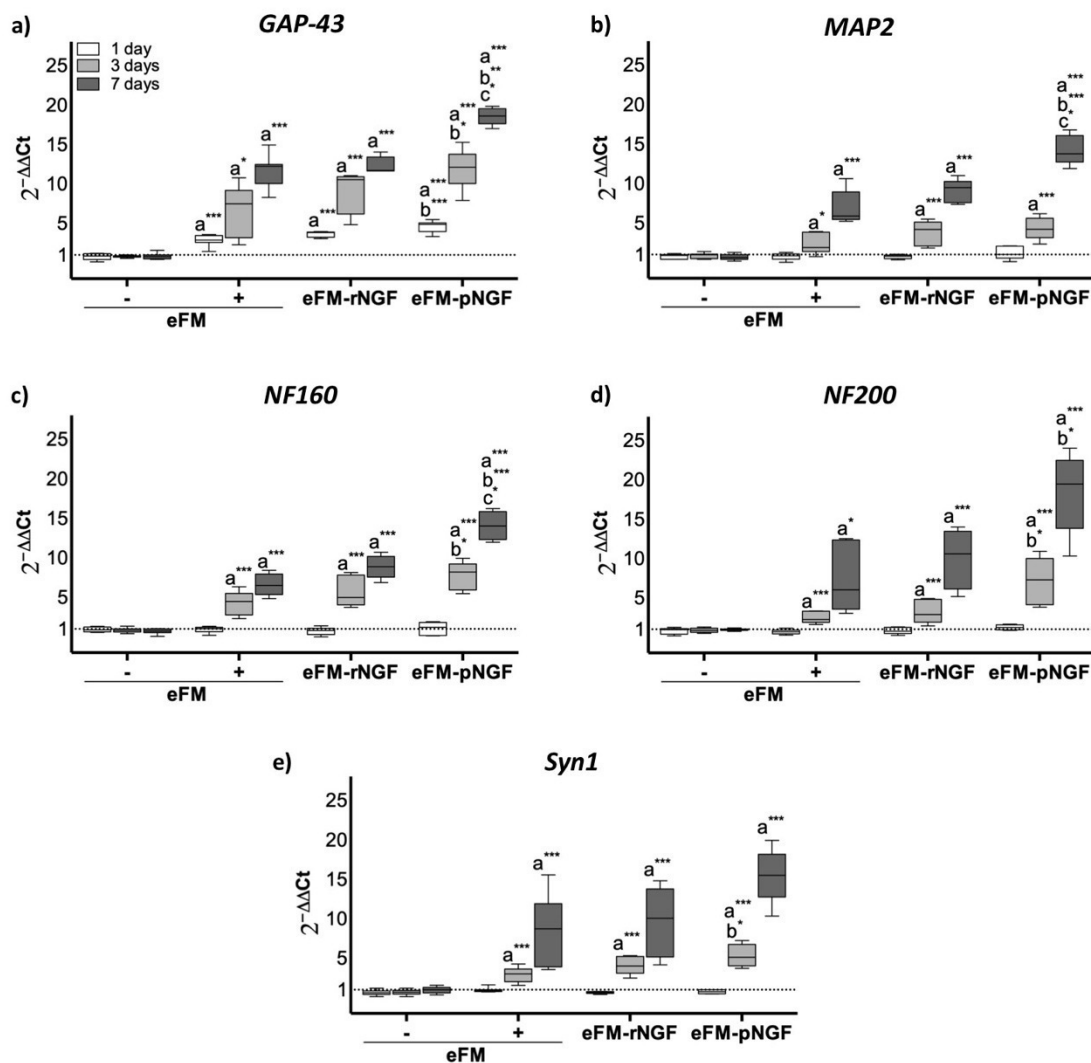
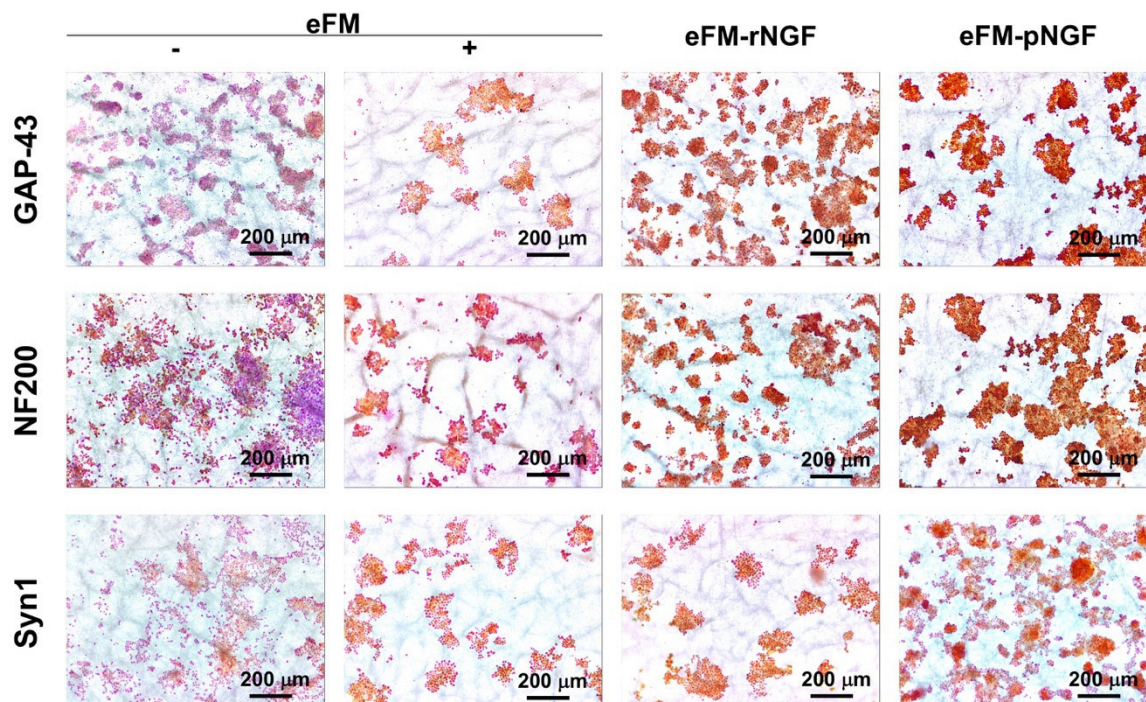


Figure VI-4 Relative expression of *GAP-43* (a), *MAP2* (b), *NF160* (c), *NF200* (d) and *Syn1* (e) genes by PC12 cells cultured on different culture condition, along culturing time. The expression was normalized against the *GAPDH* gene and the quantification was performed according to the Livak method, considering the negative control (*NFM-*) as calibrator. Data were analysed by the Kruskal-Wallis test, followed by the Tukey's HSD test ( $p < 0.01$ ): a denotes significant differences compared to *NFM-*; b denotes significant differences compared to *NFM+*; and c denotes significant differences compared to *NFM-rNGF*; \* $p < 0.01$ ; \*\* $p < 0.001$ ; \*\*\* $p < 0.0001$ ;

After 7 days of culture, the PC12 cells were immunostained for GAP-43, NF200 and Syn1. **Figure VI-5** demonstrated that NGF-stimulated differentiation of PC12 cells toward the neural cell phenotype in NFM+ condition was similar to, although a slight lower than, that in *NFM-pNGF* condition or *NFM-rNGF*. Furthermore, neuronal differentiation in both NFM-NGF systems was significantly higher than in the negative control condition (*NFM-*). Collectively, these phenotypic results confirm the previously described genotypic results.



**Figure VI-5** Immunoeexpression of GAP-43, NF-200 and Syn1 proteins by the PC12 cells cultured on the different condition, at the 7<sup>th</sup> day.

#### VI-4. DISCUSSION

Nerve regeneration involves neuronal growth and the formation of extracellular matrix [37]. Basic requirements to form the new nerve are the migration of the Schwann cells, the formation of new blood vessels, and axonal outgrowth into a matrix of fibrin [38]. The purpose of nerve guidance grafts is to stimulate the regenerative microenvironment of the nerve to facilitate the local neurogenesis, with a suitable environment that limits scar formation. Between the growth factors in use, NGF is the most potent neurotrophic factor due to its role over survival and differentiation of sensory neurons [27]. After nerve injury, lymphocytes T

and B, as well as Schwann cells, produce NGF and its gradient enables injured nerve ends to extend their axons through the injury site, overcoming degeneration [39, 40]. NGF binds to a high affinity receptor (TrkA) expressed by nerve cells and activates signaling pathways such as MAPK, Akt and PKC pathways for the survival and differentiation of nerve cells [41, 42]. Due to the crucial roles of NGF in the peripheral nervous system, we developed a neurogenesis-inductive NFM system through the endogenous NGF immobilization at the surface of NFM, capable to promote axonal outgrowth *in vitro*.

The present study aims to study the developed PCL electrospun fibrous meshes functionalized with endogenous NGF via antibody-antigen bound. Herein a non-neutralizing antibody against NGF was successfully immobilized at the surface of activated and functionalized NFM, achieving the maximum immobilization capacity at 10  $\mu\text{g/mL}$ . Early studies reported that the immobilization capacity of electrospun nanofibrous substrates differ among antibodies, namely 12  $\mu\text{g/mL}$  for anti-TGF $\beta$ 1, 8  $\mu\text{g/mL}$  for anti-bFGF, 6  $\mu\text{g/mL}$  for anti-TNF- $\alpha$  and 4  $\mu\text{g/mL}$  for anti-VEGF, anti-TGF $\beta$ 3 and anti-IGF-I [32, 43, 44].

Platelet-rich plasma has been used to stimulate tissue regeneration, especially in peripheral nerve regeneration with growing evidences at the research and clinical levels [45-48]. Plasma-derived NGF levels in healthy human patients varies between 100 - 752  $\rho\text{g/mL}$  [49-51], while in healthy rats varies between 400 – 1 000  $\rho\text{g/mL}$  [52-54]. Considering these values, the amount of NFG in the pool of rat blood plasma presented similar concentration,  $597 \pm 40 \rho\text{g/mL}$ , to the ones reported in the literature. Further on, the feasibility of anti-NGF immobilized on NFM, for the selective retrieval of the corresponding growth factor, was evaluated by using a biological fluid (i.e. rat blood plasma) and a recombinant NGF. The developed biofunctional NFM displayed a higher binding efficiency (approximately 95%), being the amount of growth factor bound limited by the concentration of protein existing in the plasma solution.

PC12 cells are extensively used as a model to study neuronal cell differentiation [21-23, 28, 33-36]. They can be triggered by NGF to differentiate into neuron-like cells, forming myelin structures. Undifferentiated PC12 cells are a type of semi-suspended and aggregate cells with a weak sensing toward the culturing substrates. The viability and proliferation of PC12 cells was favorable on the NFM-NGF systems. Moreover, the neurite outgrowth was significantly enhanced on the NFM-NGF systems, especially on the *NFM-pNGF* system. These results were further confirmed by analyzing the expression of neuronal markers (*GAP-43*, *MAP2*, *NF160*, *NF200* and *Syn1*) by qPCR and immunocytochemistry, which confirmed the prior observation that

the NFM-NGF systems induces differentiation of PC12 cells into neuron-like cells. Indeed, during neuronal differentiation, neurite extension and outgrowth are regulated by molecular cues in addition to alterations in gene expression. As examples, the GAP-43 is an axonal membrane protein involved in the neuronal outgrowth and synaptic plasticity of developing neurons; Syn1 is a neuronal phosphoprotein associated with the membranes of small synaptic vesicles involved in the neuronal development; and NF200 is commonly used as neuronal cell marker. Therefore, our immobilization strategy guarantees the bioactivity of the bound NGF, extending the half-life of the protein when compared to its free form, as confirmed by the direct culture of PC12 cells over the biofunctionalized NFM systems (*NFM-rNGF* and *NFM-pNGF*).

Taken together, the *NFM-pNGF* system promotes axonal outgrowth, exhibiting a higher potential to differentiate PC12 cells towards neurogenesis lineage, as compared to the *NFM-rNGF* system, even with a lower concentration of bound pNGF. Therefore, NGF from blood plasma is more effective than the recombinant NGF. Therefore, our neurogenesis-inductive NFM system might have application in peripheral nerve tissue engineering, which is an unmet clinical need.

## VI-5. CONCLUSIONS

This study shows evidence that NFM-NGF systems comprising NGF from different sources (recombinant or rat blood plasma) is able to successfully induce the neurogenic differentiation of PC12 cells, displaying typical phenotypic and genotypic neuronal markers. Moreover, the NFM functionalized with endogenous NGF (*NFM-pNGF* system) is more bioactive than recombinant NGF, either immobilized (*NFM-rNGF* system) or in the free form (positive control condition). Our autologous approach (*NFM-pNGF* system) is more effective in promoting the neurogenesis, avoiding the need to use medium supplementation. We hypothesize that our system maximizes the exposure of the PC12 cells to the immobilized NGF, by the close contact established between them and the NGF bound at the surface of the substrate. Therefore, the proposed *NFM-pNGF* system can act as an effective neural tissue engineering approach, with a strong potential to be translated into the clinical setting.

## VI-6. ACKNOWLEDGMENTS

The authors would like to acknowledge the Portuguese Foundation for Science and Technology (FCT) for the PhD grant of M.R.C. (PD/BD/113797/2015) financed by the FCT Doctoral Program on Advanced Therapies for Health (PATH) (FSE/POCH/PD/169/2013), the IF grant of A.M. (IF/00376/2014), and the projects SPARTAN (PTDC/CTM-BIO/4388/2014) and FRONthera (NORTE-01-0145-FEDER-0000232).

## VI-7. REFERENCES

- [1] C.A. Taylor, D. Braza, J.B. Rice, T. Dillingham, The incidence of peripheral nerve injury in extremity trauma, *Am J Phys Med Rehabil* 87(5) (2008) 381-5.
- [2] W. Wang, J. Gao, L. Na, H. Jiang, J. Xue, Z. Yang, P. Wang, Craniocerebral injury promotes the repair of peripheral nerve injury, *Neural Regen Res* 9(18) (2014) 1703-8.
- [3] M.P. Coleman, M.R. Freeman, Wallerian degeneration, wld(s), and nmnat, *Annu Rev Neurosci* 33 (2010) 245-67.
- [4] B. Chang, Q. Quan, S. Lu, Y. Wang, J. Peng, Molecular mechanisms in the initiation phase of Wallerian degeneration, *Eur J Neurosci* 44(4) (2016) 2040-8.
- [5] R. Deumens, A. Bozkurt, M.F. Meek, M.A. Marcus, E.A. Joosten, J. Weis, G.A. Brook, Repairing injured peripheral nerves: Bridging the gap, *Prog Neurobiol* 92(3) (2010) 245-76.
- [6] J.W. Griffin, M.V. Hogan, A.B. Chhabra, D.N. Deal, Peripheral nerve repair and reconstruction, *J Bone Joint Surg Am* 95(23) (2013) 2144-51.
- [7] L.F. Bulstra, N. Rbia, M.F. Kircher, R.J. Spinner, A.T. Bishop, A.Y. Shin, Spinal accessory nerve to triceps muscle transfer using long autologous nerve grafts for recovery of elbow extension in traumatic brachial plexus injuries, *J Neurosurg* 129(4) (2018) 1041-1047.
- [8] S. Geuna, I. Papalia, G. Ronchi, F.S. d'Alcontres, K. Natsis, N.A. Papadopoulos, M.R. Colonna, The reasons for end-to-side coaptation: how does lateral axon sprouting work?, *Neural Regen Res* 12(4) (2017) 529-533.
- [9] H. Millesi, Bridging defects: autologous nerve grafts, *Acta Neurochir Suppl* 100 (2007) 37-8.
- [10] M.D. Sarker, S. Naghieh, A.D. McInnes, D.J. Schreyer, X. Chen, Regeneration of peripheral nerves by nerve guidance conduits: Influence of design, biopolymers, cells, growth factors, and physical stimuli, *Prog Neurobiol* 171 (2018) 125-150.
- [11] S.J. Forbes, N. Rosenthal, Preparing the ground for tissue regeneration: from mechanism to therapy, *Nat Med* 20(8) (2014) 857-869.

- [12] L.M. Marquardt, S.E. Sakiyama-Elbert, Engineering peripheral nerve repair, *Curr Opin Biotechnol* 24(5) (2013) 887-92.
- [13] F. May, A. Buchner, K. Matiasek, B. Schlenker, C. Stief, N. Weidner, Recovery of erectile function comparing autologous nerve grafts, unseeded conduits, Schwann-cell-seeded guidance tubes and GDNF-overexpressing Schwann cell grafts, *Dis Model Mech* 9(12) (2016) 1507-1511.
- [14] D. Grinsell, C.P. Keating, Peripheral Nerve Reconstruction after Injury: A Review of Clinical and Experimental Therapies, *Biomed Research International* (2014).
- [15] M.L. Wang, M. Rivlin, J.G. Graham, P.K. Beredjikian, Peripheral nerve injury, scarring, and recovery, *Connect Tissue Res* 60(1) (2019) 3-9.
- [16] M. Moattari, H.M. Kouchesfehiani, G. Kaka, S.H. Sadraie, M. Naghdi, Evaluation of nerve growth factor (NGF) treated mesenchymal stem cells for recovery in neurotmesis model of peripheral nerve injury, *J Cranio Maxill Surg* 46(6) (2018) 898-904.
- [17] G.C. Li, Q.Z. Xiao, L.Z. Zhang, Y.H. Zhao, Y.M. Yang, Nerve growth factor loaded heparin/chitosan scaffolds for accelerating peripheral nerve regeneration, *Carbohydr Polym* 171 (2017) 39-49.
- [18] W. Zeng, M.Y. Rong, X.Y. Hu, W. Xiao, F.Y. Qi, J.H. Huang, Z.J. Luo, Incorporation of Chitosan Microspheres into Collagen-Chitosan Scaffolds for the Controlled Release of Nerve Growth Factor, *Plos One* 9(7) (2014).
- [19] C. Carvalho, J. Pedro, K.W. Ng, N. Neves, R. Reis, M. Oliveira, Keratin/chitosan as novel grafts for peripheral nerve regeneration, *J Tissue Eng Regen M* 8 (2014) 434-434.
- [20] A.J. Salgado, N. Sousa, N.A. Silva, N.M. Neves, R.L. Reis, Hydrogels for spinal cord injury regeneration, *Woodhead Publ Mater* (2008) 570-594.
- [21] H.S. Koh, T. Yong, C.K. Chan, S. Ramakrishna, Enhancement of neurite outgrowth using nano-structured scaffolds coupled with laminin, *Biomaterials* 29(26) (2008) 3574-3582.
- [22] Q. Quan, H.Y. Meng, B. Chang, G.B. Liu, X.Q. Cheng, H. Tang, Y. Wang, J. Peng, Q. Zhao, S.B. Lu, Aligned fibers enhance nerve guide conduits when bridging peripheral nerve defects focused on early repair stage, *Neural Regeneration Research* 14(5) (2019) 903-912.
- [23] J. Wang, L.L. Tian, L.M. He, N. Chen, S. Ramakrishna, K.F. So, X.M. Mo, Lycium barbarum polysaccharide encapsulated Poly lactic-co-glycolic acid Nanofibers: cost effective herbal medicine for potential application in peripheral nerve tissue engineering, *Sci Rep-Uk* 8 (2018).
- [24] K. Tajdaran, T. Gordon, M.D. Wood, M.S. Shoichet, G.H. Borschel, A glial cell line-derived neurotrophic factor delivery system enhances nerve regeneration across acellular nerve allografts, *Acta Biomater* 29 (2016) 62-70.
- [25] G. Terenghi, Peripheral nerve regeneration and neurotrophic factors, *Journal of Anatomy* 194 (1999) 1-14.



- [26] C.A. Ribeiro, J.S. Fraga, M. Graos, N.M. Neves, R.L. Reis, J.M. Gimble, N. Sousa, A.J. Salgado, The secretome of stem cells isolated from the adipose tissue and Wharton jelly acts differently on central nervous system derived cell populations, *Stem Cell Research & Therapy* 3 (2012).
- [27] R.R. Zhang, Y. Zhang, S. Yi, Identification of critical growth factors for peripheral nerve regeneration, *Rsc Adv* 9(19) (2019) 10760-10765.
- [28] T. Geetha, S.D. Rege, S.E. Mathews, S.O. Meakin, M.F. White, J.R. Babu, Nerve Growth Factor Receptor TrkA, a New Receptor in Insulin Signaling Pathway in PC12 Cells, *J Biol Chem* 288(33) (2013) 23807-23813.
- [29] K.B. Santosa, N.J. Jesuraj, A. Viader, M. MacEwan, P. Newton, D.A. Hunter, S.E. Mackinnon, P.J. Johnson, Nerve allografts supplemented with schwann cells overexpressing glial-cell-line-derived neurotrophic factor, *Muscle & Nerve* 47(2) (2013) 213-223.
- [30] J. Etulain, H.A. Mena, R.P. Meiss, G. Frechtel, S. Gutt, S. Negrotto, M. Schattner, An optimised protocol for plateletrich plasma preparation to improve its angiogenic and regenerative properties, *Sci Rep-Uk* 8 (2018).
- [31] M.R. Casanova, M.A. Da Silva, A.R. Costa-Pinto, R.L. Reis, A. Martins, N.M. Neves, Chondrogenesis-inductive nanofibrous substrate using both biological fluids and mesenchymal stem cells from an autologous source, *Mat Sci Eng C-Mater* 98 (2019) 1169-1178.
- [32] C. Oliveira, A.R. Costa-Pinto, R.L. Reis, A. Martins, N.M. Neves, Biofunctional Nanofibrous Substrate Comprising Immobilized Antibodies and Selective Binding of Autologous Growth Factors, *Biomacromolecules* 15(6) (2014) 2196-2205.
- [33] S.F. Chang, C.P. Yang, C.C. Tai, H. Tseng, Gene Expression and Behavior Analysis of PC12 Cells Grown on Biodegradable Nano-fibrous Membranes, *Curr Nanosci* 7(6) (2011) 886-892.
- [34] L. Shang, Z.B. Huang, X.M. Pu, G.F. Yin, X.C. Chen, Preparation of Graphene Oxide-Doped Polypyrrole Composite Films with Stable Conductivity and Their Effect on the Elongation and Alignment of Neurite, *Acs Biomater Sci Eng* 5(3) (2019) 1268-1278.
- [35] H. Kawakami, K. Hiraka, S. Nagaoka, Y. Suzuki, M. Iwaki, Neuronal attachment and outgrowth on a micropatterned fluorinated polyimide surface, *J Artif Organs* 7(2) (2004) 83-90.
- [36] Y.M. Yang, W.J. Zhao, J.H. He, Y.H. Zhao, F. Ding, X.S. Gu, Nerve conduits based on immobilization of nerve growth factor onto modified chitosan by using genipin as a crosslinking agent, *Eur J Pharm Biopharm* 79(3) (2011) 519-525.
- [37] X. Gu, F. Ding, D.F. Williams, Neural tissue engineering options for peripheral nerve regeneration, *Biomaterials* 35(24) (2014) 6143-56.
- [38] E. Schnell, K. Klinkhammer, S. Balzer, G. Brook, D. Klee, P. Dalton, J. Mey, Guidance of glial cell migration and axonal growth on electrospun nanofibers of poly-epsilon-caprolactone and a collagen/poly-epsilon-caprolactone blend, *Biomaterials* 28(19) (2007) 3012-25.

- [39] H. Saito, L.B. Dahlin, Expression of ATF3 and axonal outgrowth are impaired after delayed nerve repair, *BMC Neurosci* 9 (2008) 88.
- [40] Y. Tsuda, M. Kanje, L.B. Dahlin, Axonal outgrowth is associated with increased ERK 1/2 activation but decreased caspase 3 linked cell death in Schwann cells after immediate nerve repair in rats, *BMC Neurosci* 12 (2011) 12.
- [41] R.T. Uren, A.M. Turnley, Regulation of neurotrophin receptor (Trk) signaling: suppressor of cytokine signaling 2 (SOCS2) is a new player, *Front Mol Neurosci* 7 (2014) 39.
- [42] T.L. Nguyen, C.K. Kim, J.H. Cho, K.H. Lee, J.Y. Ahn, Neuroprotection signaling pathway of nerve growth factor and brain-derived neurotrophic factor against staurosporine induced apoptosis in hippocampal H19-7/IGF-IR [corrected], *Exp Mol Med* 42(8) (2010) 583-95.
- [43] M.R. Casanova, M. Alves da Silva, A.R. Costa-Pinto, R.L. Reis, A. Martins, N.M. Neves, Chondrogenesis-inductive nanofibrous substrate using both biological fluids and mesenchymal stem cells from an autologous source, *Mater Sci Eng C Mater Biol Appl* 98 (2019) 1169-1178.
- [44] E. Bacelo, M.A. da Silva, C. Cunha, S. Faria, A. Carvalho, R.L. Reis, A. Martins, N.M. Neves, Biofunctional Nanofibrous Substrate for Local TNF-Capturing as a Strategy to Control Inflammation in Arthritic Joints, *Nanomaterials-Basel* 9(4) (2019).
- [45] F. Bastami, P. Vares, A. Khojasteh, Healing Effects of Platelet-Rich Plasma on Peripheral Nerve Injuries, *J Craniofac Surg* 28(1) (2017) e49-e57.
- [46] M. Sanchez, A. Garate, D. Delgado, S. Padilla, Platelet-rich plasma, an adjuvant biological therapy to assist peripheral nerve repair, *Neural Regen Res* 12(1) (2017) 47-52.
- [47] N.P. Patel, K.A. Lyon, J.H. Huang, An update-tissue engineered nerve grafts for the repair of peripheral nerve injuries, *Neural Regen Res* 13(5) (2018) 764-774.
- [48] M. Sanchez, E. Anitua, D. Delgado, P. Sanchez, R. Prado, G. Orive, S. Padilla, Platelet-rich plasma, a source of autologous growth factors and biomimetic scaffold for peripheral nerve regeneration, *Expert Opin Biol Ther* 17(2) (2017) 197-212.
- [49] M. Hadjiconstantinou, L. McGuire, A.M. Duchemin, B. Laskowski, J. Kiecolt-Glaser, R. Glaser, Changes in plasma nerve growth factor levels in older adults associated with chronic stress, *J Neuroimmunol* 116(1) (2001) 102-6.
- [50] B.C. Lee, I.G. Choi, Y.K. Kim, B.J. Ham, B.H. Yang, S. Roh, J. Choi, J.S. Lee, D.Y. Oh, Y.G. Chai, Relation between plasma brain-derived neurotrophic factor and nerve growth factor in the male patients with alcohol dependence, *Alcohol* 43(4) (2009) 265-9.
- [51] E. Emanuele, P. Politi, M. Bianchi, P. Minoretti, M. Bertona, D. Geroldi, Raised plasma nerve growth factor levels associated with early-stage romantic love, *Psychoneuroendocrinology* 31(3) (2006) 288-94.
- [52] M.B. Levanti, A. Germana, F. de Carlos, E. Ciriaco, J.A. Vega, G. Germana, Effects of increased nerve growth factor plasma levels on the expression of TrkA and p75 in rat testicles, *J Anat* 208(3) (2006) 373-9.

[53] L. Aloe, S. Rossi, L. Manni, Altered expression of nerve growth factor and its receptors in the kidneys of diabetic rats, *J Nephrol* 24(6) (2011) 798-805.

[54] J. Liu, J.D. Li, J. Lu, J. Xing, J. Li, Contribution of nerve growth factor to upregulation of P2X(3) expression in DRG neurons of rats with femoral artery occlusion, *Am J Physiol Heart Circ Physiol* 301(3) (2011) H1070-9.

## **SECTION 5**

# **STRATEGIES FOR BONE REGENERATION**

## **Chapter VII**

# **Spatial Immobilization of Endogenous Growth Factors to Control Vascularization in Bone Tissue Engineering**

## Chapter VII

### Spatial Immobilization of Endogenous Growth Factors to Control Vascularization in Bone Tissue Engineering<sup>††</sup>

#### ABSTRACT

The intimate crosstalk, between endothelial and bone cells is essential for the reconstruction of bone defects. Indeed, a successful bone repair is greatly dependent on the formation of new blood vessels, to ensure the supply of nutrients and excretion of metabolites. Bone morphogenetic proteins (BMPs) and vascular endothelial growth factor (VEGF) are involved on cell differentiation and bone vascularization to develop viable bone tissue. Herein it is hypothesized that endogenous BMP-2 and VEGF bound in a parallel arrangement over a single nanofiber mesh (NFM) can lead to a successful osteogenic and angiogenic differentiation of mesenchymal stem cells. An engineered biofunctional system was developed comprising anti-BMP-2 and anti-VEGF antibodies immobilized over the same NFMs in a parallel pattern design, in an attempt to recreate the vasculature of a bone tissue. The osteogenic and angiogenic potential of this engineered biofunctional system was demonstrated by culturing human bone marrow-derived mesenchymal stem cells (hBM-MSCs) during 21 days without exogenous induction. A chick chorioallantoic membrane (CAM) assay showed that the engineered biofunctional system comprising endogenous BMP-2 and VEGF bound induced an increased angiogenic response. The angiogenic ability of this system, together with the osteogenic inductor BMP-2 enable obtaining an effective vascularized bone tissue engineering approach.

---

<sup>††</sup> This chapter is based on the following publication:

Casanova M. R., Oliveira C., Fernandes E. M., Reis R. L., Silva T. H., Martins A. and Neves N. M., "Spatial Immobilization of Endogenous Growth Factors to Control Vascularization in Bone Tissue Engineering", Submitted for publication.

## VII-1. INTRODUCTION

Skeletal development and fracture repair includes the synchronization of multiple events such as migration, differentiation, and activation of multiple cell types and tissues.[1] The development of a microvasculature and microcirculation is critical for the homeostasis and regeneration of living bone. Reconstruction of large bone defects still remains a major clinical orthopedic challenge, since the repair of a bone defect is not only dependent on new bone formation, but also it requires the formation of new blood vessels - angiogenesis.[2] Bone is a highly vascularized tissue and, therefore, angiogenesis is crucial for bone homeostasis and regeneration.[3, 4] Thus, both angiogenic and osteogenic processes must be considered when designing a bone graft.[5-8] Bone repair is a complex process involving chemotaxis, mitogenesis and differentiation, orchestrated by various cytokines and growth factors, in a sequential manner, starting from the wound healing process and involving into bone remodeling.[9-11] Vascular endothelial growth factor (VEGF) is a signaling protein that plays an important role in blood vessel formation.[12] Additionally, VEGF most likely enhances bone healing by its involvement in osteoblast maturation, ossification, and bone turnover.[7, 13, 14] By its side, bone morphogenetic protein-2 (BMP-2) is the most potent bone inductor and it is involved in different phases of bone repair playing a key role in skeletal tissue homeostasis.[2, 15-18] The combination of VEGF with BMP-2 may lead to augmented bone regeneration compared with that achieved by BMP-2 alone, which indicates that synergistic effects can be accomplished.[5, 6, 16, 19-21] Consequently, engineered matrices that can induce a concerted development of bone and blood vessels are very promising for the treatment of bone injuries.

Mesenchymal stem cells (MSCs) have the ability of self-renewal and differentiation into mesodermal lineages such as osteocytes, chondrocytes, cardiac muscle, and endothelial cells.[22-26] These unique biological characteristics, especially their osteogenic and angiogenic potential, make them excellent candidates for cell and tissue engineering therapies. Autologous regeneration of tissues, where both cells and bioactive factors are obtained from the same patient, is an ideal approach due to avoid an immune responses and, therefore, obviates the need for immunosuppression.[10] Platelet-rich plasma (PRP) is a refined product of autologous blood, rich in biologic factors (growth factors, cytokines, proteins, cellular components) essential to the body's response to injury.[27, 28] The use of PRP in the treatment of musculoskeletal conditions has become more frequent in recent years and several studies demonstrated that PRP is safe and can potentially accelerate or augment the bone tissue healing

process.[29-31] Platelet lysate (PL) consists of a cocktail of different growth factors (e.g., bFGF, VEGF, TGF- $\beta$ , BMPs, PDGF- $\beta\beta$ , EGF, and IGF-I) obtained from the platelets by cellular disruption, providing an autologous complex mixture of biological signals to the cells at the injury site.[31-35] Therefore, PL is a promising source of growth factors to induce MSCs differentiation and, ultimately, tissue regeneration.

Electrospun nanofibrous meshes (NFMs) are promising substrates for cell culture because of the high specific surface area, flexibility in surface functionality and the physical structure mimics the morphology of the native extracellular matrix of many connective tissues.[36, 37] Electrospun NFM surfaces were already chemically functionalized to achieve sustained delivery of various bioactive molecules [37] targeting bone tissue engineering, including dexamethasone-loaded liposomes [38] and Runt-related transcription factor 2- loaded liposomes [23]. This substrate can also be chemically modified to allow the immobilization of an antibody of interest able to bind the corresponding protein from a complex biological fluid, taking advantage of the specific and efficient interaction between an antibody and its antigen.[39, 40]

This proof-of-principle study aim to demonstrate that two growth factors can be bound in a spatial controlled way over a same nanofibrous substrate. For that, we immobilized anti-BMP-2 and anti-VEGF antibodies at the surface of an activated and functionalized NFM, on a parallel pattern design. This biofunctional system will be able to bind endogenous BMP-2 and VEGF, from human platelet lysates, envisioning an autologous vascularized bone tissue engineering strategy. The bioactivity of the bound growth factors was tested with hBM-MSCs, aiming to assessed the simultaneous induction of osteogenesis and angiogenesis on the a same nanofibrous substrate. The *in vivo* angiogenic potential of the engineered system was also assessed in a chick chorioallantoic membrane (CAM) assay.

## **VII-2. MATERIALS AND METHODS**

### **VII-2.1. Production and functionalization of electrospun polycaprolactone NFMs**

The production and surface modification of electrospun polycaprolactone (PCL) NFMs were both performed as described elsewhere.[38] Briefly, a polymeric solution of PCL (Polycaprolactone- Mn 70,000-90,000 by GPC, Sigma-Aldrich, UK) at 15% (w/v) was



prepared using an organic solvent mixture of chloroform (Fisher Scientific UK) and dimethylformamide (Fisher Scientific UK) (7:3 ratio). A voltage of 12 kV, a needle tip to ground collector distance of 20 cm, and a flow rate of 1 mL h<sup>-1</sup> were established to electrospin the PCL solution. After the complete processing of 1 mL of PCL solution, the NFM was allowed to dry. The processed NFM were cut into samples of 1.3×1.3 cm<sup>2</sup> for further assays.

The NFMs surfaces were activated by UV-ozone irradiation followed by aminolysis.[38] Briefly, it was applied UV light (ProCleaner 220 system, Bioforce Nanoscience) during 4 minutes at both sides of the NFM, and kept under sterile conditions for the biological assays. Then, the electrospun NFMs were subjected to aminolysis to introduce primary amines onto their surface by immersion in 1M 1,6-hexanediamine (HMD) solution (Sigma-Aldrich Química, S.L., Portugal) and incubated for 1h at 37 °C.

### **VII-2.2. Optimization of antibody immobilization**

Biofunctionalization of activated NFMs with growth factors using an antibody-antigen strategy was performed as described in detail elsewhere.[39] In brief, a defined antibody was immobilized at the surface of NFMs by a covalent bond mediated by a coupling agent, namely 1-ethyl-3-(3-(dimethylamino)-propyl)carbodiimide / hydroxysuccinimide mixture (EDC/NHS; Sigma-Aldrich Química, S.L., Portugal). A 1 % (v/v) antibody solution was prepared with an EDC/NHS mixture (1:4 ratio) and incubated 15 min at room temperature (RT) for antibody activation.

The maximum immobilization capacity of the NFMs was determined for each the following non-neutralizing antibodies, anti-BMP-2 (Rabbit anti-human BMP-2, Merck Millipore, German) and anti-VEGF (Mouse anti-human VEGF (JH121), Santa Cruz Biotechnology Inc., USA). For that, a wide range of primary antibody concentrations were tested. NFMs were incubated with 200 µL of primary antibody solution for 2h at RT followed by a washing step with 0.1 M PBS. A blocking step with 3 % BSA solution (Sigma-Aldrich Química, S.L., Portugal) for 30 min at RT was performed to block non-specific antibody binding. The biofunctionalized NFM was incubated with the secondary antibody (1:200 in PBS) for 1h at RT. Alexa Fluor® 488 donkey anti-rabbit (495 nm / 519 nm) and Alexa Fluor® 594 goat anti-mouse (590 nm / 617 nm) (Life Technologies, USA) were used as secondary antibodies against rabbit anti-BMP-2 and mouse anti-VEGF antibodies, respectively. The unbound secondary antibody fluorescence was measured by a microplate reader (Synergy HT,

Bio-TEK). Negative control samples were also performed, where all antibody immobilization steps were performed in the absence of the primary antibody, which was substituted by PBS.

## VII-2.3. Engineered biofunctional system

### VII-2.3.1. Immobilization of antibodies

In order to achieve the two antibodies immobilized in a parallel pattern design over the same NFM, a patterning device was developed (**Figure VII-1**). The patterning device consist on a flat acrylic plate at the bottom and an acrylic plate with 5 slits of 0.1 cm x 1 cm. In the first stage, the anti-BMP-2 antibody was immobilized at the surface of activated NFMs using the patterning mask that allows only to functionalized the areas that are not protect by the acrylic plate. The anti-BMP-2 antibody solution was prepared at previous determined concentration, dropped (30  $\mu$ L) over each slit of the patterning device and incubated for 2h at RT. After anti-BMP-2 immobilization, a blocking step with 0.3 % BSA solution for 30 min (RT) was performed to prevent the non-specific bound of the other antibody, followed by a washing step with 0.1 M PBS. In the second stage, the patterning device was disassembled and the anti-VEGF antibody was immobilized onto the binding sites previously covered of the NFMs biofunctionalized with anti-BMP-2. Those NFMs were incubated with 200  $\mu$ L of anti-VEGF antibody solution (previous determined concentration) for 2h at RT. All of the antibody immobilization steps (washing, BSA blocking, and secondary antibody incubation) were performed as previously described for the optimization of antibody immobilization. The samples were recovered to characterize the spatial distribution of the antibodies by fluorescence inverted microscope (Axio Observer; Zeiss). The fluorescently labeled biological molecules were analyzed by the green (Alexa Fluor<sup>®</sup> 488) and red channels (Alexa Fluor<sup>®</sup> 594).

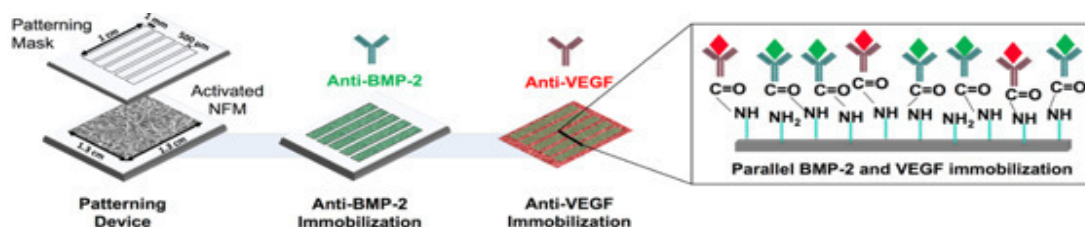


**Figure VII-1** Schematic representation of the compartments in the patterning device that allows the immobilization of antibodies in a parallel pattern design of a single NFM.

### **VII-2.3.2. Endogenous BMP-2 and VEGF binding**

The biological fluid used as an endogenous source of the growth factors (BMP-2 and VEGF) was PL. Platelet lysate (PL) was prepared from a pool of platelet concentrates obtained by plasma apheresis from six healthy O Pos male donors. Those samples were provided by Hospital de São João (HSJ, Serviço de Imunohemoterapia do Centro Hospitalar São João, Porto, Portugal) under an established collaboration protocol, approved by the ethical committee. In particular, the number of platelets were counted and concentrates with a platelet count below 1 million platelets/ $\mu\text{L}$  were rejected. Platelet concentrates were processed as previously described. [39, 41] Briefly, platelet concentrates were subjected to three freeze/thaw cycles (i.e., frozen with liquid nitrogen at  $-196\text{ }^{\circ}\text{C}$  and thawed in a  $37^{\circ}\text{C}$  water bath). The platelet debris were removed by centrifugation at  $1400g$  for 10 min at  $4^{\circ}\text{C}$  and supernatants were filtered ( $0.22\text{ }\mu\text{m}$  filter) and stored at  $-20^{\circ}\text{C}$  until further use.

The endogenous BMP-2 and VEGF binding capacity of the biofunctionalized NFMs with anti-BMP-2 and anti-VEGF antibodies, in parallel pattern design, was performed as described elsewhere.[39] Briefly, the biofunctionalized NFMs were incubated with  $400\text{ }\mu\text{L}$  of PL for 1 h (RT). The unbound protein solutions were collected and stored at  $-20\text{ }^{\circ}\text{C}$  until further quantification by *enzyme-linked immunosorbent assay* (ELISA). The quantification of BMP-2 and VEGF presented on PL samples and on the unbound protein solutions were performed to access the binding capacity of our engineered system by using the human BMP-2 and VEGF development ELISA kits (PeproTech, USA). The assay was conducted according to the respective manufacturer's protocol.

## **VII-2.4. Biological activity**

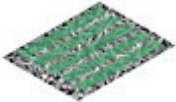
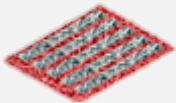
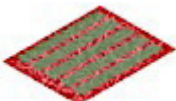
### **VII-2.4.1. hBM-MSCs isolation and culture**

hBM-MSCs were obtained from the patients undergoing knee arthroplasty after signing an informed consent under an accordance with a protocol established between the 3B's Research Group, University of Minho and the Hospital Center of Alto Ave, Guimarães, and approved by the ethics committee of this hospital. hBM-MSCs were characterized and cultured using our established standard protocols.[42] hBM-MSCs were expanded in basal medium consisting of  $\alpha\text{-MEM}$  (Sigma-Aldrich, Germany), supplemented with 10% heat-inactivated fetal bovine

serum (FBS; Life Technologies, Europe) and 1% antibiotic/antimycotic solution (FBS; Life Technologies, USA), and cultured at 37 °C in a humidified atmosphere of 5% CO<sub>2</sub>.

Before the *in vitro* studies, the NFMs were biofunctionalized with endogenous BMP-2 and/or VEGF, in parallel pattern design (**Table VII-1**), under sterile condition. Confluent hBM-MSCs at passage 4 were harvested for seeding onto these engineered biofunctional systems (*BMP-2*; *VEGF*; *BMP-2|VEGF*) at a concentration of 200000 cells/50 µL/NFM and cultured under static conditions in basal medium. The experimental controls comprise hBM-MSCs cultured on functionalized NFMs under static conditions, in *Basal medium*, standard *Osteogenic medium* (basal medium supplemented with 50 µg/mL ascorbic acid, 10 mM β-glycerophosphate and 10<sup>-7</sup> M dexamethasone) and *Angiogenic medium* (α-MEM medium supplemented with 2 % FBS and 50 ng mL<sup>-1</sup> VEGF). The constructs were retrieved at predefined culturing times, namely 0, 7, 14, and 21 days. All experiments were performed in triplicate and repeated at least three times, independently.

**Table VII-1** The engineered biofunctional systems.

CONDITIONS	BMP-2	VEGF	Pattern
<i>BMP-2</i>	Single parallel pattern (+)	(-)	
<i>VEGF</i>	(-)	Single parallel pattern (+)	
<i>BMP-2 VEGF</i>	Combined parallel pattern (+ +)		

#### VII-2.4.2. Cellular biochemistry analysis

Cell proliferation was evaluated by DNA quantification (Quant-iTPicoGreen dsDNA assay, Invitrogen, Alfacene), metabolic activity by the MTS assay (CellTiter 96 AQueous One Solution, Promega) and protein synthesis by Micro BCA assay (Micro BCA™ Protein Assay Kit, Thermo Fisher Scientific, USA), according to the manufacturer's instructions; and alkaline phosphatase specific activity by a colorimetric assay.[38]

### VII-2.4.3. Gene expression analysis

At each culturing time, the hBM-MSCs were washed with PBS, immersed in Tri reagent<sup>®</sup> (Life Science, VWR, USA), and kept at -80 °C for later RNA extraction. Total RNA was isolated and reverse transcribed into cDNA (qScript cDNA synthesis kit, Quanta Biosciences, VWR, USA), according to the manufacturer instructions. Afterwards, the obtained cDNA was used as a template for the amplification of the target genes shown in **Table VII-2**, according to manufacturer's instructions of the PerfeCta<sup>™</sup> SYBR<sup>®</sup> Green system (Quanta Biosciences, VWR, USA). The qPCR reactions were carried out in a Mastercycler<sup>®</sup> ep Gradient S realplex<sup>®</sup> thermocycler (Eppendorf; Hamburg, Germany) for all genes. The transcript expression data were normalized to the housekeeping gene *Glyceraldehydes-3-phosphate-dehydrogenase* (*GAPDH*) and the quantification performed according to the Livak method ( $2^{-\Delta\Delta CT}$  method), considering the basal medium condition (negative control) as calibrator.

**Table VII-2** Primer sequences used for RT-PCR procedures<sup>a)</sup>.

	gene	forward (5' - 3')	reverse (5' - 3')
Ref.	<i>GAPDH</i>	AGCCTCAAGATCATCAGCAA	GTCATGAGTCCTTCCACGAT
	<i>Runx 2</i>	TTCCAGACCAGCAGCACTC	CAGCGTCAACACCATCATTC
	<i>Osteocalcin</i>	GTGCAGAGTCCAGCAAAGG	TCAGCCACTCGTCACAGC
Osteogenic	<i>Osteopontin</i>	GGGGACAACCTGGAGTGAAAA	CCCACAGACCCTTCCAAGTA
	<i>Oxterix</i>	CCCTTTACAAGCACTAATGG	AACTGGGCAGACAGTCAG
	<i>BMP-2</i>	TGAATCAGAATGCAAGCAGG	TCTTTTGTGGAGAGGATGCC
	<i>ALP</i>	CTCCTCGGAAGACACTCTG	AGACTGCGCCTGGTAGTTG
	<i>COL 1<math>\alpha</math></i>	AAGAACCCCAAGGACAAGAG	GTAGGTGATGTTCTGGGAGG
Angiogenic	<i>VEGFR2</i>	AGCGATGGCCTCTTCTGTAA	ACACGACTCCATGTTGGTCA
	<i>PECAM</i>	AAGGCCAGATGCACATCC	TTCTACCCAACATTAAGTAGCAGG
	<i>VEGF A</i>	GATCCGCAGACGTGTAAATG	CTGGTGAGAGATCTGGTTCC

<sup>a)</sup> *GAPDH* = glyceraldehyde 3-phosphate dehydrogenase; *Runx 2* = Runt-related transcription factor 2; *BMP-2* = Bone morphogenetic protein 2; *ALP* = Alkaline phosphatase; *COL 1 $\alpha$*  = collagen type 1 alpha; *VEGFR2* = Vascular endothelial growth factor receptor 2; *PECAM* = Platelet and endothelial cell adhesion molecule; *VEGF A* = Vascular endothelial growth factor A.

#### **VII-2.4.4. Immunodetection of bone/vascular-specific proteins**

The osteogenic and angiogenic phenotype of hBM-MSCs seeded onto the vascularized bone tissue engineered system was assessed by immunodetection of bone-specific proteins and endothelial cell markers. Samples were collected at 21 days of culture, fixed in a 10% paraformaldehyde solution, and kept at 4 °C until further used. Immunocytochemistry was performed following the streptavidin/biotin peroxidase complex approach (R.T.U. VECTASTAIN® Universal ABC Elite® Kit; Vector Laboratories; USA), using a rabbit polyclonal antibody against osteopontin (Abcam Ltd., UK; dilution 1:1000), a mouse monoclonal antibody against osteocalcin (clone OC4-30, Abcam Ltd., UK; dilution 1:100), a goat polyclonal antibody against collagen type I $\alpha$ I (COL1A1 (C-18); Santa Cruz Biotechnology, Europe; dilution 1:2500), a rabbit polyclonal antibody against Von Willebrand Factor (vWF; Abcam Ltd., UK; dilution 1:400), a mouse monoclonal antibody against CD31 (P2B1; Abcam Ltd., UK; dilution 1:100). Briefly, the samples were treated with 0.3% hydrogen peroxide solution for 30 min to inactivate the endogenous peroxidase activity. After blocking unspecific binding, primary antibodies were incubated overnight at 4 °C, followed by the biotinylated secondary antibody and the streptavidin-peroxidase complex incubations. The immune reaction was revealed by using the Peroxidase Substrate Kit (DAB) (Vector Laboratories; USA). By the end, samples were washed in water for 5 min and then counterstained with hematoxylin for nuclei visualization. The samples were mounted and observed in an optical microscope (Leica DM750 microscope).

#### **VII-2.5. *In vivo* angiogenesis evaluation**

##### **VII-2.5.1. Chick chorioalantoic membrane (CAM) assay**

Fertilized chicken eggs from Pinto Bar (Portugal) were incubated at 37°C (Laboratory Incubator model B8420; Termarks) for 3 days. A window was open into the eggshell to evaluate embryo viability, after puncturing the air chamber, to allowed dissociation of the CAM from the shell membrane. The window was then sealed with transparent tape (~50 x 30 mm, AXTON 50 mm) to prevent dehydration. On the 10<sup>th</sup> day of embryonic development, the engineered biofunctional systems (**Table VII-1**) and controls (without NFM and with activated NFM) were placed on the CAM. At the 17<sup>th</sup> day, the chicken embryos were sacrificed by adding a

paraformaldehyde (Merck) solution at 4% (v/v), followed by its incubation at -80° C for 10 min. The implanted specimens and the immediately adjacent CAM portions were cut and fixed with 4% paraformaldehyde. *Ex ovo* images were captured using the AxioVision imaging software (release 4.8; Zeiss) connected to an AxioCAM ICc1 digital camera (Zeiss) attached to a stereomicroscope (Stemi 2000- C; Zeiss), for each condition in both sides (i.e. chorionic and allantoic epithelium). Three independent CAM assays were performed and a minimum of 10 eggs/samples were used for each condition.

### **VII-2.5.2. Analysis of blood vessel convergence**

The macroscopic evaluation of the angiogenic response was carried out using a semiquantitative method previously described by Ribatti, *et al.*, [43] which consists in analyzing the convergence of blood vessels toward the implanted engineered biofunctional systems. The chorionic epithelium images (*ex ovo*) obtained at day 17 of embryonic development were processed using the ImageJ 1.52a software program (National Institutes of Health, USA) to count the total number of blood vessels converging toward the implanted scaffolds. For quantification purposes, the magnification of the stereomicroscope images was kept constant (0.65 X), as well as the image-processed area (800 x 800 pixels). The total number of macroscopic microvessels that converged toward the graft was counted blindly for each egg by three independent observers.

An automated angiogenesis quantification method was also conducted by using the *Vessel Analysis* plugin with Fiji (ImageJ 1.52i) to perform in a reliable and repeatable way a sequence of operations leading to a robust segmentation of EC images and a reproducible extraction of the skeleton representing the microvascular network.[44] Measurements of vascular density (i.e. ratio of vasculature area to total selection area) and vascular length density (i.e. ratio of skeletonized vasculature area to total area) are expressed as % area.

### **VII-2.6. Statistical analysis**

Statistical analysis was performed using the SPSS statistic software (release 24.0.0.0 for Mac). First, a Shapiro-Wilk test was used to ascertain the data normality and Levene test for the homogeneity of variances. When data follow a normal distribution, parametric tests were used (one-way ANOVA test followed by Tukey's HSD test). When the normality and variance

homogeneity were rejected, non-parametric tests were used (Kruskal-Wallis test followed by Tukey's HSD test). *P* values than 0.01 were considered statistically significant in non-parametric tests.

### VII-3. RESULTS

#### VII-3.1. Development and characterization of the engineered biofunctional systems

Prior to the development of the engineered biofunctional system, BMP-2 and VEGF antibodies were immobilized at the surface of NFMs. The maximum immobilization capacity of each antibody (anti-BMP-2 or anti-VEGF) was determined by using an indirect quantification method (**Figure VII-2 a, b**). The fluorescence signal of the unbound secondary antibody correlates inversely with the amount of immobilized primary antibody. The maximum immobilization capacity of the nanofibrous substrate is  $6 \mu\text{g mL}^{-1}$  for anti-BMP-2 antibody and  $4 \mu\text{g mL}^{-1}$  for anti-VEGF antibody, representing the saturation point of the nanofibrous substrate.

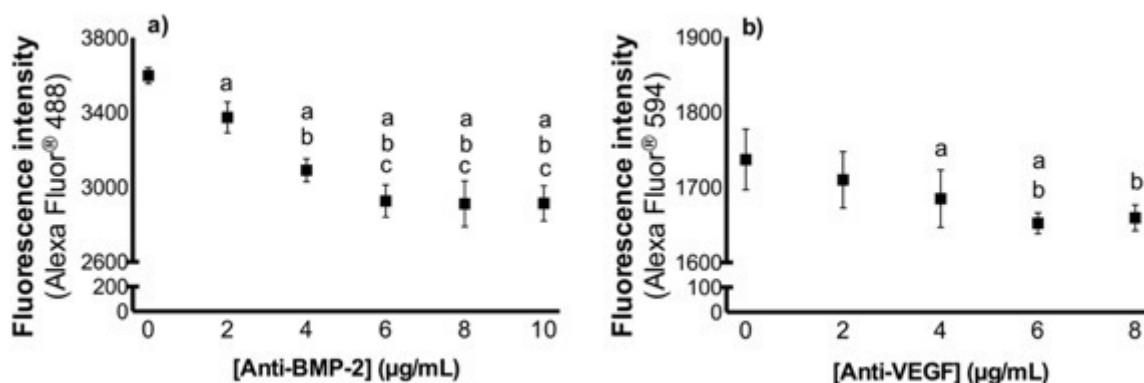


**Figure VII-2** Maximum immobilization capacity of a single antibody at the surface of activated and functionalized NFM: immobilization of anti-BMP-2 (a) and immobilization of anti-VEGF (b). Data were analyzed by the one-way ANOVA test, followed by the Tukey's HSD test ( $p < 0.01$ ): *a* denotes significant differences compared to concentration  $0 \mu\text{g mL}^{-1}$ ; *b* denotes significant differences compared to concentration  $2 \mu\text{g mL}^{-1}$  and *c* denotes significant differences compared to concentration  $4 \mu\text{g mL}^{-1}$ .

To develop an engineered biofunctional system envisioning a vascularized bone tissue engineering approach, the antibodies against BMP-2 and VEGF were immobilized over the



same nanofibrous substrate, in a parallel pattern design. Both antibodies were successfully immobilized at  $4 \mu\text{g mL}^{-1}$  since it corresponds to the maximum concentration achieved for anti-VEGF. In this sense, hBM-MSCs will have access to the same amount of bound PL-derived growth factors. A patterning mask was in house developed to enable the creation of distinct areas on the same nanofibrous substrate (**Figure VII-1**). The NFMs were firstly incubated with anti-BMP-2 antibody, using the patterning mask, followed by the incubation of VEGF antibody. By the end, NFMs with parallel immobilized anti-BMP-2 and anti-VEGF antibodies were incubated with the corresponding secondary antibodies, leading to the patterned configuration and distribution presented in **Figure VII-3**. The reddish fluorescent area of the nanofibrous substrate corresponds to the immobilized anti-VEGF antibody whereas the green area represents the immobilized anti-BMP-2 antibody (**Figure VII-3 c**). In the nanofibrous substrate with immobilized anti-BMP-2, it was not detected fluorescence on the anti-VEGF antibody immobilization area (**Figure VII-3 a**); as well as, no fluorescence was observed on the nanofibrous substrate with immobilized anti-VEGF (**Figure VII-3 b**) on the anti-BMP-2 antibody immobilization area. Activated and functionalized nanofibrous substrate without primary antibodies immobilization was used as a control of the parallel immobilization process (**Figure VII-3 d**).

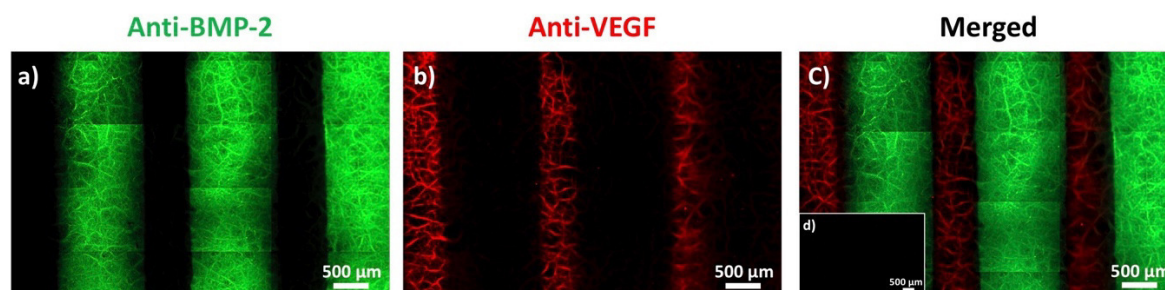


**Figure VII-3** Spatial distribution of immobilized primary antibodies at the surface of activated and functionalized nanofibrous substrates, in a parallel pattern design:  $4 \mu\text{g mL}^{-1}$  anti-BMP-2 (a);  $4 \mu\text{g mL}^{-1}$  VEGF (b); merged view (c) and activated and functionalized nanofibrous substrates without primary antibodies immobilization (d).

The herein engineered biofunctional system comprising parallel immobilized anti-BMP-2 and anti-VEGF was capable of selectively bound the respective growth factor from a biological fluid (i.e. PL). The binding capacity of the engineered biofunctional system was assessed by quantifying the total amount of the proteins of interest (BMP-2, VEGF) that can bound to the biofunctionalized nanofibrous substrate (**Table VII-3**). The herein used PL samples present BMP-2 and VEGF concentrations ranging from 106 to 781  $\mu\text{g mL}^{-1}$  and 702 to 1536  $\mu\text{g mL}^{-1}$ ,

respectively. These concentrations are within the range of values reported in the literature, i.e. from 310 to 1500  $\mu\text{g mL}^{-1}$  of BMP-2 [45, 46] and from 0.0949 to 854  $\text{ng mL}^{-1}$  of VEGF [47]. Those PL-derived proteins were successfully bound to the biofunctionalized nanofibrous substrate at the similar amount of the pool PL-derived growth factors, namely  $379 \pm 34 \mu\text{g mL}^{-1}$  of BMP-2 and  $403 \pm 7 \mu\text{g mL}^{-1}$  of VEGF.

**Table VII-3 Quantification of the growth factors of interest (i.e. BMP-2, VEGF) derived from human PL samples and the binding capacity of the engineered biofunctional system.**

$(\mu\text{g mL}^{-1})$		Donor 1	Donor 2	Pool <sup>a)</sup>
<b>BMP-2</b>	[PL]	$106 \pm 71$	$781 \pm 39$	$473 \pm 57$
	bound	$98 \pm 7$	$596 \pm 1145$	$379 \pm 34$
<b>VEGF</b>	[PL]	$702 \pm 49$	$1536 \pm 136$	$932 \pm 7$
	bound	$286 \pm 9$	$747 \pm 21$	$403 \pm 7$

<sup>a)</sup> Pool of six independent donors;

### VII-3.2. Differentiation of hBM-MSCs on the engineered biofunctional systems

The effectiveness of the engineered biofunctional systems comprising endogenous BMP-2 and/or VEGF parallel bound (**Table VII-1**) were assessed by culturing hBM-MSCs during 21 days in basal medium. Activated NFMs cultured with hBM-MSCs under standard osteogenic or angiogenic differentiation media were used as positive controls, while bare NFM constructs cultured under basal medium were used as negative control.

The biochemical performance of hBM-MSCs cultured on the engineered biofunctional systems was assessed by using standard cell biology assays, namely cell viability (MTS assay), cell proliferation (PicoGreen assay) and total protein synthesis (MicoBCA assay) (**Figure VII-4**). Biological data demonstrate that, the different culture conditions did not induce significant changes over hBM-MSCs activity along the culturing time ( $p < 0.01$ ). Moreover, hBM-MSCs cultured on the engineered biofunctional systems with endogenous BMP-2 and VEGF parallel bound ( $BMP-2|VEGF$ ) or in single parallel pattern design ( $BMP-2$ ;  $VEGF$ ) seems to have higher viability and proliferation when compared to the positive control conditions (*Osteogenic medium*; *Angiogenic medium*), although not statistically significant. In terms of the hBM-MSCs' total protein synthesis (**Figure VII-4c**) no statistically significant differences were

observed between the different culture conditions over the culturing time. The hBM-MSCs cultured on the engineered biofunctional systems displayed a high protein concentration than the control conditions.

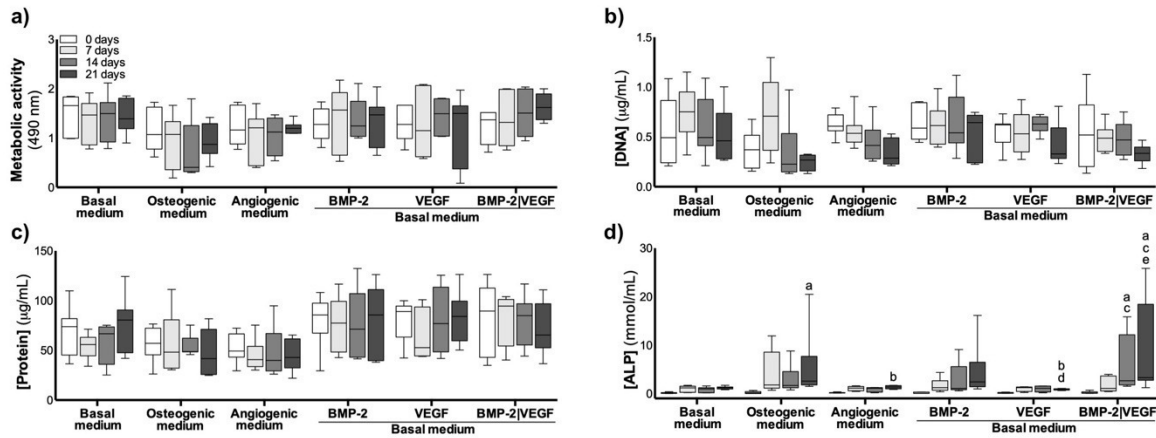


**Figure VII-4** Biochemical performance (i.e. metabolic activity (a) and proliferation (b), total protein synthesis (c) and ALP activity (d) of the hBM-MSCs cultured on nanofibrous substrates with endogenous BMP-2 and/or VEGF parallel bound, under basal medium. Activated NFMs cultured with hBM-MSCs under standard Osteogenic or Angiogenic differentiation media were used as positive controls, while NFM/hBM-MSCs constructs cultured under Basal medium was used as negative control. Data were analysed by the Kruskal-Wallis test, followed by the Tukey's HSD test ( $p < 0.01$ ): *a* denotes significant differences compared to *Basal medium*; *b* denotes significant differences compared to *Osteogenic medium*; *c* denotes significant differences compared to *Angiogenic medium*; *d* denotes significant differences compared to *BMP-2*; *e* denotes significant differences compared to *VEGF*;

In order to assess the onset of the osteoblastic activity of cultured hBM-MSCs, the quantification of the alkaline phosphatase activity was performed according to the p-nitrophenol assay. As shown in **Figure VII-4d**, the *Osteogenic medium* condition and the constructs that contained BMP-2 (*BMP-2*; *BMP-2|VEGF*) exhibited higher ALP activity. Particularly, the engineered biofunctional construct (*BMP-2|VEGF*) showed significantly higher ALP activity, indicating some synergetic effect of both growth factors over the osteogenic differentiation.

A genotypic quantification of osteogenic and angiogenic transcripts was performed to ascertain about the differentiation level of the cultured hBM-MSCs on the engineered biofunctional systems. A constitutive expression of all osteogenic mRNA transcripts was observed during the culture time for the osteogenic conditions (*Osteogenic medium*, *BMP-2* and *BMP-2|VEGF*), presenting significantly higher expression when compared with the angiogenic conditions (*Angiogenic medium*, *VEGF* and *BMP-2|VEGF*) ( $p < 0.01$ ) (**Figure VII-**

5). At 14 days, hBM-MSMs cultured on engineered biofunctional systems, *BMP-2* and *BMP-2|VEGF*, presented significantly higher Collagen type I $\alpha$  expression than the positive osteogenic condition (*Osteogenic medium*;  $p < 0.01$ ). Nevertheless, the constructs cultured under *Osteogenic medium* presents significantly higher ALP expression ( $p < 0.01$ ), at 7 days, when compared to the *BMP-2* constructs, since those conditions did not have a source of phosphate in the culture medium. Moreover, the engineered biofunctional systems (*BMP-2*; *BMP-2|VEGF*) are effective in promoting the Runx 2 expression as the osteogenic condition (*Osteogenic medium*).

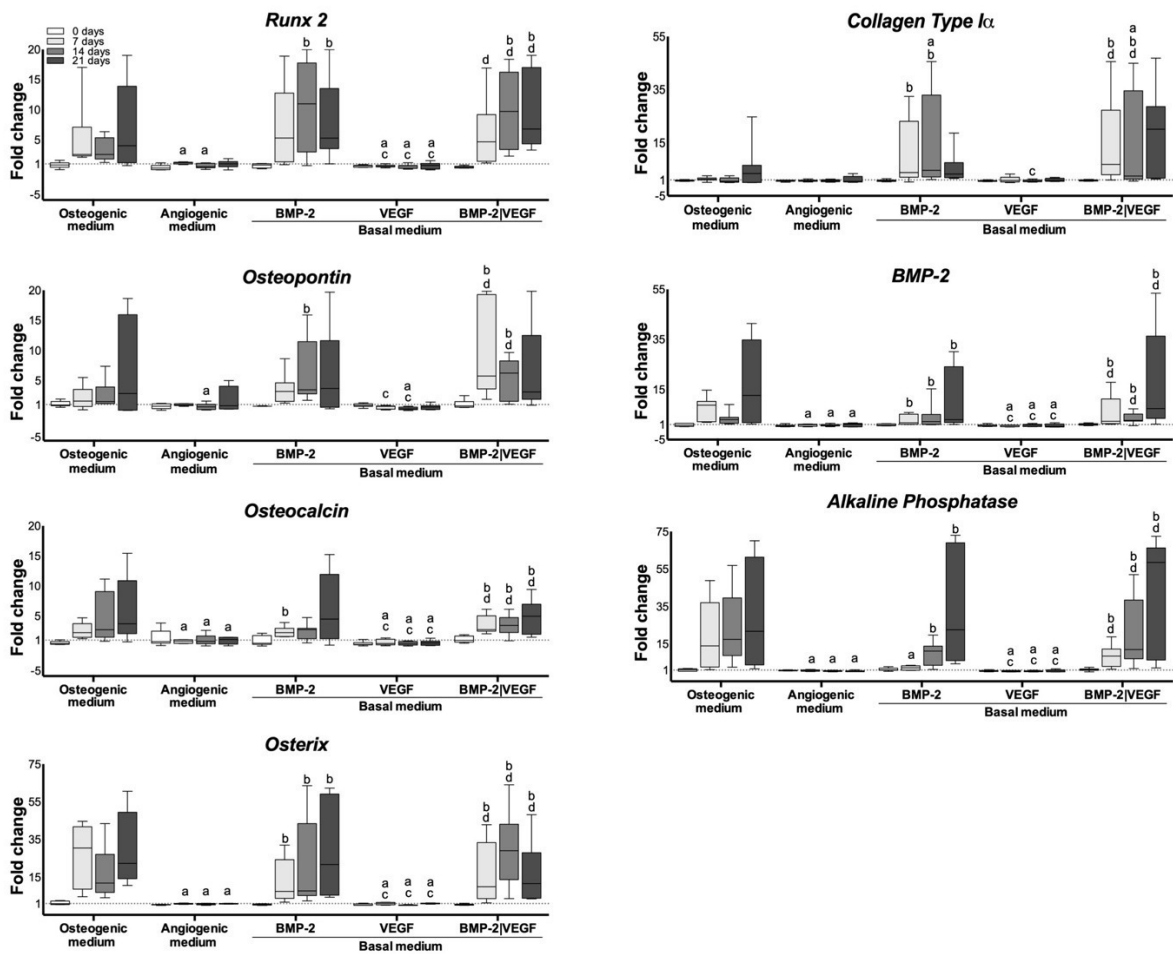
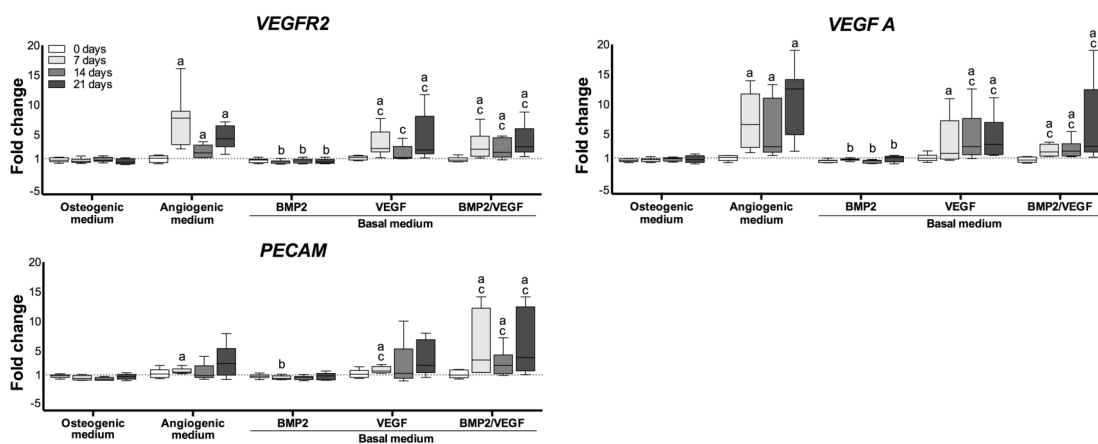


Figure VII-5 Relative expression of osteogenic markers by hBM-MSCs cultured on engineered biofunctional systems. The expression was normalized against the GAPDH gene and the quantification was performed according to the Livak method. Data were analysed by the Kruskal-Wallis test, followed by the Tukey's HSD test ( $p < 0.01$ ): a denotes significant differences compared to Basal medium; b denotes significant differences compared to *Osteogenic medium*; c denotes significant differences compared to *Angiogenic medium*; d denotes significant differences compared to *BMP-2*; e denotes significant differences compared to *VEGF*;

The quantification of angiogenic transcripts expression revealed that in the *Angiogenic medium*, *VEGF* and *BMP-2|VEGF* conditions, hBM-MSCs expressed endothelial-related genes (**Figure VII-6**). Those conditions present significantly higher expression when compared with hBM-MSCs cultured under *Osteogenic medium* and *BMP-2* constructs ( $p < 0.01$ ). In terms of VEGFR2, PECAM and VEGF A expression, no statistically significant differences were found between the angiogenic conditions (*Angiogenic medium*, *VEGF* and *BMP-2|VEGF*). However, when comparing the PECAM expression levels of the engineered biofunctional system (*BMP-2|VEGF*) with the positive osteogenic condition (*Osteogenic medium*), it is more effective in promoting the expression of PECAM gene.



**Figure VII-6** Relative expression of angiogenic markers by hBM-MSCs cultured on engineered biofunctional systems. The expression was normalized against the GAPDH gene and the quantification was performed according to the Livak method. Data were analysed by the Kruskal-Wallis test, followed by the Tukey's HSD test ( $p < 0.01$ ): a denotes significant differences compared to *Basal medium*; b denotes significant differences compared to *Osteogenic medium*; c denotes significant differences compared to *Angiogenic medium*; d denotes significant differences compared to *BMP-2*; e denotes significant differences compared to *VEGF*;

The osteogenic and angiogenic phenotype of hBM-MSCs cultured on the different culture conditions, at 21 days, was also assessed by immunodetection of some specific osteoblastic proteins (i.e. collagen type I $\alpha$ , osteocalcin and osteopontin) and endothelial cell markers (i.e. CD31 and vWF) (**Figure VII-7**). Photomicrographs shown an expression of the specific osteoblastic glycoprotein assessed on the *Osteogenic medium*, *BMP-2* and *BMP-2|VEGF* constructs, indicating their capacity to induce the deposition of a mineralized extracellular matrix. Interestingly, on the *BMP-2* and *BMP-2|VEGF* constructs, the stained areas correspond to the parallel alignment of the endogenous BMP-2 bound at the surface of the NFMs substrates. Similar endothelial cell markers expression pattern was observed on the *VEGF* and *BMP-*

2|*VEGF* constructs, where the stained areas correspond to the parallel alignment of the endogenous VEGF bound at the NFMs surface. The expression of endothelial cell markers by hBM-MSCs cultured under Angiogenic medium was also observed. On the other hand, as expected, the osteogenic and/or angiogenic phenotype of the hBM-MSCs was not observed when cultured on the *Basal Medium*, *Osteogenic Medium*, *Angiogenic Medium*, *BMP-2* and *VEGF* conditions.

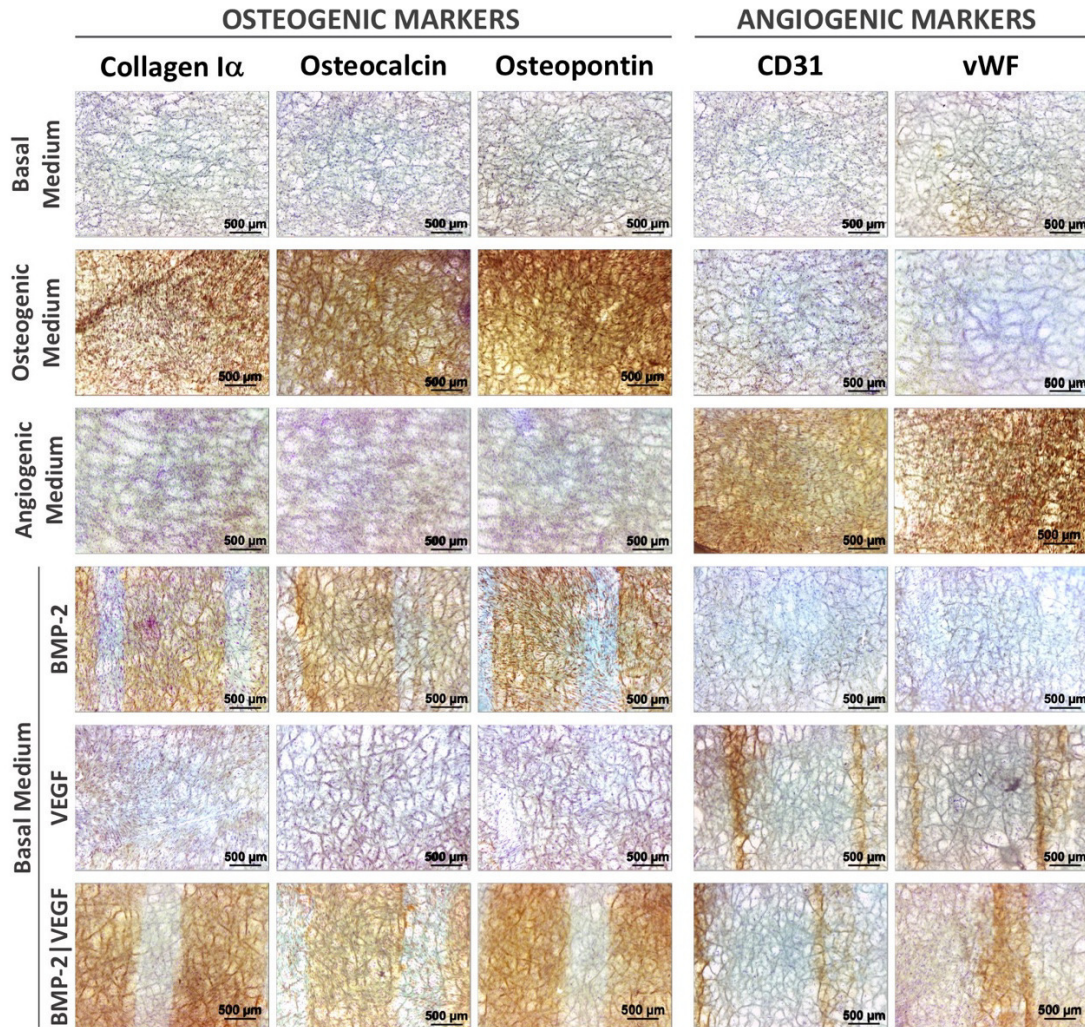
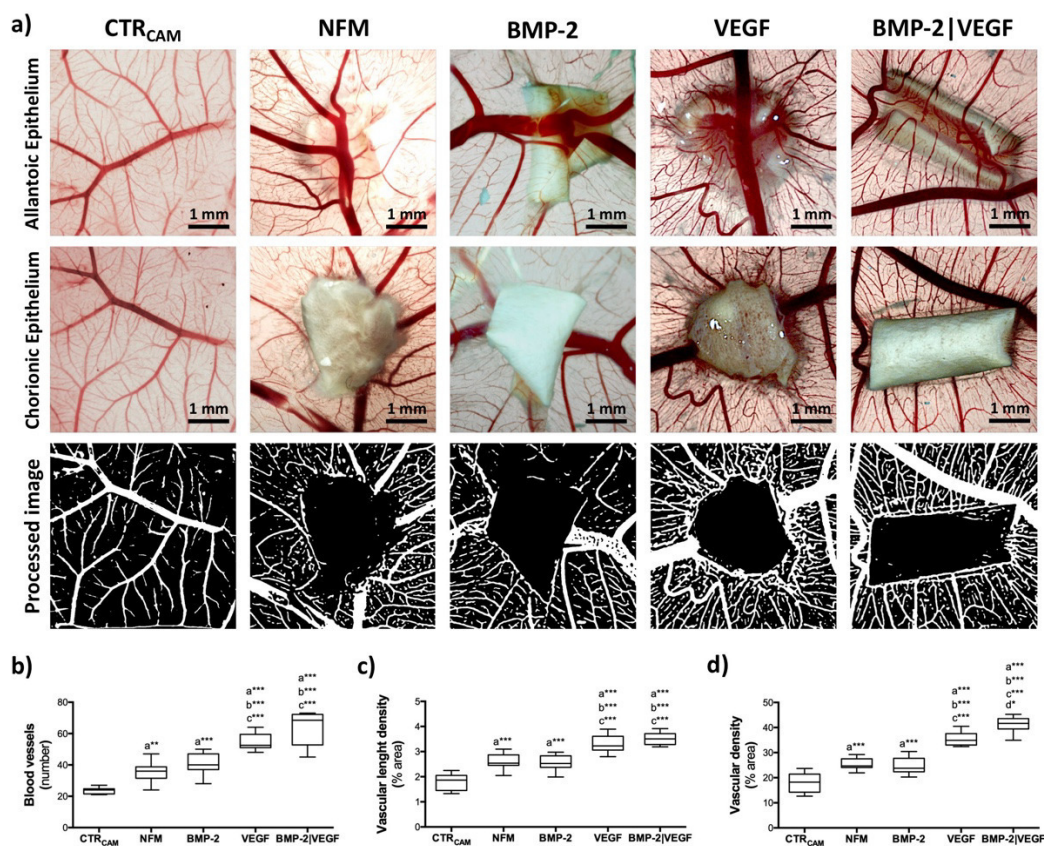


Figure VII-7 Immunoexpression of osteogenic (Collagen  $\alpha$ ; Osteocalcin; Osteopontin) and angiogenic (CD31; vWF) markers in engineered biofunctional systems, after 21 days of culture (10X magnifications).

### VII-3.3. Construct Angiogenic potential of the engineered biofunctional systems

CAM assay was carried out in order to evaluate *in vivo* the ability of the proposed engineered biofunctional system to induce angiogenesis. Representative photographs of the

chorionic and allantoic epithelium of *ex ovo* CAM after 7 days of implantation were presented in **Figure VII-8a**, where the engineered biofunctional systems comprising endogenous BMP-2 and/or VEGF parallel bound were used. Eggs without NFMs and with the activated NFMs were the controls, used in our test. The NFMs substrates significantly increased the sprouting of mature vasculature (**Figure VII-8b**). In the case of the engineered biofunctional systems comprising endogenous VEGF (*VEGF* and *BMP2|VEGF* conditions), large number of mature blood vessels with highly branched capillary network could be observed. On the other hand, the activated NFM and the engineered biofunctional systems comprising endogenous BMP-2 did not induce a significant angiogenesis, as expected.



**Figure VII-8** Stereomicroscope photographs of *ex ovo* NFMs substrates after incubation on the chorioallantoic membrane of the chick embryo (a). Macroscopic quantification of blood vessels conversing towards implanted structures (b). Vascular Length Density (i.e. ratio of skeletonized vasculature area to total area) (c), and Vascular Density (i.e. ratio of vasculature area to total selection area) (d). Data were analysed by the Kruskal-Wallis test, followed by the Tukey's HSD test (\* $p < 0.01$ ; \*\* $p < 0.001$ ; \*\*\* $p < 0.0001$ ): *a* denotes significant differences compared to *CTR<sub>CAM</sub>*; *b* denotes significant differences compared to *NFM*; *c* denotes significant differences compared to *BMP-2*; *d* denotes significant differences compared to *VEGF*;

To quantify the convergence of blood vessels towards the implanted engineered biofunctional systems, the vascular length density and the vascular density was investigated by analyzing the *ex ovo* chorionic epithelium (**Figure VII-8 c and d**). All the conditions assessed showed statistically significant proangiogenic property compared to the control CAM ( $p < 0.0001$ ), including the bare NFM substrate ( $p < 0.001$ ). Furthermore, there was no statistical significance between the activated NFM and engineered biofunctional system comprising endogenous BMP-2. When comparing the engineered biofunctional systems comprising endogenous VEGF, both the *VEGF* and *BMP-2|VEGF* conditions showed statistically significant higher proangiogenic activity ( $p < 0.0001$ ). Considering those results, it is clear that the engineered biofunctional systems comprising endogenous VEGF (*VEGF* and *BMP-2|VEGF* conditions) are the most proangiogenic ones. Nevertheless, the *BMP-2|VEGF* condition present significantly higher vascular density, when compared to the *VEGF* condition ( $p < 0.01$ ), showing some synergic effect of the two inductors.

#### VII-4. DISCUSSION

Considerable efforts have been made to create biofunctional bone tissue engineered constructs. However, low bone regeneration levels and insufficient vascularization remain the most important challenges that must be overcome to develop effective tissue engineering strategies, in order to be consistently implemented in the reconstruction of large volume bone defects.[3, 37, 48] An active and functional blood vessel network is an essential pre-requisite in the survival and integration of a bone tissue engineered construct within an existing host tissue. A variety of strategies have been implemented trying to enhance the formation of vascular networks within the engineered constructs for bone regeneration. These strategies include growth factor delivery, co-culture systems, biomaterials with appropriate mechanical properties and incorporation of microfabricated cues.[4, 20, 49-57] Herein, we present a novel approach for upgrading a nanofibrous substrate with spatially bound growth factors, in order to locally induce the differentiation of MSCs into either osteogenic or endothelial lineage. Furthermore, it allows the patterning of endogenous growth factors, defining vascularization areas adjacent to the new target tissue formation, by using cells from the own patient.

In a bone fracture healing process, the expression of VEGF occurs at an early healing stage (strongly observed in 5-10 days),[58] while the BMP-2 secretion occurs during the entire process.[59] Based on this information from wound healing, endogenous BMP-2 and VEGF



were bound at the surface of a nanofibrous substrate, in a parallel pattern design, envisioning an autologous vascularized bone tissue engineering approach. To fulfil this design, a patterning device was developed with the intent to enable immobilizing non-neutralized anti-BMP-2 and anti-VEGF antibodies that recognize non-binding sites of those growth factors. These antibodies were able to selectively bind the respective growth factors obtained from platelet lysates. The engineered biofunctional system comprising immobilized anti-BMP-2 and anti-VEGF antibodies, in a side-by-side fashion, was able to bound  $378.2 \pm 280 \mu\text{g mL}^{-1}$  and  $403 \pm 4 \mu\text{g mL}^{-1}$  of pool PL-derived BMP-2 and VEGF, respectively.

The scientific literature reported that bound growth factors can maintain their bioactivity over time, providing a more controlled and sustained induction over cells in culture when compared to the transient effect of soluble growth factors.[16, 20, 39, 60] Moreover, bound growth factors can provide extended signaling because the ligand is not internalized as a ligand/receptor complex.[61-64] Using the herein presented strategy, we can promote a spatial regulation and control over cellular activity, namely the osteogenic and angiogenic differentiation of hBM-MSCs. Therefore, to determine the bioactivity of parallel bound BMP-2 and VEGF at the surface of a nanofibrous substrate, osteogenic and angiogenic phenotyping and genotyping was conducted. ALP activity results demonstrated that the engineered biofunctional nanofibrous substrates comprising BMP-2 are able to successfully induce the osteogenic differentiation of hBM-MSCs, even in the absence of organic or inorganic phosphate source (e.g.  $\beta$ -Glycerophosphate and monosodium phosphate). Indeed, previous studies have demonstrated that BMP-2 enhanced the osteogenic differentiation capacity of MSCs by increasing ALP activity.[6, 16, 59, 65, 66] Conversely, the presence of VEGF showed no influence on the ALP activity, suggesting that VEGF alone cannot effectively enhance the osteogenic differentiation *in vitro*. Although, the presence of both BMP-2 and VEGF present a synergetic effect enhancing the ALP activity.

A successful bone regeneration strategy implies the formation of new blood vessels. Therefore, it is desirable to deliver of a growth factors cascade (in this case VEGF and BMP-2) to simultaneously induce angiogenesis and osteogenesis to develop a vascularized and functional bone tissue graft. As demonstrated by Wang *et al.*, the *in vitro* delivery of low doses of BMP-2 and VEGF by a silk fibroin-nanohydroxyapatite scaffold resulted in vascularized bone regeneration.[20] Shah *et at.* developed a dual delivery system where different ratios of BMP-2 and VEGF were entrapped within polyelectrolyte multilayer (PEM) films.[8] After implantation, the mineral density within the *de novo* bone was increased by 33% in the PEM

films containing both BMP-2 and VEGF when compared to those containing BMP-2 only, which suggests a more complete remodeling due to an increase local vascular network. The herein engineered biofunctional system present the highest osteogenic activity, indicating that the bound VEGF did not interfere with the bioactivity of BMP-2, but instead provide a synergetic effect on the development of osteogenesis. These observations were supported by the expression of osteogenic and angiogenic transcripts. As expected, the highest expression of osteogenic markers was observed when BMP-2 is presented, while high expression of angiogenic markers was observed only on the constructs having VEGF. Accordingly, the histological analysis of the vascularized bone tissue engineered system indicated that hBM-MSCs positively label for osteoblastic proteins on the areas corresponding to the parallel bound endogenous BMP-2, whereas angiogenic markers are present on the areas corresponding to the parallel bound endogenous VEGF.

Using the chick CAM *in vivo* angiogenic model, we demonstrated that the engineered biofunctional system comprising endogenous BMP-2 and VEGF bound in a side-by-side fashion presented a significantly higher angiogenic capacity. The vascular invasion showed in the engineered biofunctional systems could be attributed to bound VEGF presented in the NFM substrates. In fact, the *in vivo* angiogenic potential of a described bioscaffold was associated with matrix-dependent delivery/release of VEGF.[67-69] Interestingly, the presence of both BMP-2 and VEGF present a synergetic effect enhancing the angiogenic capacity of the engineered biofunctional system. Our results are in line with others reported in the literature,[20, 54, 70, 71] supporting the hypothesis that VEGF could indirectly enhance bone regeneration by promoting the formation of a vascular network.

Envisioning the clinical translation of the vascularized bone tissue engineered system herein reported, we foreseen its potential use as a guided bone regeneration membrane applied in the internal fixture of bone fractures or as a substrate accelerating healing in flat bones (i.e. cranial bones, scapulae). Indeed, electrospun nanofibrous meshes were applied as a scaffold to improve bone formation in a critical-sized rat calvarial bone defect model system [72-74]. Therefore, it is hypothesized that, by creating an initial synthetic ECM architecture with spatially localized growth factors, cells will be guide into either osteogenic or endothelial lineage, facilitating the formation of a neo-tissue with enhanced functional characteristics. The application of the spatially localized growth factors bound on biomaterial substrate for the regeneration of complex tissues, involving more than one cell communities, may provide helpful cues enabling its self-organized.

## VII-5. CONCLUSIONS

This proof-of-principle study showed that two growth factors can be bound parallel in an arrangement on the same nanofibrous substrate, remaining bioactivity upon bounding the immobilized antibodies. A vascularized bone tissue engineered system was developed, comprising endogenous BMP-2 and VEGF bound in a side-by-side fashion, envisioning its use as autologous bone regeneration. Our data demonstrates that this system containing BMP-2 is able to promote the osteogenic differentiation of hBM-MSCs, as well as, the bound VEGF is able to promote angiogenesis. Therefore, the herein proposed biofunctional system is able to promote spatial angiogenesis and osteogenesis of hBM-MSCs, resulting in a synergistic effect on vascularized bone regeneration. The *in vivo* study revealed that the engineered biofunctional system comprising endogenous BMP-2 and VEGF bound in a parallel arrangement present a higher angiogenic effect. Our experiments provide new evidences supporting the application of these biofunctionalized nanofibrous substrates to develop vascularized bone tissue engineering strategies and to help bone fracture healing, particularly when vascularization is severally compromised.

## VII-6. ACKNOWLEDGEMENTS

The authors would like to acknowledge Norte 2020, for financing the PhD scholarship of C.O. (Norte-08-5369-000037) and Portuguese Foundation for Science and Technology (FCT) for the PhD grant of M.R.C. (PD/BD/113797/2015) financed by the FCT Doctoral Program on Advanced Therapies for Health (PATH) (FSE/POCH/PD/169/2013), the post-doctoral grant of E.M.F (SFRH/BPD/96197/2013), the IF grant of A.M. (IF/00376/2014), and the projects SPARTAN (PTDC/CTM-BIO/4388/2014) and FRONthera (NORTE-01-0145-FEDER-000023).

This work was developed under the framework of the Cooperation Agreement established with the Serviço de Imuno-Hemoterapia do Centro Hospitalar de S. João, EPE.

## VII-7. REFERENCES

[1] C. Colnot, D.M. Romero, S. Huang, J.A. Helms, Mechanisms of action of demineralized bone matrix in the repair of cortical bone defects, *Clin Orthop Relat Res* (435) (2005) 69-78.

- [2] S. Almubarak, H. Nethercott, M. Freeberg, C. Beaudon, A. Jha, W. Jackson, R. Marcucio, T. Miclau, K. Healy, C. Bahney, Tissue engineering strategies for promoting vascularized bone regeneration, *Bone* 83 (2016) 197-209.
- [3] U. Saran, S.G. Piperni, S. Chatterjee, Role of angiogenesis in bone repair, *Arch Biochem Biophys* 561 (2014) 109-117.
- [4] C.C. Yang, B. Han, C.L. Cao, D. Yang, X.Z. Qu, X.Y. Wang, An injectable double-network hydrogel for the co-culture of vascular endothelial cells and bone marrow mesenchymal stem cells for simultaneously enhancing vascularization and osteogenesis, *J Mater Chem B* 6(47) (2018).
- [5] N. Cakir-Ozkan, S. Egri, E. Bekar, B.Z. Altunkaynak, Y.B. Kabak, E.G. Kivrak, The Use of Sequential VEGF- and BMP2-Releasing Biodegradable Scaffolds in Rabbit Mandibular Defects, *J Oral Maxil Surg* 75(1) (2017).
- [6] R. Subbiah, M.P. Hwang, S.Y. Van, S.H. Do, H. Park, K. Lee, S.H. Kim, K. Yun, K. Park, Osteogenic/angiogenic dual growth factor delivery microcapsules for regeneration of vascularized bone tissue, *Adv Healthc Mater* 4(13) (2015) 1982-92.
- [7] W.L. Xu, H.S. Ong, Y. Zhu, S.W. Liu, L.M. Liu, K.H. Zhou, Z.Q. Xu, J. Gao, Y. Zhang, J.H. Ye, W.J. Yang, In Situ Release of VEGF Enhances Osteogenesis in 3D Porous Scaffolds Engineered with Osterix-Modified Adipose-Derived Stem Cells, *Tissue Eng Part A* 23(9-10) (2017) 445-457.
- [8] N.J. Shah, M.L. Macdonald, Y.M. Beben, R.F. Padera, R.E. Samuel, P.T. Hammond, Tunable dual growth factor delivery from polyelectrolyte multilayer films, *Biomaterials* 32(26) (2011) 6183-93.
- [9] Z.S. Ai-Aql, A.S. Alagl, D.T. Graves, L.C. Gerstenfeld, T.A. Einhorn, Molecular mechanisms controlling bone formation during fracture healing and distraction osteogenesis, *J Dent Res* 87(2) (2008) 107-18.
- [10] S.J. Forbes, N. Rosenthal, Preparing the ground for tissue regeneration: from mechanism to therapy, *Nat Med* 20(8) (2014) 857-69.
- [11] S. Stegen, G. Carmeliet, The skeletal vascular system - Breathing life into bone tissue, *Bone* 115 (2018) 50-58.
- [12] H.P. Gerber, T.H. Vu, A.M. Ryan, J. Kowalski, Z. Werb, N. Ferrara, VEGF couples hypertrophic cartilage remodeling, ossification and angiogenesis during endochondral bone formation, *Nature Medicine* 5(6) (1999) 623-628.
- [13] Y.Q. Yang, Y.Y. Tan, R. Wong, A. Wenden, L.K. Zhang, A.B. Rabie, The role of vascular endothelial growth factor in ossification, *Int J Oral Sci* 4(2) (2012) 64-8.
- [14] J. Street, M. Bao, L. deGuzman, S. Bunting, F.V. Peale, Jr., N. Ferrara, H. Steinmetz, J. Hoeffel, J.L. Cleland, A. Daugherty, N. van Bruggen, H.P. Redmond, R.A. Carano, E.H. Filvaroff, Vascular endothelial growth factor stimulates bone repair by promoting angiogenesis and bone turnover, *Proc Natl Acad Sci U S A* 99(15) (2002) 9656-61.

- [15] E.A. Bayer, R. Gottardi, M.V. Fedorchak, S.R. Little, The scope and sequence of growth factor delivery for vascularized bone tissue regeneration, *J Control Release* 219 (2015) 129-140.
- [16] M. Bouyer, R. Guillot, J. Lavaud, C. Plettinx, C. Olivier, V. Curry, J. Boutonnat, J.L. Coll, F. Peyrin, V. Josserand, G. Bettega, C. Picart, Surface delivery of tunable doses of BMP-2 from an adaptable polymeric scaffold induces volumetric bone regeneration, *Biomaterials* 104 (2016) 168-181.
- [17] A. Asadi, A.A. Barati, K. Kalantari, I. Odeh, Study of Relationship Between Roads Network Development and Agricultural Land Conversion in Iran NorthWest, *Int J Environ Res* 10(1) (2016) 51-58.
- [18] M.R. Urist, Bone - Formation by Autoinduction, *Science* 150(3698) (1965) 893-&.
- [19] H. Peng, A. Usas, A. Olshanski, A.M. Ho, B. Gearhart, G.M. Cooper, J. Huard, VEGF improves, whereas sFlt1 inhibits, BMP2-induced bone formation and bone healing through modulation of angiogenesis, *J Bone Miner Res* 20(11) (2005) 2017-27.
- [20] Q. Wang, Y.X. Zhang, B. Li, L. Chen, Controlled dual delivery of low doses of BMP-2 and VEGF in a silk fibroin-nanohydroxyapatite scaffold for vascularized bone regeneration, *J Mater Chem B* 5(33) (2017) 6963-6972.
- [21] J.Y. Park, J.H. Shim, S.A. Choi, J. Jang, M. Kim, S.H. Lee, D.W. Cho, 3D printing technology to control BMP-2 and VEGF delivery spatially and temporally to promote large-volume bone regeneration, *J Mater Chem B* 3(27) (2015) 5415-5425.
- [22] E. Hasanzadeh, G. Amoabediny, N. Haghighipour, N. Gholami, J. Mohammadnejad, S. Shojaei, N. Salehi-Nik, The stability evaluation of mesenchymal stem cells differentiation toward endothelial cells by chemical and mechanical stimulation, *In Vitro Cell Dev-An* 53(9) (2017) 818-826.
- [23] N. Monteiro, D. Ribeiro, A. Martins, S. Faria, N.A. Fonseca, J.N. Moreira, R.L. Reis, N.M. Neves, Instructive Nanofibrous Scaffold Comprising Runt-Related Transcription Factor 2 Gene Delivery for Bone Tissue Engineering, *Acs Nano* 8(8) (2014) 8082-8094.
- [24] M. Alves da Silva, A. Martins, A.R. Costa-Pinto, V.M. Correlo, P. Sol, M. Bhattacharya, S. Faria, R.L. Reis, N.M. Neves, Chondrogenic differentiation of human bone marrow mesenchymal stem cells in chitosan-based scaffolds using a flow-perfusion bioreactor, *J Tissue Eng Regen M* 5(9) (2011) 722-732.
- [25] F.X. Zhang, C.R. Wang, J.T. Lin, X.W. Wang, Oxidized low-density lipoprotein (ox-LDL) promotes cardiac differentiation of bone marrow mesenchymal stem cells via activating ERK1/2 signaling, *Cardiovasc Ther* 35(6) (2017).
- [26] C. Wiraja, D.C. Yeo, M.S.K. Chong, C.J. Xu, Nanosensors for Continuous and Noninvasive Monitoring of Mesenchymal Stem Cell Osteogenic Differentiation, *Small* 12(10) (2016) 1342-1350.
- [27] P.N. Williams, G. Moran, J.P. Bradley, S.E. N, J.S. Dines, Platelet-rich plasma and other cellular strategies in orthopedic surgery, *Curr Rev Musculoskelet Med* 8(1) (2015) 32-39.

- [28] C.S. Cohn, E. Lockhart, J.J. McCullough, The use of autologous platelet-rich plasma in the orthopedic setting, *Transfusion* 55(7) (2015) 1812-20.
- [29] G. Fernandes, C. Wang, X. Yuan, Z. Liu, R. Dziak, S. Yang, Combination of Controlled Release Platelet-Rich Plasma Alginate Beads and Bone Morphogenetic Protein-2 Genetically Modified Mesenchymal Stem Cells for Bone Regeneration, *J Periodontol* 87(4) (2016) 470-80.
- [30] V. Galanis, A. Fiska, S. Kapetanakis, K. Kazakos, T. Demetriou, Effect of platelet-rich plasma combined with demineralised bone matrix on bone healing in rabbit ulnar defects, *Singapore Med J* 58(9) (2017) 551-556.
- [31] M.W. Joo, S.J. Chung, S.H. Shin, Y.G. Chung, The Effect of Autologous Platelet-Rich Plasma on Bone Regeneration by Autologous Mesenchymal Stem Cells Loaded onto Allogeneic Cancellous Bone Granules, *Cells Tissues Organs* 203(6) (2017) 327-338.
- [32] E. Anitua, M. Sanchez, R. Prado, G. Orive, Plasma rich in growth factors: the pioneering autologous technology for tissue regeneration, *J Biomed Mater Res A* 97(4) (2011) 536.
- [33] J. Pierce, E. Benedetti, A. Preslar, P. Jacobson, P. Jin, D.F. Stroncek, J.A. Reems, Comparative analyses of industrial-scale human platelet lysate preparations, *Transfusion* (2017).
- [34] G. Strandberg, F. Sellberg, P. Sommar, M. Ronaghi, N. Lubenow, F. Knutson, D. Berglund, Standardizing the freeze-thaw preparation of growth factors from platelet lysate, *Transfusion* 57(4) (2017) 1058-1065.
- [35] Y.D. Shanskii, N.S. Sergeeva, I.K. Sviridova, M.S. Kirakozov, V.A. Kirsanova, S.A. Akhmedova, A.I. Antokhin, V.I. Chissov, Human platelet lysate as a promising growth-stimulating additive for culturing of stem cells and other cell types, *Bull Exp Biol Med* 156(1) (2013) 146-51.
- [36] J.V. Araujo, A. Martins, I.B. Leonor, E.D. Pinho, R.L. Reis, N.M. Neves, Surface controlled biomimetic coating of polycaprolactone nanofiber meshes to be used as bone extracellular matrix analogues, *J Biomat Sci-Polym E* 19(10) (2008) 1261-1278.
- [37] Y.P. Ding, W. Li, F. Zhang, Z.H. Liu, N.Z. Ezazi, D.F. Liu, H.A. Santos, Electrospun Fibrous Architectures for Drug Delivery, *Tissue Engineering and Cancer Therapy*, *Adv Funct Mater* 29(2) (2019).
- [38] N. Monteiro, A. Martins, R. Pires, S. Faria, N.A. Fonseca, J.N. Moreira, R.L. Reisa, N.M. Neves, Immobilization of bioactive factor-loaded liposomes on the surface of electrospun nanofibers targeting tissue engineering, *Biomater Sci-Uk* 2(9) (2014) 1195-1209.
- [39] C. Oliveira, A.R. Costa-Pinto, R.L. Reis, A. Martins, N.M. Neves, Biofunctional Nanofibrous Substrate Comprising Immobilized Antibodies and Selective Binding of Autologous Growth Factors, *Biomacromolecules* 15(6) (2014) 2196-2205.
- [40] M.R. Casanova, M. Alves da Silva, A.R. Costa-Pinto, R.L. Reis, A. Martins, N.M. Neves, Chondrogenesis-inductive nanofibrous substrate using both biological fluids and mesenchymal stem cells from an autologous source, *Materials Science and Engineering: C Volume* 98 (2019) 1169-1178.

- [41] V.E. Santo, M.E. Gomes, J.F. Mano, R.L. Reis, Chitosan-chondroitin sulphate nanoparticles for controlled delivery of platelet lysates in bone regenerative medicine, *J Tissue Eng Regen M* 6 (2012) s47-s59.
- [42] M.L.A. da Silva, A. Martins, A.R. Costa-Pinto, P. Costa, S. Faria, M. Gomes, R.L. Reis, N.M. Neves, Cartilage Tissue Engineering Using Electrospun PCL Nanofiber Meshes and MSCs, *Biomacromolecules* 11(12) (2010) 3228-3236.
- [43] D. Ribatti, B. Nico, A. Vacca, M. Presta, The gelatin sponge-chorioallantoic membrane assay, *Nat Protoc* 1(1) (2006) 85-91.
- [44] P. Nowak-Sliwinska, J.P. Ballini, G. Wagnieres, H. van den Bergh, Processing of Fluorescence Angiograms for the Quantification of Vascular Effects Induced by Anti-angiogenic Agents in the CAM model (vol 79, pg 21, 2010), *Microvascular Research* 80(1) (2010) 177-177.
- [45] J.P. Kruger, U. Freymannx, S. Vetterlein, K. Neumann, M. Endres, C. Kaps, Bioactive factors in platelet-rich plasma obtained by apheresis, *Transfus Med Hemother* 40(6) (2013) 432-40.
- [46] F. Sellberg, E. Berglund, M. Ronaghi, G. Strandberg, H. Lof, P. Sommar, N. Lubenow, F. Knutson, D. Berglund, Composition of growth factors and cytokines in lysates obtained from fresh versus stored pathogen-inactivated platelet units, *Transfus Apher Sci* 55(3) (2016) 333-337.
- [47] J. Alsousou, M. Thompson, P. Hulley, A. Noble, K. Willett, The biology of platelet-rich plasma and its application in trauma and orthopaedic surgery: a review of the literature, *J Bone Joint Surg Br* 91(8) (2009) 987-96.
- [48] B.M. Roux, M.H. Cheng, E.M. Brey, Engineering clinically relevant volumes of vascularized bone, *J Cell Mol Med* 19(5) (2015) 903-914.
- [49] H.F. Zhang, X.Y. Mao, D.Y. Zhao, W.B. Jiang, Z.J. Du, Q.F. Li, C.H. Jiang, D. Han, Three dimensional printed polylactic acid-hydroxyapatite composite scaffolds for prefabricating vascularized tissue engineered bone: An in vivo bioreactor model, *Sci Rep-Uk* 7 (2017).
- [50] L. Keller, A. Regiel-Futyra, M. Gimeno, S. Eap, G. Mendoza, V. Andreu, Q. Wagner, A. Kyziol, V. Sebastian, G. Stochel, M. Arruebo, N. Benkirane-Jessel, Chitosan-based nanocomposites for the repair of bone defects, *Nanomed-Nanotechnol* 13(7) (2017) 2231-2240.
- [51] H.W. Kang, S.J. Lee, I.K. Ko, C. Kengla, J.J. Yoo, A. Atala, A 3D bioprinting system to produce human-scale tissue constructs with structural integrity, *Nature Biotechnology* 34(3) (2016) 312-+.
- [52] J. Zhou, H. Lin, T. Fang, X. Li, W. Dai, T. Uemura, J. Dong, The repair of large segmental bone defects in the rabbit with vascularized tissue engineered bone, *Biomaterials* 31(6) (2010) 1171-9.
- [53] T. Fernandez, G. Olave, C.H. Valencia, S. Arce, J.M. Quinn, G.A. Thouas, Q.Z. Chen, Effects of calcium phosphate/chitosan composite on bone healing in rats: calcium phosphate induces osteon formation, *Tissue Eng Part A* 20(13-14) (2014) 1948-60.

- [54] Z.S. Patel, S. Young, Y. Tabata, J.A. Jansen, M.E.K. Wong, A.G. Mikos, Dual delivery of an angiogenic and an osteogenic growth factor for bone regeneration in a critical size defect model, *Bone* 43(5) (2008) 931-940.
- [55] Y.C. Chen, R.Z. Lin, H. Qi, Y.Z. Yang, H.J. Bae, J.M. Melero-Martin, A. Khademhosseini, Functional Human Vascular Network Generated in Photocrosslinkable Gelatin Methacrylate Hydrogels, *Adv Funct Mater* 22(10) (2012) 2027-2039.
- [56] T. Gong, K. Zhao, X. Liu, L.X. Lu, D. Liu, S.B. Zhou, A Dynamically Tunable, Bioinspired Micropatterned Surface Regulates Vascular Endothelial and Smooth Muscle Cells Growth at Vascularization, *Small* 12(41) (2016) 5769-5778.
- [57] H.R. Nejad, Z.G. Malekabadi, M.K. Narbat, N. Annabi, P. Mostafalu, F. Tarlan, Y.S. Zhang, M. Hoorfar, A. Tamayol, A. Khademhosseini, Laterally Confined Microfluidic Patterning of Cells for Engineering Spatially Defined Vascularization, *Small* 12(37) (2016) 5132-5139.
- [58] S. Uchida, A. Sakai, H. Kudo, H. Otomo, M. Watanuki, M. Tanaka, M. Nagashima, T. Nakamura, Vascular endothelial growth factor is expressed along with its receptors during the healing process of bone and bone marrow after drill-hole injury in rats, *Bone* 32(5) (2003) 491-501.
- [59] K.D. Hankenson, K. Gagne, M. Shaughnessy, Extracellular signaling molecules to promote fracture healing and bone regeneration, *Adv Drug Deliver Rev* 94 (2015) 3-12.
- [60] L.L.Y. Chiu, R.D. Weisel, R.K. Li, M. Radisic, Defining conditions for covalent immobilization of angiogenic growth factors onto scaffolds for tissue engineering, *J Tissue Eng Regen M* 5(1) (2011) 69-84.
- [61] C.S. Abhinand, R. Raju, S.J. Soumya, P.S. Arya, P.R. Sudhakaran, VEGF-A/VEGFR2 signaling network in endothelial cells relevant to angiogenesis, *J Cell Commun Signal* 10(4) (2016) 347-354.
- [62] M. Shibuya, Vascular Endothelial Growth Factor (VEGF) and Its Receptor (VEGFR) Signaling in Angiogenesis: A Crucial Target for Anti- and Pro-Angiogenic Therapies, *Genes Cancer* 2(12) (2011) 1097-105.
- [63] M. Beederman, J.D. Lamplot, G. Nan, J. Wang, X. Liu, L. Yin, R. Li, W. Shui, H. Zhang, S.H. Kim, W. Zhang, J. Zhang, Y. Kong, S. Denduluri, M.R. Rogers, A. Pratt, R.C. Haydon, H.H. Luu, J. Angeles, L.L. Shi, T.C. He, BMP signaling in mesenchymal stem cell differentiation and bone formation, *J Biomed Sci Eng* 6(8A) (2013) 32-52.
- [64] M. Wu, G. Chen, Y.P. Li, TGF-beta and BMP signaling in osteoblast, skeletal development, and bone formation, homeostasis and disease, *Bone Res* 4 (2016) 16009.
- [65] D. Barati, S.R.P. Shariati, S. Moeinzadeh, J.M. Melero-Martin, A. Khademhosseini, E. Jabbari, Spatiotemporal release of BMP-2 and VEGF enhances osteogenic and vasculogenic differentiation of human mesenchymal stem cells and endothelial colony-forming cells co-encapsulated in a patterned hydrogel, *J Control Release* 223 (2016) 126-136.



- [66] K. Marupanthorn, C. Tantrawatpan, P. Kheolamai, D. Tantikanlayaporn, S. Manochantr, Bone morphogenetic protein-2 enhances the osteogenic differentiation capacity of mesenchymal stromal cells derived from human bone marrow and umbilical cord, *International Journal of Molecular Medicine* 39(3) (2017) 654-662.
- [67] Y. Bai, Y. Leng, G.F. Yin, X.M. Pu, Z.B. Huang, X.M. Liao, X.C. Chen, Y.D. Yao, Effects of combinations of BMP-2 with FGF-2 and/or VEGF on HUVECs angiogenesis in vitro and CAM angiogenesis in vivo, *Cell and Tissue Research* 356(1) (2014) 109-121.
- [68] S.P. Ayalasomayajula, P. Ashton, U.B. Kompella, Fluocinolone Inhibits VEGF Expression via Glucocorticoid Receptor in Human Retinal Pigment Epithelial (ARPE-19) Cells and TNF-alpha-Induced Angiogenesis in Chick Chorioallantoic Membrane (CAM), *J Ocul Pharmacol Th* 25(2) (2009) 97-103.
- [69] Y. Bai, L.J. Bai, J. Zhou, H.L. Chen, L.K. Zhang, Sequential delivery of VEGF, FGF-2 and PDGF from the polymeric system enhance HUVECs angiogenesis in vitro and CAM angiogenesis, *Cell Immunol* 323 (2018) 19-32.
- [70] H. Peng, V. Wright, A. Usas, B. Gearhart, H.C. Shen, J. Cummins, J. Huard, Synergistic enhancement of bone formation and healing by stem cell-expressed VEGF and bone morphogenetic protein-4, *J Clin Invest* 110(6) (2002) 751-9.
- [71] J.H. Lee, D.K. Woo, T.H. Kim, J.G. Kang, J.W. Yun, J.H. Park, B.W. Park, Y.H. Kang, G.J. Rho, S.J. Jang, J.S. Park, H.C. Lee, Y.M. Yoon, T.S. Hwang, D.R. Kim, S.C. Hwang, D.H. Lee, H.Y. Kim, S.H. Oh, J.H. Byun, In vitro and long-term (2-year follow-up) in vivo osteogenic activities of human periosteum-derived osteoblasts seeded into growth factor-releasing polycaprolactone/pluronic F127 beads scaffolds, *J Biomed Mater Res A* 105(2) (2017) 363-376.
- [72] G. Cheng, C.C. Yin, H. Tu, S. Jiang, Q. Wang, X. Zhou, X. Xing, C.Y. Xie, X.W. Shi, Y.M. Du, H.B. Deng, Z.B. Li, Controlled Co-delivery of Growth Factors through Layer-by-Layer Assembly of Core-Shell Nanofibers for Improving Bone Regeneration, *Acs Nano* 13(6) (2019) 6372-6382.
- [73] J.H. Lee, Y.J. Lee, H.J. Cho, H. Shin, Guidance of In Vitro Migration of Human Mesenchymal Stem Cells and In Vivo Guided Bone Regeneration Using Aligned Electrospun Fibers, *Tissue Eng Pt A* 20(15-16) (2014) 2031-2042.
- [74] K. Balagangadharan, R. Trivedi, M. Vairamani, N. Selvamurugan, Sinapic acid-loaded chitosan nanoparticles in polycaprolactone electrospun fibers for bone regeneration in vitro and in vivo, *Carbohydr Polym* 216 (2019) 1-16.

## **SECTION 6**

# **GENERAL CONCLUSIONS**

# **Chapter VIII**

## **General Conclusions and Future Perspectives.**

## Chapter VIII

### General Conclusions and Future Perspectives.

#### VIII-1. GENERAL CONCLUSIONS

The biofunctionalization of a biomaterial surface with bioactive agents has attracted increasing interest, aiming to boost its biological activity. The functionalization of biomaterial substrates with biological cues can be an effective approach to overcome the major problems related with implantable biomaterials, namely the limited bioactivity and suboptimal integration with the host tissue. In this sense, the work performed under the scope of this thesis aimed to develop highly biofunctional nanofibrous substrates which can provide a biocompatible and bioactive environment. The biofunctionalization of the nanofibrous meshes was based on the activation, functionalization and covalent immobilization of antibodies in order to selectively bind endogenous bioactive molecules to promote chondrogenesis, neurogenesis, osteogenesis and angiogenesis. The surface biofunctionalization of the nanofibrous meshes has the advantage of a local exposure of bioactive molecules with more prolonged activity, avoiding their degradation by biological means and the systemic side effects. The proposed approaches intended to overcome the recognized drawbacks of currently available treatments in neural and skeletal tissues, using pioneering and personalized strategies.

The low efficacy of clinical interventions to regenerate articular cartilage results from its limited or no self-repair potential. Therefore, different biofunctionalization strategies were proposed aiming to developed biofunctional nanofibrous substrates with chondrogenic inductive properties (**Chapters III to V**). The chondrogenesis-inductive systems were based on the use of different biomolecules, namely an extracellular matrix protein (fibronectin), lipidic particles with potent cargo (extracellular vesicles (EVs)) or chondrogenic growth factors (TGF- $\beta$ 3 and IGF-I).

The chondrogenic potential of human fibronectin bound at the surface of a nanofibrous substrate was evaluated in **Chapter III**. For that, an anti-fibronectin antibody was immobilized at the nanofibers' surface, which allows the binding of fibronectin. Human bone marrow-derived mesenchymal stem cells (hBM-MSCs) cultured on the fibronectin-functionalized

nanofibrous substrates under basal conditions display the typical phenotypic and genotypic markers of articular chondrocytes. Indeed, immobilized fibronectin seems to be more effective than the standard chondrogenic differentiation obtained with soluble growth factors. Furthermore, the soluble human fibronectin seems to not have the potential to induce the differentiation of hBM-MSCs towards the chondrogenic lineage as compared to its immobilized form. Therefore, the immobilization of endogenous fibronectin at the surface of a nanofibrous substrate has the advantage of inducing the chondrogenesis by exposing the bioactive domains of fibronectin correctly. However, the fibronectin orientation/conformation changes when bound at the surface of a biomaterial scaffold have to be assessed.

Aiming to exploit the regenerative potential of EVs present in conditioned medium from human articular chondrocytes (hACs) or chondrogenically induced hBM-MSC, an EVs functionalized system were developed in **Chapter IV**. Those EVs were successfully bound at the surface of biofunctional nanofibrous substrates, immobilizing a CD63 antibody. The *in vitro* biological assays demonstrated that the EVs-biofunctionalized nanofibrous substrates successfully induce the chondrogenic commitment of homotypic cells more efficiently than the current chondroinductive strategies. Furthermore, the EVs biofunctionalized nanofibrous substrates comprising EVs derived from mature hACs demonstrate to be the most effective. One of the main benefits of this strategy is the ability to use the total EVs' cargo to induce chondrogenesis, although its content needs to be further analyzed.

Another chondrogenesis-inductive nanofibrous substrate was developed comprising endogenous TGF- $\beta$ 3 and IGF-I bound at the surface of the same nanofibrous substrate (**Chapter V**). The immobilization of defined antibodies (i.e. anti-TGF- $\beta$ 3 and anti-IGF-I) allows the selective retrieval of the abovementioned growth factors from human platelet lysates. The *in vitro* cellular assays confirmed the bioactivity of bound TGF- $\beta$ 3 and IGF-I by enabling the successful chondrogenic differentiation of hBM-MSCs cultured under basal conditions. However, it seems that hBM-MSCs cultured on biofunctionalized nanofibrous substrates with individually bound TGF- $\beta$ 3 or IGF-I has similar chondrogenic gene expression profile as hBM-MSCs cultured in the presence of bound TGF- $\beta$ 3 and IGF-I.

The availability of endogenous fibronectin, EVs derived from mature hACs or chondrogenically induced hBM-MSCs, or TGF- $\beta$ 3 and IGF-I at the surface of a nanofibrous substrate are capable of induce the chondrogenic differentiation of hBM-MSCs under basal culture medium. These chondrogenesis-inductive nanofibrous substrates possibly allow the

implementation of very effective and personalized therapies tailored for specific clinical conditions, by using both biological fluids and cells from an autologous source. However, an *in vivo* study is necessary to fully validate these strategies and confirm that local and sustained exposure of those bioactive molecules is effective in promoting cartilage regeneration.

Envisioning the clinical translation of the different chondrogenesis-inductive nanofibrous substrates herein reported, we foreseen their potential use as an autologous cartilage regeneration strategy. For example, in the microfactory technique, the chondrogenesis-inductive nanofibrous substrates can be implanted over the defect site, where uncommitted homotypic cells migrating from microperforations could be induced to properly differentiate into the chondrogenic lineage by the bound biomolecules. In an *ex vivo* attempt, both the MSCs and the bioactive factors isolated from the same patient can be cultured on a biofunctional nanofibrous substrate, which will be then implanted into the defect site as a matrix-induced autologous chondrocyte implantation (MACI) approach. Both approaches could lead to the regeneration of cartilage, envisioning a personalized therapy for cartilage repair.

The versatility of the biofunctional nanofibrous substrates strategy herein proposed was also applied to others unmet clinical needs, namely nerve regeneration and reconstruction of bone defects. Therefore, the development of biofunctional nanofibrous substrates with neurogenic inductive properties or osteogenic and angiogenic potential were carried out.

Taking into consideration the state of the art of peripheral nerve regeneration, it is noticeable that more effective approaches are needed. In an attempt to contribute to this goal, in **Chapter VI**, a novel nerve stimulation nanofibrous substrates biofunctionalized with NGF was developed. The immobilization of anti-NGF antibody at the surface of nanofibrous substrates allowed for the selective retrieval of endogenous NGF, derived from rat blood plasma. The *in vitro* biological assays demonstrated that the NGF delivery system promotes neuronal differentiation of rat pheochromocytoma (PC12) cells, displaying the typical phenotypic and genotypic neuronal markers. Moreover, the nanofibrous substrates biofunctionalized with endogenous NGF is more bioactive than recombinant NGF, either immobilized or in the free form. However, in light of the results achieved, a complementary *in vivo* study in a rat nerve defect model is necessary to fully validate these endogenous NGF delivery system and confirm the hypothesis envisioned by the authors. This is a crucial pre-clinical step to validate that the presence of NGF at the surface of nanofibrous substrate will improve peripheral nerve regeneration.

Ideally, to create a bone tissue-engineered substitute capable of regenerate a fully functional tissue, it should allow the formation of new blood vessels. In the reconstruction of bone defects, it is essential an intimate crosstalk between endothelial and bone cells. In this sense, in **Chapter VII**, an engineered biofunctional system was developed comprising anti-BMP-2 and anti-VEGF antibodies immobilized over the same nanofibrous substrate in a parallel pattern design. The spatial immobilization of endogenous BMP-2 and VEGF, derived from human platelet lysates, enabled the spatial osteogenic and angiogenic differentiation of human hBM-MSCs under basal culture conditions, as confirmed in the *in vitro* biological assays. A chick chorioallantoic membrane (CAM) assay revealed that this biofunctional system induced a significant angiogenic response. The versatility of the herein described vascularization-inductive strategy can be potentially use as a guided bone regeneration membrane applied in the internal fixture of bone fractures or as a substrate accelerating healing in flat bones (i.e. cranial bones, scapulae). However, an *in vivo* study in a critical-sized rat calvarial bone defect model is necessary to fully validate this biofunctional system and confirm the synergistic effect of endogenous BMP-2 and VEGF bound in a parallel arrangement on vascularized bone regeneration.

The work developed in this thesis enabled overcoming some challenges of implantable biomaterials, namely this limited bioactivity. Particularly, the bound bioactive molecules require that the biofunctionalized nanofibrous substrates can provide a biocompatible and bioactive environment. Using surface functionalization strategies, we were able to develop effective and personalized biofunctional nanofibrous substrates, tailored for specific clinical conditions. The substrates' surface was biofunctionalized with specific antibodies, taking advantage of the specific and efficient interactions between a specific antibody and its antigen. The method consists on the generating of functional groups (i.e. amine groups) at the surface of nanofiber, which will allow the covalent and irreversible immobilization of an antibody by its carboxyl group. This immobilization strategy guarantees the efficacy/availability of the antibody binding epitopes, as well as an extended half-life of the antibodies when compared to its free form. However, one of the disadvantages on the use of antibodies is that some of them can have a neutralizing activity over the protein bound. To overcome this drawback, the antibodies used in this work do not present neutralizing activity, remaining the cell receptor binding domain free to perform their biological activity.

The presented approach of biofunctionalized nanofibrous substrates by the immobilization of antibodies allows to selectively bind, from a pool of different biomolecules present in

biological fluids (e.g. blood plasma, platelet lysate or conditioned medium), just the ones of interest for the envisioned application. However, to achieve such specificity, overcoming the drawback of possible binding of other proteins or isoforms or even cell-secreted proteins, we perform a blocking step with BSA to not allow non-specific binding of such bioactive molecules.

As a general conclusion, the work developed in this thesis is a step forward on precision medicine approaches providing alternatives for surface biofunctionalization of personalized biomaterial substrates for neural and skeletal tissues regeneration.

## **VIII-2. FUTURE PERSPECTIVES**

The development process in science is a never-ending journey. The work developed under the scope of this thesis, although answering some questions, opens a new range of questions that can be further exploited in multiple directions. In this sense, some future studies related with the work developed were previously suggested. Of particular interest is the evaluation of the *in vivo* efficacy of the immobilized antibody or bound bioactive factors at the surface of a nanofibrous substrate. The translation of novel technologies from bench to bedside is extremely dependent on these pre-clinical animal models.

The biomaterial surface biofunctionalization strategy applied in this thesis allows for the immobilization of single or multiple antibodies, and the corresponding biomolecule binding, in a spatial controlled way over a same nanofibrous substrate. The engineered biofunctional system comprising distinct biomolecules in different areas of the same substrate can be exploited to other target applications. For example, this system could enable the elucidation of its functional role over distinct cell types. The types of cells (e.g. endothelial, osteoblasts and/or chondrocytes) could be seeded over the distinct areas of the nanofibrous substrate, where a certain antibody and the corresponding biomolecule were previously immobilized. With this strategy would be possible to obtain tailored co-culture systems, allowing to study bioactive molecules-mediated cellular interactions.

The application of the spatially localized bioactive molecules bound on biomaterial substrate for the regeneration of complex tissues, involving more than one cell communities, may provide helpful cues enabling their self-organization. For example, an osteochondral regeneration model can be developed by the functionalization of a same nanofibrous substrate



divided into parts. One part will be able to promote chondrogenesis, as the other will be able to promote osteogenesis and angiogenesis. The implementation of this model could elucidate the synergistic effect of chondrogenesis, osteogenesis and angiogenesis in osteochondral tissue. Furthermore, the parallel arrangement of bioactive molecules bound on biomaterial substrate could also be applied to regenerate innervated tissue by taking advantage of the knowledge achieved with the nerve stimulation nanofibrous substrates biofunctionalized with NGF.

The potential of this versatile immobilization strategy can be transposed to different polymeric substrates currently in use in the clinic, namely bioresorbable devices (i.e. meshes, screws). As example, wound dressing meshes (for diabetic ulcers) or membranes for guided tissue regeneration in the context of dentistry. Therefore, the substrates biofunctionalization strategies developed under the scope of this thesis have remarkable biochemical properties, namely a localized and prolonged bioactivity of the bound molecules, making them a great alternative to the current available treatments.